Interplay between cholesterol homeostasis and neural development *in vitro*

Swansea University
Prifysgol Abertawe

Submitted to Swansea University in fulfilment of the requirements for the Degree of Doctor of Philosophy

2025

Emily Jane Stonelake

Summary

Cholesterol metabolism plays a critical role in brain development, with dysregulated cholesterol homeostasis implicated in the pathogenesis of multiple neural developmental disorders. However, regulation of cholesterol homeostasis and it impact on human neural development remains to be fully understood. Both cholesterol itself as well as specific oxidised metabolites of cholesterol, known as oxysterols, are demonstrated to act as bioactive signalling molecules and interact with key signalling pathways involved in neural developmental processes. However, there is a lack of evidence for the presence of these molecules endogenously in developing human neural cells and it remains to be determined which of these sterols may be responsible for aberrant human neurogenesis. In this thesis, temporal sterolomic profiles were generated from *in vitr*o models of human pluripotent stem cell (hPSC)-derived cortical neurons and astrocytes to investigate cholesterol homeostasis and identify the presence of bioactive sterols involved in key neurodevelopmental signalling pathways. We confirmed the endogenous presence of several oxysterols in human neuronal cultures, including 24S-hydroxycholesterol (24S-HC) and 24S,25-epoxycholesterol (24S,25-EC), both implicated in neurogenesis. Notably, 24S-HC was identified as the predominant oxysterol, consistent with its abundance in the adult human brain. hPSC-derived astrocytes were similarly shown to produce both 24S-HC and 24S,25-EC and express the enzyme CYP46A1, indicating active sterol metabolism. This sterolomic profiling was further applied to a model of neural developmental disorder associated with the 15q11.2 copy number variation (CNV), which demonstrated both aberrant neurogenesis and significant alterations in

cholesterol metabolism and biosynthesis. Collectively, these findings establish an *in vitro* framework for investigating the role of cholesterol dysregulation in neurodevelopmental disorders and provide new insight into the sterolomic profiles of developing human neural cells.

Declaration

This work has not previously been accepted in substance for any degree and is not being concurrently submitted in candidature for any degree.

Signed 

Date…26/9/25……..

Statement 1
This thesis is the result of my own investigations, except where otherwise stated. Other sources are acknowledged by footnotes giving explicit references. A bibliography is appended.

Signed 

Date…26/9/25……..

Statement 2

I hereby give consent for my thesis, if accepted, to be available for photocopying and for inter-library loan, and for the title and summary to be made available to outside organisations.

Signed 

Date…26/9/25……..

Statement 3

The University's ethical procedures have been followed and, where appropriate, that ethical approval has been granted.

Signed 

Date... 26/9/25.....

Table of Contents

Acknowledgments

Firstly I'd like to thank my supervisors Prof. Yuqin Wang and Prof. Meng Li for providing me with the opportunity to undertake this project, I'm grateful to have had the opportunity to benefit from your mentorship. I'd also like to thank the BBSRC and SWBio DTP for funding this project.

I want to thank Dani for everything you've taught me and all your guidance and encouragement, you've been an incredible mentor and I'm grateful for having had the chance to learn from you. I want to say a huge thanks to Emma, Kanoon and Laura for being both amazing lab mates and housemates during this journey. It's been so great working and living with you all (even in what might be the coldest, mouldiest house in Cathays), and I'm incredibly thankful for all of your support, inspiration and laughs along the way. I'd also like to say a huge thank you to everyone in the NMHII in Cardiff; I couldn't have asked for better people to share this experience with and working alongside you all has been an absolute joy. I'd like to thank all members of Li Lab for their support and advice throughout this project, with a special thanks to Zongze for kindly providing the astrocyte samples for the LC-MS analysis. I'd like to thank members of the Griffiths-Wang group in Swansea, with particular thanks to Eylan, Manuela and Mohsen for teaching me so much of what I know today about LC-MS.

I'd like to thank my family and friends for all of their support over the last few years. I would like to thank my boyfriend Dave for all of his support and patience, and importantly for helping to keep me somewhat sane whilst writing these last few months. Thanks to my brother Tom, who, despite warning me

that doing a PhD would be tough, still supported me by regularly listening to me rant over a coffee.

Finally, I want to express my sincerest gratitude to my parents Julie and Peter for their unwavering support and for everything they've done to help me get to where I am today. Thank you for always encouraging me to pursue my passions and for consistently being there to cheer me on, I just hope that I've made you both proud.

List of Figures

List of Tables

List of Abbreviations

3β,7α-diHCA: 3β,7α-dihydroxycholestenoic acid

6β-HC: 6β-hydroxycholesterol

7-DHC: 7-dehydrocholesterol

7-OC: 7-oxocholesterol

7α-HC: 7α-hydroxycholesterol

7β-HC: 7β-hydroxycholesterol

7αH,3O-CA: 7α-hydroxy-3-oxocholestenoic acid

7α,25-diHC: 7α,25-dihydroxycholesterol

7α,25-diHCO: 7α,25-dihydroxycholestenone

7α,(25R)26-diHC – 7α,(25R)26-dihydroxycholesterol

20S-HC: 20S-hydroxycholesterol

22R-HC: 22R-hydroxycholesterol

24R-HC: 24R-hydroxycholesterol

24S-HC: 24S-hydroxycholesterol

24S,25-EC: 24S,25-epoxycholesterol

25-HC: 25-hydroxycholesterol

μg: micrograms

μL: microlitres

ABC: adenosine triphosphase (ATP) -binding cassette

ADHD: Attention deficit hyperactivity disorder

APOE: Apolipoprotein E

ASD: Autism Spectrum Disorder

BBB: Blood brain barrier

CH25H: cholesterol 25-hydroxylase

CNS: central nervous system

CNV: Copy number variant

CYFIP1: Cytoplasmic FMR1 Interacting Protein 1

CYP: Cytochrome P450

DHCR7: 7-dehydrocholesterol reductase

DHCR24: 24-dehydroxycholesterol reductase

EADSA: Enzyme Assisted Derivitisation for Sterol Analysis

ESI: Electrospray ionisation

EtOH: Ethanol

FMRP: Fragile X mental retardation protein

FXS: Fragile X Syndrome

GFAP: glial fibrillary acidic protein

GP: Girard P

hESCs: Human embryonic stem cells

HMGCR: 3-hydroxy-3-methyl-glutaryl CoA reductase

hPSCs: Human pluripotent stem cells

HPLC: High performance liquid chromatography

ID: Intellectual disability

INSIG: Insulin induced gene 1 protein

iPSCs: Induced pluripotent stem cells

iSTDs: Internal standards

KO: Knockout

K-R: Kandutsch-Russell

LC-MS: Liquid chromatography-mass spectrometry

LXR: Liver X receptor

MeOH: Methanol

mg: milligrams

mL: millilitres

mRNA: messenger ribonucleic acid (RNA)

MS: Mass spectrometry

MS^n: tandem mass spectrometry

NEC: Neuroepithelial cell

NPC: Neural progenitor cell

PBS: phosphate-buffered saline

PFA: paraformaldehyde

RGC: Radial glial cell

RIC: Reconstructed ion chromatogram

RP: reverse phase

Shh: Sonic Hedgehog

SLOS: Smith-Lemli-Opitz syndrome

SREBP: Sterol Regulatory Element Binding Protein

WT: Wild type

Chapter 1

Introduction

1.1 Sterol lipids

Lipids are a major class of biomolecules, defined as small molecules that are either hydrophobic or amphipathic, where part of their structure is hydrophilic whilst the other, usually larger, part is hydrophobic. Lipids are formed in part or entirely by carbanion-based condensation of thioesters and/or the carbocation-based condensation of isoprene units, as defined by the Lipid Maps classification system (LIPID MAPS®). They include any of a diverse group of organic compounds including fats, oils, hormones and certain components of cell membranes. These molecules are classified into the following 8 primary categories based on their chemical structures: fatty acyls, glycerolipids, glycerophospholipids, sphingolipids, sterol lipids, prenol lipids, saccharolipids and polyketides (Fahy et al., 2005).

Sterol lipids can be further subcategorised based on their biological function. Sterol lipids form one of 8 classes of lipids containing a cyclopentanoperhydrophenanthrene structure. They are further subdivided into the sub-classes sterols, cholesteryl esters, steryl esters, sterylglycosides, acylsterylglycosides, bile acids and derivatives (LIPID MAPS®). Of these sterol lipids, cholesterol and its derivatives are the most extensively studied in the context of mammalian systems. Cholesterol is the dominant sterol lipid in animal cells, forming an essential component of membrane lipids, composing approximately 20-25% of the lipid molecules in the plasma membrane (Dietschy and Turley, 2004).

1.1.1 Cholesterol

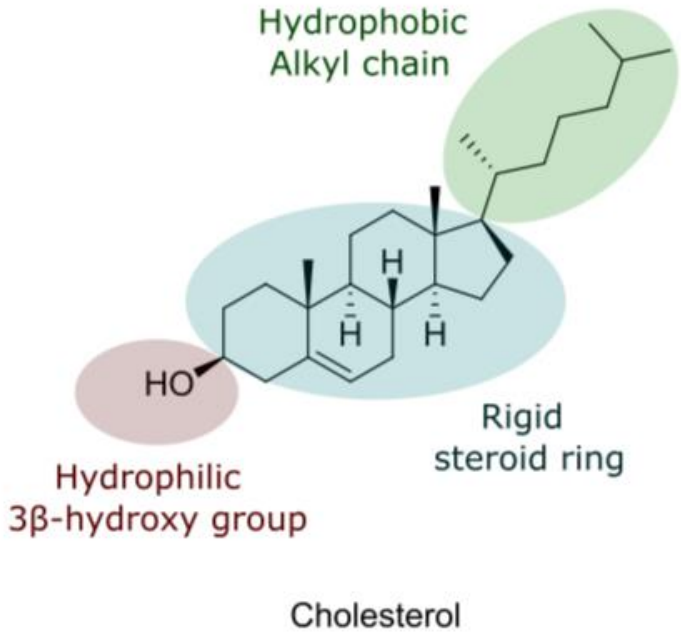

Figure 1.1. Structure of Cholesterol. Regions highlighted demonstrate the 3 structural domains of cholesterol.

Cholesterol contains 3 main structural domains: a proximal hydrophilic group, a central 4-ring structure which provides the molecule with a high rigidity and a distal hydrophobic group (**Figure 1.1**). Due to its unique structure, cholesterol is involved in various functions key to normal cellular function. Cholesterol is an essential component of the cell membrane, and due to its highly rigid core structure provides rigidity to the cell. In the typical cell, most cholesterol is unesterified and located in either the outer or inner leaflet of the plasma membrane . Cholesterol affects cell permeability, aiding influx and efflux, with increased cholesterol content in the cell membrane making the cell less

permeable to ions and gases (Itel et al., 2012). Cholesterol provides organisation in the plasma membrane for many cellular receptors and transmembrane proteins and transporters within the membrane. Additionally, cholesterol also forms “rafts” in the plasma membrane that provide compartmentalisation for cell processes across the membrane including the organisation of cell signalling molecules, membrane protein trafficking and regulation of neurotransmission (Krause and Regen, 2014; Toppozini et al., 2014).

Cholesterol is obtained mainly from diet; however, it can be synthesised by the endoplasmic reticulum (ER) of almost all cells, and around 50% of human cholesterol synthesis occurs in the liver (Repa and Mangelsdorf, 2000a). In mammalian cells, cholesterol is synthesised from acetyl CoA through a series of around 30 enzymatic reactions, with the final stages of cholesterol biosynthesis split into two major pathways known as the Kandutsch-Russell (K-R) and Bloch pathways (**Figure 1.2**). Cells can also obtain cholesterol from the circulation through uptake of low-density lipoproteins (LDL) via LDL receptors on the cell surface which are then hydrolysed to free cholesterol within lysosomes (Defesche, 2004) .

It is crucial that membrane lipid homeostasis is maintained, with external and internal sources of cholesterol carefully balanced to avoid sterol shortage or over-accumulation. Cholesterol homeostasis is tightly controlled at the transcriptional level by two factors: the sterol regulatory element binding protein (SREBP) transcription factors and the Liver X receptor/Retinoic acid receptor (LXR/RXR) transcription factors:

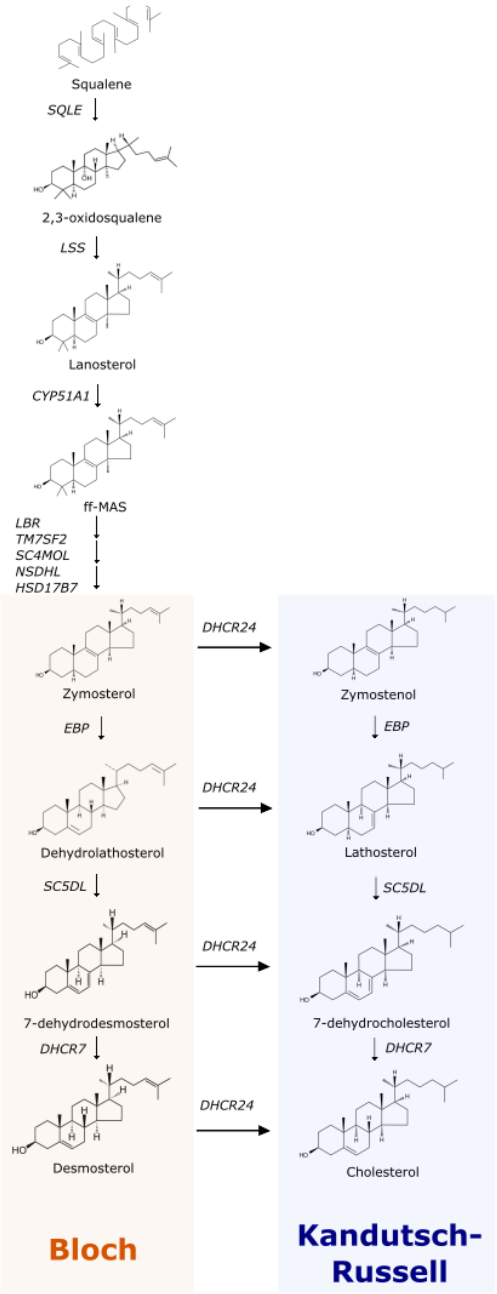

Figure 1.2. Cholesterol biosynthetic pathway. Diagram of the biosynthesis of cholesterol by the mevalonate pathway, and sub-pathways Bloch and Kandutsch-Russell (K-R).

SREBPs are transcription factors containing a basic helix-loop-helix-leucine zipper (bHLH-Zip) motif present in the ER membrane and are responsible for regulating the gene expression of enzymes involved in cholesterol biosynthetic pathways (Sato, 2010). In mammals, 2 genes *SREBF1* and *SREBF2* encode three family member subtypes SREBP1a, SREBP1c and SREBP2. Of these subtypes, SREBP2 is evidenced to be involved in regulation of cholesterol homeostasis and is ubiquitously expressed in all tissues, including the brain, whereas SREBP1 is expressed primarily in the adrenal gland and liver and regulates fatty acid metabolism (Sato, 2010). SREBP1 and SREBP2 subtypes are 47% identical, sharing a transcriptionally active NH2-terminal bHLH-Zip domain followed by a membrane attachment domain (Sato, 2010). SREBP1 and SREBP2 both interact with and forms complexes with the ER membrane protein SREBP-cleavage activating protein (SCAP). SCAP contains two distinct N-terminal and C-terminal domains, and within the N-terminal domain is a “sterol-sensing” domain (SSD), with a sequence similar to that of proteins which are also postulated to interact with sterols including HMG CoA reductase, Niemann-Pick C1 and Patched (Brown and Goldstein, 1999). Over-accumulation of cholesterol in cells and an increased concentration in the ER membrane causes a conformational change in SCAP through binding of cholesterol to the SSD within the N-terminus. This conformational change triggers binding of SCAP to another ER membrane protein known as INSIG, negatively impacting the formation of SREBP/SCAP complex and preventing proteolytic activation of SREBP (Sato, 2010).

The LXR-RXR transcription factors are involved in the upregulation of genes involved in cholesterol efflux. LXRs are nuclear receptors which heterodimerise with RXRs, remaining bound to DNA elements of target genes (Teboul et al.,

1995). LXRs have two isoforms LXRα and LXRβ, with LXRα expressed primarily in the liver whilst LXRβ has a broader expression, mainly found in the brain and the liver (Repa and Mangelsdorf, 2000b). In the absence of LXR ligand, a co-repressor complex acts to prevent transcription. Ligand-binding of LXR causes a conformational change that results in dissociation from the co-repressor complex and recruitment of a coactivator complex which promotes target gene expression.

1.1.2 Formation of oxysterols

Oxysterols are oxidised forms of cholesterol and its precursors, containing an additional hydroxyl, carbonyl or ketone group (Schroepfer, 2000). Oxysterols are formed either via the autoxidation of cholesterol or its precursors, or by enzymatic conversion by specific cytochrome P450 (CYP) enzymes, cholesterol esterase and transferases (**Figure 1.3**). Oxysterols are derived as various pathway intermediates within the bile acid synthesis and steroid hormone synthesis pathways. The nomenclature used in this thesis will follow that outlined by the LIPID MAPS® Lipid Classification System and the International Union of Pure and Applied Chemistry (IUPAC), regarding the oxidation of the terminal carbon of the sterol side chain.

The most highly abundant circulating oxysterols found in human serum are those formed via enzymatic reactions (Meaney et al., 2001), including 24(S)-hydroxycholesterol (24S-HC) produced by CYP46A1-mediated oxidation of cholesterol and 27-hydroxycholesterol (27-HC) formed by the CYP27A1 enzyme (**Figure 1.3**). A primary autoxidation product of cholesterol is 7-

hydroperoxidecholesterol, which rapidly forms major oxidised products 7-ketocholesterol (7-OC), 7α-hydroxycholesterol (7α-HC) and 7β-hydroxycholesterol (7β-HC) (**Figure 1.3**).

24S,25-epoxycholesterol is formed in a shunt pathway of the mevalonate pathway of cholesterol biosynthesis via the enzymes squalene monooxygenase and 2,3-oxidosqualene cyclase (**Figure 1.3**) and is produced in all cells that produce cholesterol. 24S,25-EC is structurally similar to cholesterol but contains an additional epoxide group in its side chain at C-24,25, thus making it more polar than cholesterol.

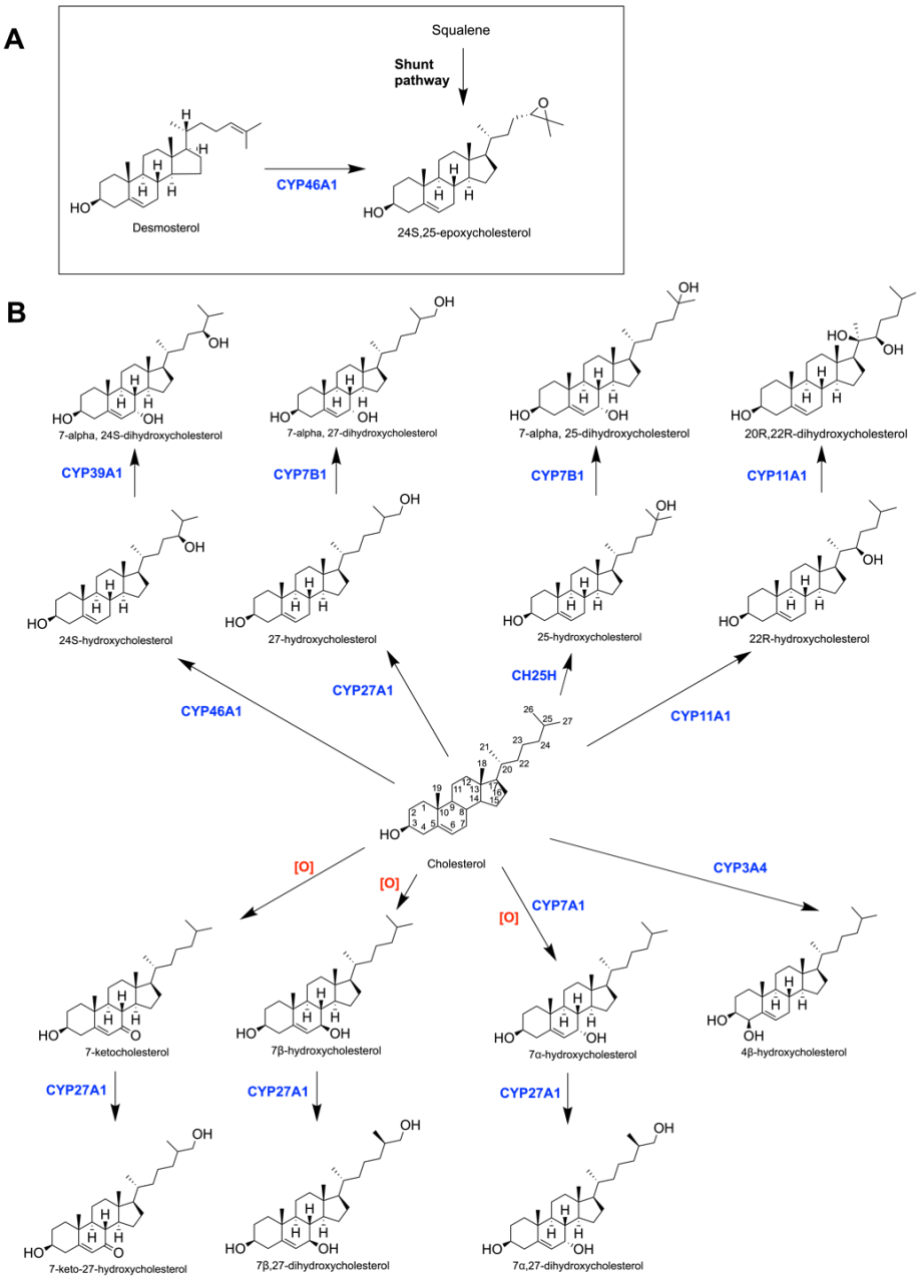

Figure 1.3. Formation of mono- and dihydroxycholesterols from cholesterol via autooxidation and enzymatic conversion. (**A**) Formation of 24S,25-EC via the shunt pathway and derived from desmosterol. (**B**) Formation of common oxysterols via enzymatic reactions and autooxidation ([O]).

1.2. Role of cholesterol in the brain

The human brain comprises only 2.1% of body weight but contains almost 25% of the total body unesterified cholesterol (Dietschy and Turley, 2001). The estimated mean concentration of cholesterol in the CNS is ~23mg/g, approximately 10 times higher than other tissues, signifying the importance of this lipid in the brain (Dietschy and Turley, 2004). In terms of its function within the CNS, cholesterol is a major component of cellular membranes, is involved in myelination (Saher et al., 2005), synapse formation and function (Mauch et al., 2001) and additionally is essential for embryonic development via the hedgehog signalling pathway (Porter et al., 1996). It is estimated that approximately 70% of cholesterol in the brain is contained within the myelin sheath (oligodendrocytes), whilst the rest is contained within the plasma membranes of neurons and astrocytes (Björkhem and Meaney, 2004).

1.2.1 Cholesterol homeostasis within the brain

Cholesterol production and disposal in the human body is reliant upon dietary intake, *de novo* synthesis in each organ, and lipoprotein-mediated transport via the circulation. However, cholesterol cannot cross the blood-brain barrier (BBB), and so excess cholesterol cannot be excreted directly from the brain into the circulation (Björkhem and Meaney, 2004). Maintaining tight cholesterol homeostasis in the brain is highly important for proper function, thus levels of cholesterol must be carefully balanced.

The cellular population of the brain is comprised of neurons and glial cells, which includes astrocytes, microglia and oligodendrocytes. Glial cells provide

structural and logistical support to neurons, allowing them to function and develop correctly. Depending on neuronal cell type and specific brain areas, it has been estimated that turnover in neurons may be as high as 20% (Dietschy and Turley, 2004).

Within the context of adult brain cholesterol homeostasis, astrocytes are though to be majorly responsible for the production of cholesterol (Pfrieger, 2003), which is assembled with ApoE for transport into neurons via the highly expressed ApoE receptor LRP1 (**Figure 1.4**). It is suggested that astrocytes also secrete precursors via lipoproteins, due to the presence of cholesterol precursors including lathosterol and desmosterol within glia-derived lipoproteins (Mutka et al., 2004; Wang et al., 2008). Rodent studies have shown that astrocytes have strong expression of SREBP2, suggesting that they have a primary role in the production of cholesterol (Ferris et al., 2017).

Upon accumulation of cholesterol beyond cellular requirements, cholesterol is eliminated from the brain via several different routes:

1. *Esterification*

Cells can store excess cholesterol as esterified cholesterol, in what are known as lipid droplets. Cholesterol can be esterified by acetyl-CoA acetyltransferase 1 (ACAT1), also referred to as Sterol O-acyltransferase 1 (SOAT1), localised to the ER (Olzmann and Carvalho, 2019). ACAT1 has been found to be expressed in neurons but not observed in astrocytes (Sakashita et al., 2000). A study has demonstrated that ACAT1-mediated cholesterol esterification is inducible in astrocytes following cholesterol loading or removal of APOE (Karten et al.,

2006). Cholesteryl esters are then stored in lipid droplets within intracellular organelles, and this forms ~1% of total cholesterol content.

2. *Direct export*

Cholesterol can be directly exported as part of a complex with apolipoproteins ApoA-I or ApoE (**Figure 1.4**). To export lipoproteins, cells express ATP-binding cassette (ABC) transporters that are able to mediate sterol efflux i.e. ABCA1, ABCG1 and ABCG4 (**Figure 1.4**). ABCA1 has been shown to be expressed in astrocytes as well as both embryonic and adult neurons in rodents (Fukumoto et al., 2002; Koldamova et al., 2003; Tachikawa et al., 2005; Wellington et al., 2002). ApoE is regarded as the most important transport protein for cholesterol within the brain, with astrocytes found to be majorly responsible for its production (Boyles et al., 1985). However, this cholesterol elimination pathway is estimated to be relatively minor and result in the elimination of ~2mg cholesterol/day.

3. *Conversion into 24S-HC*

The most significant elimination pathway of cholesterol from the brain is its conversion to 24S-HC, also referred as “cerebrosterol” (**Figure 1.4**). Cholesterol is hydroxylated at carbon-24 by the CYP P450 enzyme cholesterol 24-hydroxylase (CYP46A1) forming 24S-HC (**Figure 1.3**). Unlike cholesterol, 24S-HC is able to cross lipophilic membranes i.e. the BBB much more readily, due to the presence of the side-chain hydroxyl group. Upon interaction with the membrane phospholipid bilayer, the presence of this hydroxyl group leads to a rearrangement of the phospholipids that results in it being more energetically favourable to expel the sterol. 24S-HC is released into the circulation at a rate of ~6mg per day (Björkhem et al., 1998), with 24S-HC flux from the brain into

the CSF accounting for ~1% of 24S-HC-mediated export from the brain, whilst 99% occurs via diffusion through the BBB (Lütjohann et al., 1996). Once excreted, 24S-HC is eliminated as bile (Björkhem et al., 2001a, 1998).

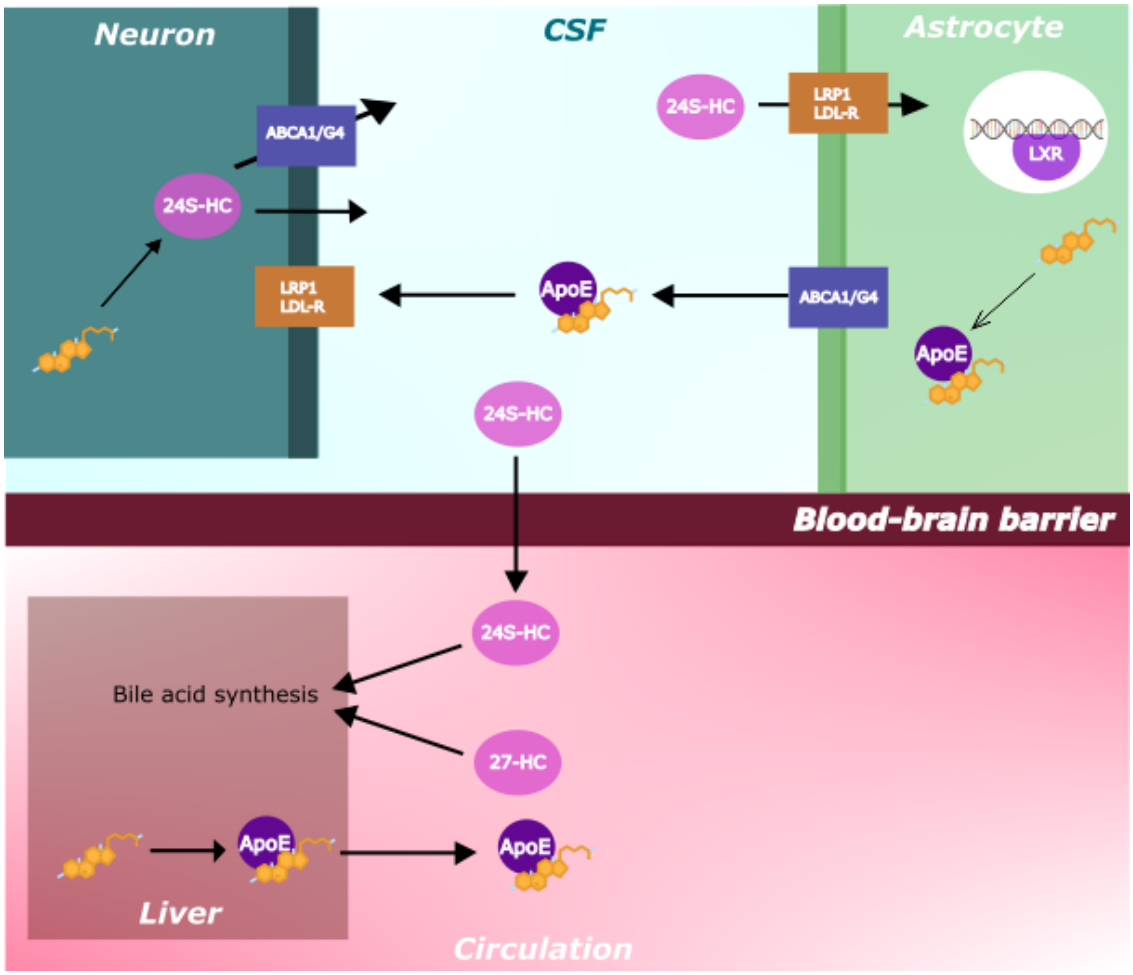

Figure 1.4. Transport of cholesterol and oxysterols between neurons and astrocytes and cholesterol homeostasis across the blood-brain barrier (BBB). ApoE: Apolipoprotein E, CSF: Cerebral spinal fluid.

Due to an efficient recycling system, the rate of cholesterol synthesis in the adult human brain is relatively low, with cholesterol having a long half-life of approximately 5 years (Björkhem et al., 1998). However, the rate of cholesterol synthesis during development is much higher than that of the adult brain. Whilst astrocytes are demonstrated to have a key role in the production of cholesterol, neurons are essential to its catabolism. Interestingly, there has been a noted cell-specific distribution of proteins involved in the metabolism of cholesterol (**Figure 1.4**). For example, CYP46A1 expression has so far only been demonstrated in neurons not astrocytes, with exception to abnormal expression in models of disease and brain injury (Brown et al., 2004; Cataldi et al., 2023; Smiljanic et al., 2010).

1.2.2 Function of cholesterol in neuronal processes

Cholesterol has a key role in neuronal physiology, forming a major component of cell membranes and as a precursor of steroid hormones, cholesterol plays a role in the regulation of ion permeability, cellular organisation, cell-to-cell interaction and transmembrane signaling (Martín et al., 2014). The majority of cholesterol present in the brain is contained within myelin membranes, with cholesterol forming an essential component of myelin, and its depletion in myelin has major consequences for brain maturation.

Cholesterol is enriched in synapses, and is essential in shaping the structure, strength and functioning of synapses. Glial-derived cholesterol has been demonstrated to be essential for the formation of synapses during the developmental stage (Mauch et al., 2001). Astrocyte-derived ApoE-cholesterol

complexes are shown to promote the formation, maturation and maintenance of synapses in vitro (Mauch et al., 2001).

The importance of cholesterol in learning and memory processes in the brain has been highlighted by various studies. Dysregulation of cholesterol homeostasis has been shown to have an impact on synaptic transmission, with altered cholesterol levels impacting synaptic vesicle release at the presynaptic membrane and postsynaptic responses via neurotransmitter receptors reliant on membrane compartmentalisation and membrane-bound signalling (Pfrieger, 2003). Depletion of cholesterol by methyl-β-cyclodextrin (MβCD)-sequestion has been shown to reduce EPSCs and impair glutamate uptake and release in rodent neurons (Krysanova et al., 2007).

1.3 Oxysterols in the brain

1.3.1 Evidence of oxysterols presence in the adult brain

Multiple studies have carried out profiling of the oxysterols present in adult brain tissue. The most well-studied oxysterol present in the brain is 24S-HC which, as outlined previously in this chapter, acts as a transport form of cholesterol and is synthesised by the enzyme CYP46A1. 24S-HC has been termed “cerebrosterol” due to its high concentration in the adult brain compared to other oxysterols. The brain contains around 80% of the body’s total 24S-HC (Björkhem et al., 1998). Circulating levels of 24S-HC in plasma are relatively low (approximately 50ng/mg of cholesterol) in adults, however this is found to be up to 5-fold higher in children (Lütjohann et al., 1996).

Immunohistochemical data has localised CYP46A1 expression to specific neuronal subtypes, including cortical pyramidal cells, Purkinje cells, hippocampal and thalamic neurons (Lund et al., 1999). The neuronal subtype-specific expression of CYP46A1 implies a specific role of 24S-HC in these cells. Whilst CYP46A1 is not widely expressed by glia, studies have noted CYP46A1 expression in astrocytes and microglia, with most evidence for this expression seen in circumstances of disease and brain injury (Brown et al., 2004; Cataldi et al., 2023; Smiljanic et al., 2010), however it is unknown what the significance is of this atypical expression. Thus, neurons are thought to be the primary site of 24S-HC production in the brain.

Analysis of the spatial distribution of sterols, oxysterols and cholestenoic acids in the mouse brain have revealed distinct expression of various sterols within certain brain regions (Yutuc et al., 2020). This study confirmed 24S-HC to be most abundant in the striatum and thalamus, with the lowest levels observed in the cerebellum (Yutuc et al., 2020). Importantly, there is evidenced to be high *Cyp46a1* expression in the striatum and thalamus, with low levels of expression observed in the cerebellum (Yutuc et al., 2020). This comparison of *Cyp46a1* expression and localisation of 24S-HC production in the mouse brain suggests that 24S-HC is not rapidly transported in the brain following its formation.

Whilst 24S-HC is by far the most abundant oxysterol identified in the adult mouse brain, using Cyp46a1-/- mice, featuring deletion of Cyp46a1 and therefore abolished synthesis of 24S-HC, it has been possible to identify isomers and other minor oxysterols present in the mouse brain. Yutuc et al. (2020) were able to identify the epimer of 24S-HC, 24R-HC, which interestingly

was noted to be highly expressed in the cerebellum. Other isomers detected included 12α-HC, 25-HC, 7-OC and 20S-HC (Yutuc et al., 2020). However, when measuring oxysterol content, it is important to consider whether the oxysterol is enzymatically formed or produced from free radical autooxidation. For example, 7-OC is found at low levels ubiquitously in the brain, however the enzyme CYP7A1 which is responsible for 7-OC formation from 7-DHC is not expressed in the brain. Thus, the presence of this oxysterol is likely from either free radical mediation oxidation from cholesterol or via its import across the BBB.

Analysis of CYP enzyme expression in the brain provides an indication of the sterols produced in each region, however as there are shared enzymes responsible for the production of various sterols it is difficult to determine exactly which sterols are produced from enzyme expression alone. Thus, accurate measurements of the sterol content of each region are required.

1.3.2 Role of oxysterols in regulation of cholesterol biosynthesis

Sterols and oxysterols are involved in the regulation of cholesterol biosynthesis through interaction with SCAP and INSIG, and through SREBP2-modulated expression of enzymes within the cholesterol biosynthetic pathway (Radhakrishnan et al., 2020). Various oxysterols are thought to be more involved in the “fine-tuning” of the regulation of cholesterol biosynthesis (Gill, et al. 2008). Side chain oxysterols, including 22R-HC, 24S-HC and 24S,25-EC are demonstrated to bind INSIG and tether the SCAP-SREBP2 complex in the ER (Radhakrishnan et al., 2007). SREBP2 is known as the master regulator of

cholesterol biosynthesis and regulate transcription of many cholesterol-related genes including those encoding key enzymes involved in cholesterol biosynthesis.

1.3.3 Presence of oxysterols in the developing brain

In the developing brain, evidence from the embryonic mouse brain has suggested that 24S-HC is not the predominant oxysterol present, with evidence from embryonic day 11 (E11) demonstrating 24S,25-EC to be present at levels ~0.165µg/g in cortical tissue extracts, compared to 24S-HC which is present at ~0.026µg/g (Wang et al., 2009). At E11, levels of cholesterol are also lower, at ~1mg/g tissue compared to ~20mg/g tissue in the adult mouse (Wang et al., 2009). However, the rate of cholesterol biosynthesis is indicated to be higher, due to increase ratios of the cholesterol precursors desmosterol and lathosterol compared to the adult mouse CNS (Wang et al., 2009). As 24S,25-EC is not formed directly from cholesterol but rather in parallel in a shunt pathway from mevalonate, this may indicate high level of activity of the mevalonate pathway. With formation of the BBB at E11, it is of interest to assess whether these sterols are being formed *in situ*, or if they are being taken up by the circulation.

1.4 Oxysterols as bioactive signalling molecules: role in modulation of cellular processes and signalling involved in development

Several oxysterols are demonstrated to act as biologically active signalling molecules. Specific oxysterol isomers are biologically active, for example 24(S)-

HC and 25-HC are both suppressors of cholesterol synthesis and enhance cholesterol export, whereas 7α-hydroxycholesterol and 7-oxocholesterol weakly suppress cholesterol synthesis, and are not LXR ligands (Lehmann et al., 1997). Therefore, the specific chemical structure of these molecules is essential to their biological activity.

1.4.1. Hedgehog signalling pathway

The Hedgehog (Hh) signalling pathway is a key signalling pathway involved in embryonic development and is essential in neural developmental patterning (Ingham and McMahon, 2001). There are 3 identified mammalian Hh ligands, with the ligand involved in human neural development known as Sonic Hedgehog (Shh) (Choudhry et al., 2014). During neural development, Shh is crucial in regulation of the dorsal-ventral patterning of the neural tube (Fuccillo et al., 2004). Aberrant Hh signalling is shown to cause neural developmental defects including holoprosencephaly and other congenital malformations (Nieuwenhuis and Hui, 2005).

Hh signalling is a complex signalling cascade occurring in a specialised region of the cell membrane known as the primary cilia (Choudhry et al., 2014). The secreted Shh ligand is cleaved and dual lipid-modified (Porter et al., 1996) by cholesterol at its N-terminus (Lee et al., 1994) and palmitic acid to the exposed N-terminal cysteine following the protein's cleavage (Pepinsky et al., 1998). The dual lipid-modified Shh is an active signalling molecule, and binds the receptor Patched-1 (PTCH1) (Choudhry et al., 2014). In the absence of Shh, PTCH1 inhibits the transmembrane protein Smoothened (Smo), a G-protein coupled receptor. Upon binding of Shh to PTCH1, the receptor is internalised, relieving

inhibition of Smo and activating downstream signalling that leads to transcription of Hh target genes (Choudhry et al., 2014). The precise mechanism of PTCH1-mediated inhibition of Smo remains unclear, but it may involve regulation of small-molecule agonists that control Smo activity (Sharpe et al., 2015).

Multiple studies attempting to identify this endogenous Smo ligand have determined that the most probable candidate to be a sterol, with both cholesterol and oxysterols shown to both directly bind Smo and induce Hh signalling (Corcoran and Scott, 2006; Deshpande et al., 2019; Dwyer et al., 2007; Luchetti et al., 2016; Myers et al., 2013; Nachtergaele et al., 2013; Nedelcu et al., 2013; Raleigh et al., 2018; Sharpe et al., 2015). There are two "sterol-binding" sites that have been identified in the structure of Smo (**Figure 1.5**), one located in the cysteine-rich domain (CRD) and at least one in the transmembrane domains (TMD) (Byrne et al., 2016; Deshpande et al., 2019; Huang et al., 2016; Luchetti et al., 2016; Qi et al., 2019).

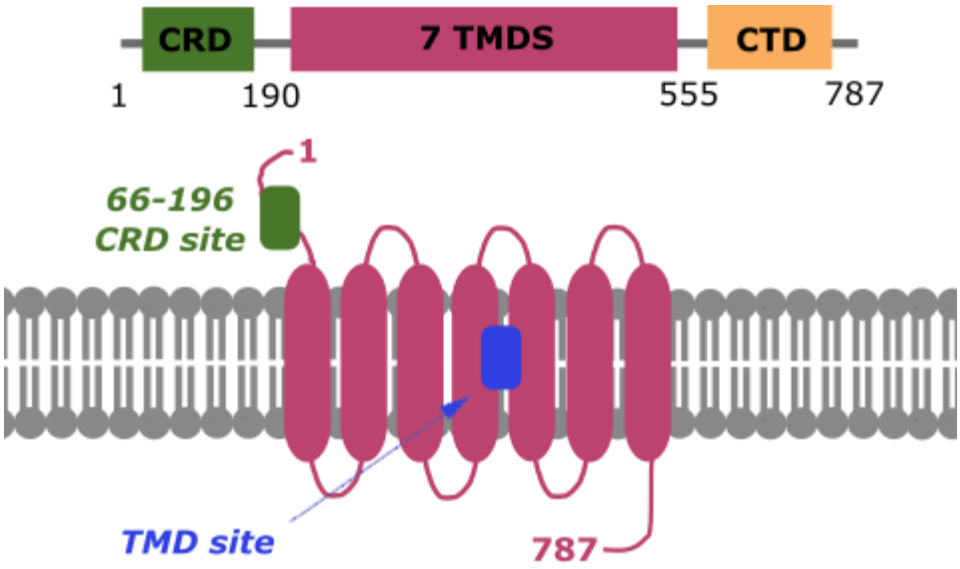

Figure 1.5. Simplified structure of Smoothened (Smo), demonstrating the 2 "sterol-binding" sites identified by recent structural studies. Smo is a 787 amino acid G-protein coupled receptor and member of the Frizzled (Fz) family of 7 transmembrane proteins. Structural studies have identified sites in the cysteine-rich domain (CRD site) and within the transmembrane domain (TMD site).

Multiple studies have demonstrated oxysterols, albeit mostly synthetically, regulate Smo activity, with multiple oxysterols demonstrated to bind directly to Smo and both activate and inhibit its activity, even in absence of Shh (**Table 1.1**). Importantly, some oxysterols are demonstrated to induce the accumulation of Smo in primary cilia, a key step in Hh signalling (Nachtergaele et al., 2013).

Table 1.1. Evidence for oxysterol interaction with Hedgehog signalling pathway

Oxysterol	Effect on Hh signalling	Present endogenously OR synthetic?	Reference(s)
7-keto-C	Present in primary cilia Does **not** activate Hh signalling	Endogenous	(Raleigh et al., 2018) (Dwyer *et al.,* 2007)
24,25-EC	Present in cilia Binds Smo in cytoplasmic binding pocket (CBP) within the TMD Activates Hh signalling	Endogenous	(Raleigh et al., 2018)
7β,27-diHC	Present in cilia Binds Smo CRD Activates Hh signalling	Endogenous	(Raleigh et al., 2018)
24-keto-C	Present in cilia Binds SMO CBP Activates Hh signalling	Endogenous	(Raleigh et al., 2018) (Qi et al 2019)

24S-HC	Smo agonist	Endogenous + Synthetic	Qi et al (2019)
20(S)-HC	Smo agonist	Synthetic	(Myers et al., 2013)
		Synthetic	(Nachtergaele et al., 2013, 2012)
		Synthetic	(Kim et al., 2007)
		Synthetic (20-OHC beads)	(Nedelcu et al., 2013)
		Synthetic	(Huang et al., 2016)
7-Keto-27-HC	Smo agonist	Exogenous (Naturally occurring oxysterol added exogenously)	(Myers et al., 2013)
	Induces Gli1 expression	Exogenous stimulation of NIH/3T3 cells with oxysterols	(Abdel-Khalik et al., 2021)
7-keto-25-HC	Smo agonist	Exogenous	(Myers et al., 2013)

	Induces Gli1 expression	Exogenous stimulation of NIH/3T3 cells with oxysterols	(Abdel-Khalik et al., 2021)
7α-27-diHC	Minimal activation of Hh signalling No known action on Smo	Exogenous	(Myers et al., 2013)
7α-27-dihydroxycholestenone	Minimal activation of Hh signalling No known action on Smo	Exogenous	(Myers et al., 2013)
25-HC	Activates Hh signalling	Synthetic	(Corcoran and Scott, 2006)
7β-HC	No known effect on Hh signalling	Synthetic	(Corcoran and Scott, 2006)
19-HC	No known effect on Hh signalling	Synthetic	(Corcoran and Scott, 2006)
22(S)-HC	Smo agonist	Synthetic	(Dwyer et al., 2007) (Corcoran and Scott, 2006)
22R-HC	Smo agonist	Synthetic	(Dwyer et al., 2007)
7α-HC	No effect on Hh signalling	Synthetic	(Dwyer et al., 2007)

B-ring oxysterol: 3β,5α-dihydroxycholest-7-en-6-one (DHCEO)	Inhibits Smo Blocks Hh signalling	Exogenous addition of naturally occurring B ring oxysterol	(Sever et al., 2016)
7β,26-diHC	Induces *GLI1* expression	Exogenous stimulation of NIH/3T3 cells with oxysterols	(Abdel-Khalik et al., 2021)
7β,25-diHC	Induces *GLI1* expression		
3βH,7O-CA	Induces *GLI1* expression		
3β,7β-diHCA	Induces *GLI1* expression		

1.4.2. LXR signalling pathway

Liver X receptors (LXRs) are ligand-dependent transcription factors, part of the nuclear hormone receptor family, and are obligate heterodimeric partners of the retinoid X receptors (RXRs) (**Figure 1.6**). Upon discovery in the 1990s, LXRβ was initially referred to as OR-1 (Teboul et al., 1995). OR-1 was found to be homologous to LXR and so both were termed LXR with the following isoforms: LXRα and LXRβ, encoded by *NR1H3* and *NR1H2* respectively, with a 78% similarity between their ligand binding domains (Alberti et al., 2000). Initially described as orphan receptors, *in vitro* studies since revealed the endogenous ligands of these receptors to be oxysterols (Lehmann et al., 1997).

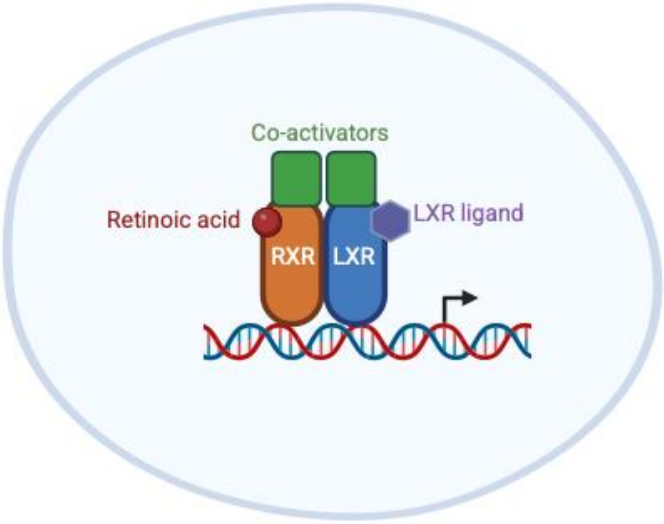

Figure 1.6. Liver X receptor (LXR) structure.

Ligand binding of LXRs appears to be structurally specific, with evidence that the oxysterols 24S,25-EC and 24S-HC are potent activators of both LXRα and LXRβ but not 7α-hydroxycholesterol or its bile acid derivatives (Lehmann et al.,

1997). Importantly, LXRs were shown to be activated by these oxysterols at concentrations consistent with that at which they are measured in human tissues (Lehmann et al., 1997).

The most well-described function of LXRs is in the regulation of lipid metabolism and homeostasis, through the modulation of cholesterol efflux across the cell membrane and maintaining cholesterol levels below that of toxicity . LXR target genes include ABCA1 and ABCG1, ATP-binding cassette proteins involved in cholesterol efflux from cells. The sterol transcription factor SREBP1-c is also a LXR target, however oxysterol-induced activation of SREBP1-c is counteracted by oxysterol binding to INSIG, suppressing SREBP1-c activation.

LXRβ is expressed in the brain, immune system and gut epithelium. In the brain, LXRβ shown to be highly expressed in cortex after embryonic day 14.5 (E14.5) (Fan et al., 2008). Recently, a role for LXRβ in neural development has been demonstrated, with expression of LXRβ shown to be essential in cortical patterning and the migration of late-born cortical neurons (Fan et al., 2008). The oxysterol 24S,25-EC has been identified as the most potent LXRβ ligand in the developing mouse brain (Theofilopoulos et al., 2013). Interestingly, it has been demonstrated that 24S,25-EC enhances midbrain dopaminergic neurogenesis and has been shown to promote the dopaminergic differentiation of embryonic stem cells *in vitro* (Theofilopoulos et al., 2013).

1.4.3. Wnt signalling pathway

The Wnt/β-catenin signalling pathway involves a family of proteins that are critically involved in embryonic development (Logan and Nusse, 2004). Wnt

signalling is comprised of canonical and noncanonical pathways. The canonical pathway, also known as the Wnt/β-catenin signalling pathway, is highly conserved and features the degradation or nuclear translocation of β-catenin and subsequent activation of target genes through the TCF/LEF transcription factors. In canonical Wnt signalling, Wnt ligands bind the cell-surface G-protein coupled receptor Frizzled (FZD) and low-density lipoprotein receptor-related protein 5/6 (LRP5/6), resulting in the recruitment of Dishevelled (DVL) and Axin to the FZD-Wnt-LRP5/6 complex. Upon activation by the binding of extracellular Wnt ligands, activation of membrane receptors induces stabilisation of β-catenin and subsequent translocation into the nucleus and induced expression of genes involved in cellular proliferation, survival, differentiation and migration. The canonical Wnt pathway is involved in control of cellular proliferation, whilst the noncanonical Wnt pathways are involved in regulating cell polarity and migration and is independent of β-catenin/TCF/LEF. Importantly, these two pathways are mutually regulated (Liu et al., 2022).

In mammals there are so far 19 Wnt genes identified, with several shown to be expressed with specific spatiotemporal expression during cortical development, including Wnt7a, Wnt7b, Wnt2b and Wnt8b (Fougerousse et al., 2000; Grove et al., 1998; Kim et al., 2001; Lee et al., 2000). It has been demonstrated that the activation of the canonical Wnt pathway is important for neuronal differentiation of neocortical neural progenitor cells *in vitro* (Hirabayashi et al., 2004).

Similarly to Hedgehog signalling, where the hedgehog protein is palmitoylated, posttranslational lipid modification is also necessary for Wnt activity (Willert et al., 2003). The Wnt3a protein is palmitoylated on a conserved cysteine by

PORCN, a member of the membrane-bound O-acyltransferases (MBOATs) located in the endoplasmic reticulum, and removal of the palmitoleate group at this site results in loss of Wnt activity (Willert et al., 2003). However, the opposite effect is observed for the glycosylation of the Wnt protein, which is shown to result in loss of activity (Willert et al., 2003).

Furthermore, cholesterol has been shown to selectively activate the canonical Wnt pathway, by playing an essential role in the recruitment of the PDZ domain of the DVL protein to the membrane (Sheng et al., 2014). It has been proposed that local cholesterol enrichment in the membrane surrounding the canonical Wnt signalling complex results in selective activation of canonical Wnt signalling over non-canonical signalling (Sheng et al., 2014).

Defects in Wnt/β-catenin signalling have been implicated in Smith-Lemli-Opitz syndrome (SLOS), a malformation disorder characterised by cognitive impairment, behavioural problems and neurodevelopmental defects (Francis et al., 2016). SLOS is caused by a mutation in the gene encoding the DHCR7 enzyme responsible for formation of cholesterol from 7-dehydrocholesterol (7-DHC), resulting in a deficiency of DHCR7 resulting in an accumulation of 7-DHC. It's been demonstrated in an iPSC model of SLOS that direct inhibitory effects of the 7-DHC on formation of the active Wnt receptor complex is responsible for downregulation of Wnt/β-catenin signalling resulting in neuronal differentiation defects (Francis et al., 2016).

1.4.4. NMDA receptors

N-methyl D-aspartate receptors (NMDARs) are ligand-gated cation channels activated by the excitatory neurotransmitter glutamate and are involved in excitatory synaptic function. 24S-HC has been demonstrated to be a positive allosteric modulator of the NMDAR and interacts with NMDARs at a distinct site from other positive allosteric modulators (Paul et al., 2013). 24S-HC is shown to enhance long-term potentiation and potentiate NMDAR-mediated EPSCs at sub-micromolar concentrations in rat hippocampal neurons (Paul et al., 2013). A key finding is that this effect is independent of nuclear receptors i.e. LXRs, as 24S-HC does not alter membrane currents in the absence of NMDA (Paul et al., 2013).

1.5. Evidence associating dysregulated cholesterol metabolism and neural developmental defects

Neurodevelopmental disorders (NDDs) are common psychiatric conditions thought to arise during early brain development and share a common genetic aetiology. There have been major advances in recent years in uncovering the genetic basis of these disorders, with high throughput screening and genetic studies associating specific mutations with the development of brain structural malformations and NDDs. Increasingly, it is being recognised that altered cholesterol metabolism may contribute toward development of these neurodevelopmental disorders. Cholesterol is essential for embryonic development (Tozawa et al., 1999), and inborn errors of cholesterol metabolism, including Smith-Lemli-Opitz syndrome (SLOS), mevalonate kinase deficiency and desmosterolosis, are all associated with various developmental defects. Both cholesterol and its immediate oxidised metabolites in the bile acid synthesis pathway, known as oxysterols, are identified to be bioactive signalling molecules and are demonstrated to have a role in key signalling pathways involved in neural development.

Cholesterol is implicated in many essential processes in the developing nervous system, including myelin formation, membrane lipid rafts, neurosteroid formation and Hedgehog signalling (Griffiths and Wang, 2021; Wang et al., 2021). Alterations to these key processes have been linked to neurodevelopmental defects, with altered cholesterol biosynthesis and metabolism associated with the development of several NDDs (**Table 1.2**).

Table 1.2. Evidence of altered serum and plasma levels of cholesterol and derivatives in neural developmental disorders.

Disorder	Evidence	Study design	Reference
Autism Spectrum Disorder (ASD)	~20% of children with an ASD presented with hypocholesterolaemia i.e. lower than 100mg/dL	Analysis of 100 serum samples taken from the Autism Genetic Resource Exchange	(Tierney et al., 2021)
	↑ 24S-HC levels in plasma	Oxysterol profiling of plasma samples from 36 children with Autism Spectrum Disorders and 38 healthy children, matched for age and sex	(Grayaa et al., 2018)
	↓ 27-HC levels in children with ASD	Lipid profiling of a cohort of 107 children with ASD and 103 control children aged 2-18 years old.	(Menteşe Babayiğit et al., 2024)

	↑ total cholesterol, LDL and triglyceride levels in ASD children.	Lipid panel generated on a Beckman Coulter 5800, oxysterol analysis performed by LC-MS/MS.	
Fragile X syndrome (FXS)	↓ serum cholesterol content	*Fmr1-Δexon 8* rat model of FXS	(Parente et al., 2022)
	↓ serum cholesterol content	Analysis of FXS patient serum samples	(Çaku et al., 2017; Lisik et al., 2016)
Smith-Lemli Opitz syndrome (SLOS)	↓ 24S-HC plasma levels ↑ 27-HC plasma levels	Plasma levels of six infants with SLOS were measured and compared to 59 control infants aged 1-15 years old	(Björkhem et al., 2001b)

1.5.1 Smith-Lemli-Opitz Syndrome (SLOS)

Smith-Lemli-Opitz syndrome (SLOS) is an autosomal recessive malformation syndrome caused by mutations in the gene encoding the enzyme 7-dehydrocholesterol reductase (DHCR7) located on chromosome 11q12-13. This results in a disruption of the final enzymatic step in cholesterol biosynthesis, with reduced conversion of the cholesterol precursor 7-DHC to cholesterol. As a result, SLOS symptoms include intellectual disability and behavioural disorders as well as physical abnormalities include microencephaly and a variety of anatomical defects (DeBarber et al., 2011; Kelley and Hennekam, 2000). SLOS is also associated with ASD in approximately 50-75% of cases, however the mechanism behind this link is not well understood. Individuals with SLOS are documented to have elevated plasma levels of the cholesterol precursor 7-DHC and its isomer 8-DHC, and a reduction in total serum cholesterol levels. However, due to disrupted cholesterol biosynthesis, the production of other sterols is further affected. This includes an approximately 50% reduction in the levels of 24S-HC observed in infants with SLOS (Björkhem et al., 2001b). Additionally, the levels of 27-HC are shown to be increased in the periphery (Björkhem et al., 2001b). It is hypothesised that the accumulation of 7-DHC rather than depletion of cholesterol may be responsible for the pathophysiology of SLOS, with 7-DHC itself or its oxidised derivatives may be biologically active and play a role in SLOS pathology. Indeed, 7-DHC-derived oxysterols have been demonstrated to reduce cell viability of the neuroblastoma Neuro2a cell line in a dose-dependent manner (Korade et al., 2010). However the exact mechanism behind the pathological effect of these sterols is not fully understood.

1.5.2. Fragile X Syndrome (FXS)

Fragile X syndrome (FXS) is an X-linked neurodevelopmental disorder, and is the most frequent form of X-linked pathology and first monogenic cause of ASD (Hagerman and Hagerman, 2021). FXS is caused by a mutation in the *FMR1* gene (Hagerman and Hagerman, 2021). Altered cholesterol synthesis has been associated with FXS, with FXS patients demonstrated to have low levels of total serum cholesterol compared to unaffected controls (Çaku et al., 2017; Lisik et al., 2016). A preclinical study of a FXS rat model was found to mimic the lower serum cholesterol content seen in humans, as well as further revealing alterations to key enzymes involved in the mevalonate pathway of cholesterol biosynthesis (Parente et al., 2022).

1.5.3. Autism Spectrum Disorders (ASDs)

Autism spectrum disorders (ASDs) are a group of NDDs that include a wide spectrum of disorders that feature various symptoms including difficulties in social communication and interaction, nonverbal communication and impaired speech, and restrictive repetitive patterns of behaviour and interests (Bauman, 2010). These symptoms are a result of altered neural development, yet the full extent of the underlying mechanisms contributing to the pathogenesis of ASDs remains unknown. Dysregulated cholesterol homeostasis has been associated with the pathogenesis of ASDs, including its observed comorbidity in cases of inborn errors of cholesterol metabolism including SLOS.

Analysis of 100 serum samples taken from the Autism Genetic Resource Exchange found that ~20% of children with an ASD presented with

hypocholesterolaemia i.e. lower than 100mg/dL (Tierney et al., 2006). It has been hypothesised that altered cholesterol metabolism results in ASDs via 3 core mechanisms during neural development, potentially working together to contribute to the development of ASD: impaired Shh signal patterning, altered membrane lipid raft structure impacting synaptic activity and impaired neurosteroid synthesis (Tierney et al., 2006).

A recent study profiling oxysterol levels in plasma samples taken from individuals with ASD has demonstrated altered oxysterol profiles, with significantly higher levels of the oxysterol 24S-HC compared to control individuals (Grayaa et al., 2018). It has been proposed that 24S-HC could be used as a potential biomarker for ASD diagnosis, however further research would be required to confirm this relationship between altered 24S-HC and the mechanisms underlying the development of an ASD. GC-MS analysis has also revealed significantly higher concentrations in other oxysterols, including 27-HC, 7α-HC, 7β-HC and 7-keto-C (Grayaa et al., 2018). However, further work is needed to determine how these changes in sterol profiles relates to the pathophysiology of ASDs.

With the increasing wealth of evidence linking dysregulated cholesterol metabolism with disorders featuring neurodevelopmental defects, a need to further understand how these molecules potentially contribute to neural developmental processes is required.

1.6 Human cortical development

The cerebral cortex is responsible for mediation of higher cognitive functions, the processing of sensory information and personality, and thus is of interest in the context of psychiatric disorders. Development of the human cerebral cortex is a highly regulated and complex process, and dysregulation of this tightly controlled process is shown to result in a variety of neurodevelopmental conditions. The cerebral cortex contains around 80% of the total brain mass and diversity of neuronal subtypes (Cadwell et al., 2019). Of this, the most abundant subtype of neurons are the excitatory pyramidal neurons which represent around 85% of cells in the cerebral cortex (Marín and Müller, 2014).

Most of current understanding of cortical development has been established largely through structural, cellular and molecular studies of the neocortical development of rodent models. Whilst the mouse and rat brain closely recapitulate human cortical development, there are limitations in the extrapolation of findings in these models to that of the human cortex. For instance, in terms of structure, the rodent cortex is unfolded and approximately 1000 times smaller than that of the human (Loomba et al., 2022). Furthermore, in terms of developmental time periods, whilst the process of human cortical neurogenesis takes months, in the mouse this process takes a mere 7 days (Angevine and Sidman, 1961; Rakic, 1974).

With the inherent limitations of the use of rodent models to study human cortical development, recent advances in stem-cell technology have allowed for the modelling of human cortical development *in vitro*. Various protocols have been

developed recapitulating developmental processes and enabled the production and validation of cortical cells. Furthermore, advances in molecular profiling at a single-cell resolution has provided increasing information on the genes and regulatory pathways underlying these developmental processes.

1.6.1. Early stages of cortical development

Development of the human brain is a highly complex and regulated process. Following the formation of the neural tube at approximately 3-4 weeks gestation, processes of neurogenesis, cell proliferation and neuronal migration occur, leading to the formation of general brain regions (Villalba et al., 2021). Synaptogenesis and myelination occur at later stages, majority postnatally.

The developing embryo is subdivided into specified regions, the endoderm, mesoderm and ectoderm, through a process known as gastrulation (Villalba et al., 2021). The CNS is derived from the neuroectoderm, and a layer of neural progenitor cells are located in this top layer and form the neural plate. A rod-shaped structure in the mesoderm known as the notochord, plays an important role in neural patterning. Formation of the neural tube, a process known as neurulation, involves formation of ridges in the neural plate and the production of neural crest cells (Villalba et al., 2021). The developing neural tube is populated by neural epithelial cells (NECs), and in the ventricular zone (VZ), also known as the “proliferative zone”, this pool of neural epithelial cells form radial glial cells (RGCs) at the onset of neurogenesis (Cadwell et al., 2019).

Cerebral cortex development begins following formation of the telencephalic vesicles and the specification of sub-regions. The primary brain vesicles are known as the anterior prosencephalon, the middle mesencephalon and the posterior rhombencephalon . These regions are further specified into 5 brain vesicles, with the prosencephalon subdividing into the telencephalon (precursor to the cerebral regions) and diencephalon (precursor to the thalamus and hypothalamus). The

rhombencephalon further subdivides into the metencephalon (precursor to pons and cerebellum) and myelencephalon (precursor to medulla).

In the developing telencephalon, the cortical primordium is formed of a monolayer of NECs (Bishop et al., 2000; Sur and Rubenstein, 2005). NECs are highly polarised cells, with two thin processes extending from the soma in the radial direction, one contacting the apical surface of the neuroepithelium (apical process) and one contacting the basal lamina (basal process) (**Figure 1.7**). NECs are associated at the apical surface via adherent and tight junctions. NECs self-proliferate, producing two NECs from each cellular division. After completing several cell division and amplification events, NECs lose apical tight junctions whilst retaining adherent junctions and become apical radial glial cells (aRGCs), marking the onset of cortical neurogenesis. aRGCs are the primary cortical progenitor cells, expressing Paired-box transcription factor 6 (PAX6) and are the precursor cells for all excitatory cortical neurons (Wong et al., 2015). At the onset of neurogenesis, aRGCs mostly self-renew, producing two aRGC daughter cells, with some production of neurons. As neurogenesis proceeds, this switches to the increased production of secondary progenitor cells and neurons.

The human cerebral cortex is highly organised into six layers, defined as cortical layers I-VI. The formation of these layers during development is highly regulated and formed in an “inside-out” gradient, with the deeper cortical layers i.e. layer VI formed first (**Figure 1.7**). The cortex is subdivided into areas with specialized functions, including the somatosensory, visual and motor cortical areas. Despite the different functions of these subregions of the cortex, they all share the same basic structural organisation, described as a columnar structure with a specific laminar appearance due to the arrangement of diverse subtypes of excitatory projection neurons and inhibitory interneurons into well-defined cell layers (Marín and Müller, 2014)

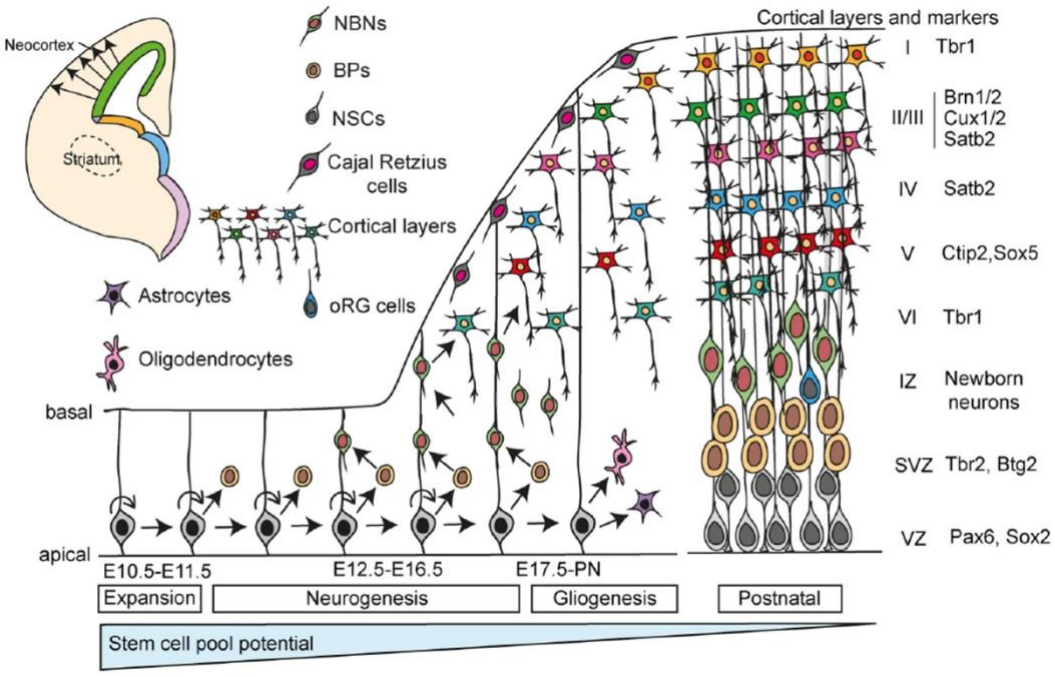

Figure 1.7. Migration pattern of neocortical projection neurons. Neuroepithelial cells give rise to radial glial cells, which divide and produce glutamatergic neurons. Radial glia proliferate to produce intermediate progenitors, through several rounds of differentiation before producing neurons. NBNs: Newborn Neurons; NSCs: Neural stem cells; BPs; Basal Progenitors; oRG cells: outer radial glia cells; SVZ: Subventricular Zone; VZ: Ventricular Zone; IZ: intermediate zone. Figure from (Mukhtar and Taylor, 2018).

1.6.2. Altered cortical development

Corticogenesis is a complex highly-ordered process, and alterations to this tight regulation can massively impact normal brain structure and function, with alterations to cortical development being responsible for several neurological diseases, including neural developmental disorders (NDDs). Cortical malformations include altered brain size including micro- and megalencephaly, and cortical folding including lissencephaly or polymicrogyria (Subramanian et al., 2020). Such malformations are associated with intellectual disability, epilepsy and autism spectrum disorder (ASD) (Barkovich et al., 2012).

One of the best studied NDDs in this regard is ASD, with both syndromic and idiopathic causes of ASD linked to changes in brain size across the developmental time course, from birth to adulthood (Redcay and Courchesne, 2005). Cases of idiopathic ASD have also been noted to feature altered laminar structures in prefrontal and temporal cortex (Stoner et al., 2014) as well as increased neuronal numbers in the prefrontal cortex (Courchesne et al., 2011)..

Corticogenesis is broadly subdivided into 3 overall stages of proliferation, neuronal migration and post-migration organisation, with alterations to any one of these processes leading to cortical malformation. Thus, there is a wide spectrum of developmental disorders that feature various aberrant cortical morphology, genetic or extrinsic etiology and a range of clinical symptoms. The majority of developmental cortical malformations are thought to be due to underlying genetic mutations associated with molecular signalling involved in the stages of cortical development (Barkovich et al., 2012). In recent years, advancements in sequencing technologies and genetic models have developed our understanding of the genes and signalling pathways underlying these malformations. Several mutations have been associated with genes that interact with key mechanisms involved in neuronal proliferation, migration and the differentiation of progenitors into neuronal subtypes. There is increasing evidence that changes in temporal dynamics of developmental processes such as the timing and numbers of defined subtypes of neuron may result in errors in neuronal migration and connectivity, which may contribute to the phenotypes observed in various NDDs (Marchetto et al., 2017; Paulsen et al., 2022).

1.7 15q11.2 Copy Number Variant (CNV): Role of CYFIP1 in altered cortical development

1.7.1 15q11.2 CNV

Copy number variations (CNVs) are defined as molecular events where sequences of the genome are repeated, with the number of repeats varying between individuals. CNVs can occur in the form of insertions, deletions or duplications of segments of DNA, and range from approximately 50 base pairs up to several megabases (Mb) in size (Gordeeva et al., 2022; Malhotra and Sebat, 2012). CNVs can occur either as inherited or *de novo* events. Biological effects of CNVs can range widely, from no effect on biological variability to having a substantial contribution to defined genetic disorders/syndromes.

Microdeletions and duplications of the proximal region of the long arm of chromosome 15 have been associated with the development of neuropsychiatric disorders and have been identified as a high penetrant risk CNV for both autism spectrum disorders and schizophrenia (Cox and Butler, 2015). This chromosomal region contains 5 breakpoints (BP1-5), with BP1-2 located on the proximal end of the 15q11-q13 regions whilst BP3-5 are located more distally. Combinations of these regions can be affected by various deletions and duplications (**Figure 1.8**). Multiple loci in the 15q11-q13 region are subject to genomic imprinting, whereby the expression of the gene is dependent on the parental origin of the allele. Genomic imprinting in mammals involves methylation of specific alleles inherited by a parent leading to silencing of the allele and the non-equivalence of the maternal and paternal genomes (Ferguson-Smith, 2011). Two syndromes are associated with genomic imprinting within the 15q11-13 region, with deletion of the paternal chromosome linked to Prader-Willi syndrome and deletion of the maternal chromosome linked to Angelman syndrome (Butler, 2017). These two syndromes are clinically different, and are typically classified as type I deletions involving a 6.6Mb deletion of the region involving BP1 and BP3; or type II deletions involving a 5.3Mb deletion within BP2 and BP3. Individuals with type I deletion typically have

more severe learning and behavioural problems compared to those with the smaller type II deletion, indicating the importance of genes present within this region in neurodevelopmental processes.

CNVs of this 15q11.2 region have been estimated to affect around 0.3-1% of those who undergo genetic screening, making it one of the most common CNVs documented (Sønderby et al., 2021). The CNV in this region has been shown to be associated with cognitive and neurological problems (Cox and Butler, 2015), with patients featuring the 15q11.2 deletion having been reported to exhibit structural differences including a smaller brain surface area, increased cortical thickness and reduced size of the nucleus accumbens (Sønderby et al., 2021). Interestingly, not all patients affected by this CNV appear to be clinically affected, and CNV results in a broad severity of symptoms.

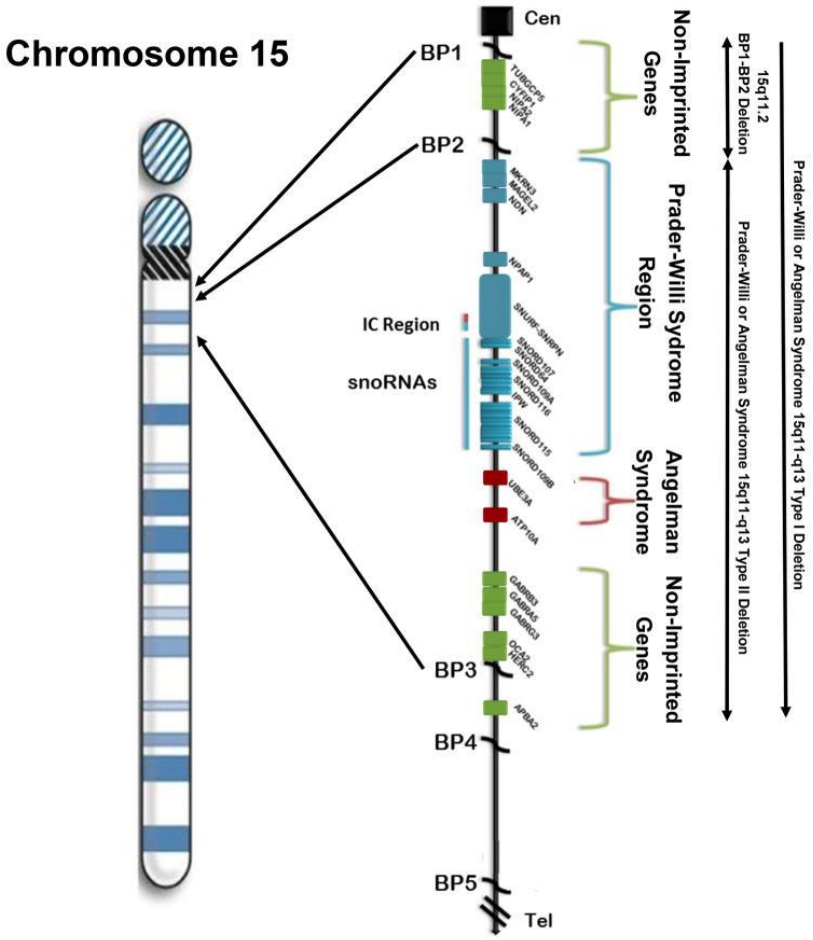

Figure 1.8. Ideogram of 15q11-q13 region of the chromosome. The five chromosome breakpoints (BPs) are shown and the locations of three recognised 15q deletions, including 15q11.2 BP1-BP2. Non-imprinted genes are shown in green, genes expressed from the paternal allele (Prader-Willi Syndrome critical region) shown in blue and genes expressed only from the maternal allele (Angelman Syndrome critical region) shown in red. Figure taken from Butler (2017).

1.7.2. 15q11.2 BP1-BP2 microdeletion

The 15q11.2 BP1-BP2 region is a 500kb region located between the breakpoints BP1 and BP2 on the chromosome, and encompasses 4 non-imprinted protein-coding genes; Cytoplasmic fragile X mental retardation 1 FMR1 interacting protein 1 (*CYFIP1)*, Non-imprinted in Prader-Willi/Angelman syndrome 1 (*NIPA1)*, *NIPA2* and Tubulin gamma complex associated protein 5 (*TUBGCP5)* (**Figure 1.8**). All four genes are highly conserved, and when affected individually each of these

genes are known to be implicated in neurological, cognitive and behavioural symptoms.

NIPA1 is perhaps the most well-studied of these genes, is known to be involved in Mg^{2+} transport and is highly expressed in the developing brain (van der Zwaag et al., 2010). Mutations in this gene cause autosomal dominant hereditary spastic paraplegia and postural disturbance. *NIPA2* encodes a protein involved in renal Mg^{2+} transport. Mutations in NIPA2 are known to result in childhood absence epilepsy (Goytain et al., 2007). *TUBGCP5* has been associated with attention deficit hyperactivity disorder (ADHD) and obsessive compulsive disorder (OCD) (De Wolf et al., 2013). *CYFIP1* encodes a protein which interacts with distinct protein complexes, including FMRP, a protein encoded by the *FMR1* gene and associated with Fragile X syndrome (FXS).

Microdeletion of the 15q11.2 BP1-BP2 region results in a wide range of clinical symptoms, with more than two-thirds of those affected presenting with intellectual disabilities and language delays (Butler, 2017). Other symptoms include neurodevelopmental disorders (ASDs, ataxia, ADD, seizures), psychiatric disorders (schizophrenia) or mild dysmorphism (Butler, 2017). Not all those with this deletion develop clinical symptoms, and the non-penetrant nature of this microdeletion syndrome is not fully understood.

1.7.3 Role of CYFIP1 in cortical development

Of the genes located in the 15q11.2 deletion, cytoplasmic FMR1-interacting protein 1 (*CYFIP1*) has been linked to both ASDs (Noroozi et al., 2018) and schizophrenia (Domínguez-Iturza et al., 2019). Patients with duplication of the 15q11.2 region who also present with an ASD have been specifically demonstrated to have upregulated *CYFIP1* mRNA levels (Nishimura et al., 2007; Oguro-Ando et al., 2015), suggesting this gene may play a role in the neuropsychiatric phenotype observed.

The CYFIP1 protein, previously referred to as p140Sra-1 (Specifically Rac1-associated Protein), has been shown to interact with two distinct protein complexes (**Figure 1.9**) (De Rubeis et al., 2013). CYFIP1 and CYFIP2, which share 88% amino acid sequence identity, both interact with Fragile X mental retardation protein (FMRP) and form a component of the CYFIP1-EIF4E-FMRP complex (Schenck et al., 2001). Unlike CYFIP2 which interacts with other FMRP related proteins FXR1P/2P, CYFIP1 interacts with FMRP only. This complex has been demonstrated to act to repress neuronal protein synthesis (Napoli et al., 2008).

CYFIP1 has further been shown to play a role in the WAVE regulatory complex (WRC), involved in the modulation of cellular actin filament dynamics (Chen et al., 2010). The WRC is a pentameric complex of the following proteins: WAVE1, WAVE2 and WAVE3; CYFIP1 or CYFIP2; Nck-associated protein 1 (NCKAP1) or NCKAP1L; abl interactor 1 (ABI1) or ABI2 or ABI3: and hemopoietic stem progenitor cell 300 (HSPC300) (Chen et al., 2010).

Furthermore, several studies have provided evidence of a role for CYFIP1 in the formation of dendritic connections and axon extension, as well as a role in synaptic plasticity (Biembengut et al., 2021), suggesting that it may play an important role in neural development.

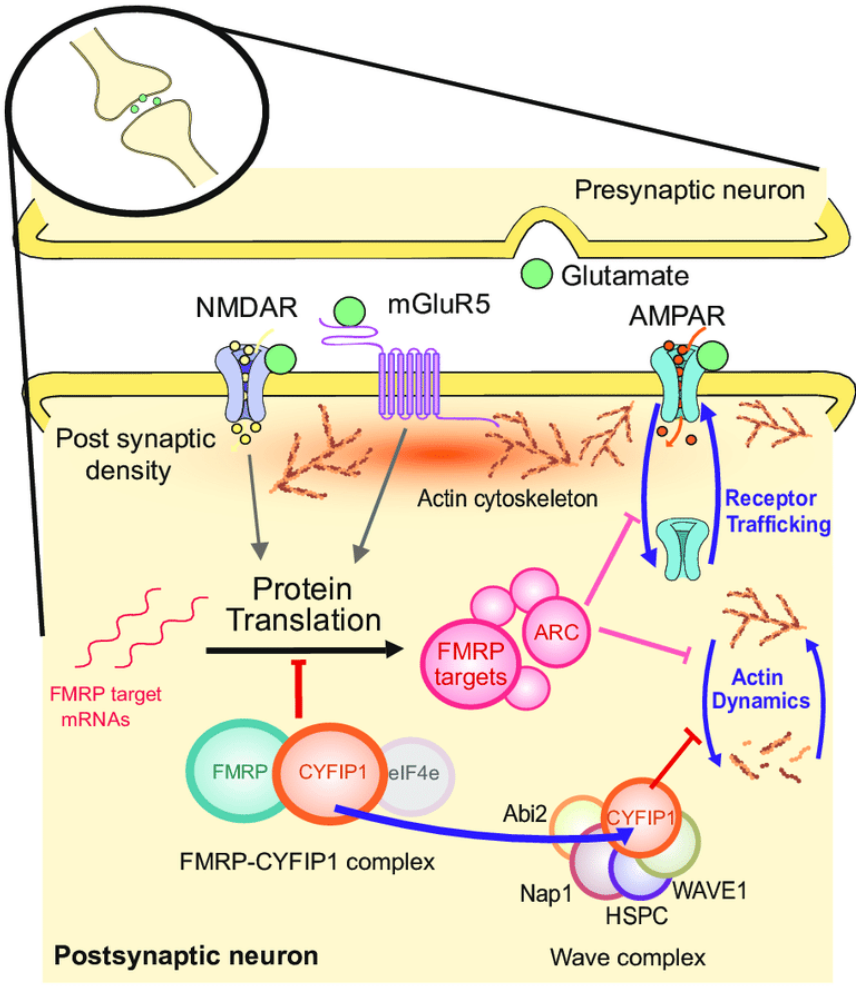

Figure 1.9. Interaction of CYFIP1 with the WAVE and FMRP protein complexes. Schematic demonstrating interaction of CYFIP1 with FMRP and WAVE in postsynaptic neurons. FMRP regulates translation of many FMRP targets, including ARC, by forming a complex with CYFIP1. CYFIP1 additionally can bind and inhibit WAVE regulatory complex, inhibiting actin cytoskeleton dynamics. ARC: Activity-regulated cytoskeleton associated; CYFIP1: Cytoplasmic FMRP-interacting Protein 1; FMRP: Fragile X Mental Retardation Protein; mGluR5: metabotropic glutamate receptor 5. Figure adapted from (Clifton et al., 2020).

1.7.4. CYFIP1 and cholesterol metabolism

There are multiple studies providing evidence that supports a potential role for CYFIP1 in the regulation of cholesterol biosynthesis. This includes interaction with the master transcription factor for genes regulating cholesterol biosynthesis and metabolism, SREBP2. SREBP2 mRNA was recently demonstrated by

immunoprecipitation sequencing (RIP-seq) to be a direct target of CYFIP1 in adult mouse cortex and hippocampal tissue (Kim et al., 2022a). Additionally, SREBP2 together with two other enzymes involved in the cholesterol biosynthetic pathway, HMGCS1 and GGPS1, were shown to be identified as high confidence FMRP targets in the brain (Darnell et al., 2011a; Sawicka et al., 2019). 14 further genes involved in cholesterol biosynthesis have also been reported to bind to FMRP in HEK cells (Ascano et al., 2012).

A recent study carried out with colleagues in Cardiff has indicated that altered levels of *CYFIP1* in cortical neural progenitors results in altered cholesterol biosynthesis and metabolism. Transcriptomic analysis of neuronal cells derived from iPSC lines generated from individuals carrying 15q11.2del and hPSC lines containing either a *CYFIP1* knockout (KO) or overexpression of *CYFIP1* revealed cholesterol metabolism as one of the top altered biological functions in these cells (Fuente, et al. 2024). Results from this study revealed that *in vitro* differentiation of these human pluripotent stem cells (hPSCs) into cortical neurons demonstrated pronounced deficits in neural progenitor maintenance and neuronal differentiation, with overexpression of *CYFIP1* leading to a bias toward proliferation and self-maintenance whilst knockout of *CYFIP1* and the 15q11.2del cells underwent premature neuronal production (Fuente, et al. 2024). Furthermore, RNASeq analysis of these neural progenitors also revealed mirror differences in LXRβ target gene expression between 15q11.2del neurons and CYFIP1 overexpressing neurons. This led to the hypothesis that oxysterol-mediated LXRβ signalling may potentially underpin the phenotype observed in both the 15q11.2del and CYFIP1 neural progenitors. However, a need for further investigation of how the sterol profiles of these cells are altered is required.

1.8 Sterol analysis of biological samples

Due to the dominating concentration of cholesterol and its esters, as well as their poor ionisation characteristics, sterols are usually under-represented in untargeted metabolomic or lipidomic analyses. Thus, there has been the development of the field of “sterolomics”, which refers to the quantitative or semi-quantitative profiling metabolites derived from cholesterol and cyclic precursors (Griffiths, W.J. *et al*. 2019). Several sample purification processes have been developed for the specific analysis of sterol content of various cell types, tissues, organs or bodily fluids. Here is detailed the specific approach utilised in this thesis.

1.8.1 Sterol extraction from human biological samples

Identification and quantification of sterols present in biological samples involves stages of sterol extraction, sterol separation and sample purification, derivatisation and either qualitative or quantitative analysis of examined extracts. This thesis will focus specifically on the profiling and the quantitative identification of cholesterol, its direct precursors and oxidised metabolites, oxysterols, using liquid chromatography-tandem mass spectrometry (LC-MS) techniques.

The analysis of cholesterol and oxysterol content of human biological samples requires initial extraction of these molecules from the samples, separating the sterols from other biomolecules present. The process of sterol extraction must be precise and avoid any unwanted contaminants whilst also preventing any loss and/or degradation of the sterols themselves.

1.8.2 Solid Phase Extraction (SPE)

A key concern in the analysis of oxysterols is the uncontrolled reaction of cholesterol or its precursors desmosterol or 7-DHC with atmospheric oxygen, a process known as autoxidation, resulting in the generation of oxysterols with similar structures to those formed *in vivo* (Zerbinati and Iuliano, 2017). This risk of potential autoxidation of cholesterol and any resultant nonenzymatic formation of

oxysterols is increased during long periods of sample handling, storage and processing. This is an issue as it can lead to unreliable identification and quantification, as oxysterols formed endogenously via enzymatic reactions can have identical structures to those formed through autoxidation reactions with oxygen in the air. Thus, efforts must be made to minimise and avoid any unnecessary delays in sample processing, including avoiding high temperatures and separating cholesterol from the sample at the earliest possible point in processing.

Traditional approaches to sample preparation for lipidomic analysis involve liquid-liquid extraction (LLE) which employs the use of various solvents or solvent mixtures, to separate lipids into a non-polar organic phase while more polar metabolites remain in a polar aqueous phase. Common LLE methods include the Bligh-Dyer method, which uses chloroform/methanol as the extraction solvent, but there are various LLE utilised (Furse et al., 2015). An alternative and well-established method for sterol analysis is solid-phase or sorbent extraction (SPE), which is carried out at the initial point in sample processing. SPE involves physical extraction, using commercial pre-packed columns containing a stationary phase such as silica gel contained within a plastic column with a Luer tip, commonly used in combination with a vacuum manifold.

This thesis utilises a SPE method using Sep-Pak tC18 200mg cartridges for the initial separation of sterols. This approach enables the separation of cholesterol from oxysterols and aims to prevent autoxidation products. In this process, the more polar lipids are retained in the column stationary phase, which is pre-conditioned in 70% EtOH, whilst the less hydrophobic lipids i.e. oxysterols are eluted from the column. The polar sterols i.e. cholesterol is then eluted from the stationary phase in absolute EtOH. Using this method, two separate oxysterol- and cholesterol-containing fractions are generated.

1.8.3 Derivatisation techniques

Chemical derivatisation methods are employed to improve ionisation characteristics of samples in LC-MS analysis. As cholesterol and oxysterols are neutral molecules, they ionise poorly in LC-ESI-MS/MS analysis. Various derivatisation methods have been devised to overcome this issue, including derivatisation to picolinyl esters and N,N-dimethylglycine esters. A common and very well-established method of derivatisation involves the use of Girard hydrazine reagents.

This thesis utilises the pre-established Enzyme Assisted Derivatisation for Sterol Analysis (EADSA) method (**Figure 1.10**), developed by Crick *et al* (2015). This charge-tagging approach specifically targets the 3β-hydroxy-5-ene group of the sterol structure, converting it to a 3-oxo group using the enzyme *Streptomyces sp*. cholesterol oxidase. This converted group can then be derivatised using Girard P hydrazine reagent, which introduces a positive charge-tag to the target molecule. Design of the Girard P charge tag is based upon a modification of procedure detailed by Girard and Sandulesco (1936).

The EADSA method is utilised for analysis of neutral sterols as it also improves specificity of their analysis in the LC-MS/MS. As the sterol backbone is composed of carbon-carbon and carbon-hydrogen bonds, plus a carbon-oxygen bond, MS^2 experiments are difficult due to the fragmentation spectra being dominated by non-specific loss of a H_2O molecule. The advantage of derivatisation with GP reagent is it results in a characteristic loss of a $[M-79]^+$ from the GP tag in MS^2, which is not a commonly observed loss in neutral molecules (Crick et al., 2015). The subsequent MS^3 scan results in a $[M]^+ \rightarrow [M-79]^+ \rightarrow$ transition that provides structural information that can be used to identify different oxysterols based on their unique spectra. The EADSA method also allows for identification of multiple cholesterol metabolites in a single assay, as it specifically targets molecules with either a 3β-hydroxy-5-ene or oxo group, which includes hydroxy- and oxo-cholesterols, cholestenoic acids and derivatives with these groups.

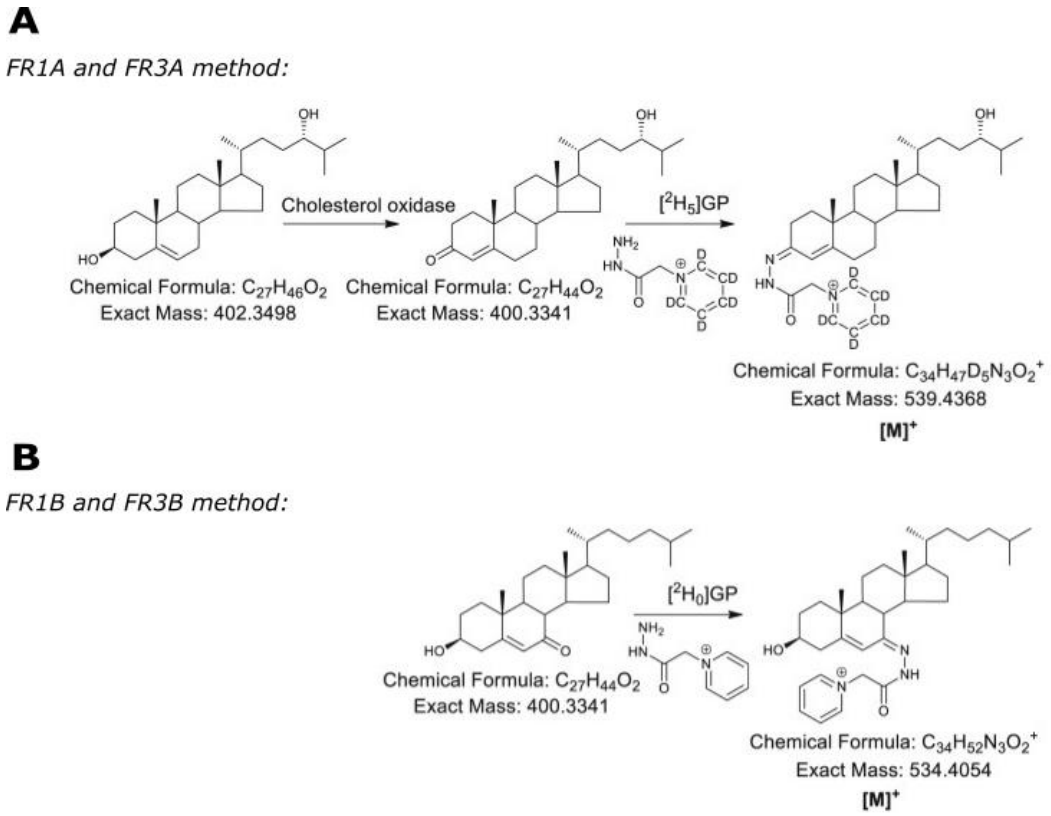

Figure 1.10. Schematic demonstrating the principle of the Enzyme Assisted Derivatisation for Sterol Analysis (EADSA) method. (**A**) EADSA of the 3β-hydroxy group with cholesterol oxidase and [$^2H_5$] GP reagent. (**B**) Derivatisation of 3-oxo group with [$^2H_0$] GP. Adapted from Abdel-Khalik, et al. (2019).

A key consideration when utilising the EADSA method is the potential of side-reactions, which is a consequence of the derivatisation process. In utilising this method for oxysterol analysis, important attention is needed in the analysis of 24S,25-EC, which via the EADSA method undergoes hydrolysis, methanolysis and isomerisation, additionally producing 24,25-dihydroxycholesterol, 24-hydroxy-25-methoxycholesterol and 24-oxocholesterol. This therefore requires the need for all side products to be detected and quantified to give a total quantification for 24S,25-EC. Another potential disadvantage of this method is the large excess of GP reagent required for the reaction. To avoid overloading of the chromatography

column or ion suppression in the LC-MS analysis, this excess reagent must be removed through a second SPE step.

1.8.4. Liquid Chromatography-Mass Spectrometry (LC-MS) analysis

Following processing of the sample, the sterolomic profile of the sterol extracts can then be measured and quantified. Gold standard techniques for the analysis of sterols include liquid chromatography (LC) and gas chromatography (GC) coupled to a mass spectrometer (MS). Nuclear Magnetic Resonance (NMR) can also be used but chromatographic techniques are preferred both due to an increased sensitivity and better spectral interpretation. Thin layer chromatography (TLC) can also be used and provides rapid analysis with very little sample preparation. However, for more in-depth analysis of complex biological samples, use of TLC has increasingly been replaced by GC and LC techniques, which are now the standard techniques for metabolomic studies, including sterolomics (Shackleton et al., 2018).

Many in the field of sterolomics, including our group, utilise high-performance liquid chromatography for the chromatographic separation of sterols. The basic LC technique involves the separation of compounds based on the number and type of interactions they have between the stationary phase and the mobile phase. Modern HPLC techniques use closed columns packed with micron-sized particles, known as the stationary phase, through which the analyte and mobile phases are pushed through under high pressure (Asensio-Ramos et al., 2017). This thesis will focus on the use of reversed phase (RP) liquid chromatography. RP chromatography refers to the use of a more polar mobile phase and less polar stationary phase, with RP columns usually composed of a hydrophobic alkylated silica stationary phase. RP is the preferred stationary phase for sterol analysis, due to its stability and easier modification, with C18 stationary phases the most utilised for sterol separation, providing a good peak resolution under gradient elution.

Following chromatographic separation, the effluent is passed to the detector, where the chemical or physical properties of the analyte is transduced into an electrical signal, measured as the solutes are eluted from the column. Mass spectrometers have become a commonly used HPLC detector, providing both structural and molecular weight (MW) information. The coupling of HPLC-MS provides the advantage over use of other detectors in that it carries out separation and identification in a single step.

The mass spectrometer design includes four main essential components: the sample inlet, ion source, mass analyser and detector (**Figure 1.11**).

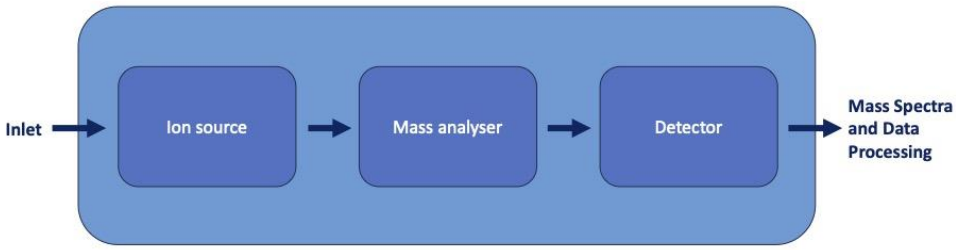

Figure 1.11. Overview of typical mass spectrometer workflow, detailing the essential components.

In recent years, multiple MS based strategies have been developed for the analysis of lipids, with the most popular methodologies based on the use of electrospray ionisation (ESI) sources and triple quadrupole analysers (Isaac et al., 2007).

Upon introduction into the MS, compounds are ionised at the ion source. Electrospray ionisation (ESI) involves applying a high voltage to a sample in solution resulting in creation of an aerosol and is the most widely used technique for MS analysis of samples in liquid state. ESI is a “soft” ionisation technique, due to the sample being ionised at low energy conditions, preventing in source fragmentation (Banerjee and Mazumdar, 2011). Following ionisation, samples are transferred to the second component of the mass spectrometer known as the mass

analyser. Here, ions are separated based on their mass, *m*, and charge, *z, i.e. m/z* values .

Quadrupole and triple quadrupole mass analysers are popular mass analysers which also use an electrical field to separate ions (Holčapek et al., 2012). Quadrupoles are often used in tandem with other mass analysers in hybrid/tribrid systems (Haag, 2016). They are termed quadrupole due to its structure, which involves ions being passed through 4 parallel rods organised equally around a central axis, which act as electrodes inside a vacuum chamber. A continuous ion source is provided, and ions are accelerated into the quadrupole. Voltage of the same polarity is applied to diagonally opposing pairs of rods, and opposite voltage polarity between adjacent rods (Haag, 2016). Both a direct current (D.C.) and high frequency alternating current or radio frequency (RF) are applied to the quadrupole. Under specific parameters, ions with the m/z of interest maintain a stable oscillation and reach the detector, whilst ions with other m/z values collide with the rods and leave the system undetected. This setup results in the selective filtering of ions with the target *m/z* passing through the quadrupole to the detector, which reads the quantity of ions present and produces an output signal (Haag, 2016).

The Orbitrap mass analyser is a high-performance mass analyser that uses the electrostatic field formed between two electrodes to trap ions in orbital motion. The orbitrap is comprised of an inner spindle electrode and outer barrel like electrodes. This form of mass analyser functions by oscillating ions in a central electrode with tapered ends. *m/z* signals are then detected based on Fourier Transforms (FT). When ions are injected into the analyser into the area between the central and outer electrodes, they follow an oscillation path along the trap, due to application of the desired voltage the radial electric field which bends the ion's trajectory toward the inner electrode, whilst the inner electrode provides an opposing centrifugal force. The axial electric field produced by the conical shape of the electrodes pushes ions towards the widest section of the trap, initiating axial harmonic oscillations with axial frequencies proportional to the *m/z* of the ion. This

technique provides both a high resolving power between ions and high mass accuracy, with the ability to calculate the m/z of ions up to 4.d.p.

A tandem combination of multiple mass analysers, known as tandem MS, involves the multi-stage fragmentation of ions of interest based on *m/z,* and provides more detailed structural information. These instrument arrangements are particularly useful in sterolomics, as there are a variety of oxysterols which have the same chemical formula and mass i.e. monohydroxycholesterols can be distinguished based on their fragmentation pattern.

Developments of “hybrid” or “tribrid” instruments, which utilise multiple mass analysers, are commonly used for their improved resolution and sensitivity. The tandem mass spectrometer systems used in this thesis are the Orbitrap Elite (hybrid) and Orbitrap ID-X (tribrid). The Orbitrap Elite is a hybrid MS instrument, which combines the use of an Orbitrap and dual pressure LIT mass analyser. Further advancements in MS/MS analytical techniques have led to the development of the tribrid instrument Orbitrap ID-X, which is the instrument utilised in this thesis. In addition to an Orbitrap and dual pressure LIT, this MS contains a quadrupole mass filter (**Figure 1.12**). The addition of the quadrupole filters the ion beam retaining the chosen mass. This specific mass is then fed into the C-trap and the Orbitrap for FT scans, or into the LIT for fragmentation.

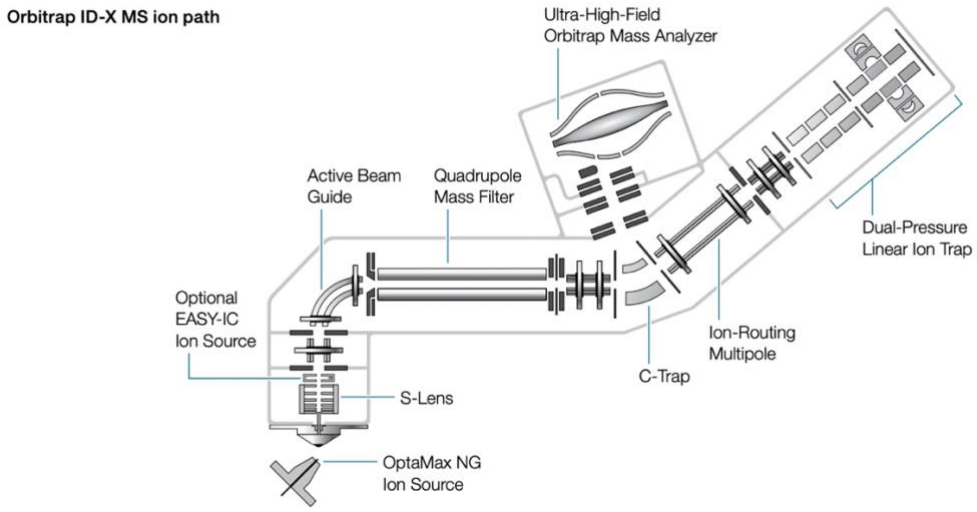

Figure 1.12. Schematic representation of MS instrument ion path of the hybrid Orbitrap ID-X. *Image taken with permission from Thermo Fisher™ Orbitrap ID-X product specification.*

1.9 Aims of this project

Cholesterol homeostasis is critical to proper neuronal development, with altered cholesterol synthesis and inborn errors of cholesterol metabolism linked to developmental defects and associated with several neurodevelopmental disorders. In recent years, focus on the bioactive signalling roles of both cholesterol and its oxidised forms, oxysterols, has led to findings that these molecules interact and modulate several key signalling pathways involved in human brain development. However, evidence for the endogenous presence of these sterols in the developing human brain is lacking. This information is vital to our understanding of how these molecules may be interacting with these pathways during development, and how alterations to cholesterol metabolism may result in neurodevelopmental defects.

This project is designed to develop an understanding of the production of these sterols during human cortical development, using *in vitro* human stem-cell derived methods which provides the ability to gain insight into each stage of early neuronal development, which is not feasible with human foetal tissue. Furthermore, this analysis will provide information on cell population-specific production, rather than whole brain tissue analysis carried out in previous studies. The development of this model and subsequent sterol analysis will provide a control system to which models of neurodevelopmental disorder which are known to feature dysregulated cholesterol metabolism can be compared.

Recent pilot data generated from colleagues in Cardiff has suggested that altered levels of CYFIP1 is associated with both dysregulated cholesterol metabolism and altered cortical neurogenesis. Transcriptomic analysis of stem cell-derived cortical neuronal models featuring altered levels of CYFIP1 revealed cholesterol metabolism as one of the top altered biological pathways in these cells. However, further investigation of how the sterol profiles of these cells is altered is required. Therefore, the above sterol analysis will be extended to investigate CYFIP1-altered human stem cell lines, in an effort to determine how cholesterol metabolism is affected and if biologically active sterols are altered in these models.

The principal objectives of this project are:

- Generate *in vitro* human embryonic stem cell (hESC)-derived models of human cortical development, verifying cell identity using immunocytochemical (ICC) analysis
- Assess protein level expression of key cholesterol biosynthetic enzymes at key developmental stages to assess cholesterol biosynthetic activity.
- Using previously published RNAseq datasets, assess gene expression of enzymes involved in both cholesterol biosynthetic and metabolic pathways in these cells.
- Through LC-MS^n analysis, develop a temporal sterol profile of these control hESC-derived models to assess oxysterols, cholesterol, cholesterol precursors desmosterol and 8(9)-DHC, and cholestenoic acids present at each stage of cortical development.
- Further assess hESC-derived astrocytic cultures to determine sterol profiles and assess expression of the CYP46A1 enzyme.
- Extend this analysis to a model of the human neurodevelopmental disorder 15q11.2del syndrome, using CYFIP1-altered hESC lines and patient-derived induced pluripotent stem cell (iPSC) lines, to assess any significant differences in sterol levels between control and disease model lines.

This thesis hypothesises that cholesterol and its oxidised derivatives ('oxysterols') are endogenously synthesised in a temporally and cell type-specific manner during human cortical development, where they play critical roles as bioactive signalling molecules regulating neurogenesis. Furthermore, it is proposed that disruption of cholesterol homeostasis, specifically through altered expression of CYFIP1, results in distinct changes in sterol profiles, contributing to abnormal cortical development. These alterations are expected to correlate with changes in the expression of cholesterol metabolic enzymes and lead to measurable defects in neuronal differentiation in human stem cell-derived models.

Chapter 2 Materials & Methods

2.1. Neuronal cell cultures and cortical differentiation

2.1.1 Cell lines used in cortical differentiation protocol

Two control human embryonic stem cell (hESC) lines are utilised in this thesis to establish baseline sterolomic profiles and distinguish developmentally regulated changes in sterol composition from cell line–specific or experimental variability over time. The H7 human embryonic stem cell (hESC) line (https://www.wicell.org/home/stem-cells/catalog-of-stem-cell-lines/wa07.cmsx) and a derivative of the HESC8 line carrying a doxycycline inducible Cas9 transgene (referred to here as iCas9 WT) (González et al., 2014) were used as control cell lines. The use of these cell lines was justified by their extensive prior validation within the same differentiation paradigm in our group.

The *CYFIP1-GoF (CYFIP1tg)* cell line is a pre-established cell line generated by previous Li Lab member Dr Claudia Tamburini and was generated by transgenic integration of a CYFIP1 constitutive expression vector into the H7 cell line (Fuente et al., 2024). The CYFIP1-GoF line features constitutive expression of exogenous CYFIP1 protein at around double the level observed in the WT H7 cell line and is used as a model of the rare 15q11.2 duplication (Fuente, et al., 2024). The H7 human embryonic stem cell (hESC) line was used as the isogenic control cell line for the *CYFIP1*-GoF cells.

CYFIP1 knockout (*CYFIP1*-LoF) human pluripotent stem cell (hESC) lines were generated using CRISPR/Cas9 directed gene editing of the iCas9 line, as detailed in (Fuente, et al., 2024). The iCas9 WT line was used as a control line for the *CYFIP1*-LoF cells.

All cell lines were cultured in standard culture conditions, at 37ºC, 5% CO_2.

Table 2.1. Human embryonic stem cell (hESC) lines used in* in vitro *differentiation protocols.

Cell Line	Cell Type	Sex	Source	Clonal lines	CNVs detected (>100kb and spanning >10 SNPs)
H7	hESC	Female	Wicell.org	1	3q26.1dup, 20p13-p11.21dup, 20q11.21-20q13.33dup
iCas9	hESC	Male	Hue 9	1	7q11.23dup, 8p23.2dup
CYFIP1-GoF	hESC	Female	Genetically modified H7 line	1	3q26.1dup, 20p13-p11.21dup, 20q11.21-20q13.33dup
CYFIP1-LoF	hESC	Male	Genetically modified iCas9 line	1	7q11.23dup, 8p23.2dup

2.1.2 Reagents

DMEM/F-12 (Gibco), Neurobasal (Gibco), DPBS (Gibco), N2 (Invitrogen), B27 (w/o RA) (Invitrogen), B27 (w/ RA) (Invitrogen), MycoZap™ Plus (Lonza), L-Glutamine (Gibco), β-mercaptoethanol (Gibco), LDN (StemGent), SB 431542 (Tocris), Rock inhibitor (Millipore), Cultrex® Basement Membrane extract (R&D systems), Essential 8™ Flex medium (Gibco), RevitaCell™ supplement (Gibco), Reduced growth factor Matrigel (Coring), Fibronectin (Millipore), 0.01% Poly-lysine (Sigma), Laminin (Sigma), DMSO (Sigma), Ethylenediaminetetraacetic acid (EDTA), Accutase® (Sigma).

2.1.3 Stem cell maintenance

hESCs were plated onto Cultrex®-coated 6-well plates and maintained in Essential 8™ Flex medium (Gibco). Once at 70-80% confluency, cells were passaged onto newly Cultrex®-coated plates. To passage, cells were washed in DPBS and incubated in 0.02% EDTA for 1-3 mins at 37ºC. EDTA was then aspirated, and cells were dissociated in Essential 8™ Flex medium by gently scratching the well with a 2ml serological pipette. Cells were then split at a 1:4-1:6 ratio onto Cultrex®-coated plates in Essential 8™ Flex medium. For the iCas9-derived lines, media required supplementation with 1X RevitaCell™ following passage to prevent cell death. hESCs were passaged approximately every 3-4 days.

Freezing of stem cell cultures was performed by collection of approximately $1x10^6$ cells. Cells were incubated in EDTA for 1-3 mins at 37ºC as described above. Cells were then dissociated into cold Essential 8™ Flex medium containing 10% DMSO. The cell suspension was then transferred to cryovials and placed in a Mr Frosty freezing container and cooled to -80ºC at a rate of 1ºC/minute. Cells were then transferred to liquid nitrogen for long-term storage. To thaw stem cell cultures, cryovials were thawed in a water bath at 37ºC. 1ml cell suspensions were immediately diluted in 9ml pre-warmed DMEM/F-12 and centrifuged at 200 x g for 5 minutes. The media was then aspirated and cells resuspended in Essential 8™ Flex medium supplemented with RevitaCell™ to improve survival.

2.1.4 Cortical neuronal differentiation

The cortical neuronal differentiation protocol outlined in this thesis has been adapted from previous published protocols (Chambers et al., 2009; Cambray et al., 2012; Arber et al., 2015) and has been described previously (De la Fuente, et al., 2024). Details of the factors and cell media used are shown in **Table 2.2.** An outline of the details of the protocol and overall timeline are shown in **Figure 2.1.** Each cell line was differentiated in two independent experiments with three technical

replicates collected per timepoint for each immunocytochemical analysis, sterolomic profiling and western blotting analysis.

Table 2.2. Details of cell media compositions used in neuronal differentiation protocols

Media	**Components**
Neural induction	• 2:1 ratio DMEM/F-12 and Neurobasal • 1X N2 supplement • 1X B27 supplement without vit A • 2mM L-Glutamine • 0.1mM β-mercaptoethanol • 0.2mM Mycozap • 100mM LDN • 10 μM SB431542
N2B27-RA	• 2:1 ratio DMEM/F-12 and Neurobasal • 1X N2 supplement • 1X B27 supplement without vit A • 2mM L-Glutamine • 0.1mM β-mercaptoethanol • 0.2mM Mycozap
N2B27+RA	• 2:1 ratio DMEM/F-12 and Neurobasal • 1X N2 supplement • 1X B27 supplement with vit A • 2mM L-Glutamine • 0.1mM β-mercaptoethanol • 0.2mM Mycozap

Stem cells were plated onto reduced growth factor Matrigel and maintained with Essential 8™ Flex media. Once cells were 80% confluent, cells were washed in DPBS and induced using the neural induction media: N2B27-RA supplemented

with dual SMAD inhibitors 100nM LDN, and 10μM SB 431542. This timepoint is referred to here as Day 0 of the differentiation (D0). Due to slight differences in the differentiation rates of the H7 and iCas9 cell lines, cells were kept in this media for 9 days for the iCas9-derived lines and 12 days for the H7-derived lines. At this stage, media was changed to N2B27-RA without LDN and SB.

When cells start to form multi-layered colonies, at approximately day 7 for the iCas9 line and day 10 for the H7 line, cells were passaged at ratio 2:3 onto fibronectin coated plates (15μg/ml in DPBS). Cells were pre-treated with 100μM ROCK inhibitor for 1 hour at 37ºC prior to splitting. Cells were then washed in DPBS and incubated in 0.02% EDTA for 3-5 mins at 37ºC. Cells were dissociated in the medium by gently scraping the well and resuspended in appropriate volume of neural induction medium for a 2:3 split ratio.

At the second passage, at approximately 10 days following the first passage, cells were split at a ratio of 1:4 onto poly-D-lysine-laminin coated plates. Plates were prepared by incubation in 0.01% poly-D-lysine in DPBS at RT for 1 hour, followed by washing in DPBS and incubation in 5μg/ml laminin solution in DPBS at 37ºC overnight. Cells were washed in DPBS and incubated in 0.02% EDTA for 3-5 minutes. Cells were dissociated in N2B27-RA media and scraping of the well and resuspended in appropriate volume of N2B27-RA before plating onto the prepared poly-D-lysine-laminin plates. A few days after the second passage, following confirmation of neuronal morphology, media was changed to N2B27 with vitamin A for promotion of neuronal maturation. Cells were then maintained in this media for the rest of the differentiation, with media changes every other day.

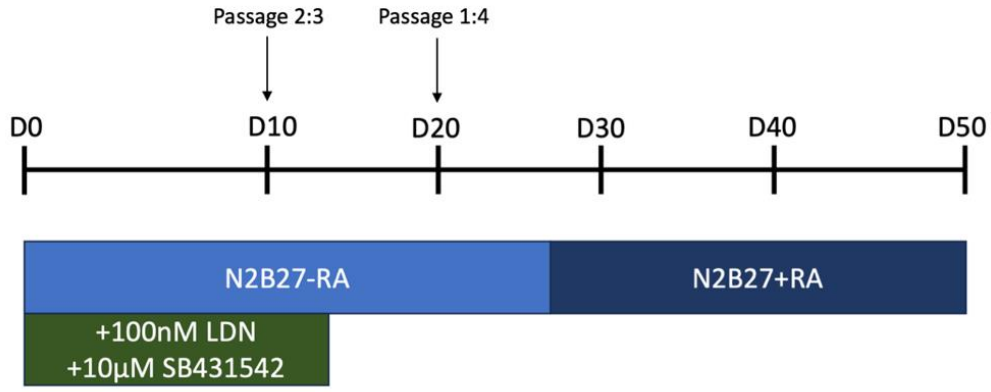

Figure 2.1. Schematic of in vitro cortical neuron differentiation protocol.

2.1.5. Astrocyte differentiation

Astrocytes were generated according to the following protocol, detailed in **Figure 2.2,** using the iCas9 line. The samples utilised in the IHC analysis and western blotting were derived from one independent experiment and three technical replicates collected per timepoint for each analysis. The samples used in the LC-MS^n analysis were kindly provided by Dr Zongze Li, who carried out one independent experiment and collected three technical replicates per timepoint using the same cell line and protocol. Following initial neural induction as described in **2.1.4.**, nascent neural progenitors were passaged at a 1:1 ratio onto Cultrex®-coated plates and induced for astrogenic switch through addition of 20ng/ml FGF2 and 10ng/ml EGF to the N2B27-RA basal medium. Between day 9 and 20, cells were maintained in this media with media replaced daily. At day 21, cells were passaged using Accutase at a 1:2 ratio and kept in the same media composition. At day 25, media was changed to N2B27+RA with 20ng/ml FGF2 and 10ng/ml EGF. At day 30, cells were passaged and plated at density 100K/cm^2. Between days 30-100, cells were maintained in the same media and passaged every 3-5 days depending on confluency and plated at a $1x10^5/cm^2$ density. At day 100, once cells determined to be majority CD44+ by ICC analysis, cells were passaged and plated at $3x10^4/cm^2$ density and media changed to N2B27+RA with 10ng/ml CNTF and 10ng/ml BMP4. At approximately day 105, cells were passaged for the final

time at density $3x10^4/cm^2$ and media switched to N2B27+RA with 10ng/ml CNTF only.

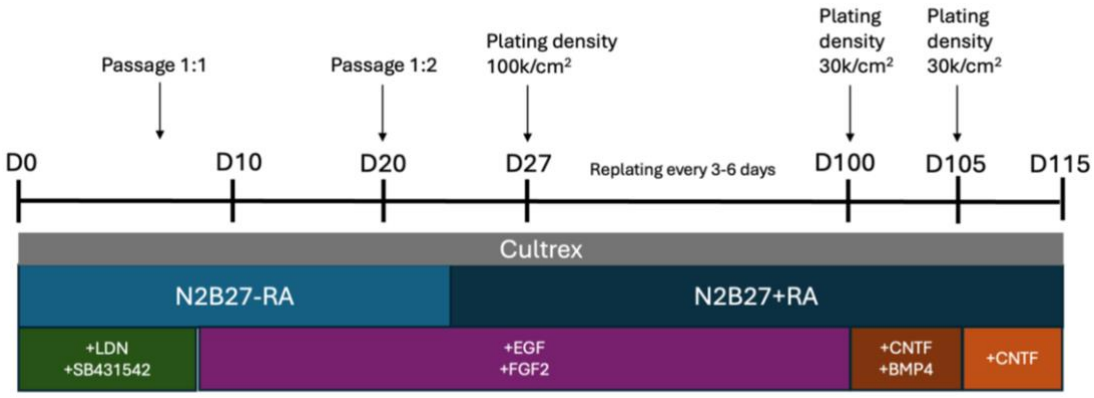

Figure 2.2. Schematic of in vitro cortical astrocyte differentiation protocol.

2.1.6. 15q11.2del patient samples

For the LC-MS^n analysis of 15q11.2del patient-derived and matched control neuronal cells, samples were kindly provided by Dr Daniel Cabezas de la Fuente, who carried out one independent differentiation with three technical replicates collected per sample timepoint. Details of cell lines used are shown in **Table 2.3.** Age and sex information were provided for the two 15q11.2del patients however phenotype details remain confidential and are therefore unable to be reported. Cells were differentiated using the same protocol outlined in **Figure 2.1**, and samples collected at the same time points described above.

Table 2.3. Details of induced pluripotent stem cell (iPSC) lines.

Cell Line	**Cell Type**	**Age**	**Sex**	**Source**	**Clonal lines**	**CNVs detected (>100kb and spanning >10 SNPs)**
900	iPSC	30 years	Male	Human control iPSC line	1	16p13.2del
EA008	iPSC	49 years	Male	Patient-derived iPSC line featuring 15q11.2 BP1-BP2 deletion	2	15q11.2del, 7q22.1dup, 14q11.2dup
EA062	iPSC	19 years	Male	Patient-derived iPSC line featuring 15q11.2 BP1-BP2 deletion	2	15q11.2del, 14q11.2del

2.2 Immunocytochemistry

2.2.1 Immunocytochemical staining

Prior to immunohistochemical analysis, cultured cells were fixed in 4% paraformaldehyde (PFA) for 10 minutes at RT and then washed twice in DPBS. For the assessment of nuclear markers, cells were permeabilised by going through increasing and then decreasing concentrations of methanol (33% and 66% for 5 mins each at RT, 100% MeOH for 20 mins at -20ºC). Cells were then washed twice in PBS and 0.3% Triton X-100 (PBS-T), before blocking in a block solution of 5% normal donkey serum, 2% bovine serum albumin (BSA) (Sigma-Aldrich) and PBS-T for 20 mins at RT. Cells were incubated in primary antibodies (**Table 2.4**), diluted in PBS-T and 3% normal donkey serum, overnight at 4ºC. Cells were then washed in 3 x PBS-T before incubation in AlexaFluor® (ThermoFisher) secondary antibodies, diluted 1:1000 in PBS-T, for 1h at RT in the dark. Cells were then counterstained with DAPI, diluted 1:3000 in PBS, for 5 min at RT in the dark. Cells were washed 3 x 10 min in PBS and mounted in fluorescent mounting medium (Aligent) using glass coverslips.

Table 2.4. Primary antibodies used for immunocytochemical analysis.

Marker	**Species**	**Dilution**	**Supplier**	**Product code**
OCT4	Mouse	1:1000	Invitrogen	MA1-104
NANOG	Rabbit	1:1000	Abcam	ab21624
PAX6	Rabbit	1:300	DSHB	PAX6

Marker	Species	Dilution	Supplier	Product code
FOXG1	Rabbit	1:500	Abcam	ab18259
NESTIN	Mouse	1:1000	BD	BD61159
NEUN	Mouse	1:1000	Abcam	ab279296
DCX	Goat	1:1000	Santa Cruz	SC-8067
βIII-Tubulin	Chicken	1:1000	Novus Biological	NB100-1612
TBR1	Rabbit	1:1000	Abcam	ab239000
CTIP2	Rat	1:1000	Abcam	ab18465
SATB2	Mouse	1:1000	Abcam	ab51502
GFAP	Rat	1:500	Thermo Fisher	13-0300
NFIA	Rabbit	1:500	Abcam	ab228897
hSOX9	Goat	1:100	R&D systems	AF3075
CD44	Mouse	1:500	CST	156-3C11
MAP2	Mouse	1:1000	Sigma Aldrich	M9942
EAAT2	Goat	1:100	Abcam	ab235202
AQP4	Rabbit	1:200	Abcam	ab259318
S100β	Rabbit	1:200	Abcam	ab52642
CYP46A1	Mouse	1:200	Merck	MAB2259

2.2.2 Imaging

Cells were imaged using Leica DM6000B Inverted Microscope (Leica) and LAS AF software (Leica). 3 replicate wells were used for each immunocytochemical staining for each cell line, with 10 fields of view captured per well. Z-stack images were 3D-deconvoluted and processed using LAS X and FIJI ImageJ software. Cell counts were then estimated for DAPI and most nuclear markers using the CellProfiler software.

2.3 Liquid Chromatography-tandem Mass Spectrometry (LC-MS^n) Analysis

2.3.1 Materials

Authentic sterol internal standards were procured from Avanti Polar Lipids (Alabaster, AL, USA) as deuterated standards and taken from stock solutions in 100% ethanol, with the following used in our analysis (Table 2.1): 24R/S-hydroxycholesterol-D6 (cat # 700018P), 7α-hydroxycholesterol-D7 (cat # LM-4103), 7-oxocholesterol-D7 (cat # LM-4107), 22S-3O-hydroxycholesterol-D7 (cat # 700051P), 7α, 25-dihydroxycholsterol-D6 (cat # 700078), 3β-hydroxycholest-5-en-26-oic acid-D5 (cat # 700151P), 7αH,3O-hydroxycholestenoic acid-D3 (cat # 700194P), desmosterol-D6 (cat # 700040P) and cholesterol-D7 (cat # 700041P). Water, ethanol, methanol and propan-2-ol all HPLC-grade (Fisher Scientific); Girard P (GP) reagent (TCI Europe); cholesterol oxidase (2mg/ml) from Streptomyces sp. (Sigma Aldrich); certified tC18 200mg Sep-Pak® solid-phase extraction (SPE) cartridges (Waters Inc., Elstree, Herts, UK); 60mg Oasis® HLB cartridges (Waters). 50 mM KH_2PO_4 (136.1gmol-) buffer (pH 7) prepared from phosphate (Sigma-Aldrich). Formic and acetic acid both HPLC grade (Sigma-Aldrich).

For the analysis of sterols in the samples used in this thesis, a combination of isotope-labelled sterol standards were used as reference internal standards for relative quantification. A master mix was generated containing several deuterated standards, and this was used for quantification for all samples analysed in this work. Details of the composition of this master mix are shown in **Table 2.5**.

Table 2.5. Internal standard master mix composition for analysis of stem cell-derived cell cultures.

Sterol		Cat no.	Concentration of iSTDs in master mix (ng/µl)	Amount Per sample (ng)
Systemic name	**Common name**			
Cholest-5-en-3β,24R/S-diol-D6	24R/S-HC-D6	700018	1	2
Cholest-5-en-3β,7α-diol-D7	7α-HC-D7	LM-4103	1	2
Δ5-Cholesterol-3β-ol-7-one-D7	7-OC-D7	LM-4107	1	2
25,26,26,26,27,27,27-heptadeuterocholest-5-ene-3β,22S-diol-D7	22S-3O-HC-D7	700051P	1	2
Cholest-5-en-3β,7α,25-triol-D6	7α,25-DiHC-D6	111117P	0.5	1
3β-Hydroxycholesta-5-en-(25R)26-oic acid-D5	3β-HCA-D5	700151P	1	2
7α-Hydroxy-3-oxocholest-4-enoic acid-D3	7αH,3O-HCA-D3	700194P	1	2
Cholesta-5,24-dien-3β-ol-D6	Desmosterol-D6	700040P	1	2
Cholest-5-en-3β-ol-D7	Cholesterol-D7	700041P	100	200

2.3.2 Sterol extraction from cell pellet

The method used for sterol extraction from cell pellet in this thesis is adapted from that used by Blanc, et al. (2013), as shown in **Figure 2.3**. At the indicated time points, cell media was removed and cells washed twice in ice-cold DPBS. Cells were then incubated with EDTA for 1-3 minutes at 37°C. Cells were then scraped into ice-cold PBS and collected into a 1.5ml microcentrifuge tube. Cells were centrifuged at 1000 x g for 5 mins and supernatant discarded. Cells were stored at 80°C prior to analysis.

Cells were thawed at 4°C on ice immediately prior to analysis to avoid freeze-thawing and minimise autooxidation of the sterols. Once cell pellets had started to thaw, cell pellet was loosened from bottom of tube. Sterols were extracted from cell pellet through the dropwise addition of 1ml 100% ethanol containing 20µl of the internal standards under sonication in an ultrasonic bath, followed by 50µl 100% ethanol and further sonicated for 5 minutes. Samples were then centrifuged at 16,000 x g (13,000rpm) at 4˚C for 30 mins to separate debris from ethanol sterol extract. Ethanol supernatant was then extracted and 400µl HPLC-grade water added to dilute sample to 70% ethanol.

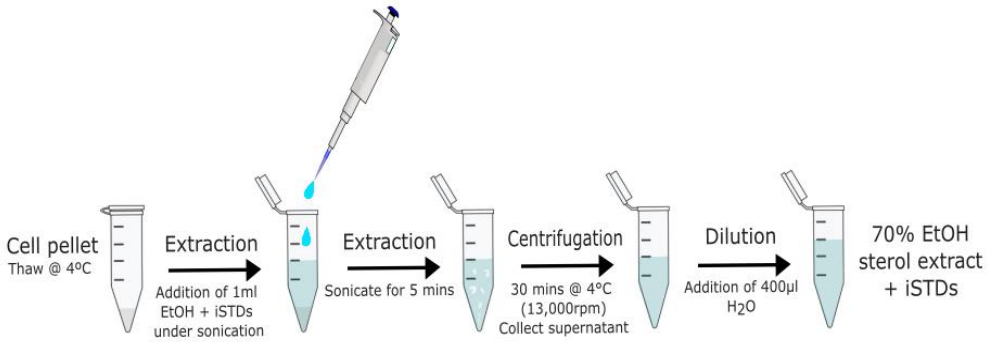

Figure 2.3. Workflow of sterol extraction method from cell pellet. EtOH: Ethanol, iSTDS: Internal standards.

2.3.3 Sterol extraction from cell media

For measurement of sterol release into the cell culture medium, cell media samples were collected from individual wells following a 48-hour incubation at the indicated time points. Due to collection at several different timepoints during differentiation, media volumes varied from 3ml to 1.5ml. A mock media sample i.e. fresh N2B27 media was also used to exclude the possibility that any components of the media may contribute to the measurements in the LC-MS^n analysis. The process for sterol extraction from the cell media samples is outlined in **Figure 2.4**. After collection, samples were stored at -80°C prior to analysis. Media samples were thawed on ice immediately prior to sterol extraction to avoid freeze-thawing and minimise autooxidation of sterols. Once thawed, media was centrifuged at 900 *x g* at 4˚C for 15 mins to remove any cell debris. Sterols were

extracted from cell medium through the dropwise addition of the cell media to an appropriate volume of 100% ethanol containing 10µl of the internal standards to form a 70% ethanol solution under sonication in an ultrasonic bath. For media volumes of 1.5ml, 3.5ml of 100% EtOH containing 10µl internal standards was added, whereas for 3ml media volumes 7ml of 100% EtOH containing 10µl internal standards was added. Samples were then further sonicated for 5 minutes. Samples were then centrifuged at 3,000 *x g* at 4˚C for 1 hour and the 70% ethanol supernatant collected for analysis.

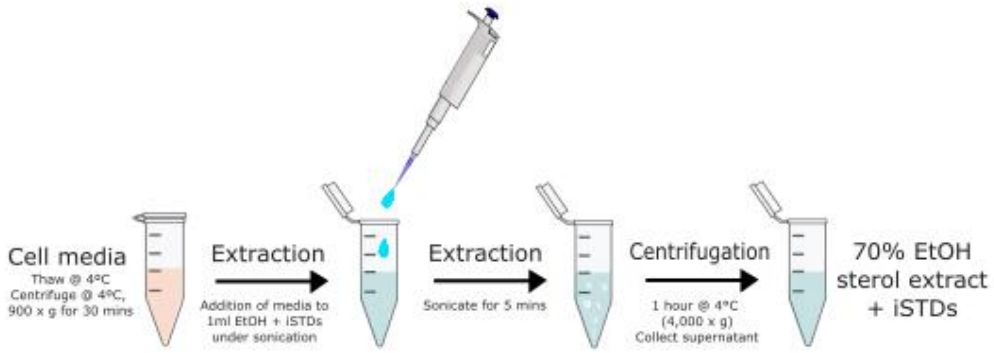

Figure 2.4. Schematic outlining workflow of sterol extraction from cell media. EtOH: Ethanol, iSTDs: Internal standards.

2.3.4 Reversed Phase (RP) Solid Phase Extraction (SPE)

Following sterol extraction, the sterols present in the extracts were separated from cholesterol and other hydrophobic sterols in the extracts by reversed solid-phase extraction (SPE) chromatography detailed in **Figure**

2.5. Separation of the sterols is based upon the sterol molecule's polarity and affinity for the silica-based reverse-phase C18 column used.

Sep-Pak® RP C18 vacuum cartridge (Waters, 200mg, 37-55 µm,186004618) is first preconditioned by washing with 4ml absolute ethanol, followed by conditioning with 6ml 70% ethanol. The sterol extract in 70% ethanol was applied to the column, with a flow rate set at 0.25 ml/min, with flow rate controlled by applying negative pressure at the column outlet using a vacuum manifold. Sterol extract volume varies depending on sample type. For extraction of cell pellet extracts, column flow-through was collected and combined with a 5.5ml column wash of 70% ethanol. For extraction of cell media samples, column flow through was collected and combined with a 1ml column wash of 70% ethanol. This initial fraction (FR1) contains the oxysterols and sterol-acids. The column was washed with a further 4ml 70% ethanol to give FR2. This additional washing step between the collection of polar and the non-polar sterols is used to minimise contamination of the hydrophobic fraction with any late eluting polar molecules. 2ml absolute ethanol was applied to the column and eluted to give FR3, the fraction containing cholesterol and its precursors. A final 2ml absolute ethanol was applied to the column to further elute more lipophilic sterols (FR4). Fractions 1 and 3 used in our analysis were then divided into two equal parts (A) and (B).

Following separation, eluted fractions containing the oxysterols and cholesterol were dried under reduced pressure for 24 hours (0.001mbar, -110^{o}C) at 1500rpm in a ScanLaf ScanSpeed vacuum concentrator (LaboGene) coupled with CoolSafe cold trap set at -110°C.

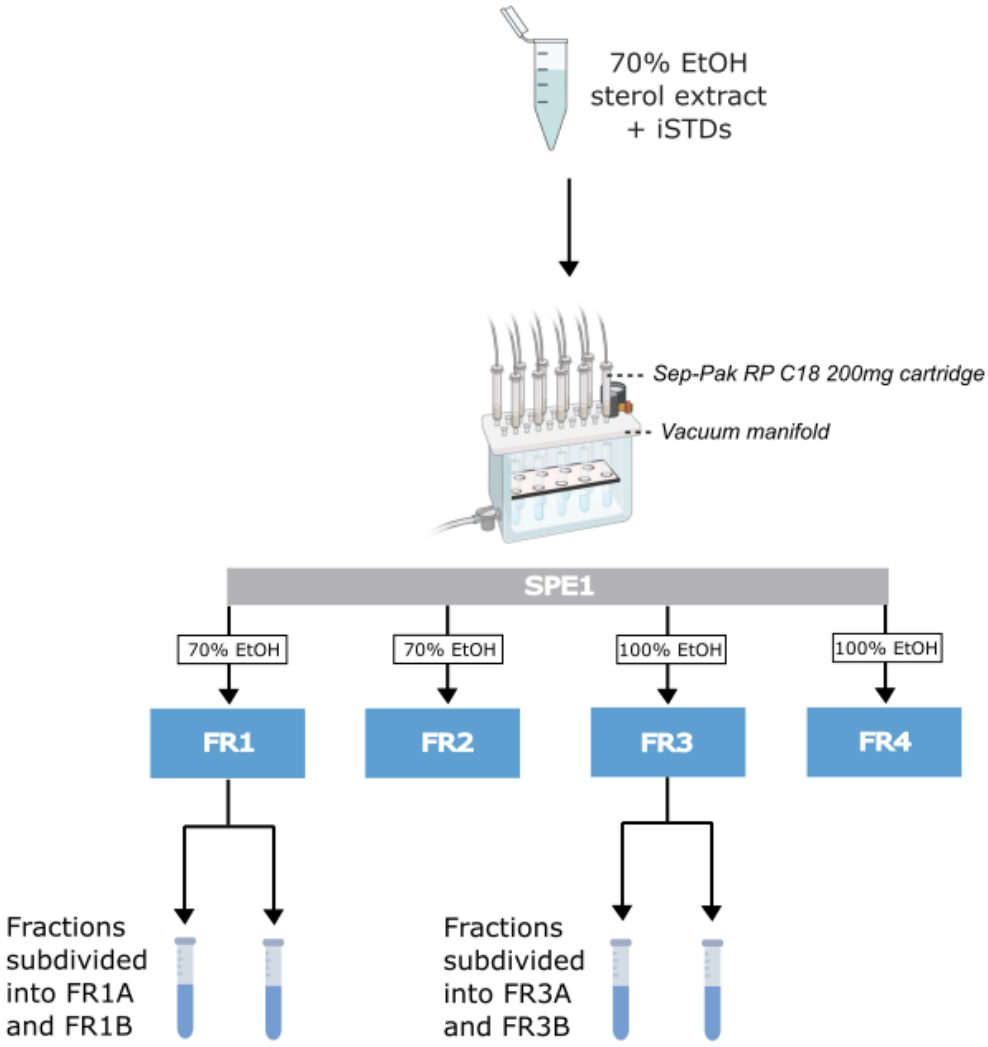

Figure 2.5. Solid Phase Extraction (SPE1) workflow for separation of oxysterols and sterols. Utilising the Sep-Pak RP C18 200mg cartridges, less-abundant oxysterols are separated from more abundant polar sterols i.e. cholesterol from the sample sterol extracts prior to LC-MS^n analysis.

2.3.5 Enzyme-Assisted Derivatization for Sterol Analysis (EADSA)

Sterols are neutral hydrophobic molecules which provides a challenge for their ionisation, particularly by mass spectrometry analysis using a mild ionisation technique such as electrospray ionisation (ESI). To overcome this issue, the method utilised here for sterol analysis involves a derivatisation reaction known as Enzyme Derivatisation for Sterol Analysis (EADSA), a method first described by Crick et al. (2015). Details of this method are outlined in **Figure 2.6**. The lyophilised fractions generated following SPE1 were first reconstituted in 100µL propan-2-ol. In FRA samples, the 3β-hydroxy-5-ene group is selectively oxidised to a 3-oxo-4-ene group (Figure 2.6.) by addition of 3µl cholesterol oxidase (2mg/ml in H_2O, 44 units/mg protein, Streptomyces sp.) and 1ml phosphate buffer (KH_2PO_4, 50mM, pH 7). To FRB, the buffer was added in the absence of cholesterol oxidase to account for sterols already containing a 3-oxo-4-ene group. Samples were then incubated for 1 hour at 37°C in a water bath. Following incubation, oxidation by cholesterol oxidase was quenched by addition of 2ml absolute methanol, forming a solution of approximately 70% methanol.

Presence of the 3-oxo-4-ene group allows for the binding of a charged hydrazine known as Girard P at the C3 position. Two Girard P reagents were used in this analysis, commercially available GPd0 (TCI Europe) and in-house synthesised GPd5. Addition of a positive charge both increases the signal intensity of analysed molecules in the mass spectrometry

analysis and improves their solubility in organic polar solvents for improved separation on the RP column. There is a characteristic neutral loss of 79Da and 84Da for GPd0- and GPd5-derivitised sterols respectively in the MS^n analysis. 150µl glacial acetic acid was added to both FR1 and FR3 and vortexed for 1 minute. Samples were then charge-tagged through the addition of 190mg GPd5 to FRA and 150mg GPd0 to FRB samples and incubated for 16 hours at room temperature in the dark.

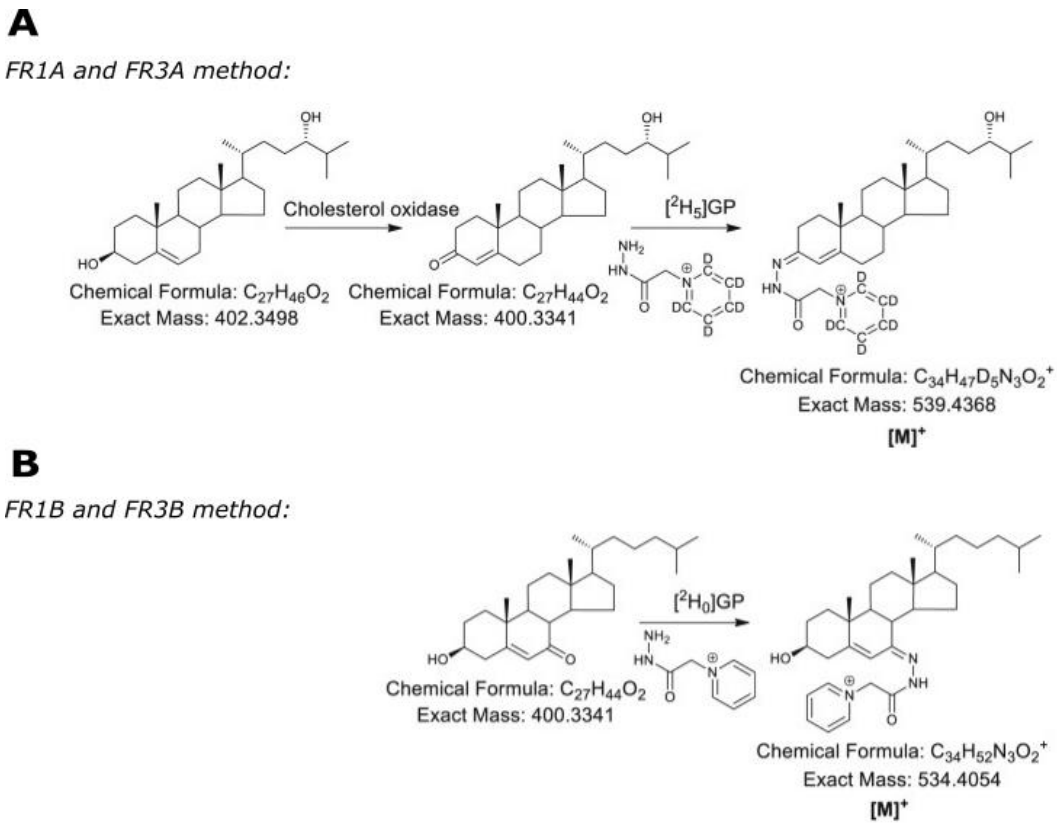

Figure 2.6. Derivitisation process using EADSA method and Girard P reagents GPd5 and GPd0. (A) Enzymatic reaction of the 3b-hydroxy group of 24S-HC in Fraction 1A with cholesterol oxidase, resulting in conversion to 3-oxo group. Subsequent reaction of this 3-oxo group with Girard P hydrazine [$^2H_5$] results in a charge-tagged molecule of mass

539.4368m/z. (B) Girard P hydrazine [$^2H_0$] reaction with naturally occurring 3-oxo group of 7-oxocholesterol in Fraction 1B, resulting in a charge-tagged molecule of mass 534.4054m/z. Image adapted from (Yutuc, et al., 2020).

2.3.6 Reversed-phase sorbent extraction (SPE2)

During the derivatisation step, the GP reagents used are added in a large excess and this excess needs to be removed prior to MS analysis to avoid heavy ion suppression which will impact the identification of the sterol lipids of interest. The excess reagent is removed by a second SPE chromatography step which involves the "recycling" of the sterol-containing solutions, enabling the recovery of sterols and elimination of excess GP reagent. The sterol-containing 70% methanol solutions are applied to the RP SPE column, then re-applied to the column in decreasing concentrations of methanol. Increasing the water content and reapplying the resulting solutions in this way enables the recovery of more polar sterols which may not be retained initially by the column at higher concentrations. The steps for this SPE2 process are outlined in **Figure 2.7**.

An Oasis® hydrophilic-lipophilic balanced (HLB) 3cc 60mg column (Waters, 186007646) was conditioned through washing with 6ml 100% MeOH, followed by washing with 6ml 10% MeOH and then 4ml 70% MeOH. Flow through the column was set at 0.25 ml/min, with flow rate controlled by applying negative pressure at the column outlet. The derivatised samples FR1As and FR1Bs or FR3As and FR3Bs were then applied to the columns and eluted. The sample tubes were then washed with 1ml 70% MeOH and this solution then applied to the column. The eluent was collected and

diluted to 35% MeOH by addition of 4ml HPLC-grade H_2O. The columns were then conditioned with 1ml 35% MeOH, and the 9ml 35% MeOH eluent reapplied. The eluent was again collected and diluted to 17.5% MeOH by addition of 9ml HPLC-grade H_2O. The column was conditioned with 1ml 17.5% MeOH and the 18ml 17.5% MeOH eluent then reapplied to the column and the eluent discarded. The columns were then washed with 6ml 10% MeOH for the removal of any excess GP reagent from the column bed. The oxysterols and cholesterol fractions were then eluted in 3 x 1ml 100% methanol and stored individually in 3 x 1ml aliquots. A final 1ml of absolute EtOH was applied and collected to remove any remaining sterols in the column. The sterol extracts were then stored at -20°C for short term or -80°C for long-term storage.

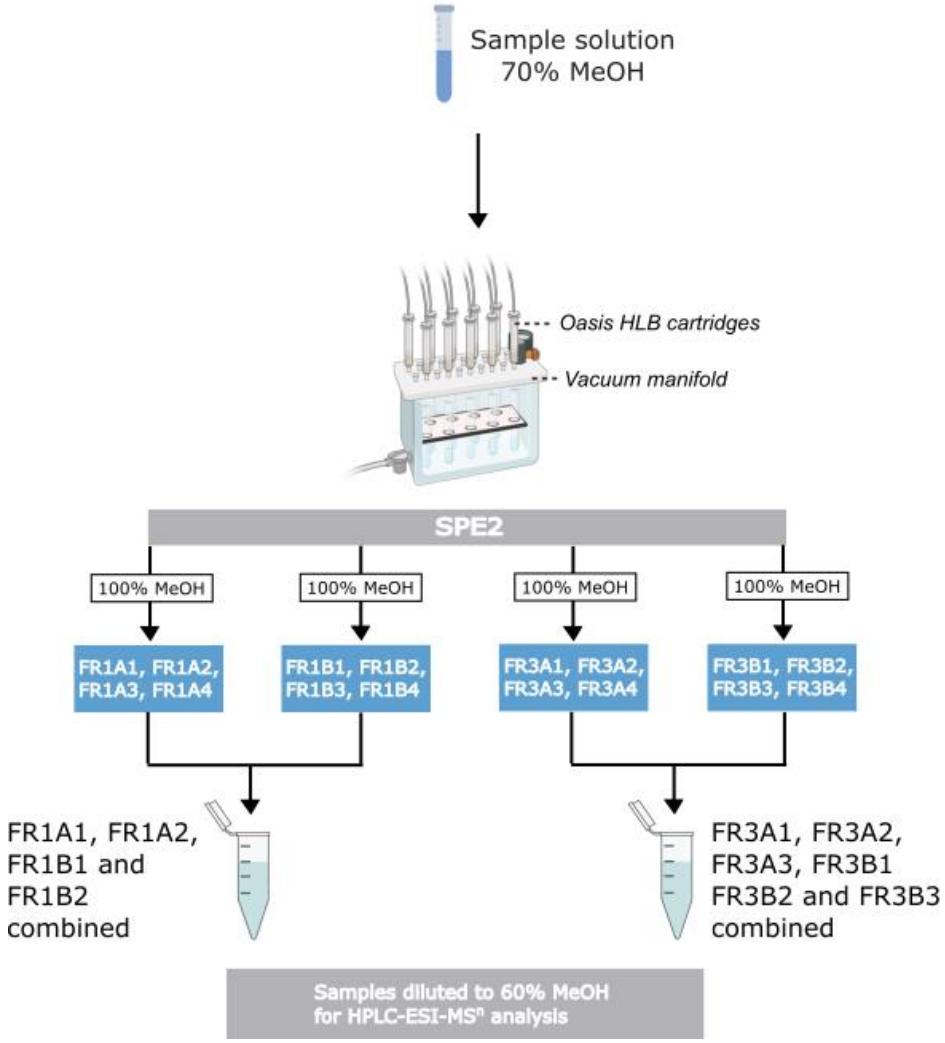

Figure 2.7. Outline of workflow of Oasis "recycling" step via Solid Phase Extraction (SPE2). A second SPE step is required for removal of excess GP reagent from samples prior to LC-ESI-MS^n analysis. Fractions are eluted in 4 x 100% MeOH washes, producing subfractions e.g. FR1A1, FR1A2, FR1A3 and FR1A4. For analysis of FR1s, the first two subfractions are combined and for FR3s the first 3 subfractions combined.

`2.3.7 Sterol Extract Analysis using Liquid Chromatography-Tandem Mass Spectrometry (LC-MS^n) Technique

Analysis of the methanolic sterol extracts were carried out using a coupled LC-ESI-MS^n technique. Chromatographic separation was performed using an UltiMate™ 3000 Micro LC system (Thermo Fisher Scientific, UK). The column used is a Hypersil™ Gold C18 RP column (50 × 2.1 mm, 1.9 µm, Thermo Fisher Scientific, UK). Two mobile phases were used and freshly prepared prior to each run, compositions for these are detailed in **Table 2.6**.

Table 2.6. Mobile phase composition used for LC separation of methanolic sterol extracts.

	% MeOH	% ACN	% Formic Acid
Mobile Phase A	33.3	16.7	0.1
Mobile Phase B	63.3	31.7	0.1

For analysis of the oxysterol-containing fractions (FR1s), 100µl of the neat 60% MeOH FR1 solutions were injected into the HPLC. For analysis of the cholesterol-rich fractions (FR3s), due to the high free cholesterol concentration i.e. in the range of µg/million cells, samples were diluted based on cell number of the sample. This is performed to avoid saturation of the RP column in the HPLC and avoid any potential carryover between

samples. For samples containing <1x10^6 cells, 10µl of the neat 60% MeOH FR3 solutions were injected. For samples >1x106 cells, the combined 60% MeOH FR3 samples were diluted 1 in 50, and 100µl injected into the HPLC. This approach allows for identification of cholesterol but avoids over diluting the sample and impacting the identification of the precursors 8(9)-dehydrocholesterol and desmosterol.

17- and 37-minute gradient methods were utilised for the separation of derivatised sterol isomers, as previously described in Griffiths et al. (2018). For better separation of closely eluting monohydroxycholesterols the longer 37-minute gradient was utilised for this specific method. The shorter 17-minute gradient was utilised for all other methods. For both methods the flow rate is maintained at 200µL/min throughout.

17-minute gradient: An initial equilibration phase is maintained at 20% mobile phase B and 80% mobile phase A for 1 minute. The proportion of mobile phase B is increased to 80% over next 7 minutes and maintained at this level for further 5 minutes. Proportion of mobile phase B is then decreased to 20% in 0.1 minutes and column recalibrated for final 3.9 minutes, giving a total run time of 17 minutes. This method allows for the elution of sterols by decreasing polarity, with the more polar sterols i.e. cholestenoic acids and dihydroxycholesterols eluted in the first few minutes, followed by the monohydroxycholesterols then finally by the least polar sterols i.e. cholesterol and precursors desmosterol and 8(9)-dehydrocholesterol.

37-minute gradient: An initial equilibration phase is maintained at 20% B for 10 minutes, then the proportion of mobile phase B is increased to 55% over next 9 minutes. The proportion of mobile phase B is then increased linearly to 80% in 10 minutes, before returning to 20% in 0.1 min. Column is recalibrated by maintaining 20% mobile phase B and 80% mobile phase A for the final 3.9 minutes, giving a total run time of 37 minutes.

Following chromatographic separation from the HPLC, eluents are passed into the ESI source of an Orbitrap ID-X™ Tribrid™ mass spectrometer (Thermo Fisher Scientific, UK). Following ionisation at the ESI source, ions are subjected to 4-6 scan events in positive ion mode. An initial high-resolution Fourier transform (FTMS) scan (resolution 120000 FWHM, 400 *m/z*), mass range 400-610 *m/z*, is performed in the Orbitrap mass analyser for the accurate identification of the molecular ions of interest (see Figure 1.8.7 for details). Four to six precursor ion scan events in the linear ion trap (LIT) are then performed, each followed by two fragmentation (MS^3) stages.

For the detection and identification of the more polar sterols e.g. oxysterols present in FR1s, we utilised 3 different methods screening for a total of 13 *m/z* values (**Supplementary tables 7.1, 7.2. and 7.3**.). For analysis of sterols in the FR3 samples, 2 different methods were used screening for a total of 9 *m/z* values (**Supplementary tables 7.4. and 7.5.**).

Thermo Fisher Scientific™ Xcalibur™ software (Thermo Fisher Scientific, UK) is used for data acquisition and processing, with the Xcalibur™ Qual browser used for data visualisation of the raw data files and identification.

2.3.8 Relative Quantification of Sterols

Sterols were identified and quantified using Thermo Fisher™ TraceFinder™ 5.1 software (Thermo Fisher Scientific, UK). Sterols were identified based on comparison of mass spectra and retention times of standards. Comparison of IT-MS fragmentation spectra was performed against the Griffiths-Wang lab's extensive spectral library, which details the retention times and mass spectra for a range of sterol lipids and has been generated using established methods for sterol analysis through LC-ESI-MS^3. Using TraceFinder™ software, quantification of endogenous sterols present in the sample can be performed by means of comparison to the internal standards (iSTDs) of known concentration (**Figure 2.8**). Relative quantification can be achieved though comparison to identical deuterated standards, for example cholesterol is quantified based on [$^2H_7$]-cholesterol. Semi-quantification is achieved when identical deuterated standards are not available, and the sterol can be quantified by comparison to similar structures, for example 27-hydroxycholesterol is estimated based on [$^2H_7$]-24(R/S)-hydroxycholesterol.

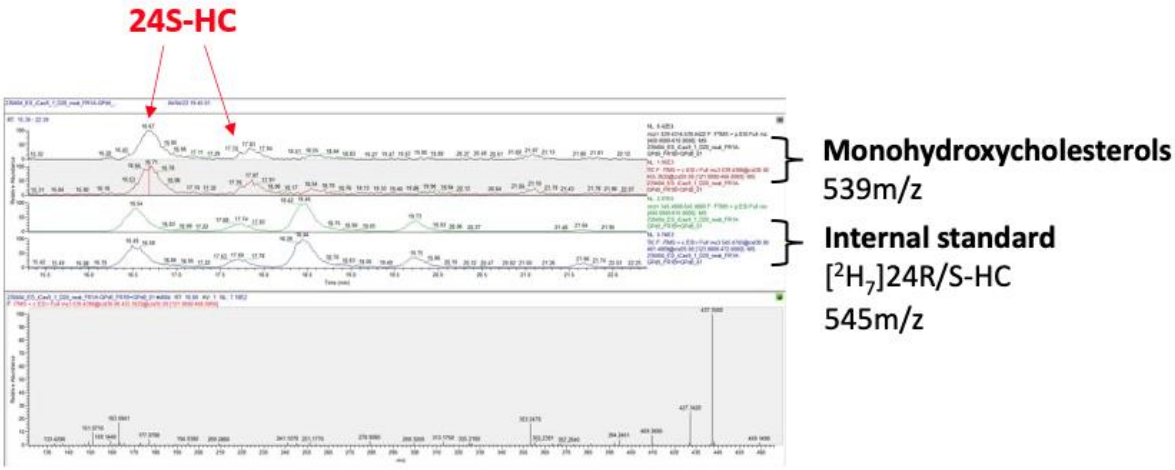

$$Conc_{analyte} = \frac{AUC_{analyte}}{AUC_{Internal\ standard}} \times Conc_{Internal\ standard}$$

Figure 2.8. Identification and relative quantification of the monohydroxycholesterol 24S-HC in neuronal cell pellet sample, using deuterated [$^2H_7$] 24R/S-HC internal standard. Peak selection is based on comparison of retention time and mass spectra of that of known standards. Peak area of endogenous 24S-HC is compared to that of the [$^2H_7$] 24R/S-HC internal standard using the ThermoFisher XCalibur™ and TraceFinder™ software.

2.4. Western Blotting

2.4.1 Protein extraction

Cell pellets were collected at the indicated time points, with cell media removed and cells washed twice in ice-cold DPBS. Cells were then incubated in 0.02% EDTA for 1-3 minutes at 37°C. Cells were then collected in ice-cold PBS and collected into a 1.5ml microcentrifuge tube. Cells were centrifuged at 1000 x g for 5 mins and supernatant discarded. Cell samples were lysed on ice in 1X RIPA buffer (Merck) supplemented with protease and phosphatase inhibitors (Sigma). Cell lysates were centrifuged for 5 min at 12000 *x g*. 120µl of the resulting supernatant was combined with 4X Bolt® LDS sample buffer (Thermo Fisher) and 1M DTT (Thermo Fisher) and incubated at 70°C for 10 mins. The remaining supernatant was used for relative protein quantification, estimated using a Bio Rad DC™ protein assay kit (500-0116) and compared against protein standard (Bio Rad). For estimation of protein quantification, absorbance was read at 750nm using the CLARIOStar® Plus (BMG Labtech). Samples were then stored at –80°C until further analysis.

2.4.2 SDS-PAGE and semi-dry transfer

Proteins were separated on either 4-12% Bolt® Bis-Tris Plus gels (Thermo Fisher) if protein of interest <100kDa or NuPage™ Tris-Acetate gels (Thermo Fisher) if protein of interest >100kDa. Amount of protein loaded was optimised to the antibody utilised, with 10µg protein loaded for both

SREBP2 and HMGSC1, 20µg for DHCR7 and 30µg for DHCR24. Proteins were then transferred onto a PVDF (0.2 µm) membrane via semi-dry transfer using the iBlot™ 2 Western Blotting system (Thermo Fisher), using the P0 transfer method with a 7-minute run time.

2.4.3 Antibodies

The membrane was blocked in 5% BSA (Sigma) in TBS-T (Tris-Buffered Saline containing 0.1% Tween-20) for 2 hours at RT. Membrane was then incubated at 4°C overnight in primary antibodies diluted in fresh blocking solution (**Table 2.7**). Following incubation, the membrane was washed 3 x TBS-T for 20 minutes at room temperature then incubated in LICOR IRDye® fluorescent secondary antibodies for 2 hours at RT in the dark. sFollowing incubation, the membranes were washed 3 x in TBS-T. The membranes were imaged using the Odyssey CLx Imaging System (LI-COR). Quantification was carried out in FIJI (ImageJ), with sample normalised to intensity of housekeeping protein GAPDH or Beta-actin.

Table 2.7. Primary antibodies used for western blotting of stem cell-derived neuronal and astrocytic cell samples.

Protein	***Supplier***	***Product code***	***Species***	***Dilution***	***Protein band***
HMGCS1	Novus biological	NBP2-16861	Rabbit	1:5000	57kDa
SREBP2	Thermo Fisher	PA1-338	Rabbit	1:1000	Full length: 125kDa Cleaved N-terminus: 67kDa
DHCR24	Novus biological	NBP1-32247	Rabbit	1:500	60kDa
DHCR7	Thermo Fisher	PA5-48204	Rabbit	1:500	54kDa
CYP46A1	Merck	MAB2259	Mouse	1:500	37kDa
GAPDH	Abcam	ab8245	Mouse	1:5000	36kDa
Beta-actin	Proteintech	20536-1-AP	Rabbit	1:2000	42kDa

2.5 Statistical analyses

All data were collected from at least 2 independent experiments with 3 technical replicates and presented as mean ± S.E.M., with exception to the 15q11.2del patient-derived samples and initial hESC-derived astrocyte samples provided for the LC-MS analysis, which were each provided as 3 technical replicates from a single *in vitro* differentiation. Data was tested for normality using the Shapiro-Wilk test and for equal variance with the Levene test. Statistical analysis was then performed by unpaired Student's *t* test or ANOVA, as specified in relevant figure legends. Post-hoc Tukey test was applied following ANOVA for multiple comparisons. The adjusted P-value was taken and used for significance, with the significance levels as follows: * $P < 0.05$, ** $P < 0.005$, *** $P < 0.0005$, **** $P < 0.0001$. Statistical analysis was performed in R (www.r-project.org).

Chapter 3

Temporal sterol profiling of stem-cell derived cortical neurons

3.1. Background

There is increasing evidence for the role of cholesterol and its metabolites in both human developmental processes and in the pathogenesis of neural developmental disorders, with various studies having focussed on assessing the interaction of these molecules with key developmental signalling pathways. However, much information on the presence of these sterols during brain development has been taken from animal models and there remains a lack of information on how levels of these sterols fluctuate across the developmental period.

Studies have utilised rodent models in an attempt to identify which of these bioactive sterols are present during embryonic development, to help shed light on which are endogenously present and thus relevant to neural developmental processes *in vivo*. During development the predominant oxysterol in the embryonic mouse brain has been found to be 24S,25-EC, identified in cortical tissue at E11 (Wang et al., 2009a). Importantly, 24S,25-EC has been evidenced to play a role in neuronal development, with a study demonstrating 24S,25-EC to be involved in the development of midbrain dopaminergic neurons through the activation of the liver X receptors (LXRs) (Theofilopoulos et al., 2013). Of the two liver X receptors, LXRβ is highly expressed in the brain, and has been shown to be essential in cortical development (Fan et al., 2008; Guo et al., 2014) and midbrain dopaminergic neurogenesis (Theofilopoulos et al., 2013). However, current evidence for the potential role of 24S,25-EC in regulating neurogenesis has

only been demonstrated in either animal models or its effects following the exogenous treatment with synthetic 24S,25-EC. Further evidence for how 24S,25-EC levels change in human neural cells during development would provide insight into how this sterol is involved in human neural development and confirm the predominate bioactive sterols present at each stage of human development.

Different cell types in the brain have been shown to have specific expression of various cholesterol metabolism enzymes and subsequently produce different sterols and metabolites. This has also been shown to differ depending on the developmental stage. During development, both neurons and astrocytes have been evidenced to produce cholesterol (Genaro-Mattos et al., 2019). Studies of embryonic mouse brain models have shown that following formation of the BBB at around E11, the brain produces essentially all sterols *in situ* (Tint et al., 2006). Up to E18, just prior to birth, cholesterol 24-hydroxylase (CYP46A1) expression, the enzyme responsible for hydroxylation of 24S-HC is low and hence biosynthesis of 24S-HC is restricted, conserving cholesterol levels in the brain (Tint et al., 2006).

Evidence so far for the role of oxysterols in neural development has been based on the analysis of animal models, whole brain tissue, primary cell cultures, and the exogenous application of oxysterols. To assess sterol production during human development *in vivo,* analysis is restricted to limited access to human foetal tissue and its associated ethical concerns. Thus, there remains a need for further information on what sterols are produced in individual cell types throughout human neural development.

This information would confirm which sterols are present endogenously that are involved in key developmental processes. It is important that these molecules are shown to both interact with these pathways and be identified endogenously during human neural development. Further, most studies that have focused on the role of cholesterol metabolism in brain development report only the levels of cholesterol and its precursors, with few having measured endogenous oxysterol levels in these models.

With ongoing developments in human stem cell technology, it is now possible to model human neural development *in vitro* without the need for human foetal tissue and animal models. With the current lack of data on the oxysterol profile of human neural cells during cortical neuronal development, the use of *in vitro* models of human cortical development would provide much needed insight into the endogenous sterol profile of developing human cortical cells. Characterising the sterol profile of human cells undergoing cortical neurogenesis will provide not only further information on what oxysterols may be produced in the developing brain but also provide a reference model for the development of further models to study neural developmental defects in the context of aberrant cholesterol metabolism.

3.2. Aims

With increasing evidence for a role for cholesterol and oxysterols in human neural development, it remains to be confirmed what the endogenous expression levels of these sterols are in neural cells during early brain development. Through the establishment of a temporal sterolomic profile of human cortical neuronal cells throughout *in vitro* neural development, this work aims to characterise both the presence of oxysterols as well as tracking changes in cholesterol metabolism during the different stages of neural development. This will also provide a reference control temporal sterol profile that can be used to further understand how altered levels of different cholesterol metabolites may impact upon neural development, potentially through their role in key neuronal signalling pathways.

This work aims to address this through:

- Cortical neuronal differentiation of two human embryonic stem cell (hESC)- and induced pluripotent stem cell (iPSC)-derived lines of a hESC line, confirming cell population identity through immunocytochemical analyses of key progenitor and neuronal markers.

- LC-MS^n analysis of the sterol content of samples at each stage of cortical neuronal differentiation to confirm which sterols are produced during *in vitro* cortical neurogenesis in each cell population. LC-MS^n technique utilises the EADSA method for the improved detection of both cholesterol and its metabolites.

- Analysis of protein expression of key enzymes involved in cholesterol biosynthesis will further enable determination of the level of cholesterol biosynthetic activity as well as compare activity of the Kandutsch-Russell and Bloch biosynthetic pathways. This will help address the question of whether different cell types i.e. neural progenitors and neurons prefer a specific biosynthetic pathway in the formation of cholesterol, and whether this is consistent through each stage of development.

Overall, these findings will provide a characterisation of how cholesterol metabolism is regulated throughout cortical development *in vitro and* confirm the levels of sterols evidenced to interact with key developmental signalling pathways. This model can be used to help further understand how altered cholesterol metabolism may impact neural development as observed in cases of neurodevelopmental disorder.

3.3. Results

3.3.1. Generation of hESC-derived cortical neuronal cell cultures

Cortical neuronal cultures were generated following the differentiation protocol detailed in Chapter 2.1. Two independent differentiations were carried out, and cell culture populations were assessed via immunocytochemical staining at 10-day intervals during *in vitro* differentiation, with three replicate wells taken at the same timepoints for sample collection for the accompanying experiments. Prior to *in vitro* differentiation, hESCs were confirmed to be pluripotent at DIV0 by expression of the pluripotency markers OCT4, SOX2 and NANOG (**Supplementary Figure 7.1**). Following neural induction, cortical neural progenitor rich cultures were identified at timepoint DIV20 by expression of the paired-box specific transcription factor PAX6 (**Figure 3.1A & C**). At later stages of the protocol following neuronal differentiation, from DIV40 onwards, neuronal-rich cultures were identified by expression of neuronal nuclei marker NeuN (**Figure 3.1B & D**). Both cell lines display a similar percentage of PAX6+ cells at the progenitor-rich stages of the differentiation (DIV 20 and D30) (**Figure 3.1 A & C**). It is noted that the iCas9-derived cells appear to produce an increased percentage NeuN+ cells earlier in the differentiation paradigm, indicating slightly different rates of differentiation dynamics between the two cell lines (**Figure 3.1B & D**).

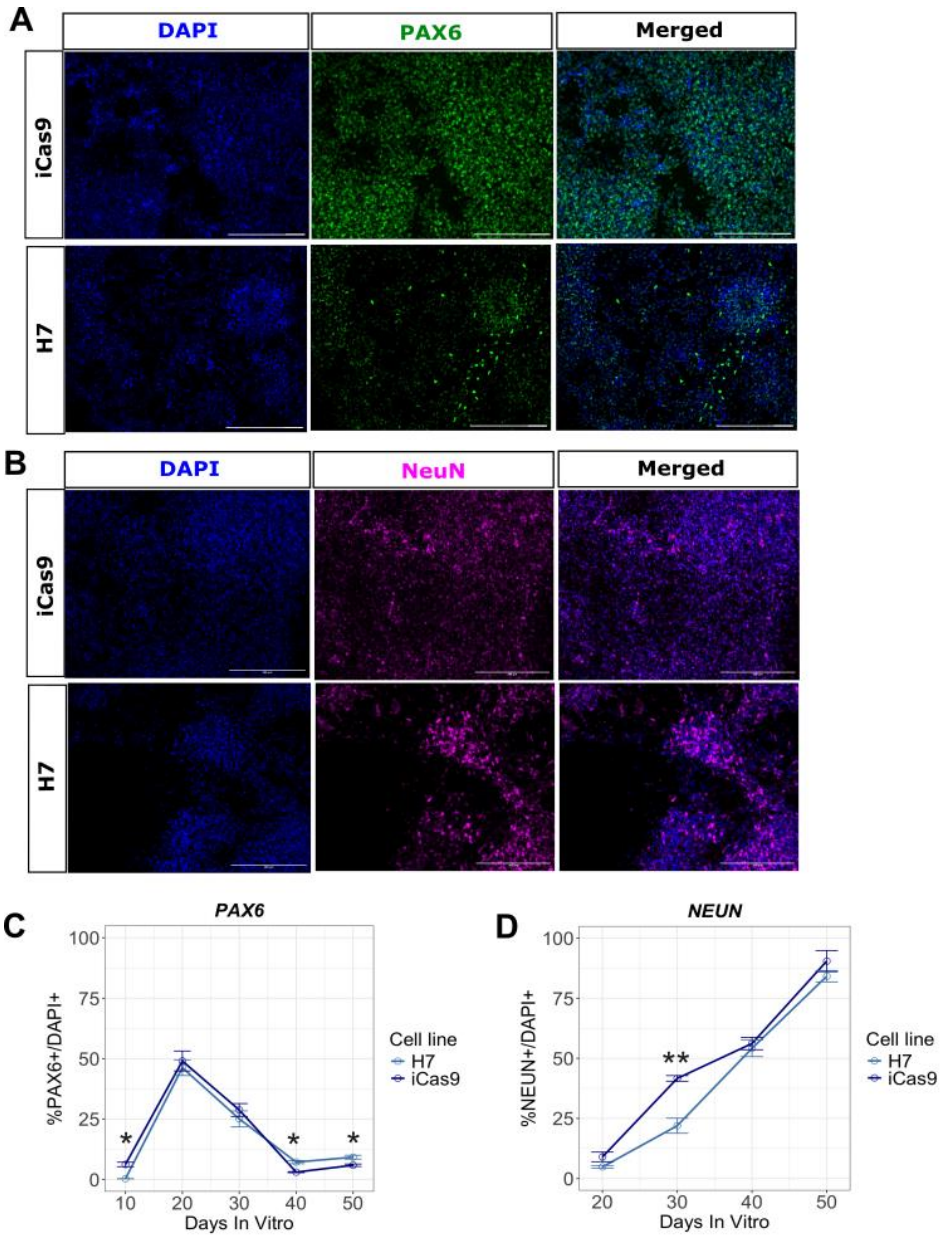

Figure 3.1. **Generation of human embryonic stem cell (hESC)-derived neural progenitor and cortical neuronal cells.** (**A**) Representative images of immunocytochemical staining of key neural progenitor marker PAX6 at 20 DIV and neuronal marker NeuN at 40 DIV. Nuclei were counterstained with DAPI (blue). (**B**) Quantification of percentage of PAX6+ and NeuN+ cells normalised to DAPI+ cells. Data

represent mean from 2 independent experiments, 3 technical well replicates, error bar = SEM. Student's t-test, *p<0.05, **p<0.01. 20X objective. Scale bar = 200μM.

Furthermore, cortical identity of the cells was confirmed by analysis of the expression of specific cortical layer markers TBR1 (layer VI), CTIP2 (layer V) and SATB2 (Layer IV) (**Figure 3.2**). Interestingly, this analysis also revealed iCas9-derived cultures to produce a higher percentage of CTIP2+ cells than the H7-derived cultures (**Figure 3.2C**).

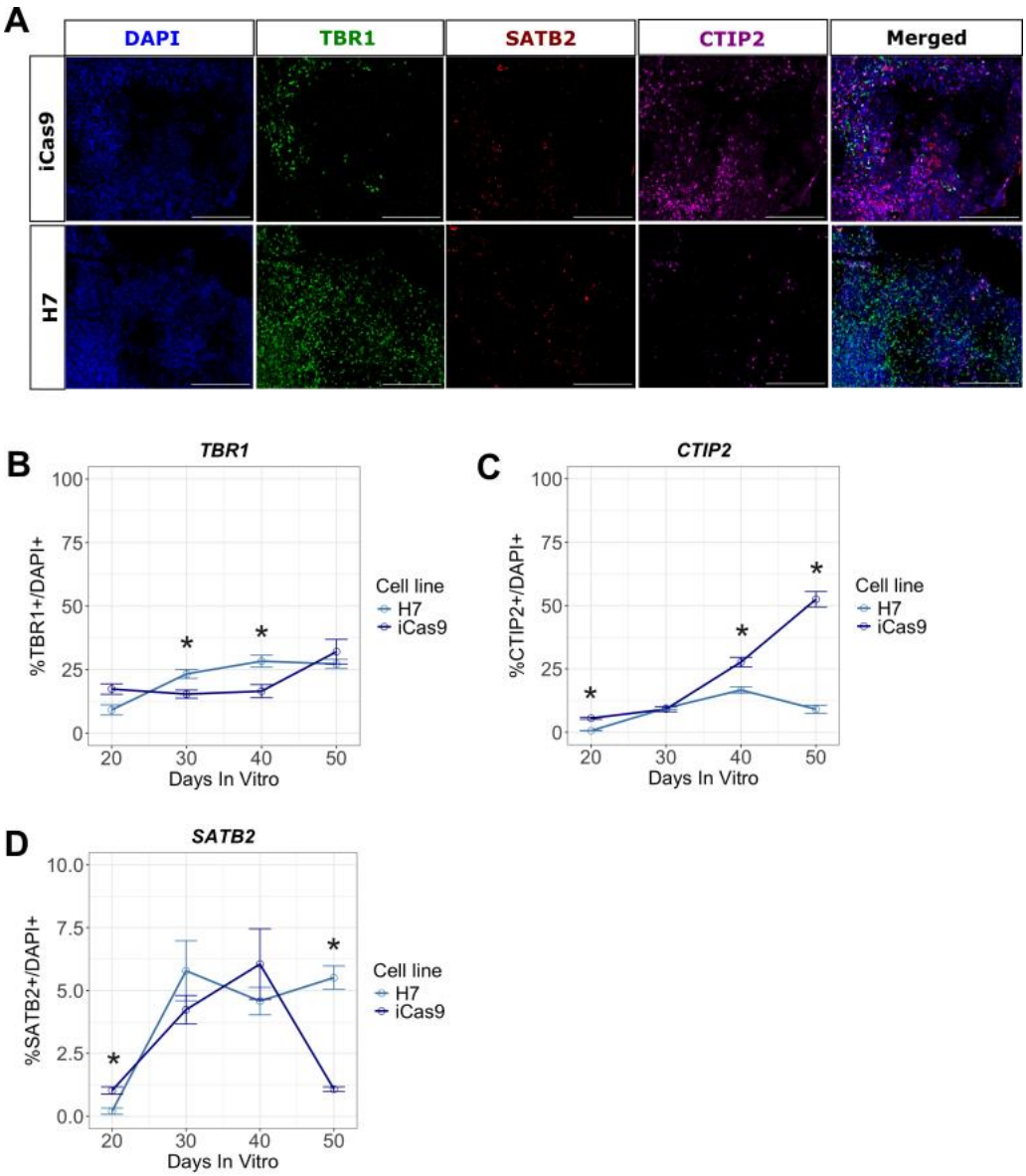

Figure 3.2. Generation of human embryonic stem cell (hESC)-derived neural progenitor and cortical neuronal cells. *(**A**) Representative images of immunocytochemical staining of key cortical markers CTIP2, SATB2 and TBR1 at 40 DIV. Nuclei were counterstained with DAPI (blue). (**B**) Quantification of percentage of CTIP2+, SATB2+ and TBR1+ cells normalised to DAPI+ cells.* Data represent mean from 2

independent experiments, 3 technical well replicates, error bar = SEM. Student's t-test, *p<0.05, **p<0.01. 20X objective. Scale bar = 200μM.

3.3.2. Temporal sterol profiling of human stem cell-derived neural progenitors and cortical neurons

Following the generation of hESC-derived neuronal cultures and collection of cell samples at each 10-day interval, sterol profiling was carried out to identify bioactive oxysterols, cholesterol and its immediate precursors present at each stage of the differentiation process. Using the pre-established EADSA method, identification and quantification of the sterols present in both cell pellet and cell media during in vitro differentiation of hESCs into cortical neurons was carried out using LC-MS^n methods detailed in Chapter 2.

With growing evidence of their role in neuronal development, it was confirmed that the oxysterols 24S-HC and 24S,25-EC were present in the neural progenitor and neuronal cultures, identified at all timepoints analysed (**Figure 3.3A & B**). 24S-HC and 24S,25-EC were both identified based on the comparison of retention times and mass spectra to those of known concentrations of internal standards. Analysis of the cell pellet revealed the levels of 24S,25-EC appear to fluctuate throughout the neuronal differentiation, and were present at similar levels to 24S-HC at the initial stages of the differentiation (**Figure 3.3A**). As neural cell fate is determined we observed an increase in 24S-HC, detected at a concentration of ~0.8 and 5ng/x10^6 cells at DIV50 in the iCas9 and H7 cultures respectively (**Figure 3.3B**). With the levels of this sterol increasing

as overall neuronal numbers increase (**Figure 3.3B**), this supports the idea that neurons produce 24S-HC. It should however be noted that at later timepoints there are significant differences in the levels of 24S-HC between the two hESC-derived lines analysed (**Figure 3.3B**). Interestingly, we were only able to detect 27-HC to be present in the H7-derived cultures, and only detectable at the initial and final stages of the differentiation, present at 0.413±0.0663 ng/x10^6 cells and 0.0814±0.0054ng/x10^6 cells at DIV10 and DIV50 respectively (**Figure 3.3C**).

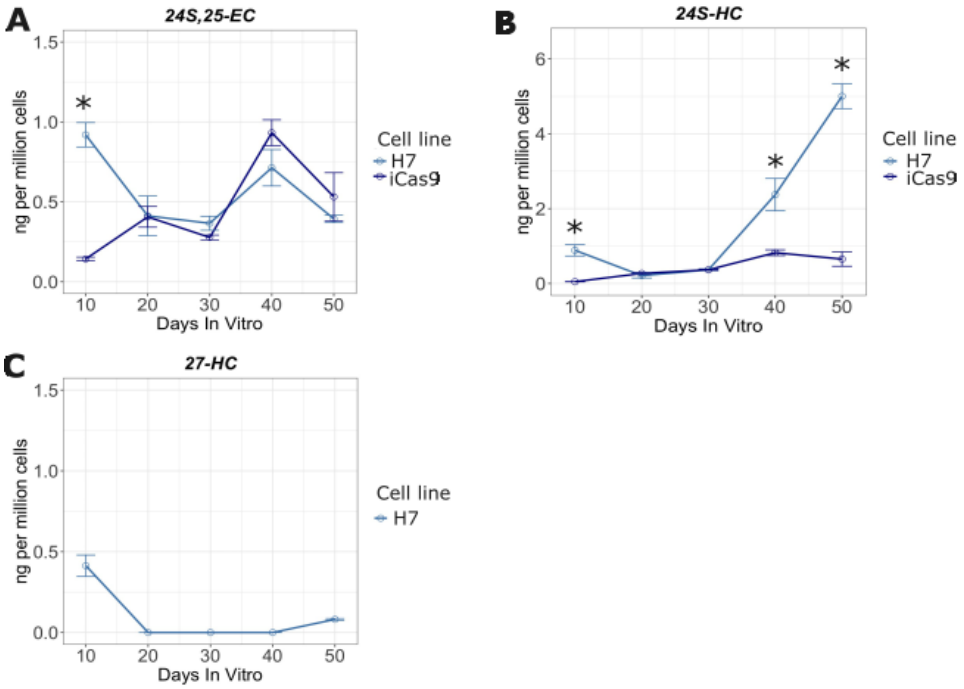

Figure 3.3. Quantification of 24S-HC and 24S,25-EC content of hESC-derived neuronal cells. Quantification of (**A**) 24S,25-EC, (**B**) 24S-HC and (**C**) 27-HC levels in neural progenitors and neuronal cells derived from H7 and iCas9 hESC lines. Data represent mean from 2 independent experiments, 2-3 technical well replicates, error bar = SEM. Student's t-test, *p<0.05.

Further analysis of the monohydroxycholesterol content at mass fragments 534 and 539*m/z* of the cell pellets revealed the presence of 7α-hydroxylated sterols 7α-hydroxycholesterol, 7β-hydroxycholesterol, 6β-hydroxycholesterol and 7-ketocholesterol (**Figure 3.4**). These were all detected in both cell lines at each timepoint (**Figure 3.4**). Of these, it should be noted that 7-ketocholesterol, 6-hydroxycholesterol and 7β-hydroxycholesterol are products of the autoxidation of cholesterol.

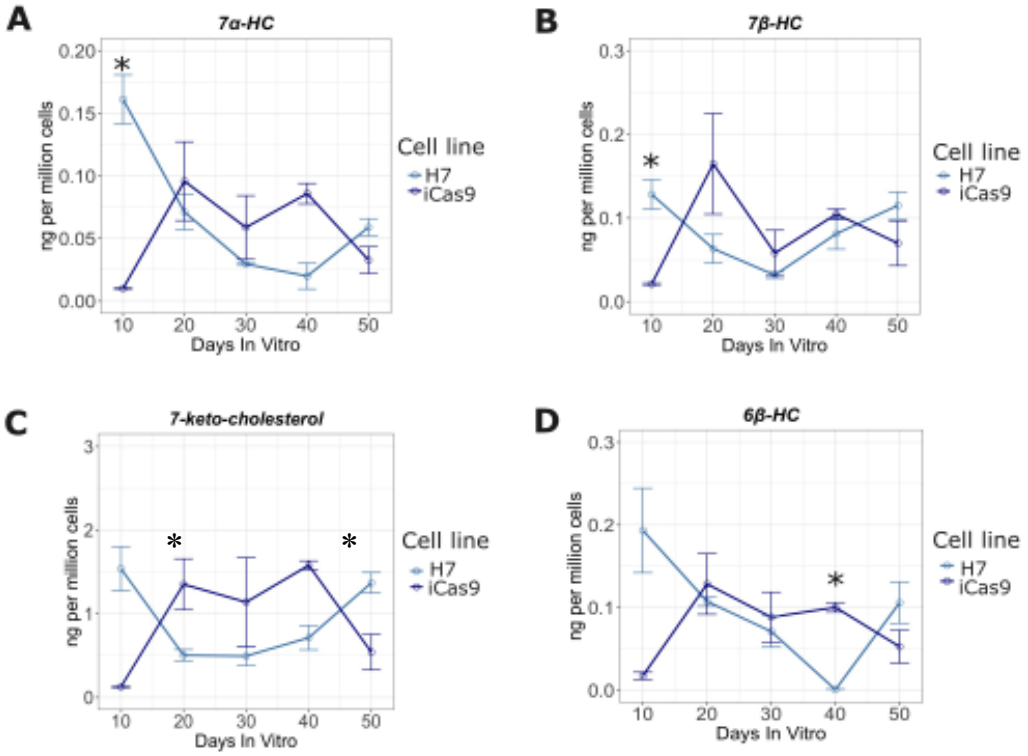

Figure 3.4. Quantification of monohydroxycholesterol content of neuronal cells. Quantification of levels of (**A**) 7α-hydroxycholesterol, (**B**) 7β-hydroxycholesterol, (**C**) 7-ketocholesterol and (**D**) 6β-hydroxycholesterol in neural progenitors and neuronal cells derived from H7 and iCas9 hESC lines. Data represent mean from 2 independent experiments, 2-3 technical well replicates, error bar = SEM. Student's t-test, *p<0.05.

Analysis of the 555*m/z* fragment revealed the presence of the dihydroxycholesterol 7α, 26-dihydroxycholesterol (7α, 26-diHC), formed via CYP7B1-mediated oxidation of 27-HC (**Figure 3.5A**). 7α, 26-diHC was detected to be present at the levels of 0.0623±0.00766ng/x10^6 cells in the H7 cells at DIV10 of the differentiation, which corresponds to the NPC-rich stage (**Figure 3.5B**). This sterol was only detectable at in the iCas9 line at DIV20, present at 0.0257±0.00970 ng/x10^6 cells.

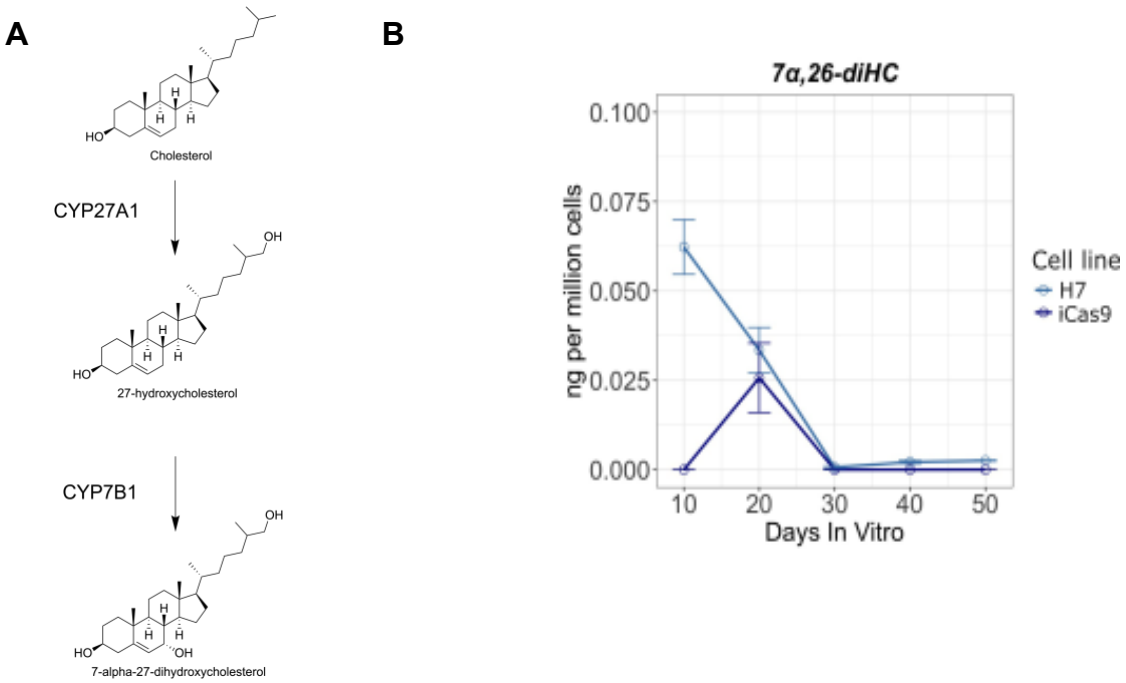

Figure 3.5. Quantification of dihydroxycholesterol 7α, 26-diHC content of neuronal cells. (**A**) Enzymatic formation of 7α, 26-diHC from cholesterol. (**B**) Quantification of monohydroxycholesterols in neural progenitors, neuronal cells and astrocytes derived from H7 and iCas9 hESC lines. Data represent mean from 2 independent experiments, 2-3 technical well replicates, error bar = SEM. Student's t-test, *p<0.05.

3.3.2. Profiling of secreted sterols in cell medium of human stem cell-derived neuronal cultures

To assess the secretion of these sterols, analysis of the cell media of the H7-derived cells was carried out to identify the presence of the sterols identified in the cell pellet and identify any other sterols that may be secreted by these cells. We confirmed the presence of both 24S-HC and 24S,25-EC (**Figure 3.6**). The concentrations of each oxysterol were noted to be lower than that detected in the cell pellet, with 24S-HC ranging from ~0.4-1ng/x10^6 cells and 24S,25-EC at 0.1-1ng/x10^6 cells (**Figure 3.6A & B**). 27-HC was also detected in the cell medium, but interestingly compared to the cell pellet, 27-HC was detectable at all timepoints but at the highest level at DIV10 (**Figure 3.6C**).

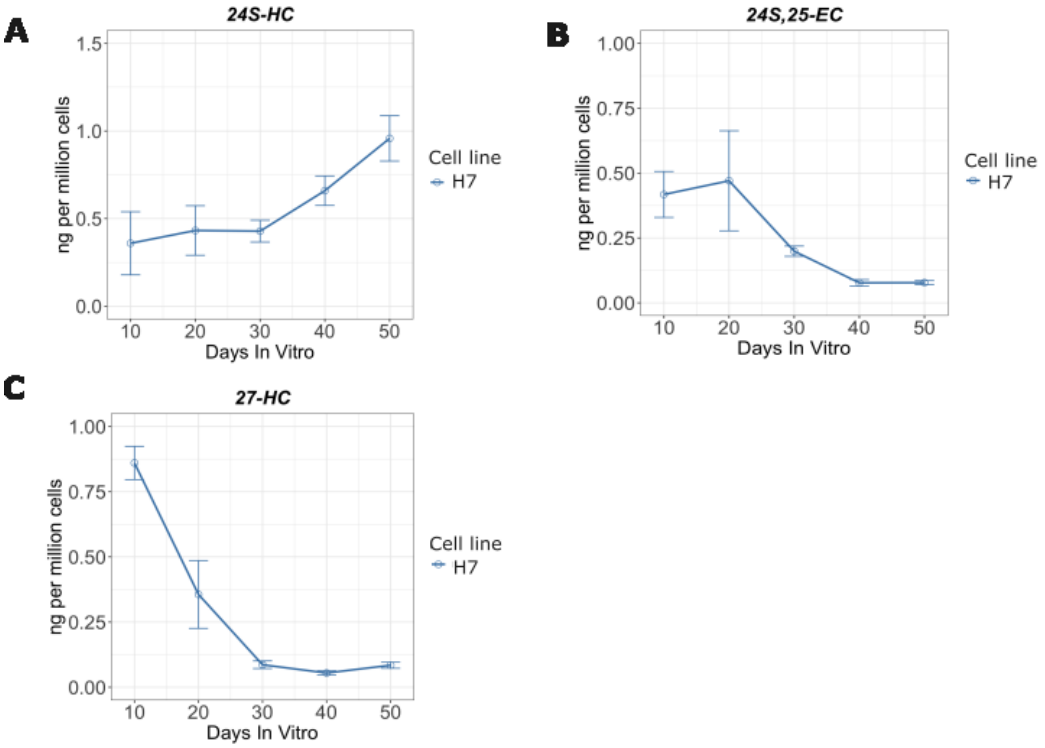

Figure 3.6. Quantification of bioactive oxysterol content of neuronal cell medium. Quantification of levels of (**A**) 7α-hydroxycholesterol, (**B**) 7β-hydroxycholesterol, (**C**) 7-ketocholesterol and (**D**) 6β-hydroxycholesterol in neural progenitors and neuronal cells derived from media taken from H7 hESC lines. Data represent mean from 1 independent experiment, 3 technical well replicates, error bar = SEM.

Further analysis of the monohydroxycholesterol content at mass fragments 534 and 539*m/z* of the media samples confirmed the presence of 7α-hydroxylated sterols previously detected in the cell pellets: 7α-hydroxycholesterol, 7β-hydroxycholesterol, 6β-hydroxycholesterol and 7-ketocholesterol (**Figure 3.7**). Similarly to the results observed for 24S-HC and 24S,25-EC, the levels of the 7α-hydroxylated sterols were all lower than that measured in the cell pellet.

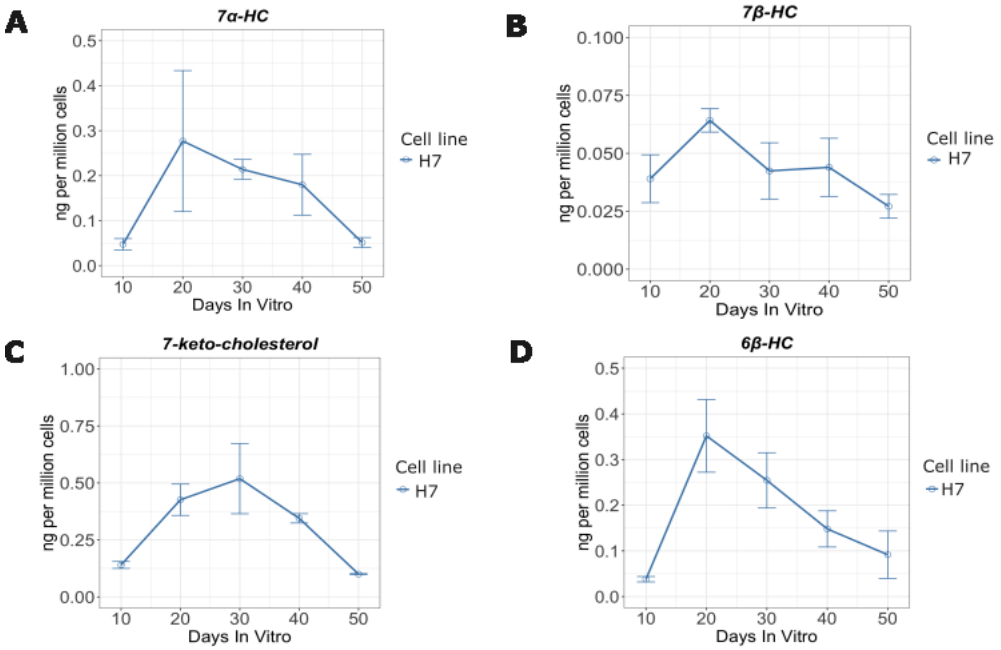

Figure 3.7. Quantification of monohydroxycholesterol content of neuronal cell medium. *Quantification of levels of (**A**) 7α-hydroxycholesterol, (**B**) 7β-hydroxycholesterol, (**C**) 7-ketocholesterol and (**D**) 6β-hydroxycholesterol in neural progenitors and neuronal cells derived from media taken from H7 hESC lines.* Data represent mean from 1 independent experiment, 3 technical well replicates, error bar = SEM.

Analysis of the cell medium confirmed the presence of the dihydroxycholesterol 7α, 26-diHC (**Figure 3.8**). It is to be noted however, that 7α, 26-diHC was observed to be present at a higher level in the cell medium (**Figure 3.8**) at DIV10 (1.500±0.343 ng/x10^6 cells) compared to the concentration in the cell pellet (0.0623±0.00766 ng/x10^6 cells) (**Figure 3.5**). As observed in the cell pellet, the levels of 7α, 26-diHC were also noted to decrease as the neuronal differentiation progressed (**Figure 3.8**).

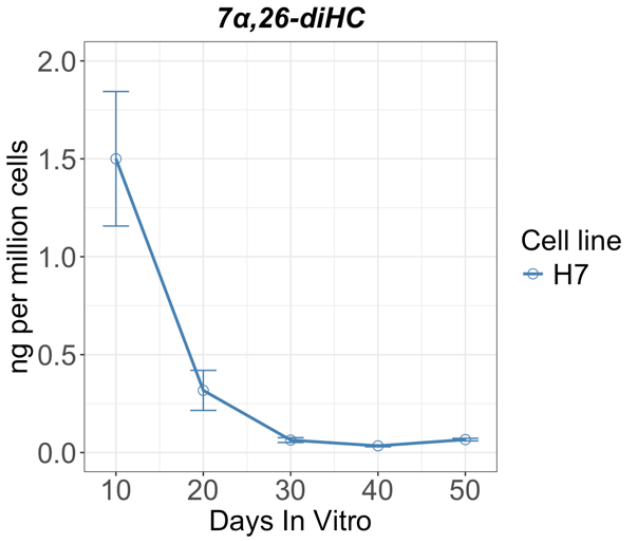

Figure 3.8. Quantification of dihydroxycholesterol 7α, 26-diHC content of neuronal cell medium. Quantification dihydroxycholesterol 7α, 26-diHC levels in neural progenitor and neuronal cell medium derived from H7 hESC line. Data represent mean from 1 independent experiment, 3 technical well replicates, error bar = SEM.

Analysis of the cell medium revealed the additional presence of the cholestenoic acids (25S)-dihydroxycholestenoic acid and 3β, 7α-dihydroxycholestenoic acid, detected at DIV10 at levels of 2.28 ±0.772 ng/x10^6 cells and 8.39±1.880ng/x10^6 cells respectively (**Figure 3.9**). There was also noted to be a decrease in the levels of these sterols after DIV10 (**Figure 3.9**).

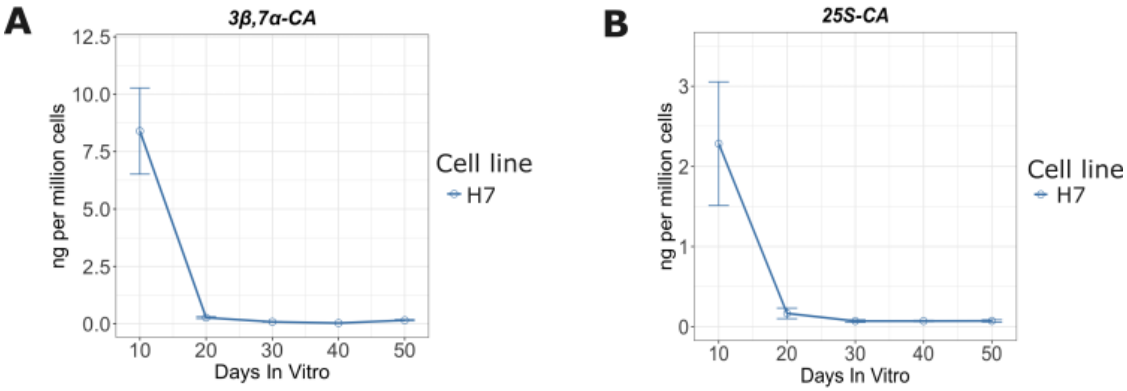

Figure 3.9. Quantification of cholestenoic acid content of neuronal cell medium. Quantification of cholestenoic acids in cell medium derived from H7 and iCas9 hESC lines. Data represent mean from 1 independent experiment, 3 technical well replicates, error bar = SEM.

Finally, to assess activity of each cholesterol biosynthesis pathway, the levels of cholesterol as well as its precursors desmosterol and 8(9)-DHC were quantified, with desmosterol being an intermediate in the Bloch pathway and 8(9)-DHC an intermediate of the K-R pathway in the formation of cholesterol (**Figure 3.10**). Identification and quantification were based on comparison of retention times and mass spectra of known standards. Cholesterol levels were observed to fluctuate over time, however there were noted differences between the levels of cholesterol production across the two cell lines, with higher levels of cholesterol seen in the iCas9-derived cells compared to H7-derived cells at DIV20, and lower at DIV10 and DIV50 (**Figure 3.10C**). These same differences were also observed for cholesterol precursor desmosterol (**Figure 3.10A**). No clear preference was observed for either the K-R or Bloch pathway in these cells, however levels observed for 8(9)-DHC were significantly higher in the H7-derived cells compared to the iCas9 cells (**Figure 3.10B**).

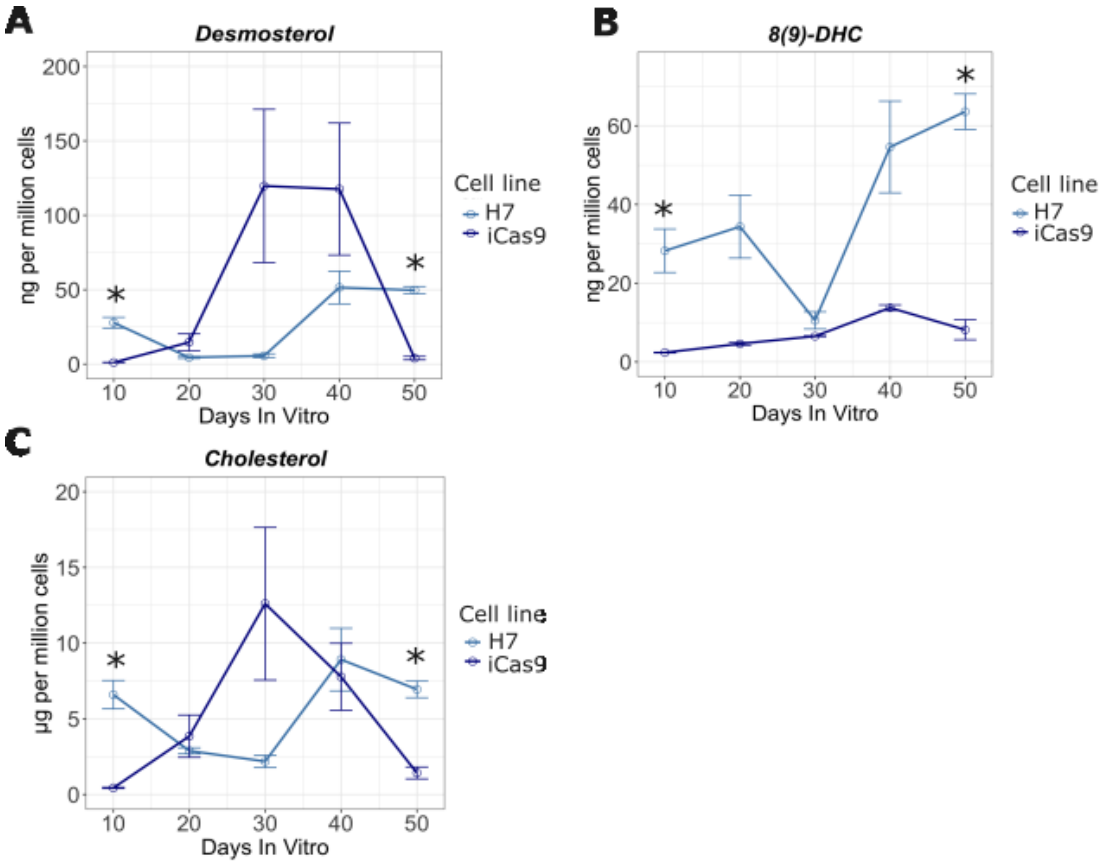

Figure 3.10. Quantification of cholesterol and precursor content of neuronal cells. Quantification of levels of cholesterol precursors (**A**) desmosterol and (**B**) 8(9)-DHC and (**C**) cholesterol in neural progenitors and neuronal cells derived from H7 and iCas9 hESC lines. Data represent mean from 2 independent experiment, 2-3 technical well replicates, error bar = SEM. *p <0.05, Student's t-test.

3.3.3. Protein levels of enzymes involved in cholesterol biosynthesis in hESC-derived cortical neuronal cells

The protein level expression of key cholesterol biosynthetic enzymes was assessed to confirm overall cholesterol biosynthetic activity in these cells. Key enzymes in the cholesterol biosynthetic pathway were selected for analysis, including sterol regulatory element binding protein 2 (SREBP2) and hydroxymethylglutaryl-CoA synthase 1 (HMGCS1), SREBP2 is the master transcription factor of cholesterol biosynthesis, which controls gene expression of enzymes in the cholesterol biosynthetic pathway. Quantification of both the full-length inactive precursor form of SREBP2 and the cleaved n-terminus of SREBP2 were included in the analysis, with the transcriptionally active form of SREBP2-n normalised to total SREBP2 protein detected. HMGCS1 is the precursor enzyme to the mevalonate pathway and rate limiting enzyme of cholesterol biosynthesis.

It was demonstrated that in the H7 hESC-derived cells, both SREBP2 and HMGCS1 protein expression decreased up to DIV40 (**Figure 3.11B & D**). It has been demonstrated that oxysterols downregulate SREBP2 and HMGCR expression (Schroepfer, 2000), and so with the observed increase in 24S-HC over time, it would be expected in these cells the SREBP2 and HMGCS1 gene expression and protein translation would be downregulated. However, the same pattern was not seen in the iCas9-derived cells, although this is also reflected in the differences in 24S-HC production at the same time points. No significant differences in SREBP2 or HMGCS1 protein expression were noted between cell lines.

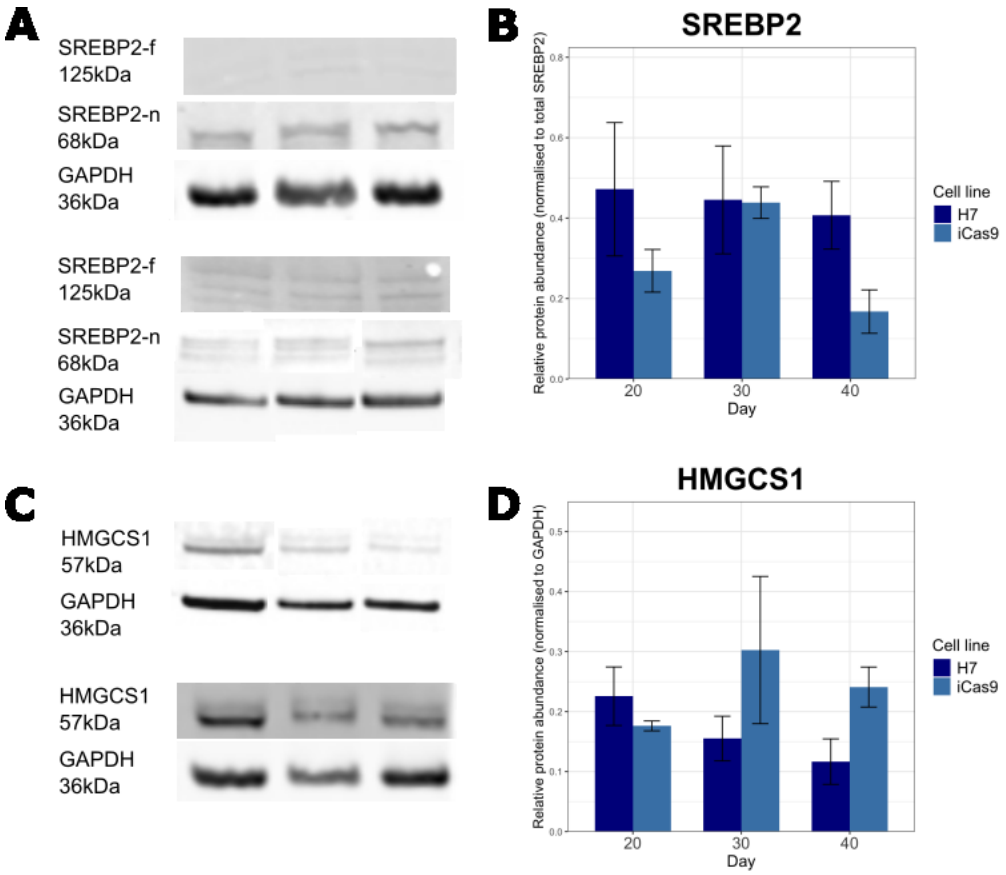

Figure 3.11. Protein expression of key cholesterol biosynthetic enzymes SREBP2 and HMGCS1 in neuronal cells. (**A**) Representative Western blot showing protein levels of mature cleaved transcriptionally active form of SREBP2 (SREBP2-n, 68kDa) and inactive precursor form of SREBP2 (SREBP2-f, 125kDa) in H7 and iCas9 cells. Equal amounts of total protein (10µg per lane) were resolved by SDS–PAGE. (**B**) Semi-quantitative measure of mature SREBP2-n normalised to total SREBP2 protein and GAPDH housekeeping protein. (**C**) Representative Western blot showing protein levels of HMGCS1 in H7 and iCas9 cells. Equal amounts of total protein (10µg per lane) were resolved by SDS–PAGE. (**D**) Relative protein abundance of HMGCS1, normalised to GAPDH. Data represent mean ± SEM from 2 independent experiments, one-way ANOVA, followed by Tukey post-hoc test.

Protein levels were also assessed for 7-dehydrocholesterol reductase (DHCR7) and 24-dehydrocholesterol reductase (DHCR24), the final enzymes in the Bloch and Kandutsch-Russell (K-R) pathways respectively. This analysis revealed similar levels of expression for both enzymes in the H7 line, with both DHCR7 and DHCR24 expression increasing over time, indicating no obvious preference for either pathway (**Figure 3.12B & D**). However, in the iCas9 line there appeared to be contrasting patterns of expression for each enzyme, with increasing expression of DHCR24, whilst the protein level of DHCR7 was observed to decrease over time, and significantly lower at DIV40 compared to the H7 line (**Figure 3.12B & D**).

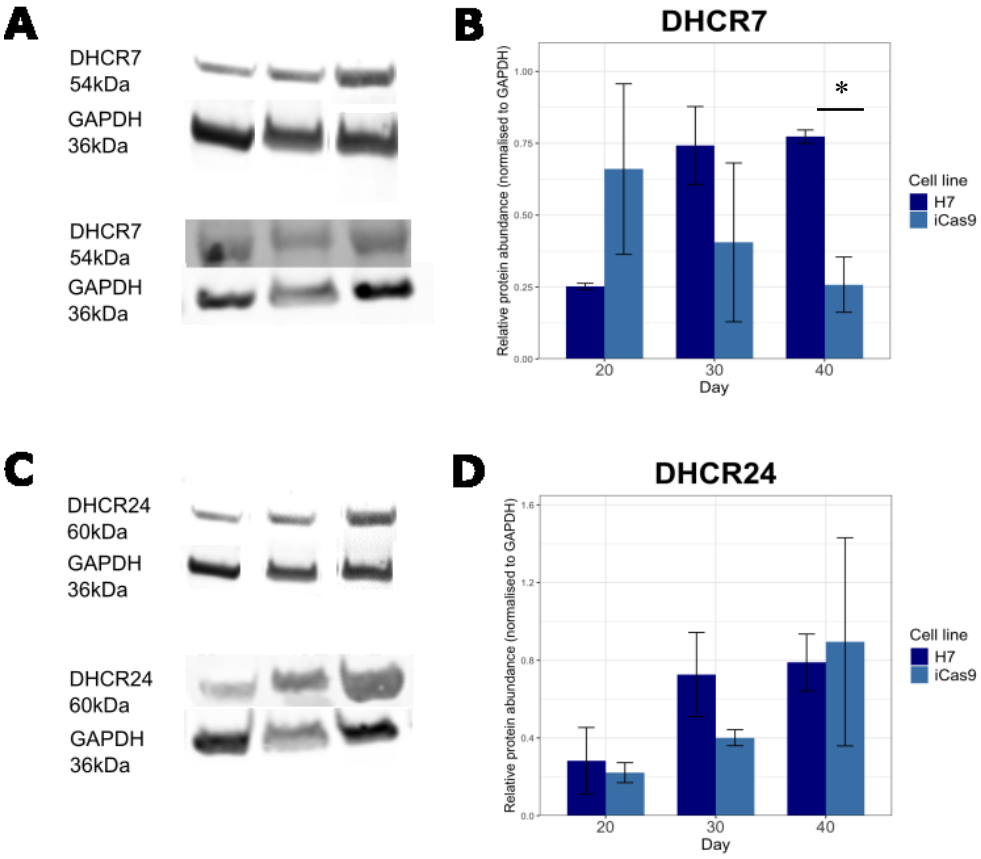

Figure 3.12. Protein expression of cholesterol biosynthetic enzymes DHCR7 and DHCR24 in neuronal cells. (**A**) Representative Western blot showing protein levels of DHCR7 in H7 and iCas9 cells. Equal amounts of total protein (20µg per lane) were resolved by SDS–PAGE. (**B**) Semi-quantitative measure of mature SREBP2-n normalised to total SREBP2 protein and GAPDH housekeeping protein. (**C**) Representative Western blot showing protein levels of DHCR24in H7 and iCas9 cells. Equal amounts of total protein (30µg per lane) were resolved by SDS–PAGE. (**D**) Relative protein abundance of HMGCS1, normalised to GAPDH. Data represent mean ± SEM from 2 independent experiments. Error bars=SEM, *p>0.05, one-way ANOVA, followed by Tukey post-hoc test.

3.4. Discussion

The importance of the role of cholesterol metabolism during human neural development has been highlighted by the finding that many inborn errors in cholesterol metabolism feature neurodevelopmental defects (Porter and Herman, 2011). Cholesterol and oxysterols have been evidenced to interact with key signalling pathways involved in cortical development, and errors in the synthesis and metabolism of cholesterol are implicated in several neurodevelopmental conditions. There is a need to further understand the production of these molecules during human neural development, however this is difficult to achieve in human developmental studies utilising foetal tissue, and thus much evidence has been derived from animal models and primary cell culture. Hence, this study reports for the first time a characterisation of the temporal profile of cholesterol and oxysterols in a stem cell model of human cortical development.

3.5.1.Monohydroxycholesterol production during cortical neurogenesis in vitro

24S-HC, also referred to as “cerebrosterol” is the dominant oxysterol found in the adult human brain. However, studies of embryonic rodent brain tissue suggest that during development other oxysterols may predominate, with evidence that 24S-25-EC levels are higher during rodent embryonic development (Wang et al., 2009a). Here, it is noted that in neuronal cells during cortical development 24S-HC levels increase as cortical neuronal identity is determined (**Figure 3.3B**) and appears to be overall higher than 24S,25-EC levels. Here, findings are focused on *in vitro* cortical neuronal

cultures, rather than embryonic brain tissue samples in which the individual cell types responsible for 24S,25-EC production cannot be determined.

In our analysis, it was noted that there were notable differences in 24S-HC production between the two cell lines at the latest timepoint in the neuronal differentiation. This may be due to the different rates of differentiation observed between the lines. An interesting potential factor underlying these differences may be the effect of sex differences on lipid profiles. However, as these lines are from male and female donors, with the female-derived H7 line and male-derived iCas9 line, sex differences may contribute to these observed differences, with multiple studies providing evidence for sex differences in the production of 24(S)-HC and 27-HC (Burkard et al., 2007; Chiappelli et al., 2020; Parrado-Fernandez et al., 2021).

3.5.2. Presence of oxysterols secreted into cell culture media

Further assessment of the secreted sterols in the cell culture media confirmed that cortical neurons can both produce and secrete 24S-HC. Monohydroxy sterols are able to cross plasma barriers through simple diffusion, with 24S-HC having previously been identified in human plasma at levels of ~5-6ng/mL (free oxysterol levels) whilst found to be present in human CSF at levels of ~0.02ng/mL (Griffiths et al., 2013). For comparison, it was identified here following a 48-hour incubation that 24S-HC was present in the cell culture media at concentrations ranging from 0.05-0.25ng/mL throughout the cortical neuronal differentiation. Interestingly, it was further noted that these cells release a higher level of 7α,26-dihydroxycholesterol (also known as cholest-(25R)-5-ene-3β,7α,26-triol)

into the media at DIV10, which corresponds to the neural epithelial cell rich stage of the differentiation, with 7α,26-dihydroxycholesterol found to be present at levels of ~1.1ng/mL (**Figure 3.8**). However, by the more neuronal rich stages of the differentiation i.e. DIV50, these levels drop to ~0.09ng/mL (**Figure 3.8**). This sterol has been evidenced to be present in human plasma at ranges of ~3-5.5ng/mL, but has not identified in human CSF (Griffiths et al., 2013). Interestingly, this oxysterol has been recently linked with inhibition of mDA neurogenesis (Hennegan et al., 2023), but its effect on cortical neurogenesis remains to be determined.

3.5.3. Synthesis of Cholesterol through the Kandutsch-Russell and Bloch Pathway during cortical development in vitro

Next, through analysis of key cholesterol biosynthetic enzymes on both the gene and protein level, we were able to determine the cholesterol biosynthetic activity of the neuronal cells. From this analysis, it was suggested that there were differences in the activity of the Bloch and K-R pathways. It was observed that both DHCR7 and DHCR24 gene and protein expression increased as neuronal differentiation progressed in the H7-derived cells, however in the iCas9-derived cells we observed a less clear pattern (**Figure 3.12**). In the iCas9-derived cells, DHCR24 expression increased over time on both the protein and gene level, however whilst gene expression levels of *DHCR7* increased over time, this was not reflected in the protein level expression. Similar differences were seen with SREBP2 and HMGSC1 protein expression, whilst on the mRNA level both were shown to increase over time.

There remains some debate over which cholesterol biosynthetic pathways is preferred by neurons. It has previously been hypothesised that neurons rely on the K-R pathway for the production of cholesterol (Nieweg et al., 2009; Zhang and Liu, 2015). However, it has also been argued that neurons preferentially use the Bloch pathway (Genaro-Mattos et al., 2019). Here, similar levels of 8(9)-DHC and desmosterol were observed in the neuronal cells derived from the H7 hESC line. However, much higher levels of desmosterol were observed in the iCas9 derived line. It is possible that there may also be differences in the preferred cholesterol biosynthetic pathways preferred between neuronal cell subtypes i.e. mature neurons and neural progenitors, with the differences noted in differentiation dynamics between the cell lines. However, due to the large variation observed in the iCas9 line, further independent experiments would be required to confirm these findings.

3.5.4. Limitations

The cultures assessed here are not purely neuronal, containing mixed populations of neural progenitors and neurons. Therefore, it cannot be confirmed the sterol profiles within the individual cell subtypes, but the sterols produced at these stages of cortical development *in vitro*. With ongoing developments in single-cell proteomics/lipidomic techniques, there is potential that individual cells could be analysed using single-cell mass spectrometry (scMS). This used in combination with derivatisation techniques allows for the potential to enable confirmation of oxysterols produced in individual cells (Li et al., 2021; Tajik et al., 2022).

It was also noted that there were differences in the levels of certain sterols between the two control lines utilised in this study. This may be due to several factors, including the slight difference in rates of differentiation observed between the lines including the increased NeuN expression in iCas9 lines observed at earlier timepoints (**Figure 3.1**). Interestingly, recent analysis comparing the proteomes of different cell lines has shown differences between proteomes of different cell lines, including proteins involved in lipid metabolism (Geiger et al., 2012). Additionally, with these 2 lines taken from male and female donors, sex differences may also be a contributing factor to these observed differences, with multiple studies providing evidence for sex differences in the production of 24S-HC and 27-HC (Burkard et al., 2007; Chiappelli et al., 2020; Parrado-Fernandez et al., 2021). Additionally, several studies of the lipid profiles of cord blood from newborns have also shown differences in both the levels of cholesterol, with female infants found to have higher total cholesterol levels in cord blood compared to male infants (Felzer-Kim et al., 2020). Therefore, further analysis of additional cell lines would aid in confirming if these differences are indeed due to sex differences, and to what extent the range of variation in sterol levels exists between cell lines.

3.5.5. Impact

This work provides for the first time a characterisation of the temporal sterol profile of a model of human cortical neurogenesis *in vitro*. This provides information on the sterols produced during human cortical development, which can be used to confirm what sterols are produced endogenously that may interact with signalling pathways relevant to human neural

development. This sterolomic profile of control cells can further be used to compare to models of neural developmental disorders and for assessment of the effects of disordered cholesterol metabolism.

3.5.6. Further work

Whilst important to have evidence of the presence of these sterols endogenously in human neural development, it remains to be confirmed that they are also contributing to neural developmental processes in this *in vitro* model. It would need to be assessed whether altering the levels of these molecules results in changes in expression of key target genes/proteins involved in neural developmental signalling pathways, such as Hh and Wnt signalling. However, it must be noted that conventional knockdown approaches may be difficult as both cholesterol biosynthesis and metabolic pathways share the same enzymes to produce various sterols and so this approach would result in the production of multiple sterols being inhibited.

Whilst this work focuses on the sterolomic profiles of cortical neurons, other neuronal cell types remain to be characterised. These include other neuronal subtypes, as well as glial cells. Of note, microglia are essential to the non-enzymatic phagocytosis-mediated clearance of cholesterol, and supply of exogenous cholesterol results in altered expression of key genes responsible for their survival and phagocytic capacity. Microglia have been shown to express high levels of the enzyme CH25H, which is responsible for the production of 25-hydroxycholesterol (25-HC) and is recognised to be the major source of this oxysterol in the brain (Cyster et al., 2014). 25-HC is categorised as an immune oxysterol and is involved in inflammatory

responses through its activation of immune cells and enhanced production of inflammatory mediators such as IL-1β (Gold et al., 2014; Kim et al., 2014; Son et al., 2013). Furthermore, microglia have been implicated in the regulation of both astrocyte lipid metabolism and APOE secretion through 25-HC-induced activation of LXR- and inhibition of SREBP2-mediated gene expression (Cashikar et al., 2023). Additionally, GC-MS analysis of oligodendrocytes and Schwann cells has confirmed production of the monohydroxysterols 24S-HC, 25-HC and 27-HC (Shackleford et al., 2013a). It has been implicated that the oxysterol 25-HC may establish a crosstalk mechanism between Schwann cells and Wnt/β-catenin signalling via interaction with LXRs (Shackleford et al., 2013a). Thus, it would be interesting to further investigate the sterols expressed in these glial cell populations during *in vitro* development. It is also interesting to speculate whether these cells would demonstrate differences in sterol levels in conditions featuring inborn error of cholesterol metabolism and whether changes in these sterol levels may contribute to the pathogenesis of developmental defects.

3.5.7. Conclusions

This study has generated the first temporal sterol profile of cholesterol, its direct precursors and oxidised metabolites, known as oxysterols, in an *in vitro* model of human cortical development. Furthermore, it has also assessed the gene and protein level expression of key enzymes involved in cholesterol biosynthesis and metabolic pathways. This has provided a characterisation of human cortical neural development, providing information on both the endogenous sterols produced during human

cortical development as well as the expression of key cholesterol biosynthetic enzymes on both the gene and protein level.

There is a high level of interest in these molecules' role in neural development due to the evidence of an interaction of these molecules with key nuclear receptors and GPCRs involved in neurodevelopmental signalling pathways as well as the association between altered cholesterol metabolism and neural developmental disorders. Additionally, due to their ability to cross the BBB, these molecule may provide therapeutic potential. Further investigation of their role in the pathogenesis of neural developmental defects is therefore an exciting avenue for further study.

Chapter 4

Altered levels of CYFIP1 results in dysregulated cholesterol metabolism in stem-cell derived cortical neuronal cultures

4.1. Background

It is evidenced that the dysregulation of cholesterol biosynthesis or metabolism results in various forms of neurological dysfunction, including an association with various neurodevelopmental defects. It has been shown that levels of certain metabolites of cholesterol, including oxysterols, are altered in the analysis of plasma and CSF of individuals with ASDs (Grayaa et al., 2018; Sun et al., 2021) and schizophrenia (Messedi and Makni-Ayadi, 2024; Moreno et al., 2025). However the exact biological mechanisms underpinning this difference remains unknown for a large proportion of these disorders. The most well-described syndrome associated with neurodevelopmental defects featuring alterations to cholesterol metabolism is Smith-Lemli-Opitz syndrome (SLOS) (Tomita et al., 2022), which is caused by a mutation in the *DHCR7* gene resulting in reduced cholesterol biosynthesis.

Whilst there are several reported studies of altered levels of cholesterol metabolites in human serum in cases of different neurodevelopmental conditions, it is not fully understood how alterations to cholesterol biosynthesis and metabolism are associated with the observed neurodevelopmental deficits. As neurodevelopmental defects can be the result of either genetic, environmental or idiopathic causes, a better understanding of the underlying pathogenesis for these underlying causes may provide further information on how this relates to the altered cholesterol metabolism.

This chapter focuses on the 15q11.2 copy number variant (CNV), which features microdeletions or duplications of a region of the chromosome containing the *CYFIP1* gene. Previous work in our lab has indicated that *in vitro* models featuring altered CYFIP1 levels result in both altered cortical neurogenesis and dysregulated cholesterol metabolism (Fuente et al., 2024). Here we aim to characterise the temporal sterol profiles of cells undergoing cortical neurogenesis in an attempt to further understand how neural developmental defects in both patient cells and genetic models are associated with altered cholesterol metabolism.

Of the genes located in the 15q11.2 deletion, whilst little is known of the function of these in mammalian neural development, *CYFIP1* has been associated with increased risk of both autism spectrum disorder (ASD) (Noroozi et al., 2018) and schizophrenia (Domínguez-Iturza et al., 2019). Patients with duplication of the 15q11.2 region who also present with an ASD have been specifically demonstrated to have upregulated CYFIP1 mRNA levels (Nishimura et al., 2007; Oguro-Ando et al., 2015), suggesting this gene may play a role in the neuropsychiatric phenotype observed.

The use of animal models for the study of CNVs is challenging due to the duplication and deletion of large areas of the chromosome spanning multiple genes. With increasing developments in generation of iPSC-based models of cortical development, these models offer the opportunity to investigate the cellular phenotype of patient-derived cells carrying these mutations. Previous research by Yoon and colleagues observed that neural differentiation of iPSCs from 15q11.2del patients resulted in disrupted neural rosette formation at the neural progenitor stage (Yoon et al., 2014).

This was supported by evidence from the developing mouse cortex, where CYFIP1 deficiency was shown to result in abnormal migration of radial glia and NPCs, resulting in the ectopic localization of radial glia outside the VZ (Yoon et al., 2014).

A recent study carried out in our lab indicated that altered levels of CYFIP1 in cortical neural progenitors results in altered cholesterol biosynthesis and metabolism (Fuente et al., 2024). Cell lines were previously generated from hESC lines featuring knockout of CYFIP1 (CYFIP1-LoF) and overexpression of CYFIP1 (CYFIP1-GoF) respectively. iPSC lines were additionally generated from two patients with 15q11.2del syndrome (referred to here as EA008 and EA062), with 2 clones generated per line. A study carried out utilising these cell lines revealed that in vitro differentiation of these human pluripotent stem cells (hPSCs) into cortical neurons demonstrated pronounced deficits in neural progenitor maintenance and neuronal differentiation, with overexpression of CYFIP1 leading to a bias toward proliferation and self-maintenance whilst knockout of CYFIP1 and the 15q11.2del cells underwent premature neuronal production (Fuente et al., 2024). Furthermore, bulk RNASeq analysis of these cells was previously carried out at neural progenitor and neuronal stages to assess any changes in gene expression (Fuente et al., 2024). Transcriptomic analysis of cortical progenitor and neuronal cells derived from iPSC lines generated from individuals carrying 15q11.2del and the CYFIP1-LoF and CYFIP1-GoF hESC-derived lines revealed cholesterol metabolism as one of the top altered biological functions in these cells (Fuente et al., 2024). This analysis also revealed mirror differences in LXRβ target gene expression between 15q11.2del and CYFIP1 overexpressing

neural progenitors (Fuente et al., 2024). LXRβ signalling has previously been shown to be essential for cortical patterning and migration of late-born cortical neurons (Fan et al., 2008). Moreover, modulation of LXRβ signalling by the oxysterol 24S,25-EC has been demonstrated to enhance midbrain dopaminergic neurogenesis and promote dopaminergic differentiation of embryonic stem cells in vitro (Theofilopoulos et al., 2013). This led to the hypothesis that oxysterol-mediated LXRβ signalling may underpin the phenotype observed in both the 15q11.2del and CYFIP1 neural progenitors.

4.2. Aims

From the previous work carried out in our lab, it has been indicated that cholesterol metabolism is altered in CYFIP1-altered cells undergoing cortical neurogenesis. However, the sterol profiles of these cells remain to be characterised, and thus how alterations to cholesterol metabolism in these cells may relate to the changes to cortical neurogenesis and LXRβ signalling observed.

This chapter will investigate how alterations in CYFIP1 levels results in altered cholesterol metabolism in these cell lines undergoing cortical neurogenesis *in vitro*. This will be addressed through:

- Generation of *in vitro* cortical neuronal cultures using pre-established CYFIP1-altered hESC lines, containing either a knockout of CYFIP1 (CYFIP1-LoF) or expressing CYFIP1 at approximately double the level observed in wild type (CYFIP1-GoF), and their respective controls.

- Immunocytochemical analysis to confirm differentiation of these lines results in altered cortical neurogenesis, confirming a bias toward proliferation in the CYFIP1-GoF and accelerated neuronal differentiation in the CYFIP1-LoF.
- Carry out additional analysis of the pre-existing published RNASeq dataset generated from the same cell lines to assess any differential expression of genes encoding key cholesterol biosynthetic and metabolic enzymes.
- Confirm any changes in protein expression of key enzymes involved in cholesterol biosynthesis to gain insight into any alterations compared to controls. This also aims to address whether the activity of each branch of the cholesterol biosynthetic pathway is affected in these cells.
- Quantify the sterol content of samples at each stage of cortical neuronal differentiation to assess if sterol profiles are significantly different in CYFIP1-altered lines.
- Further characterisation of the sterol profiles of cortical neurons generated from two 15q11.2del patients for further comparison to hESC models.

These findings seek to uncover how cholesterol metabolism is altered in these CYFIP1-altered cells, and provide candidate sterols that may be associated with the altered cortical neurogenesis and LXRβ signalling observed in these cells. This study also provides the first sterol profiling of neural cells generated from 15q11.2del patients.

4.3. Results

4.3.1. Generation of hPSC-derived cortical neuronal cell cultures derived from CYFIP1-altered lines

We first aimed to confirm altered cortical neurogenic phenotypes previously observed in the CYFIP1-altered lines by our group, as well as confirm cell population identity at the different timepoints in the differentiation collected for protein and LC-MS^n analysis. Immunocytochemical analysis of key markers of neural progenitors, neuronal cells and specific cortical markers were used to assess cell subtype-specific identity throughout the *in vitro* differentiation, to confirm defects in cortical neurogenesis in the CYFIP1-altered lines and their respective controls. Initial analysis was carried out to confirm that the starting hESC cultures showed similar levels of pluripotency, demonstrating both the CYFIP1-altered lines and their respect controls both highly express the pluripotency markers OCT4, NANOG and SOX2 (**Supplementary Figure 7.1 & 2**).

Analysis of neural progenitor and neuronal markers enabled the confirmation of the neurodevelopmental phenotypes of the CYFIP1-altered lines determined by previous studies in our lab (Fuente, et al. 2024). This was determined by significantly increased PAX6+ cells in the CYFIP1-GoF cells compared to controls at D30 and D40 of the differentiation, which would indicate a bias towards proliferation (**Figure 4.1B**). However, we noted significantly less PAX6+ at DIV10 in the CYFIP1-LoF cultures compared to the iCas9 control line (**Figure 4.1B**).

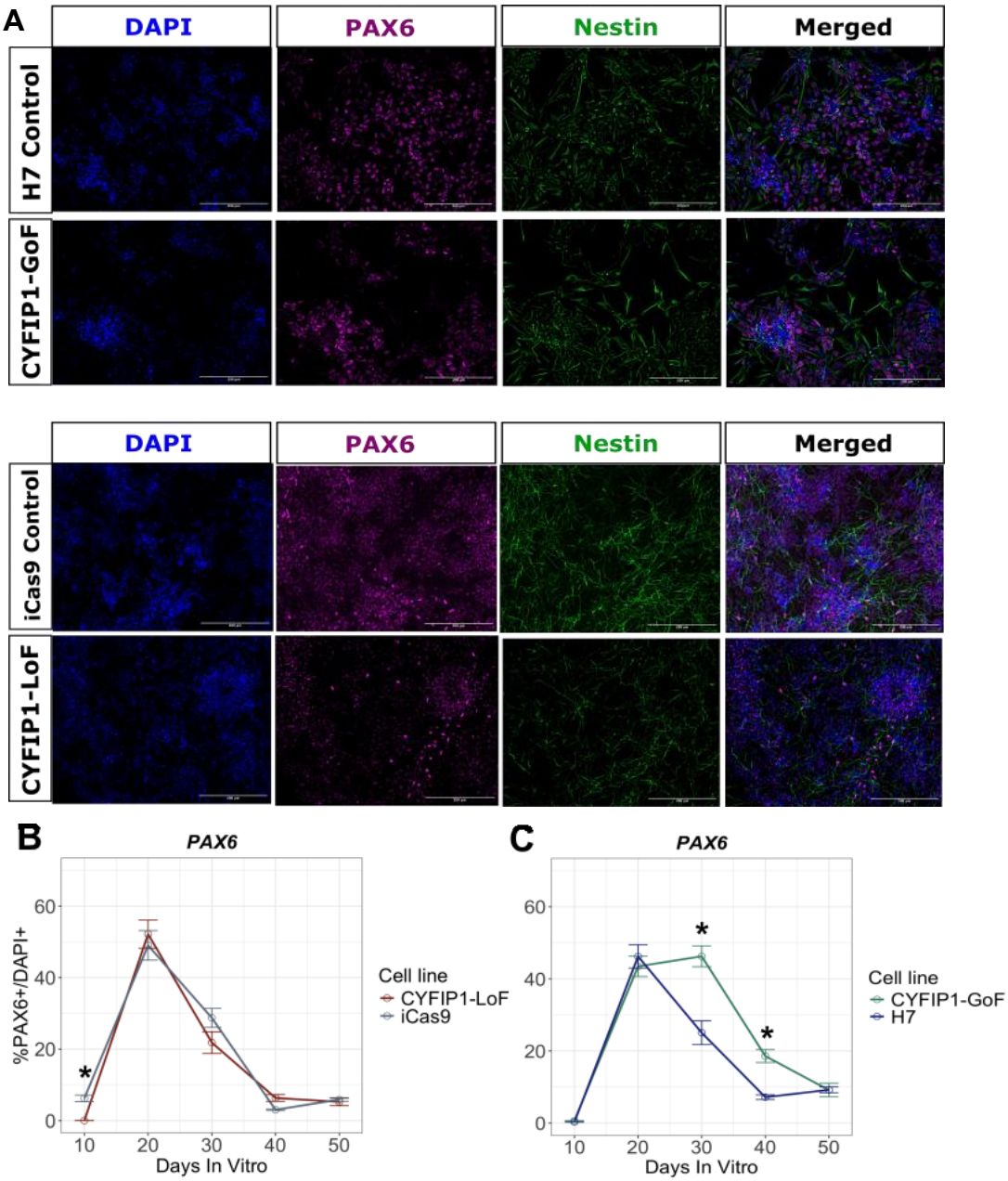

Figure 4.1. CYFIP1-altered cells demonstrate differences in cortical neural progenitors. (**A**) Nestin+ and PAX6+ neural progenitors at 20 DIV in CYFIP1-altered lines and respective controls. Quantification of PAX6+ cells in (**B**) CYFIP1-LoF and (**C**) CYFIP1-GoF cells and respective controls. Results of 2 independent experiments, 3 technical well

replicates. Results presented as mean ± SEM. Groups were compared by Student's t test between the CYFIP1-manipulated vs. isogenic control at each time point, *p<0.05. 20X objective. Scale bar 200μM.

In terms of neuronal cell markers, CYFIP1-LoF cells were found to have increased percentage of cells expressing the nuclear neuronal marker NeuN at earlier stages of the differentiation compared to controls, which would indicate accelerated neuronal production (**Figure 4.2A & C**). The CYFIP1-GoF lines demonstrated a decreased percentage of NeuN+ cells at DIV40 (**Figure 4.2B & D**). Overall, this analysis supports previous findings that the CYFIP1-LoF cells display accelerated neuronal differentiation, whilst the CYFIP1-GoF cells exhibit a bias toward proliferation.

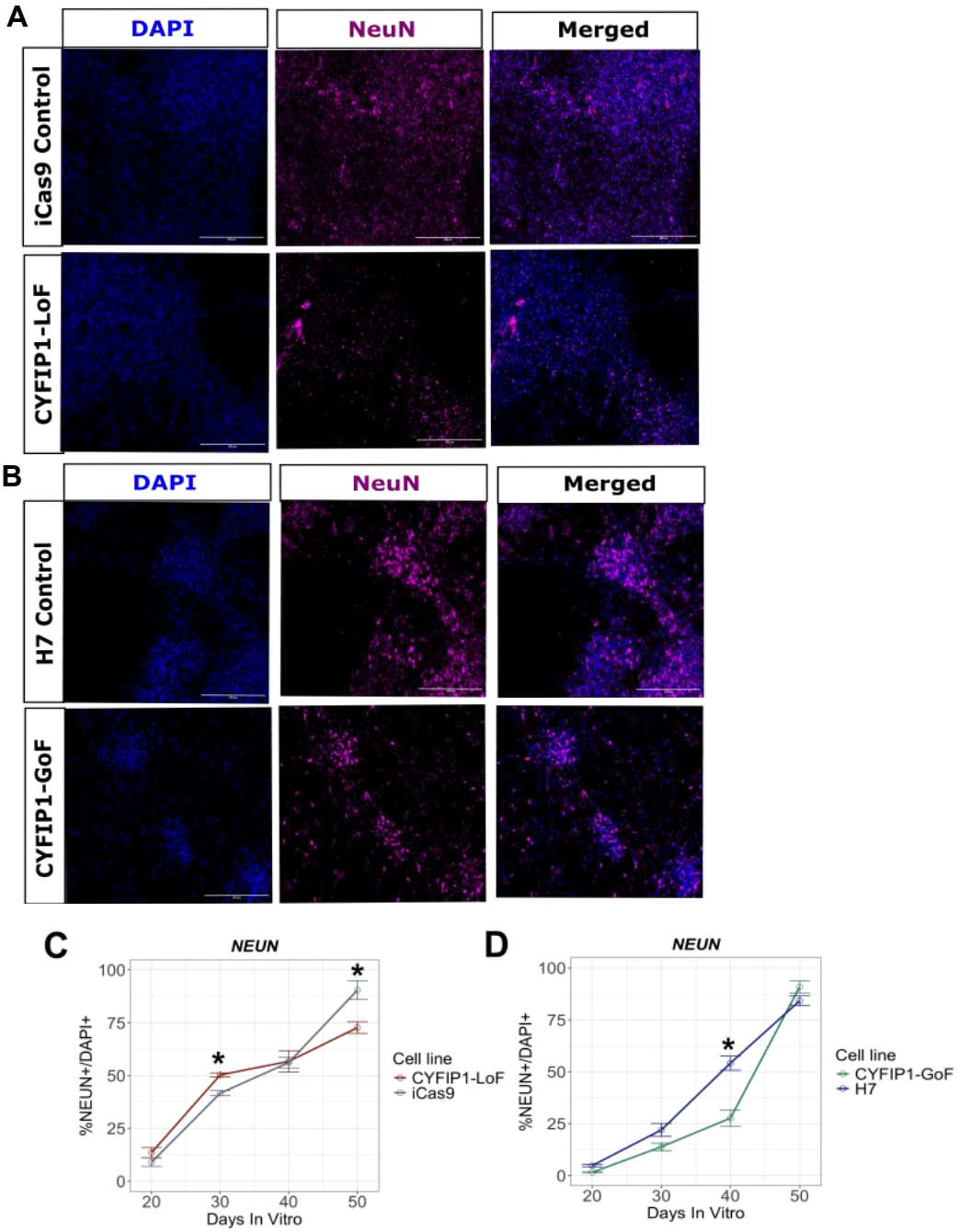

Figure 4.2. CYFIP1-altered cells demonstrate differences in neurogenesis. NeuN+ cells in (**A**) CYFIP1-LoF and (**B**) CYFIP1-GoF cells at DIV40. Percentage of NeuN+ cells normalised to DAPI+ cell counts in (**C**) CYFIP1-LoF and (**D**) CYFIP1-GoF cells compared

to their respective controls. Results presented as mean ± SEM. Groups were compared by Student's t test between the CYFIP1-manipulated vs. isogenic control at each time point, *p<0.05. 20X objective. Scale bar 200μM.

We further assessed the expression of cortical layer markers TBR1 and CTIP2 in these cells to assess any changes in the cortical cell population (**Figure 4.3**). We were consistently able to detect TBR1 and CTIP2 expression, markers of corticothalamic projection neurons in layer VI and cortical projection neurons in layer V respectively (**Figure 4.3A & B**). We observed an increase in the expression of TBR1 and CTIP2 as the differentiation progressed in all cell lines, however CYFIP1-GoF lines demonstrated significantly decreased expression of both CTIP2 and TBR1 compared to the parent H7 control lines (**Figure 4.3D & F**). A less clear pattern was observed for the CYFIP1-LoF line, which displayed similar levels of CTIP2+ expression to the iCas9 control line and lower levels of TBR1+ expression at the NPC stage of the differentiation paradigm (**Figure 4.3C & E**).

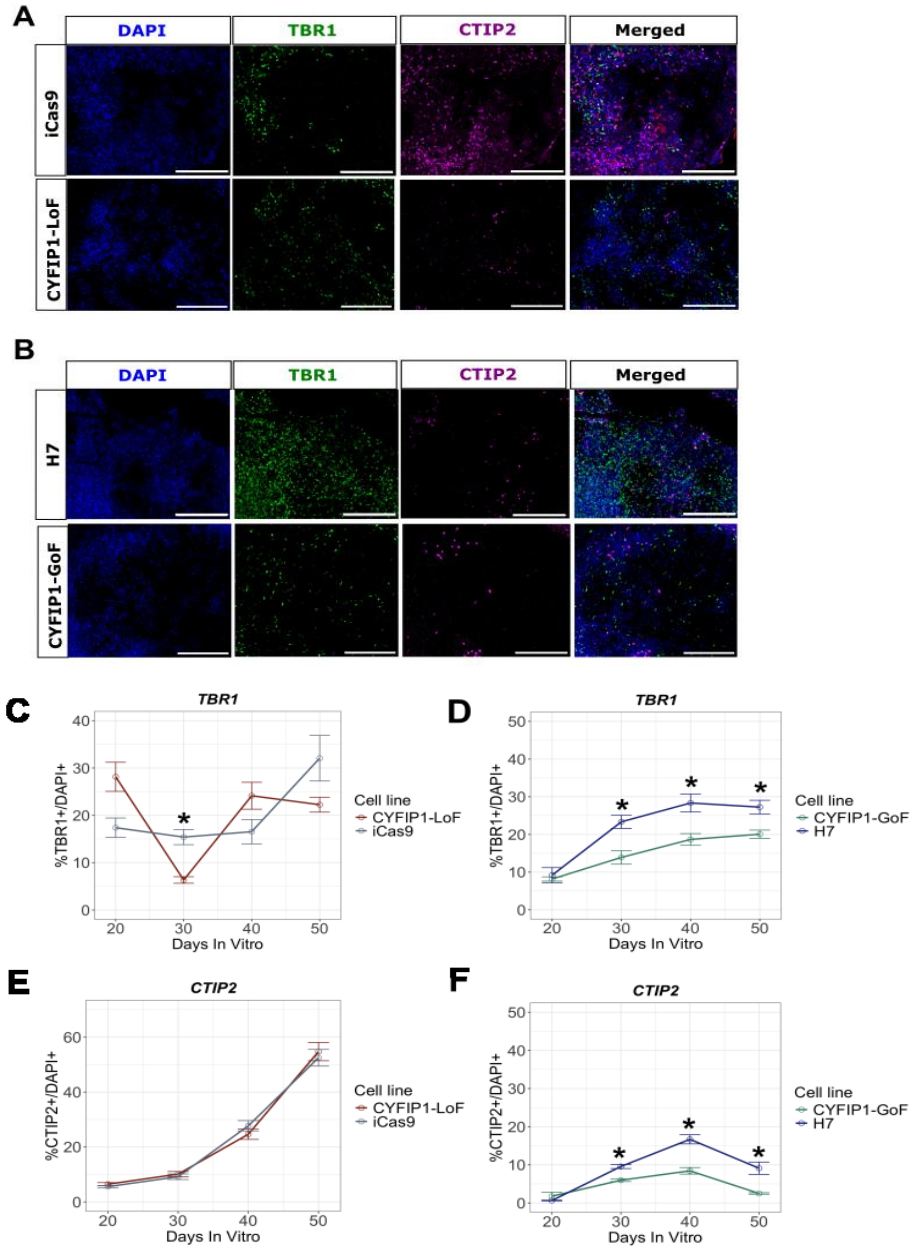

Figure 4.3. CYFIP1-altered cells demonstrate differences in cortical neurogenesis. (A & B) CTIP2 and TBR1 expressing cells in CYFIP1-LoF andCYFIP1-GoF cells at 40 DIV. Percentage of CTIP2+ cells normalised to DAPI+ cell counts in (C) CYFIP1-LoF and (D) CYFIP1-GoF cells compared to respective controls. Percentage of TBR1+ cells

normalised to DAPI+ cell counts in (E) CYFIP1-LoF and (F) CYFIP1-GoF cells compared to respective controls. Results presented as mean ± SEM. Groups were compared by Student's t test between the CYFIP1-manipulated vs. isogenic control at each time point, *p<0.05. 20X objective. Scale bar 200μM.

4.3.2. CYFIP1-altered lines demonstrate differences in expression of key genes involved in cholesterol biosynthesis and metabolism

Following previous findings from transcriptomic analysis of CYFIP1-altered cells undergoing neurogenesis, which revealed cholesterol metabolism to be a significantly altered pathway in CYFIP1-altered lines (Fuente et al., 2024), it remains to be determined the exact underlying differences in either the cholesterol biosynthetic or metabolic pathways affected. Therefore, we have carried out a further analysis of the pre-existing bulk RNAseq dataset generated from these cell lines by previous lab members Dr Daniel Cabezas de la Fuente and Dr Claudia Tamborini (Fuente et al., 2024) to investigate any differential gene expression of genes involved in cholesterol biosynthesis and metabolism. This RNA-sequencing was performed on the CYFIP1-GoF and CYFIP1-LoF lines and their respective parental control cells at three time points of cortical neural differentiation, representing and early NPC (NPC1, DIV10), peak NPC and onset of neurogenesis (NPC2, DIV20), and neuronal rich (neuronal, d40) stages, respectively.

Significant differences in the expression of several key genes (FDR padj > 0.05) involved in the cholesterol biosynthetic pathway were observed in the CYFIP1-altered lines compared to controls, with fold change expression for

these genes detailed in **Figure 4.4**. Identified differentially expressed genes (DEGs) included the *SREBF2* gene encoding SREBP2, the master transcription factor of cholesterol biosynthesis, which was found to be downregulated in the CYFIP1-GoF cells at the early NPC and neuronal stages compared to control (**Figure 4.4A**). *HMGCR*, encoding the rate-limiting enzyme HMG-CoA reductase, was observed to also be downregulated at both the NPC and neuronal stages in the CYFIP1-GoF lines (**Figure 4.4A**). Interestingly, in the CYFIP1-LoF line, *SREBF2* was not found to be differentially expressed at the early NPC stage or neuronal stages, but was upregulated at the later NPC stage (**Figure 4.4A**). However, whilst downregulated at the early NPC stage, *HMGCR* was found to be upregulated at both the late NPC and neuronal stages in the CYFIP1-LoF cells (**Figure 4.4A**).

Genes involved in either the Bloch and K-R biosynthetic pathways of cholesterol biosynthesis were investigated to assess any differences between the CYFIP1-altered lines and their respective controls. Assessment of *DHCR7* and *DHCR24*, which encode the enzymes involved in the final stages of cholesterol biosynthesis as part of the Bloch and K-R pathways respectively, revealed further differences between the CYFIP1-altered lines and their respective controls. Interestingly, *DHCR24* and *DHCR7* were both downregulated at the early NPC stage and upregulated at the late NPC stage in both the CYFIP1-GoF and CYFIP1-LoF lines compared to their controls (**Figure 4.4A**).

The most obvious differences in cholesterol biosynthetic enzyme expression when comparing DEGs between the CYFIP1-GoF and CYFIP1-

LoF and their respective controls was at the neuronal stage, where all cholesterol biosynthetic genes analysed were found to be downregulated in the CYFIP1-GoF line (**Figure 4.4A**). Meanwhile, in the CYFIP1-LoF line, *EBP*, *HMGCR*, *MVD* and *SC5D* were all found to be upregulated, whilst *LSS,* which encodes an enzyme involved in 24S,25-EC synthesis*,* was downregulated compared to its parental control line (**Figure 4.4A**).

In terms of genes directly involved in cholesterol metabolism, differential gene expression was noted for several CYP P450 enzymes responsible for oxysterol production. *CYP46A1*, which encodes the enzyme responsible for both 24S-HC from cholesterol and 24S,25-EC production from desmosterol, was found to be downregulated in the CYFIP1-GoF line (**Figure 4.4B**). *CYP46A1* however was not found to be differentially expressed in the CYFIP1-LoF cells at either the NPC or neuronal stages (**Figure 4.4B**).

CYP51A1 encodes the enzyme involved in catalysing removal of the C-14a methyl group from lanosterol, the demethylation step at the initial point for transformation of lanosterol to bioactive sterols. *CYP51A1* was found to be downregulated at all points assessed in the CYFIP1-GoF cells (**Figure 4.4B**). In the CYFIP1-LoF lines, a less clear pattern was observed, with CYP51A1 found to be downregulated at the early NPC1 stage and upregulated at the NPC2 stage (**Figure 4.4B**).

CYP39A1, which encodes the enzyme involved neural cholesterol clearance and in the production of bile acids from 24S-HC, 27-HC and 25-HC, was found to be upregulated in the CYFIP1-GoF cells at the neuronal

stage of the differentiation (**Figure 4.4B**). However, *CYP39A1* was not found to be differentially expressed in the CYFIP1-LoF cells at any of the time points analysed (**Figure 4.4B**).

CYP27A1, which encodes the enzyme responsible for 27-HC production from cholesterol, was found to be upregulated at the late NPC stage in the CYFIP1-GoF cells and downregulated at the same timepoint in the CYFIP1-LoF cells (**Figure 4.4B**). However, at the early NPC and neuronal stage, *CYP27A1* was found to be upregulated in the CYFIP1-LoF cells (**Figure 4.4B**).

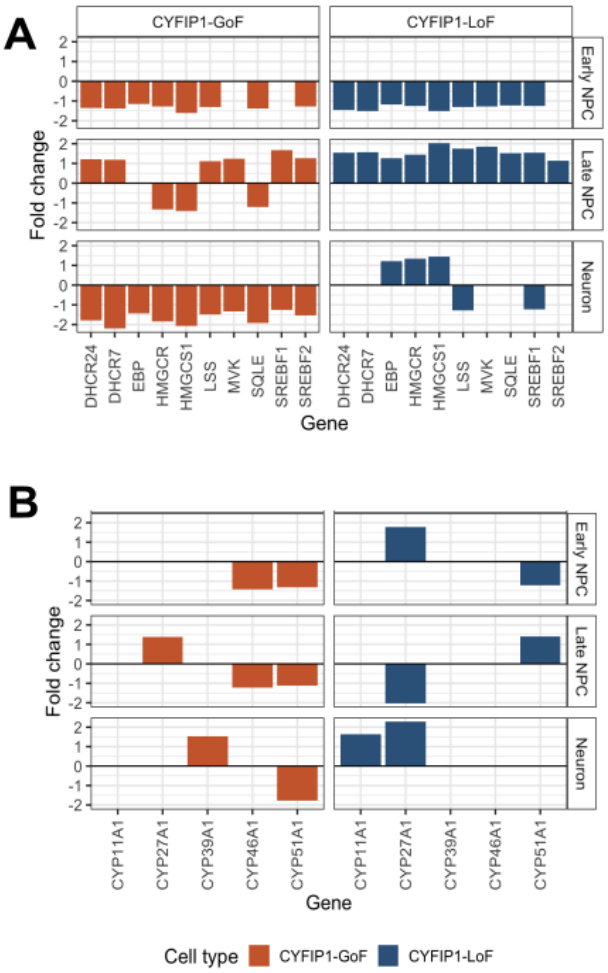

Figure 4.4. CYFIP1-altered cells demonstrate differences in expression of genes encoding key enzymes involved in cholesterol metabolism and synthesis. Differentially expressed genes (DEGs) involved in **(A)** cholesterol biosynthesis and **(B)** cholesterol metabolism. Fold changes in gene expression in NPC1 (DIV12), NPC2 (DIV25) and Neuron (DIV35) stages of cortical differentiation in CYFIP1-LoF and CYFIP1-GoF cell lines compared to respective controls. n=3, bar height represents fold change (FC) of significant DEGS (FDR p adj<0.05).

4.3.3. CYFIP1-altered lines demonstrate difference in expression of key proteins involved in cholesterol biosynthesis

Confirmation of the protein level expression of key cholesterol biosynthesis enzymes was carried out by western blotting analysis of cell pellet extracts collected from the differentiation corresponding to the neural progenitor rich timepoints (DIV20 and 30) and neuronal rich timepoints (DIV40) (**Figure 4.5**).

SREBP2 is known as the master regulator of cholesterol biosynthesis, and so with both cholesterol biosynthesis identified to be altered in these cells and altered *SREBF2* expression, we aimed to confirm if SREBP2 expression was altered on a protein level. To assess if SREBP2 protein expression was altered between these lines, quantification of both the full-length inactive form of SREBP2 (125kDa) and the cleaved transcriptionally active N-terminus (68kDa) was determined (**Figure 5.4A & B**). In CYFIP1-LoF cells at the early NPC-rich stage, protein levels of cleaved active SREBP2 were significantly higher than that of controls (**Figure 4.5A**). In CYFIP1-GoF cells, active SREBP2 appeared to be decreased compared to controls, however this was non-significant (**Figure 4.5A**).

3-hydroxy-3-methylglutaryl-CoA synthase 1 (HMGCS1) is a crucial enzyme in the mevalonate pathway, and is involved in the formation of HMG-CoA. In CYFIP1-LoF cells, HMGCS1 was significantly increased compared to controls at DIV40 (**Figure 4.5B**), which is in line with our

finding that *HMGCS1* gene expression is upregulated in CYFIP1-LoF cells. Interestingly, HMGCS1 was also shown to be increased compared to controls in the late NPC and neuron rich stages in CYFIP1-GoF cells compared to controls, however this was non-significant (**Figure 4.5B**).

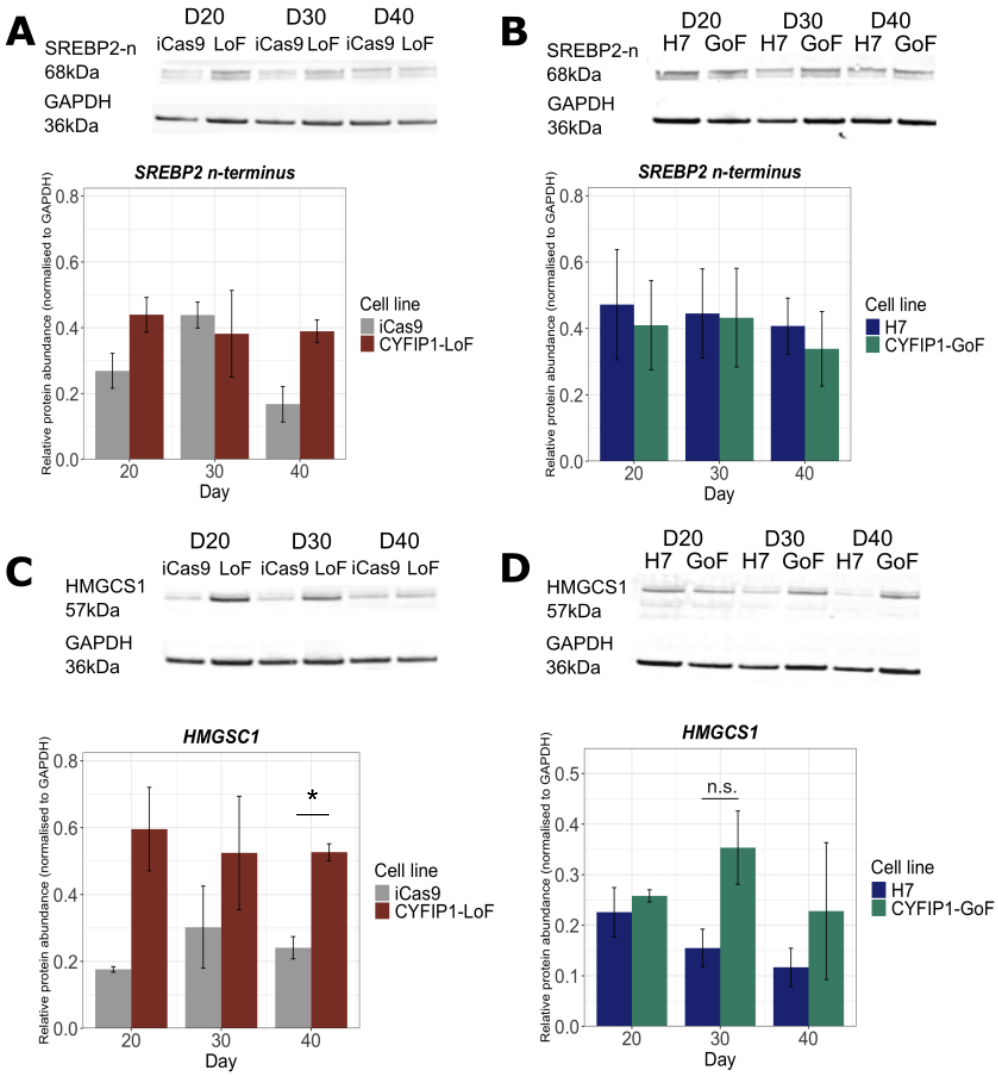

Figure 4.5. Western blotting analysis of key cholesterol biosynthetic enzymes in CYFIP1-altered lines. nSREBP2 normalised to GAPDH and total SREBP2 expression in (**A**) CYFIP1-LoF and (**B**) CYFIP1-GoF cells. HMGSC1 normalised to GAPDH expression in (**C**) CYFIP1-LoF and (**D**) CYFIP1-GoF cells. Data are shown as mean ± SEM of 3 replicate wells collected over 4 time points from two independent differentiation experiments. *p<0.05, one-way ANOVA, followed by Tukey post-hoc test.

We next aimed to assess the activity of the two parallel biosynthetic pathways and final stages of cholesterol biosynthesis. Following our finding of differential gene expression of the two final enzymes involved in cholesterol biosynthesis, DHCR7 and DHCR24, we aimed to assess the protein level expression of these enzymes between the CYFIP1-altered lines. DHCR7 protein expression did not appear to be significantly different between either of the CYFIP1-altered lines and their respective controls (**Figure 4.6A & B**). However, it is noted that DHCR7 protein levels appear to be higher at the NPC-rich stages in CYFIP1-GoF cells compared to controls (**Figure 4.6B**).

DHCR24 protein expression was shown to increase as the differentiation progressed in all lines, however CYFIP1-LoF cells were observed to have significantly higher protein expression at DIV30, which corresponds to the NPC rich stage at the onset of neurogenesis (**Figure 4.6C**). However, we did not observe any significant difference between CYFIP1-GoF and control cells (**Figure 4.6D**).

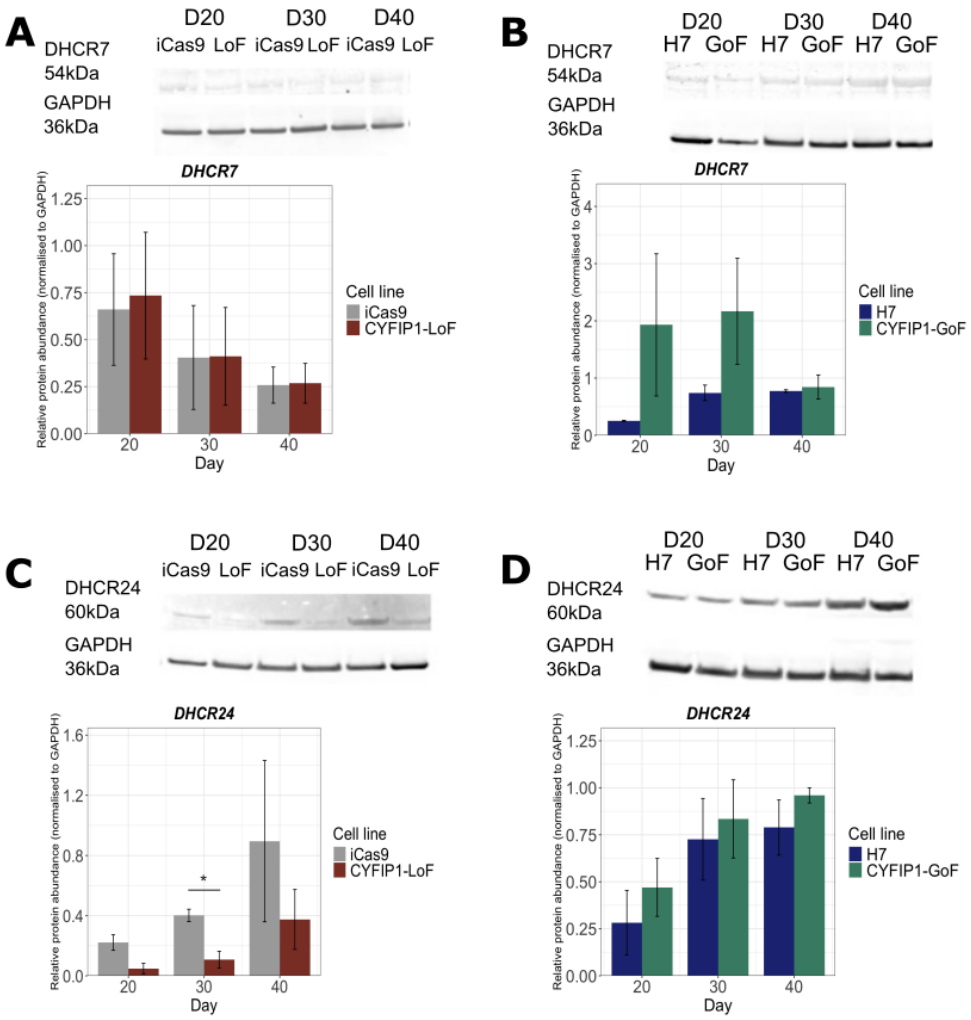

Figure 4.6. Western blotting analysis of key cholesterol biosynthetic enzymes in CYFIP1-altered lines. DHCR7 normalised to GAPDH expression in (A) CYFIP1-LoF and (B) CYFIP1-GoF cells. DHCR24 normalised to GAPDH expression in (C) CYFIP1-LoF and (D) CYFIP1-GoF cells. Data are shown as mean ± SEM of 3 replicate wells collected over 4 time points from two independent differentiation experiments, *p<0.05, one-way ANOVA, followed by Tukey post-hoc test.

4.3.4. CYFIP1-altered cell lines reveal differences in sterol profiles

Whilst assessing the activity of key enzymes provides an insight into overall cholesterol synthesis and metabolism, determining the levels of the products of these enzymes, the bioactive sterols themselves, provides crucial information of the potential contribution of these molecules to the aberrant cholesterol metabolism identified in these cells by previous transcriptomic analysis.

To determine the impact of aberrant cholesterol metabolism as a consequence of altered levels of CYFIP1, we carried out LC-MS^n analysis to characterise the sterol profiles of the CYFIP1-altered lines in comparison to their respective controls. In addition to the hESC-derived line with genetically manipulated CYFIP1 expression, samples derived from 15q11.2del BP1-BP2 patient iPSCs and matched controls were provided for LC-MS^n analysis by Dr Daniel Cabezas de la Fuente, utilising the same cortical differentiation protocol. Through use of these cells, comparisons of the effect of altered CYFIP1 expression alone to the whole 15q11.2 BP1-BP2 deletion could be made.

In the CYFIP1-GoF cells, 24S-HC levels were shown to be similar to that of the control line, increasing as differentiation progressed (**Figure 4.7A**), with CYFIP1-GoF cells having significantly higher levels of 24S-HC at DIV30 compared to controls (**Figure 4.7A**). In contrast, 24S-HC levels were shown to be significantly lower in CYFIP1-LoF cells at the neuronal rich stage (DIV 40) compared to controls (**Figure 4.7A**).

Levels of 24S,25-EC were found to be altered in the CYFIP1-LoF lines compared to controls, with significantly increased levels compared to the control line at the stage of the differentiation corresponding to the neural epithelial stage (DIV10) and also increased but non-significantly at neural progenitor stages (DIV30) ($p = 0.07$) (**Figure 4.6C**). However, at the more neuronal stage (DIV40) the opposite effect was seen, with decreased 24S,25-EC levels compared to the control ($p = 0.06$) (**Figure 4.7C**). In the CYFIP1-GoF cells, whilst initially significantly higher than controls at the stage in the differentiation corresponding to the neural epithelial stage (DIV 10), levels of 24S,25-EC were found to be significantly lower at the neuronal stage of the differentiation at DIV40 and 50 (**Figure 4.7D**).

Interestingly, whilst 24S-HC appears to be the more abundant sterol in CYFIP1-GoF and H7 cultures, levels of 24S-HC and 24S,25-EC are similar in the iCas9 and CYFIP1-LoF cells (**Figure 4.7**). It should however be taken into consideration that this may be a factor of previously observed differences between the parent cell lines.

In the two CYFIP1-altered lines and their respective controls, we were only able to identify the presence of 27-HC in the H7 and CYFIP1-GoF lines (**Figure 4.7E**). Interestingly, there were significantly higher 27-HC levels in CYFIP1-GoF lines compared to the control at the neuronal rich stages of the differentiation after DIV30 (**Figure 4.7E**). Interestingly, we also observed increased CYP27A1 expression at the late NPC stage in these cells in our RNAseq analysis (**Figure 4.7B**).

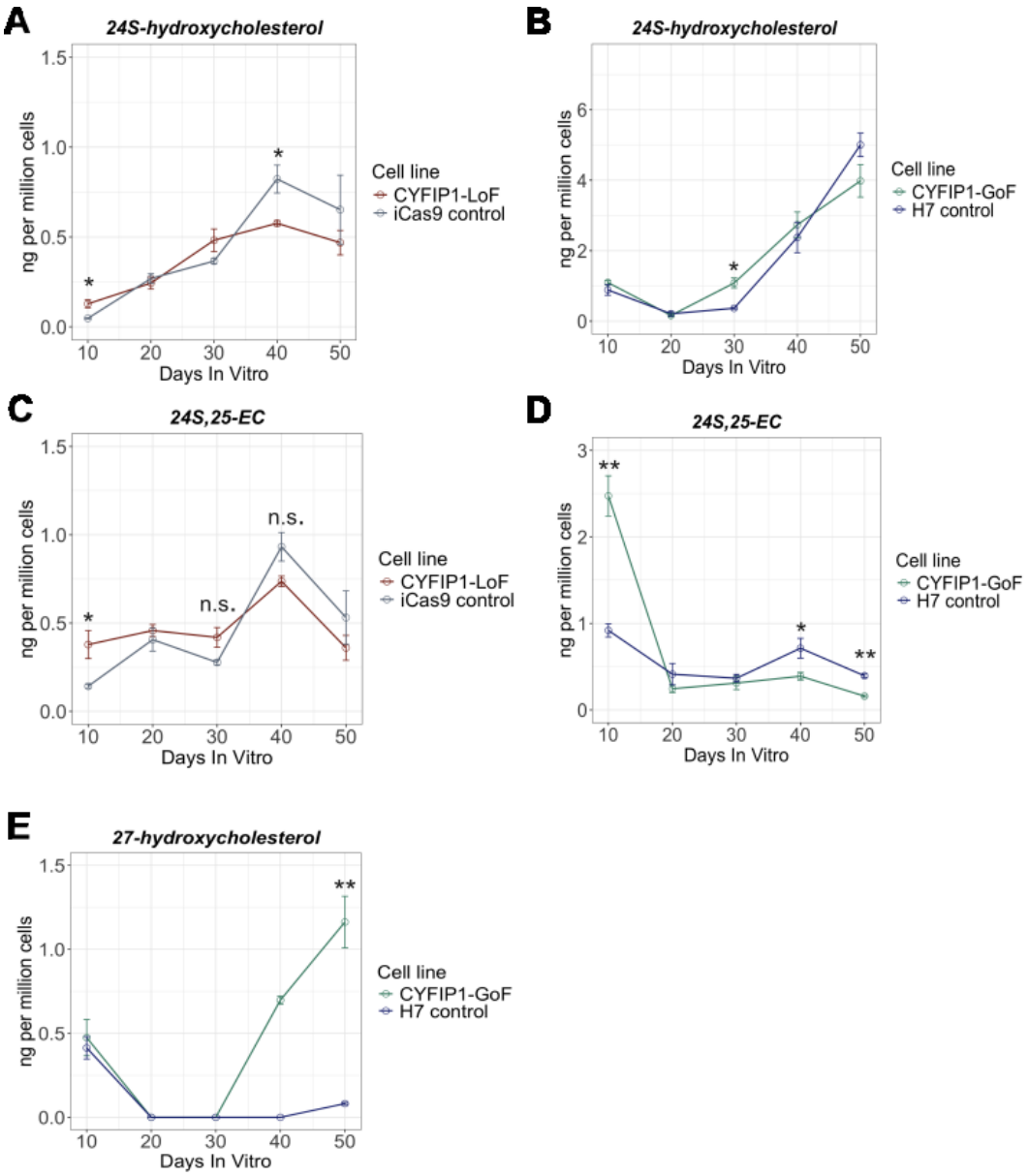

Figure 4.7. Monohydroxycholesterol content of CYFIP1-altered lines. (**A**) 24S-HC content of CYFIP1-GoF cells. (**B**) 24S-HC content of CYFIP1-LoF cells. (**C**) 24S,25-EC content of CYFIP1-GoF cells. (**D**) 24S,25-EC content of CYFIP1-LoF cells. (**E**) 27-HC content of CYFIP1-GoF cells. Data represent mean from 2 independent experiments, 2-3 technical replicates collected per timepoint, error bar = SEM. *p<0.05, Student's unpaired t test.

Further monohydroxycholesterols were identified in the CYFIP1-altered cells, including 7α-hydroxycholesterol, and autoxidation products of cholesterol 7β-hydroxycholesterol, 6β-hydroxycholesterol and 7-ketocholesterol (**Figure 4.8**). At DIV20, CYFIP1-LoF cells were found to demonstrate significantly increased levels of 7α-hydroxycholesterol (**Figure 4.8A**). No significant difference was observed in the levels of 6β-hydroxycholesterol in either the CYFIP1-LoF or CYFIP1-GoF lines compared to the control. CYFIP1-GoF cells (**Figure E & F**) were found to have increased levels of 7β-hydroxycholesterol at DIV 30, and increased 7α-hydroxycholesterol at DIV10 ($p = 0.047$) (**Figure 4.8B, D & F**). Levels of 7-ketocholesterol were shown to be significantly increased at DIV10 and DIV20 in the CYFIP1-LoF cells compared to the controls (**Figure 4.8G**). Whilst initially higher than control, levels of 7-ketocholesterol in CYFIP1-GoF cells were significantly decreased at DIV40 and DIV50 (**Figure 4.8H**).

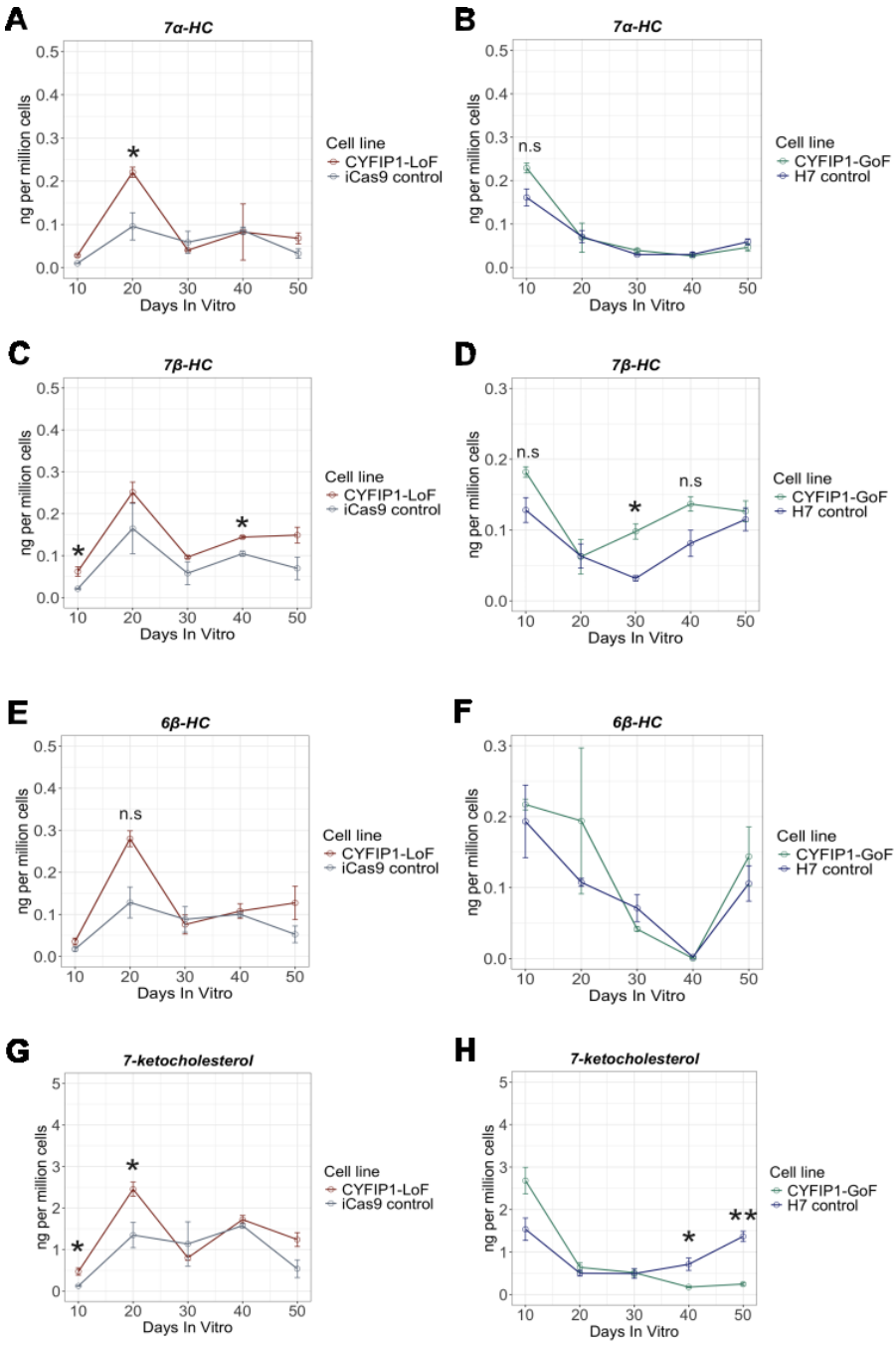

Figure 4.8. 7α-hydroxylated sterol content of CYFIP1-altered lines. 7α, 26-diHC content of (**A**) CYFIP1-GoF and (**B**) CYFIP1-LoF cells. 7α-HC content of (**C**) CYFIP1-GoF

and (**D**) CYFIP1-LoF cells. (**E**) 7β-HC content of CYFIP1-GoF cells and (**F**) CYFIP1-LoF cells. Data represent mean from 2 independent experiments, 2-3 technical replicates collected per timepoint, error bar = SEM. *p<0.05, **p<0.01, Student's unpaired t test..

We were further able to identify the presence of 7α, 26diHC in both CYFIP1-altered lines (**Figure 4.9**). No significant differences were observed in the CYFIP1-LoF cells (**Figure 4.9A**), however we observed significantly increased levels of 7α,26di-HC in the CYFIP1-GoF cells following DIV20 of the differentiation (**Figure 4.9B**).

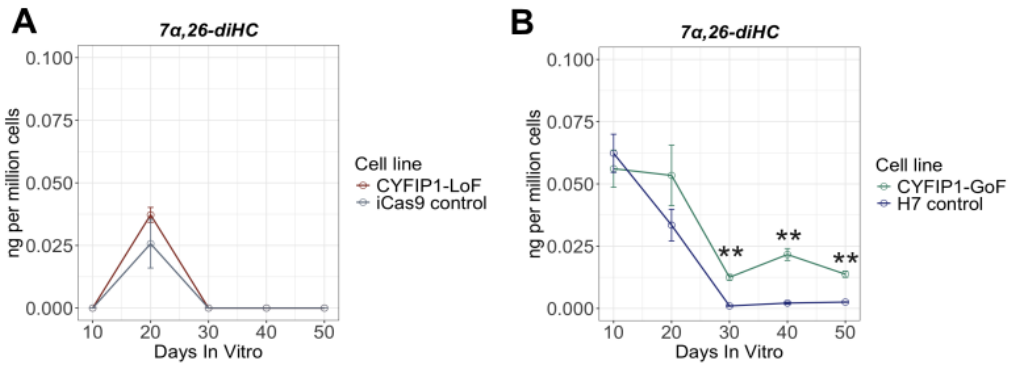

Figure 4.9. 7α,26di-HC content of CYFIP1-altered lines. 7α, 26-diHC content of (**A**) CYFIP1-GoF and (**B**) CYFIP1-LoF cells. Data represent mean from 2 independent experiments, 2-3 technical replicates collected per timepoint, error bar = SEM. *p<0.05, ***p*<0.01, Student's unpaired t test.

Assessment of the cholesterol levels in the CYFIP1-altered lines revealed in the CYFIP1-LoF cells, levels of cholesterol were observed to be significantly increased at the NPC stages DIV10 and 30 (**Figure 4.10A**). However, in the CYFIP1-GoF lines we instead observed significantly

increased levels compared to control following DIV20, at the onset of nerogenesis (**Figure 4.10B**).

Next, levels of cholesterol precursors desmosterol and 8(9)-DHC were assessed to gain an insight into the respective activity of the Bloch and K-R biosynthetic pathways (**Figure 4.10C-F**). Whilst our analysis of DHCR24 expression revealed significant downregulation on both a gene and protein level in the more neuronal stages the CYFIP1-LoF cells, levels of desmosterol and 8(9)-DHC were both significantly increased at the earlier stages of the differentiation (**Figure 4.10C**). In the CYFIP1-GoF cells, levels of desmosterol were significantly lower than that of controls in the neuronal-rich stages of the differentiation (**Figure 4.10D**). DHCR7 protein expression was noted to be higher in these cell compared to controls, but determined to be non-significant (**Figure 4.6B**). Analysis of 8(9)-DHC revealed a more mixed result, with initially levels in CYFIP1-GoF cells being significantly lower than that of controls, however the opposite situation was observed for the later neuronal-rich stages of the differentiation with levels being significantly higher compared to controls (**Figure 4.10F**).

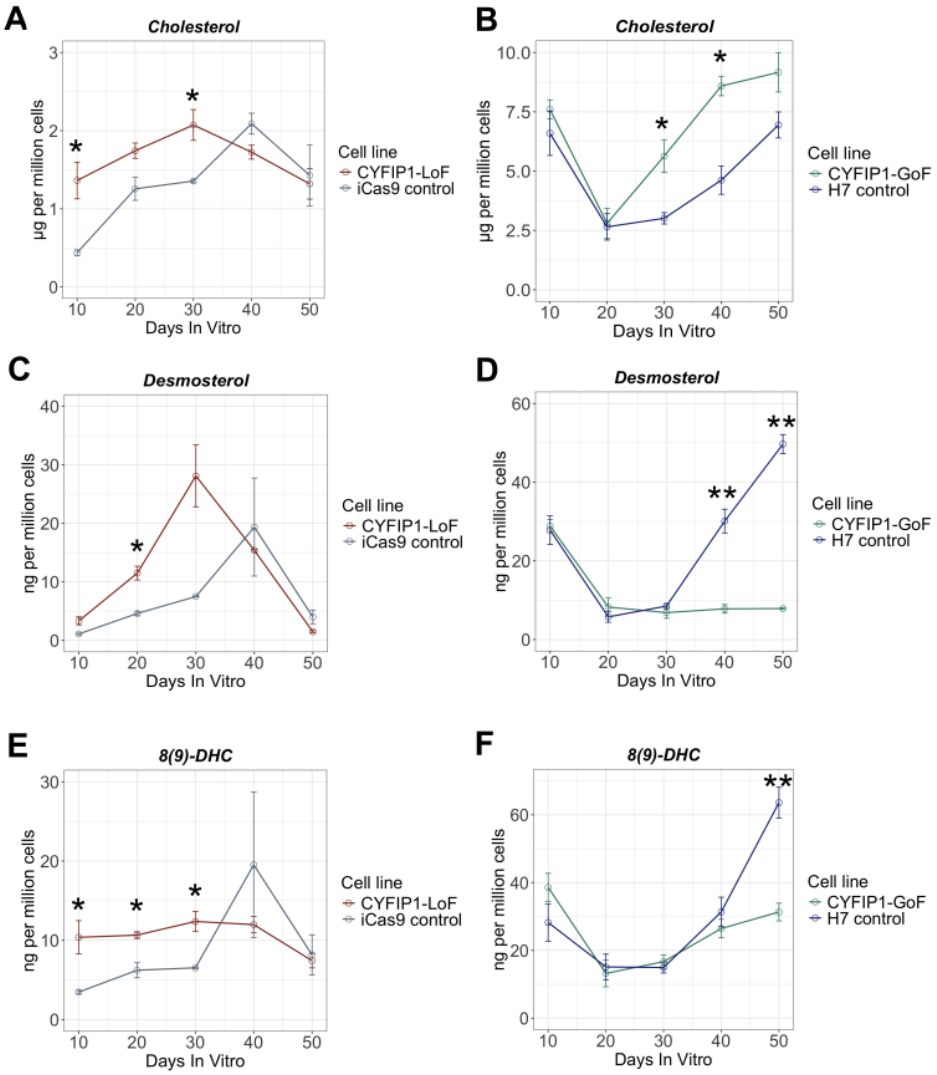

Figure 4.10. Cholesterol and precursors desmosterol and 8(9)-DHC. Cholesterol content of cortical cells derived from **(A)** CYFIP1-GoF and **(B)** CYFIP1-LoF compared to respective control lines. 8(9)-DHC and desmosterol content of cortical cells derived from **(C&D)** CYFIP1-GoF and **(D&F)** CYFIP1-LoF compared to respective control lines. Data represent mean from 2 independent experiments, 2-3 technical replicates collected per timepoint, error bar = SEM. *p<0.05, **p<0.01, Student's unpaired t test.

4.3.5. Sterol levels of 15q11.2del patient undergoing cortical neurogenesis

To confirm the altered sterol levels observed in the CYFIP1-altered models is representative of the 15q11.2 CNV and a consequence of altered levels of CYFIP1, we further analysed cell samples taken from two 15q11.2del patients utilizing the same cortical differentiation paradigm as above.
Initial ICC confirmed the altered cortical neurogenic phenotype, similar to that observed in the CYFIP1-LoF model of the deletion with a bias toward neuronal differentiation (**Supplementary Table 7.9**).

24S-HC was found to be significantly increased in the EA008 patient at DIV 30 and 40, however significant differences were instead found at DIV10 and 20 between EA062 patient and the unaffected control (**Figure 4.11A & C**). 24S,25-EC levels were found to be significantly increased in both EA008 and EA062 at DIV20, with exception to the EA062.19 clonal line (**Figure 4.11 B & D**).

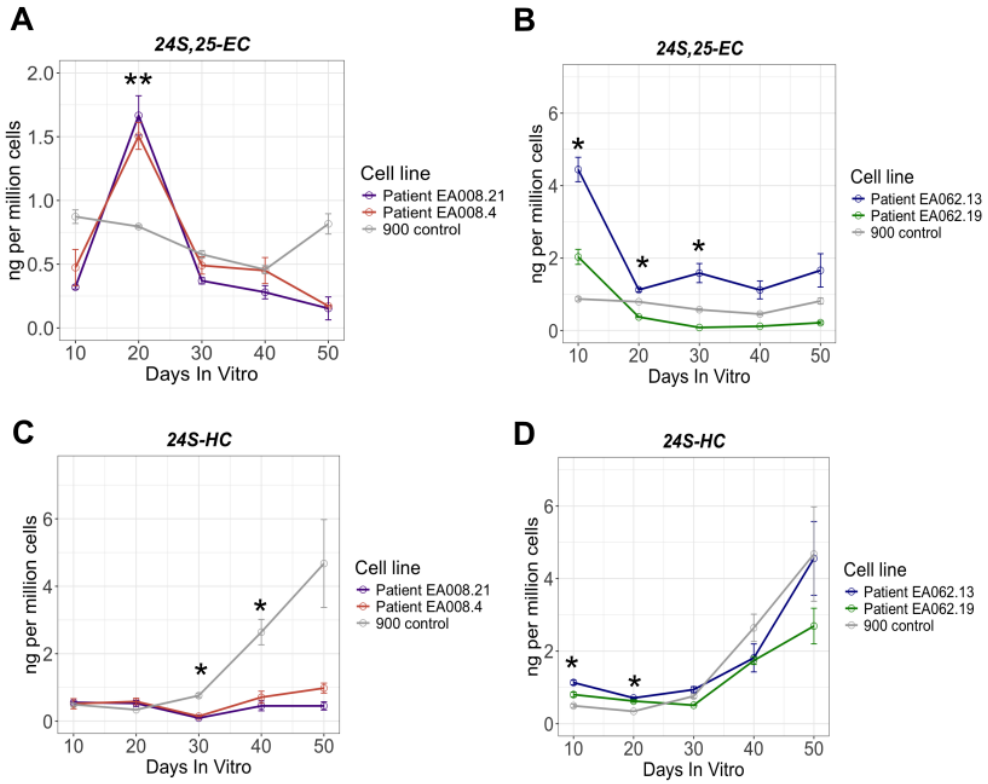

Figure 4.11. Bioactive oxysterol content of 15q11.2del patient-derived lines compared to unaffected control. 24S,25-epoxycholesterol content of 15q11.2del patient cortical cells derived from **(A)** Patient EA008 clones and **(B)** EA062 clones compared to 900 control line.24S-hydroxycholesterol content of 15q11.2del patient cortical cells derived from **(C)** Patient EA008 clones and **(D)** EA062 clones compared to 900 control line. Data represent mean from a single independent experiment, 3 well technical replicates, *p<0.05, Student's unpaired t test.

Next, we further identified the presence of same 7α-hydroxylated sterols formed via autoxidation as previously identified in the CYFIP1-altered lines (**Figure 4.12**). Differences between the two patient lines were

observed, with the EA008.4 clone demonstrating increased 7α-hydroxycholesterol levels at DIV40, whilst the EA062 lines demonstrated decreased levels of the same sterol at DIV30 (**Figure 4.12A & B**). Whilst no significant differences in 7β-hydroxycholesterol were observed in the EA008 patient lines, the EA062.19 clonal line demonstrated significantly increased 7β-hydroxycholesterol levels at DIV10, 20 and 50 (**Figure 4.12C & D**). Both EA008 and EA062 lines demonstrated increased levels of 6β-hydroxycholesterol, at DIV30 and DIV10 respectively (**Figure 4.12E & F**). A more unclear pattern was observed for the autoxidation product 7-ketocholesterol, which was found to be significantly increased at DIV40 in the EA008.4 clonal line, but opposing differences were observed in each EA062 line compared to the unaffected control (**Figure 4.12G & H**).

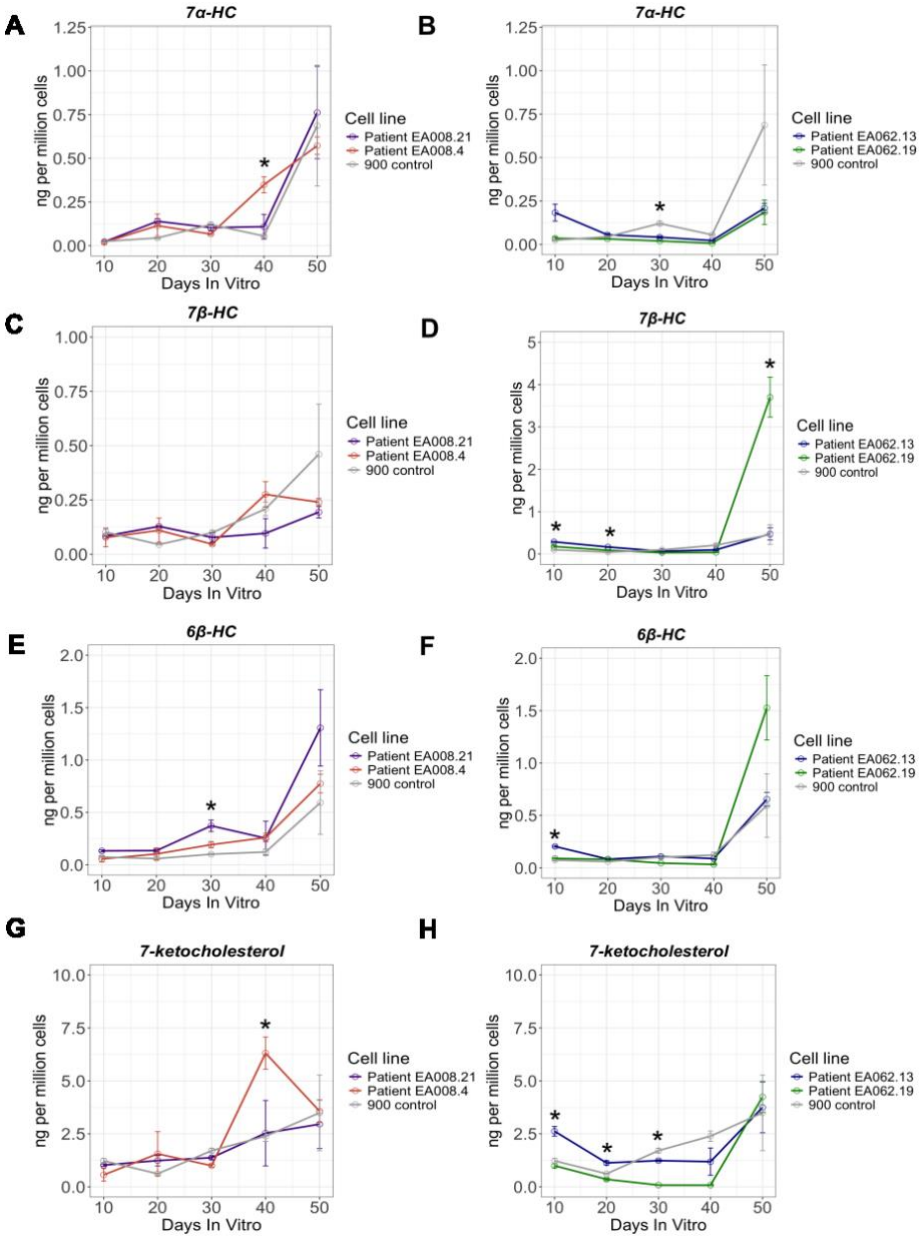

Figure 4.12. 7α-hydroxylated sterol content of 15q11.2del patient-derived lines compared to unaffected control. 7α-hydroxycholesterol content of 15q11.2del patient cortical cells derived from **(A)** Patient EA008 clones and **(B)** EA062 clones compared to 900 control line. 7β-hydroxycholesterol content of 15q11.2del patient cortical cells derived from **(C)** Patient EA008 clones and **(D)** EA062 clones compared to 900 control line. 6β-

hydroxycholesterol content of 15q11.2del patient cortical cells derived from **(E)** Patient EA008 clones and **(F)** EA062 clones compared to 900 control line. 7-ketocholesterol content of 15q11.2del patient cortical cells derived from **(G)** Patient EA008 clones and **(H)** EA062 clones compared to 900 control line. Data represent mean from a single independent experiment, 3 well technical replicates, Student's t test *p<0.05,

We were further able to identify the presence of the dihydroxycholesterol 7α,26-diHC in each of the 15q11.2del lines (**Figure 4.13**). Both the EA008.21 and EA008.13 lines were shown to be significantly increased compared to the unaffected control at DIV 20, 30 and 40 (**Figure 4.13 A & B**).

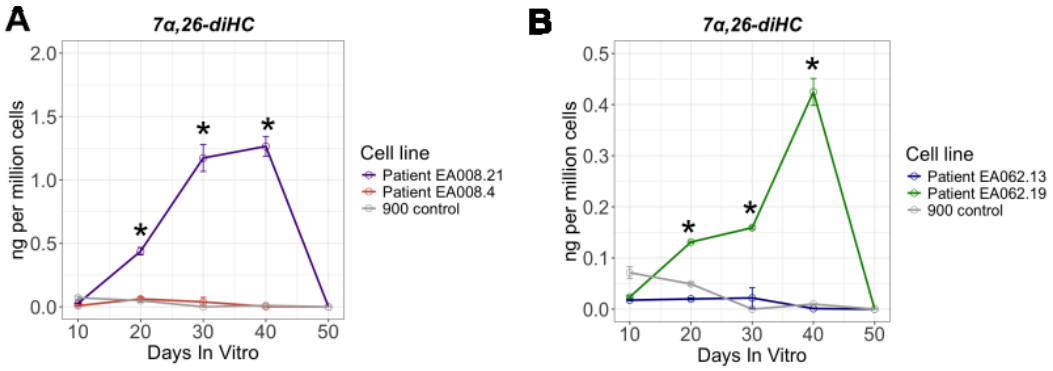

Figure 4.13. 7α,26-diHC sterol content of 15q11.2del patient-derived lines compared to unaffected control. 7α,26-diHC content of 15q11.2del patient cortical cells derived from **(A)** Patient EA008 clones and **(B)** EA062 clones compared to 900 control line. Data represent mean from a single independent experiment, 3 well technical replicates, Student's t test *p<0.05,

Analysis of the cholesterol content of the 15q11.2del patient cells revealed significantly increased cholesterol levels at DIV20 and decreased cholesterol levels at the DIV50 timepoint in both patients compared to the

unaffected control (**Figure 4.14 A&B**). Both clones generated from patient EA008 were found to have different levels of the assessed cholesterol precursors compared to the control, with significantly decreased levels of desmosterol at DIV50 (**Figure 4.14C**), and increased 8(9)-DHC compared at DIV10 to the unaffected control (**Figure 4.14E**). Significant differences in the levels of the cholesterol precursors desmosterol and 8(9)-DHC were also found in the EA062.13 clone compared to the unaffected control, with significantly increased levels of desmosterol also found at DIV50 (**Figure 4.14 D & F**). However, this analysis also revealed differences in 8(9)-DHC precursor levels between the two patient clones generated from patient EA062 (**Figure 4.14D**).

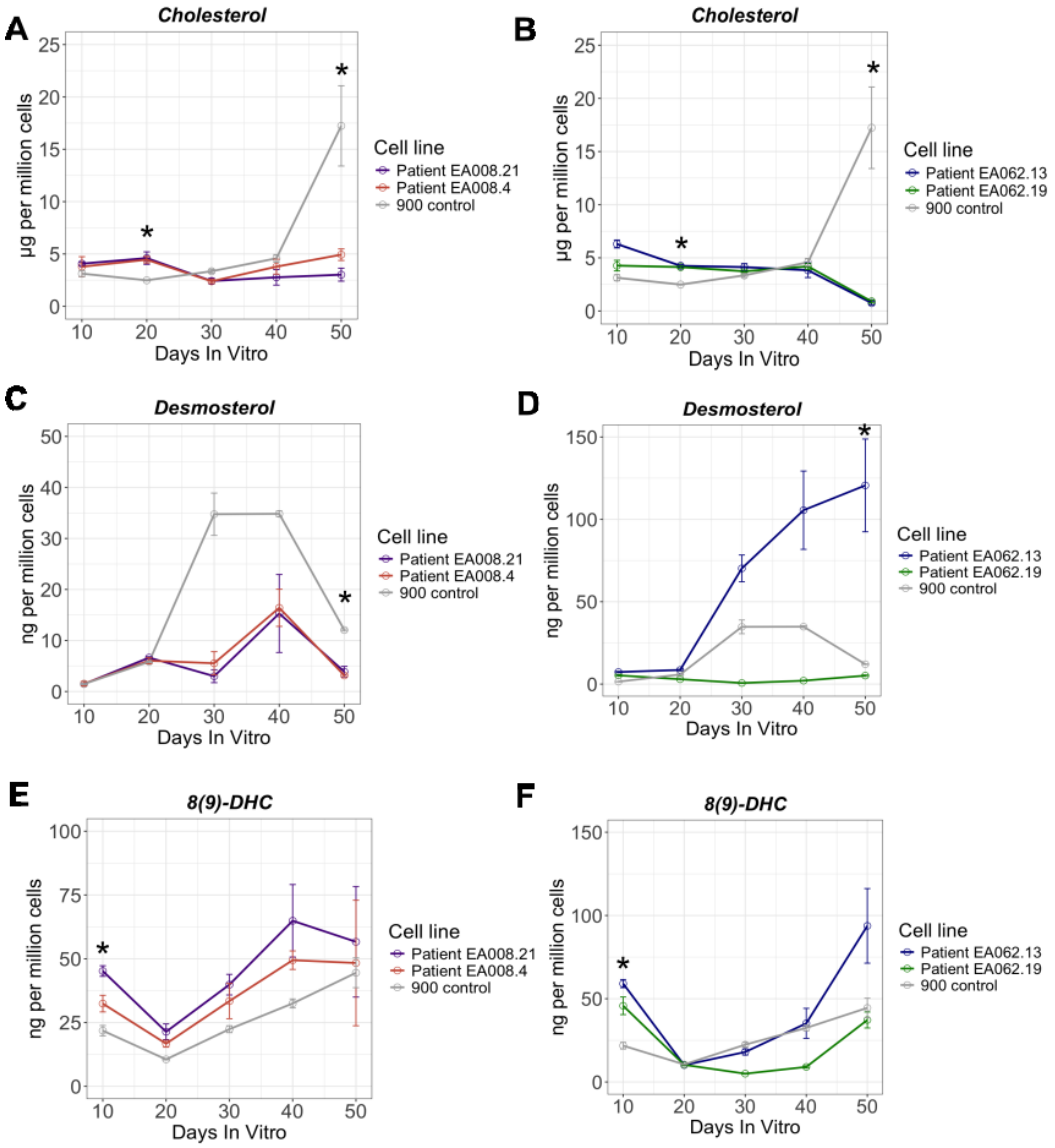

Figure 4.14. Cholesterol and precursor content of 15q11.2del patient-derived lines compared to unaffected control. Cholesterol content of 15q11.2del patient cortical cells derived from **(A)** Patient EA008 clones and **(B)** EA062 clones compared to 900 control line. Desmosterol content of 15q11.2del patient cortical cells derived from **(C)** Patient EA008 clones and **(D)** EA062 clones compared to 900 control line. 8(9)-DHC content of 15q11.2del patient cortical cells derived from **(E)** Patient EA008 clones and **(F)** EA062

clones compared to 900 control line. Data represent mean from a single independent experiment, 3 well technical replicates, Student's t test *p<0.05.

4.4. Discussion

This chapter investigates the sterol profiles of hESC-derived models of 15q11.2 CNV human cortical development featuring altered levels of CYFIP1 and iPSCs derived from patients featuring a deletion at 15q11.2 BP1-BP2. This work provides the first study into sterol profiles of 15q11.2 BP1-BP2 deletion patients and hESC-derived models of altered levels of CYFIP1 and investigates how alterations to cholesterol metabolism may relate to the altered cortical neurogenesis observed in these cells. This analysis has revealed differences on both a gene and protein level for key cholesterol biosynthetic and metabolic enzymes, and this is reflected in the measured sterol levels determined by LC-MS^n analysis.

Previous work carried out by our lab has demonstrated that altered levels of CYFIP1, either modelled by genetic manipulation in hESC-based models or in 15q11.2del patient-derived cells, results in deficits in cortical neurogenesis (Fuente et al., 2024). These deficits appear dosage-dependant, with increased levels of CYFIP1 resulting in a bias toward proliferation whilst knockout of CYFIP1 demonstrated a bias toward neuronal differentiation. In this chapter, we were able to replicate this finding as well as further show that these cells present altered sterol profiles during cortical neurogenesis *in vitro*.

4.5.1. CYFIP1-altered lines display differences in bioactive oxysterols and gene expression of the CYP enzymes involved in their formation

Following on from the previous chapter, which developed a characterisation of control hESC-derived cortical cells, it was determined that with the observed increased expression of the neuronal marker NEUN as the differentiation progressed, production of the bioactive oxysterol 24S-HC was also found to increase. Here, CYFIP1-LoF cells which display a bias toward neuronal proliferation as demonstrated by increased NEUN+ cells at earlier stages of the differentiation, also demonstrated higher 24S-HC and 24S,25-EC levels at earlier stages of the differentiation compared to controls. This may support the hypothesis that 24S-HC and 24S,25-EC promote neurogenesis through its evidenced interaction with signalling implicated in neurogenesis, including the Hegdehog and LXR signalling pathways (Deshpande et al., 2019; Dwyer et al., 2007; Lehmann et al., 1997; Nachtergaele et al., 2013; Nedelcu et al., 2013; Raleigh et al., 2018).

In line with the differences observed in cortical differentiation dynamics, we also observed significant differences in the levels of the oxysterol 24S,25-EC in both the CYFIP1-altered lines and the 15q11.2del patient lines. This sterol has previously been shown to promote dopaminergic differentiation through its activation of LXRβ (Theofilopoulos et al., 2019, 2013). Further, a recent study published by our lab has shown that this treatment of CYFIP1-altered lines with this oxysterol also rescues CYFIP1-mediated deficits in neurogenesis through LXRβ (Fuente et al., 2024). Further work would be required to determine the extent of the pro-neural activity of

24S,24-EC in cortical neurogenesis, and with observed fluctuations in its levels throughout the cortical neural differentiation paradigm in vitro, it would be interesting to determine at what stage of neurogenesis its effect on signalling is most crucial.

It is interesting to note that we observed significantly increased levels of 7α, 26-diHC in the CYFIP1-GoF cultures compared to its parent control line. Inhibition of the production of this sterol through CYP7B1 has been implicated in promotion of dopaminergic neurogenesis (Hennegan et al., 2023). However, it should be noted that this oxysterol was also found to be significantly increased in both the 15q11.2del patient lines. Whilst the exact mechanism through which inhibition of this sterol contributes to a promotion of dopaminergic neurogenesis remains unclear, and whether it also promotes cortical neurogenesis, it is theorised that it may be due to a reduction in the toxic effect of this sterol and increased levels of 24S,25-EC observed when CYP7B1 is inhibited (Hennegan et al., 2023).

A mirror difference noted in our analysis was in the gene level expression of the rate limiting enzyme *HMGCR*, which was found to be significantly downregulated in CYFIP1-LoF line and upregulated in the CYFIP1-GoF line. 24S,25-EC, which was shown to be increased in the CYFIP1-LoF line and decreased in the CYFIP1-GoF line, is formed in the shunt of the mevalonate pathway. Activity of the mevalonate pathway is rate-limited by the HMGCR enzyme. Thus, higher levels of 24S,25-EC could potentially be due to this pathway being more active as a consequence of HMGCR having decreased activity and/or being less stabilised.

Assessment of *CYP46A1* gene expression, and the levels of 24S-HC and 24S,25-EC which are produced by this enzyme from cholesterol and desmosterol respectively, revealed differences between the two CYFIP1-altered lines in our analysis. Analysis of the RNAseq dataset revealed *CYP46A1* to be downregulated in the CYFIP1-GoF line at DIV 10 and 20. This was further reflected in the sterol analysis, which found both 24S-HC and 24S,25-EC to be present at lower levels compared to the control line at DIV30 and DIV40 and 50 respectively. Downregulation of CYP46A1 has previously been implicated in cases of neurodevelopmental disorder, including both Rett (Audouard et al., 2024) and Nieman-Pick type C syndrome (Mitroi et al., 2019). However, the situation in the CYFIP1-LoF line was less clear, with *CYP46A1* not found to be differentially expressed in the CYFIP1-LoF cells at either the NPC or neuronal stages, but 24S-HC and 24S,25-EC levels found to be significantly upregulated at DIV10. Similarly, in the 15q11.2del patient lines, whilst 24S,25-EC was found to be significantly increased at the NPC stage in both patients, there was a less clear pattern for 24S-HC.

Whilst these findings focus on the 15q11.2 CNV, similar studies have looked into other neurodevelopmental conditions and have also noted differences in altered cholesterol homeostasis. A recent study has further demonstrated alterations in proteins involved in cholesterol biosynthetic pathway, including HMGCR, CYP46A1 and nSREBP2, in the prefrontal cortex, amygdala and nucleus accumbens of a rat model of Fragile X syndrome (Parente et al., 2022). Whilst here our study focuses on cortical cells, this also highlights the need for a further analysis of these proteins during development in other neural cell types and brain regions.

4.5.3. Limitations

In this study we utilised two 15q11.2del lines, with two clonal lines generated per patient. Whilst for the one patient (EA008.4) we saw the two clonal lines to behave similarly and a similar pattern for differences between 24S-HC and 24S,25-EC compared to control as the CYFIP1-LoF lines, this was not true of the second patient lines (EA062). Whilst a sex-matched unaffected control line was used, these findings highlight the importance of use of CRISPR-corrected patient lines as isogenic controls in disease modelling, which was unfortunately out of the scope of this research.

4.5.4. Conclusions

In conclusion, this chapter demonstrates that alterations to the levels of CYFIP1 resulting in deficits in neurogenesis additionally results in altered sterol profiles compared to that of control cells. We have identified key differences in bioactive sterols implicated in neural development, including differences in the neuro-oxysterol 24S,25-EC between CYFIP1-LoF and CYFIP1-GoF cells undergoing cortical neurogenesis. In the context of 15q11.2del syndrome, this study has also emphasised the need for further determination of the link between CYFIP1 and sterol metabolism. An interesting avenue may be through a possible interaction with FMRP, with evidence that various proteins involved in regulation of cholesterol biosynthesis, including SRBEP2 and HMGCS1, having been shown to be

identified as high confidence FMRP targets in the brain (Darnell et al., 2011a; Sawicka et al., 2019) .

Whilst this study focuses on a single variant associated with increased risk of autism and schizophrenia, further work is required investigating the impact of altered sterol metabolism on neurogenesis in other stem cell models of neurodevelopmental disorder. This research identifies the need for further exploration into the role these sterols are playing in cortical neurodevelopment, with previous evidence for a role of 24S,25-EC in promotion of specifically dopaminergic neurogenesis (Theofilopoulos et al., 2019, 2013). Findings here support a potential pro-neural role of 24S-HC and 24S,25-EC in cortical neurogenesis. With the potential of oxysterols as both biomarkers for disease and potential therapeutic targets, these findings highlight the need for further study of the use of these molecules as diagnostic and therapeutic targets in neurodevelopmental disorders.

Chapter 5

Cholesterol biosynthetic and metabolic enzyme activity during astrogliogenesis

5.1 Introduction

During human neural development, neurons produce cholesterol which is required to support rapid growth and the formation of synapses (Fünfschilling et al., 2012). However, in the postnatal brain, neurons are thought to outsource the production of cholesterol, with astrocytes having been theorised to be responsible for the majority of cholesterol biosynthesis in the adult brain (Pfrieger, 2003; Pfrieger and Ungerer, 2011). This hypothesis has been further supported by evidence that there is a cell-specific distribution of proteins responsible for the mediation of different steps of cholesterol metabolism between these different cell types (Zhang and Liu, 2015). Studies of mouse models have demonstrated both neurons and astrocytes to express the master transcription factor *Srebf2* as well as genes encoding enzymes involved in cholesterol biosynthesis including *Hmgcr* and *Sqle* (Suzuki et al., 2010)

In the postnatal period there is evidence that neurons switch from producing cholesterol *in situ*, to relying on cholesterol production by astrocytes (Nieweg et al., 2009; Pfrieger and Ungerer, 2011). A shuttle system has been hypothesised for the transport of cholesterol between astrocytes and neurons in the postnatal brain, with proteins involved in cholesterol transport and uptake identified in both cell types (Pfrieger, 2003). However, it remains to be determined when exactly this switch occurs in human neural development.

In terms of oxysterol production, there is some evidence for astrocytes producing the oxysterol 24S,25-EC (Wong et al., 2007). However, it is

thought that under physiological conditions astrocytes do not produce the oxysterol 24S-HC, with this oxysterol considered to be neuron-specific. Some studies have demonstrated astrocytic expression of CYP46A1; however this has mostly been observed in models of brain injury and disease, and it has been hypothesised that this production of 24S-HC may only occur in reactive astrocytes (Cataldi et al., 2023; Smiljanic et al., 2010). So far, there has been a single postmortem study has noted CYP46A1 expression in healthy human adult brain tissue (Brown, et al., 2004). However, it is unknown which sterols are produced in developing astrocytes, how this switch in cholesterol production between cell types occurs and whether this also applies to other sterols, including bioactive oxysterols.

Both neurons and astrocytes have a high demand for cholesterol, with both cell types possessing large cell membrane surface areas. In neuronal synapses alone, presynaptic vesicles and the postsynaptic spines encompass large amounts of membrane, possessing a high cholesterol content of approximately 40 mol% (Takamori et al., 2006). Comparatively, astrocytes also require large membranes, with the occupation of large cell volumes and contact with up to 100,000 synapses through many fine processes (Grosche et al., 1999; Halassa et al., 2007; Ogata and Kosaka, 2002).

Studies have also looked into potential differences in how neurons and astrocytes produce cholesterol, with suggestion that neurons and astrocytes utilise different branches of the cholesterol biosynthetic pathway. It has previously been hypothesised that neurons and astrocytes employ

different biosynthetic pathways to synthesise cholesterol, with some debate over which pathway is preferred in each cell type. It is proposed based on comparison of levels of sterols composing the two pathways that astrocytes primarily utilise the Bloch pathway, whereas neurons rely on the K-R pathway (Nieweg et al., 2009; Zhang and Liu, 2015). A study by (Nieweg et al., 2009) demonstrated this by looking at primary rat serum-free cultures of CNS neurons and glia, and demonstrated that each cell population contained different profiles of post-squalene precursors. However, it has since been argued in a study of cortical cells that both neurons and astrocytes preferentially use the Bloch pathway (Genaro-Mattos, et al. 2019). In this study, Genaro-Mattos et al. propose that neurons synthesise cholesterol via the K-R pathway, whilst astrocytes synthesis cholesterol via the Bloch pathway based upon the intermediates of each pathway being present in each cell type assessed. Thus, with it still to be determined how these cell types synthesis cholesterol, it remains to be investigated how this may differ in these cells during development.

5.2 Aims

Following Pfreiger's hypothesis that astrocytes take over the production of cholesterol postnatally, much interest has been taken in the role of these cells in the maintenance of cholesterol homeostasis in the brain. Utilising hPSC-drived cells models, we aim to explore the sterolomic profile of developing astrocytes *in vitro* as well as examine the protein expression of the enzymes responsible for formation of cholesterol. With evidence that astrocytes take over the production of cholesterol in the postnatal brain, we also aim to demonstrate whether these cells also express proteins involved

in the various steps of cholesterol biosynthesis, and if these are acquired as the astrocytic progenitors develop into cortical astrocytes.

In the previous chapter we have shown that the CYFIP1-altered cell lines demonstrate differential production of several oxysterols, including 24S,25-EC and 24S-HC, during cortical neuronal induction compared to their parental control lines, and this is correlated to the cortical developmental phenotype. As neurons are shown to interact with astrocytes *in vivo* to maintain cholesterol homeostasis, we aim to investigate whether the bioactive sterols identified in the neuronal cultures can also be produced by astrocytes during development.

This work aims to address this through:

- Cortical astrocytic differentiation of a human embryonic stem cell (hESC)-derived line, confirming cell population identity through immunocytochemical analyses of key astrocytic markers.
- LC-MS^n analysis to assess cholesterol and oxysterol production as hESC-derived lines are differentiated into cortical astrocytes.
- Immunohistochemical and western blotting analysis of CYP46A1 expression in hESC-derived astrocytic progenitors and astrocytes.
- Analysis of protein expression of key enzymes involved in cholesterol biosynthesis. Assessment of proteins involved in the Kandutsch-Russell and Bloch biosynthetic pathways to determine whether astrocytes do indeed preferentially produce cholesterol via the Bloch or K-R pathway.

Overall, these findings aim to further investigate the mechanism utilised by astrocytes in the production of the oxysterols 24S-HC and 24S,25-EC, by determining the ability of these cells to synthesise these oxysterols through CYP46A1-mediated oxidation of cholesterol and desmosterol. We are further interested in confirming if astrocytes do indeed preferentially produce cholesterol via the Bloch biosynthetic pathway. Finally, with neurons outsourcing the production of cholesterol to astrocytes postnatally, we also aim to determine if expression of the cholesterol biosynthetic enzymes changes as differentiation of hESC-derived cells to astrocytes occurs.

5.3 Results

5.3.1. LC-MS^n analysis of hESC-derived cortical astrocytic cultures

We first aimed to assess the sterolomic profiles of developing astrocytes, utilising hESC-derived models of developing astrocytes. The astrocyte cultures used for this analysis were kindly provided by Dr Zongze Li (NMHII, Cardiff University) with cell identity confirmed by immunocytochemical analysis (**Supplementary Figure 7.3**). The differentiation protocol utilised is detailed in **Figure 2.2**. Cells were analysed at several astrocytic progenitor stages (DIV70, 80 and 90) and at the final timepoint following terminal differentiation of the cells into astrocytes (DIV110).

Analysis of cholesterol levels revealed an increase in cholesterol as the differentiation progressed, with highest levels at the final timepoint following

terminal differentiation into astrocytes shown to be significantly higher than that of the DIV92 progenitors, detected at levels of 7.3 ± 0.333 μg/x10^6 cells (**Figure 5.1A**). Analysis of immediate precursors of cholesterol, 8(9)-DHC and desmosterol was carried out to assess activity of the K-R and Bloch pathways. Increased levels of 8(9)-DHC compared to desmosterol were noted in the cultures (**Figure 5.1B & C**), which could indicate a preference for the K-R biosynthetic pathway over the Bloch pathway. Levels of desmosterol were also shown to decrease as the differentiation progressed, found to be significantly lower at DIV110 compared to DIV 90 (**Figure 5.1C**).

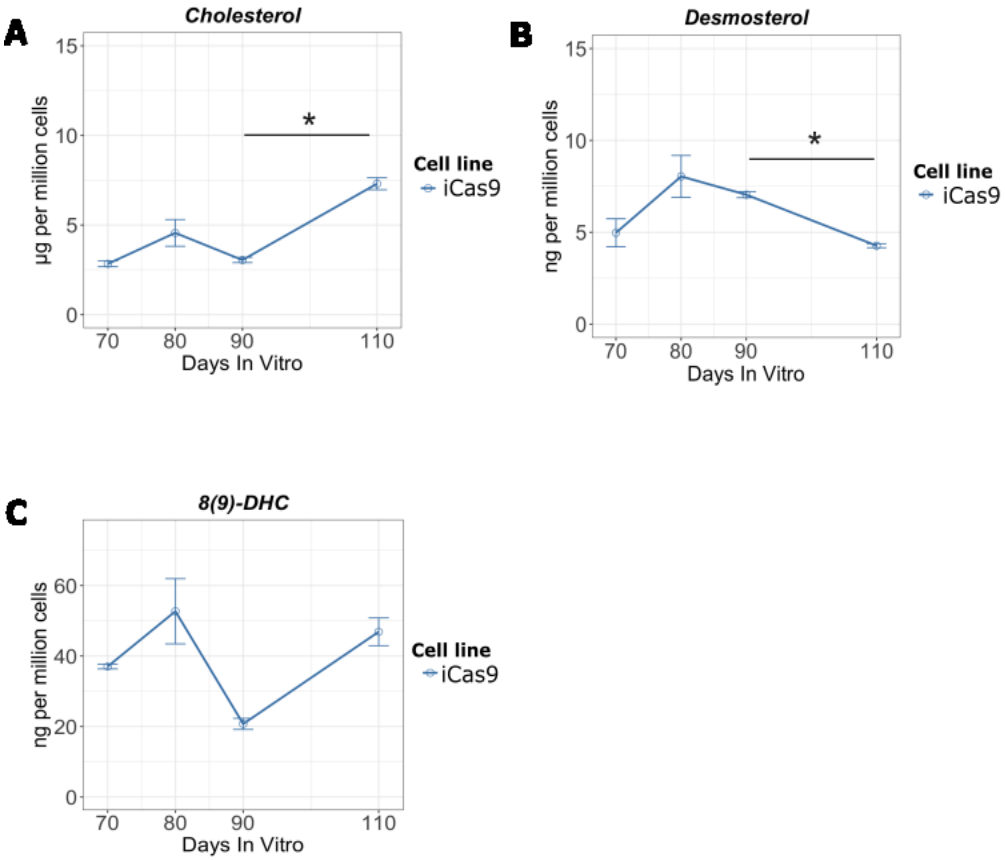

Figure 5.1. LC-MS^n analysis of cholesterol and precursor levels in hESC-derived astrocyte cultures. (**A**) Quantification of cholesterol levels in hESC-derived astrocyte cultures. (**B**) Quantification of desmosterol levels in hESC-derived astrocyte cultures. (**C**) Quantification of 8(9)-DHC levels in hESC-derived astrocyte cultures. Data are shown as mean ± SEM of 3 replicate wells collected over 4 time points from a single differentiation experiment. Repeated measures ANOVA with Bonferroni-corrected pairwise comparisons. *p<0.05.

Following analysis of cholesterol and its precursors, we next focused on assessing cholesterol metabolic activity of these cells, analysing the oxysterols produced during the differentiation. Interestingly, we observed

high levels of 24S-HC production in the terminally differentiated astrocytes, with levels similar to that observed in our neuronal cultures at DIV50 (**Figure 5.2B**). It is interesting to note that there is a sharp increase in 24S-HC in these cells following terminal differentiation of the astrocytic progenitors with the addition of factors CNTF and BMP4, with 24S-HC present at 5.22 ± 0.207 ng/x10^6 cells (**Figure 5.2B**). A similar pattern of an increase in the production of 24S,25-EC in these cells was also observed, detected at 20.5 ± 1.38 ng/x10^6 cells following terminal differentiation (**Figure 5.2A**). However, astrocyte 24S,25-EC levels were more than 40-fold higher than that observed in the neuronal cultures in the previous chapter, which were found to have a 24S,25-EC concentration of 0.5ng/x10^6 cells at DIV50 (**Figure 3.3C**). This finding is in line with previous studies, which demonstrate human primary astrocytes to produce significantly higher levels of 24S,25-EC compared to human primary neurons (Wong et al., 2007).

We were further able to detect and quantify the oxysterol 27-HC, which was present at higher levels in the astrocytic progenitors, but interestingly was undetectable upon terminal differentiation into astrocytes (**Figure 5.2C**).

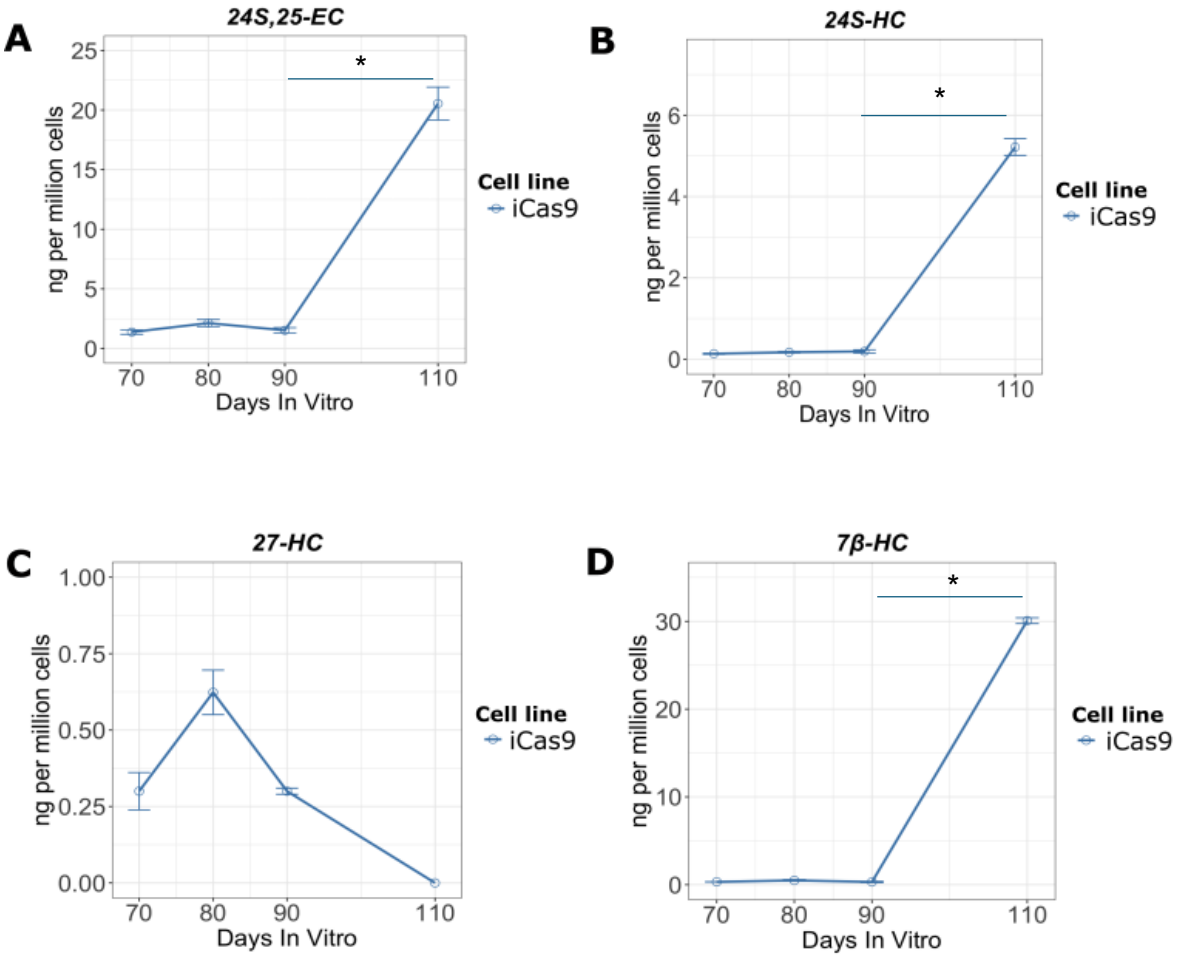

Figure 5.2. Quantification of 24S-HC and 24S,25-EC content of hESC-derived neuronal cells and astrocytes. (**A**) Quantification of total 24S,25-EC levels in hESC-derived astrocyte cultures. (**B**) Quantification of total 24S-HC levels in hESC-derived astrocyte cultures. (**C**) Quantification of 27-HC levels in hESC-derived astrocyte cultures. (**D**) Quantification of 7β-HC levels in hESC-derived astrocyte cultures. Data are shown as mean ± SEM of 3 replicate wells collected over 4 time points points from a single differentiation experiment. Repeated measures ANOVA with Bonferroni-corrected pairwise comparisons. *p<0.05.

5.3.2. Confirmation of cortical astrocytic marker expression

Following the finding that hESC-derived astrocytes produce 24S-HC and 24S,25-EC, we next aimed to confirm if these cells also express the enzyme CYP46A1, responsible for the production of 24S-HC from cholesterol and 24S,25-EC from desmosterol. We therefore repeated this differentiation utilising the same iCas9 hESC line to assess CYP46A1 expression in the astrocytic progenitors and following terminal differentiation into astrocytes.

Firstly, to confirm astrocytic identity, throughout the differentiation of the hESC-derived cell line into cortical astrocytes samples were collected at the same timepoints as the LC-MS^n analysis for ICC analysis of key markers of astrocytic cell fate (**Figure 5.3**). Expression of the astrocyte specific nuclear marker SOX9 (Sun et al., 2017) was confirmed to increase as differentiation progressed (**Figure 5.3A & 5.3C**). Further, expression of NFIA, a nuclear transcription factor that specifies glial cell identity and promotes astrocyte differentiation during embryonic development (Song et al., 2010), was noted to be consistently >90% in the later progenitor stages (**Figure 5.3B and 5.3C**).

Cells were regularly analysed for the marker CD44, a key astrocytic cell surface marker (Liu et al., 2004). This marker expression was also used as an indicator for the timing of the terminal differentiation stage of the differentiation protocol, with cells demonstrated to be 86.8%±1.46 CD44-positive prior to terminal differentiation being carried out (**Figure 5.3C**).

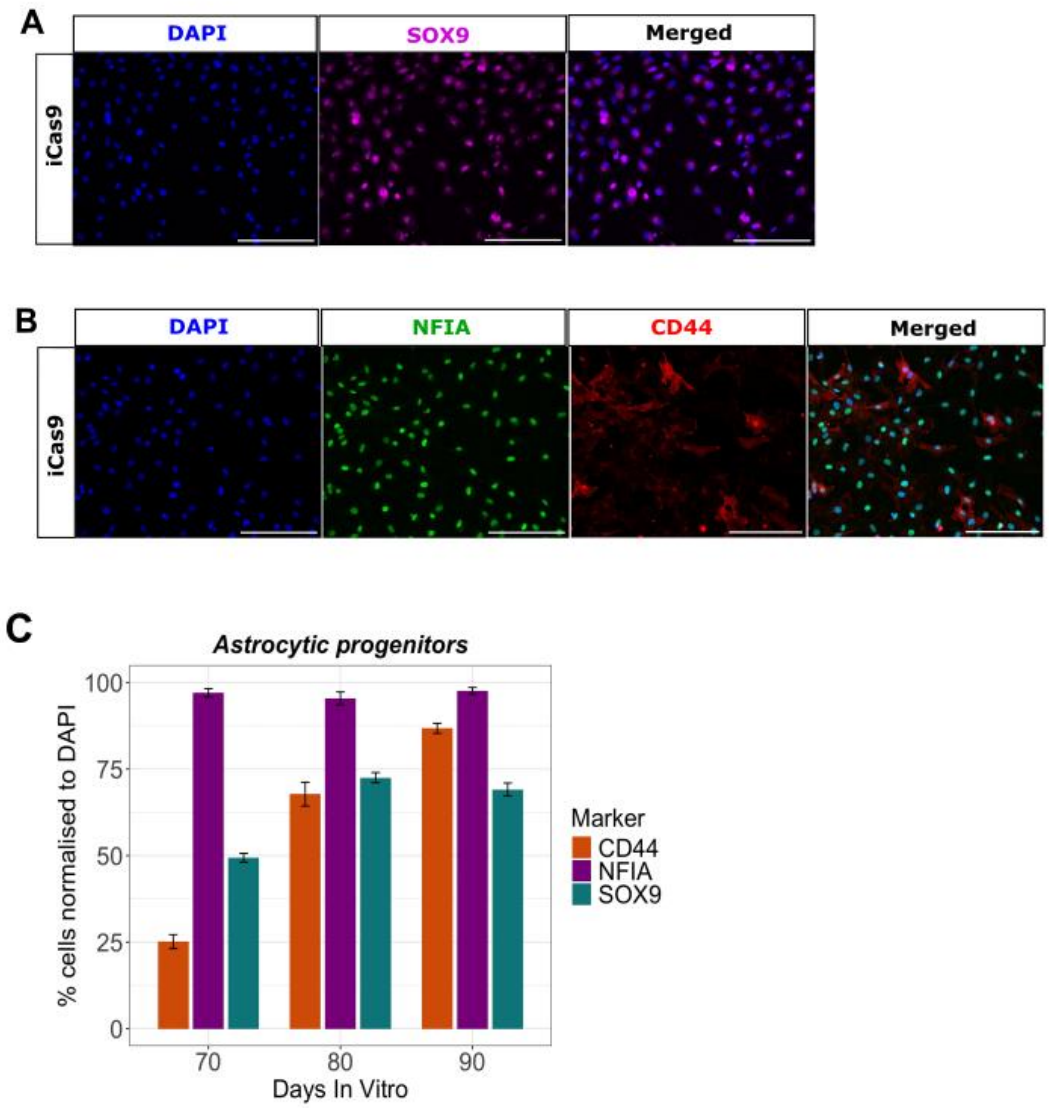

Figure 5.3. Astrocytic markers following terminal differentiation at DIV110. (A) Immunocytochemical analysis of markers NFIA and CD44. **(B)** Immunocytochemical analysis of markers EAAT2 and AQP4. **(C)** Quantification of astrocytic markers detected by immunocytochemistry. Data are shown as mean ± SEM of 3 replicate wells collected over 4 time points from a single differentiation experiment. 20X objective, 200μM scale bar.

Following the terminal differentiation of the astrocytic progenitors into astrocytes, with the addition of BMP4 and CNTF, astrocytic cell identity was confirmed by the expression of key astrocytic markers (**Figure 5.4**). As noted in the previous differentiation used for the LC-MS^n analysis and previous experiments by colleagues utilising this protocol (Li et al., 2025), whilst we weren't able to consistently detect GFAP expression in our cultures, a panel of other cortical astrocytic-specific markers were used to confirm cell identity (Clavreul et al., 2022). We were able to detect high levels of expression of the key astrocytic markers S100β, EAAT2, AQP4, SOX9 and NFIA (**Figure 5.3**).

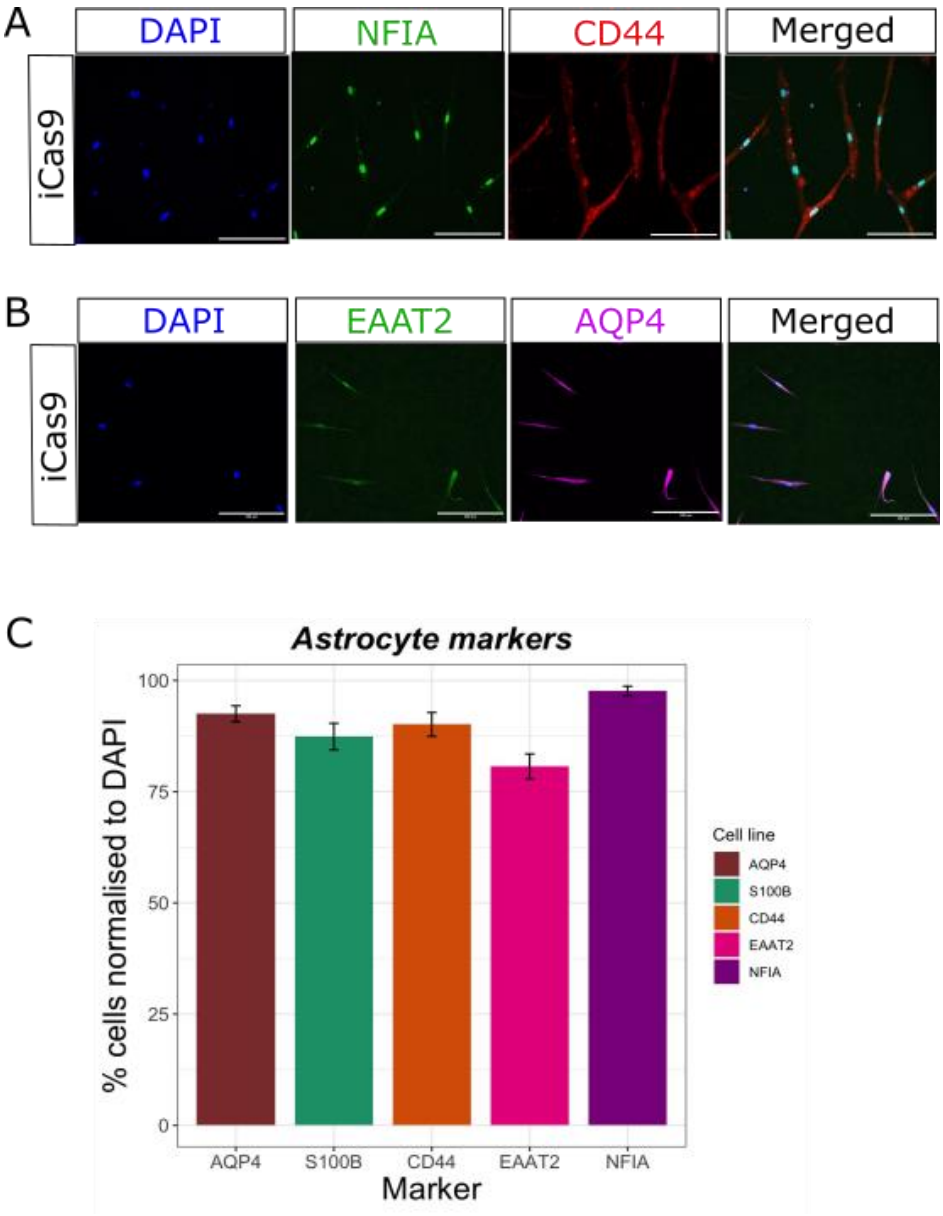

Figure 5.4. Astrocytic markers following terminal differentiation at DIV110. (A) Immunocytochemical analysis of markers NFIA and CD44. **(B)** Immunocytochemical analysis of markers EAAT2 and AQP4. **(C)** Quantification of astrocytic markers detected by immunocytochemistry. Data are shown as mean ± SEM of 3 replicate wells collected over 4 time points from a single differentiation experiment. 20X objective, 200μM scale bar.

5.3.3. hESC-derived cortical astrocytic cells express CYP46A1 enzyme

Following the assessment of cell population astrocytic identity, we aimed to investigate if these cells expressed CYP46A1, by determining both if we able to detect expression in our cultures and if this was co-expressed with key astrocytic markers. Thus, we carried out immunocytochemical analysis staining for CYP46A1 at the astrocytic progenitor stages and astrocytic timepoints used for the LC-MS^n analysis.

Interestingly, this immunocytochemical analysis revealed undetectable expression of CYP46A1 until the final timepoint analysed, following the terminal differentiation of astrocyte precursors into astrocytes (**Figure 5.5**). At this final timepoint we were able to demonstrate co-expression of CYP46A1 with the astrocytic marker S100β (**Figure 5.5A**). We were able to demonstrate that 88.7%±3.07 of cells expressed CYP46A1, with 99.1%±0.754 showed co-expression of CYP46A1 and S100β (**Figure 5.5B & C**). This finding supports the results from our LC-MS^n analysis, which demonstrated a sharp increase in 24S-HC and 24S,25-EC levels in these cultures following terminal differentiation.

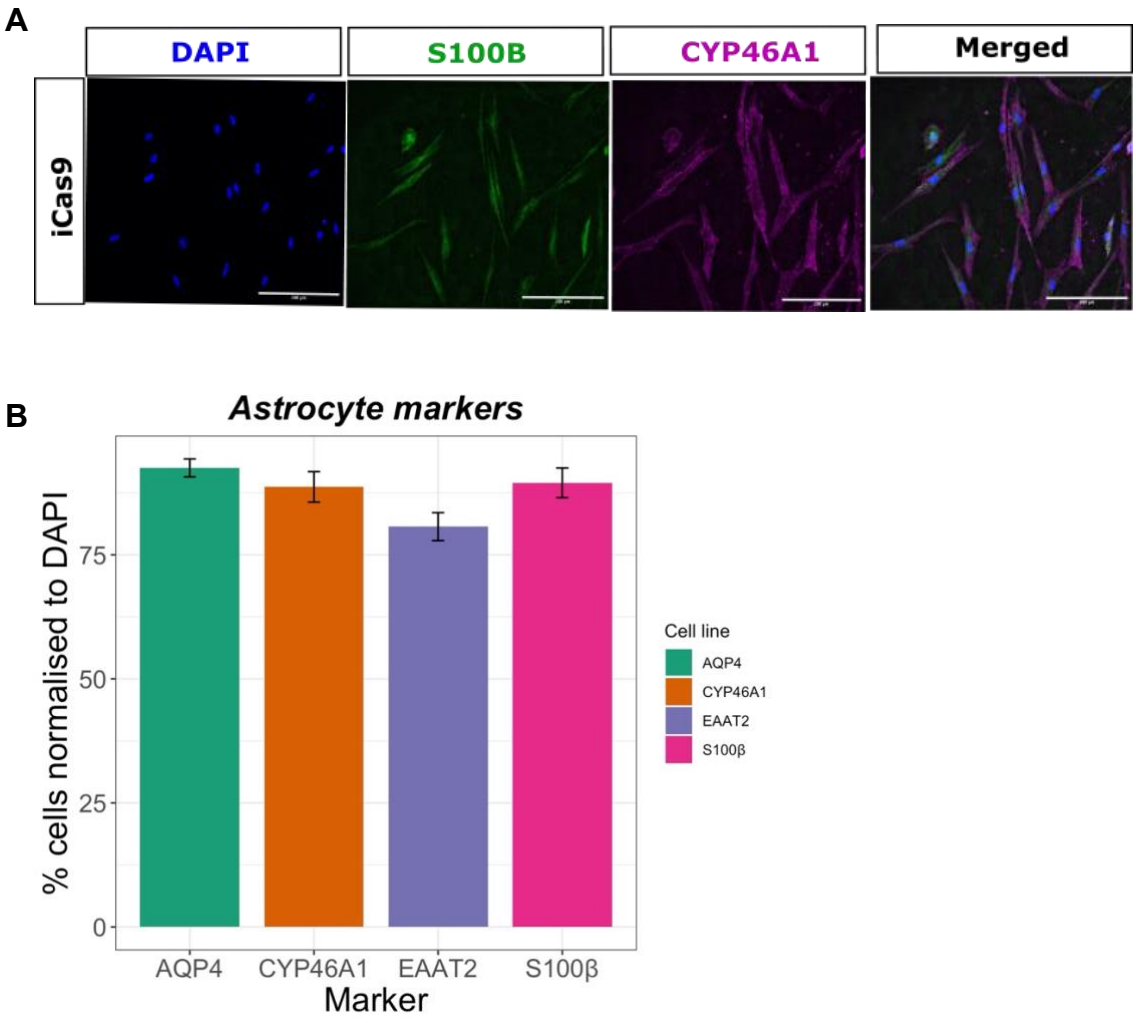

Figure 5.5. CYP46A1 expression co-localises with astrocyte marker expression in hESC-derived cortical astrocyte cultures. (**A**) CYP46A1 expression co-localised with S100β marker expression. (**B**) Percentage of positive cells at DIV115 normalised to DAPI nuclear marker. Data are shown as mean ± SEM of 3 replicate wells collected over 4 time points from a single differentiation experiment.. 20X objective, scale bar = 200μM.

We next aimed to confirm CYP46A1 expression on a protein level, using western blots to confirm CYP46A1 expression present in our cultures. We observed low levels of CYP46A1 protein at earlier timepoints rich in astrocytic progenitors (**Figure 5.6**). However, interestingly we observed increased CYP46A1 protein expression at the later timepoints and following terminal differentiation (**Figure 5.6**).

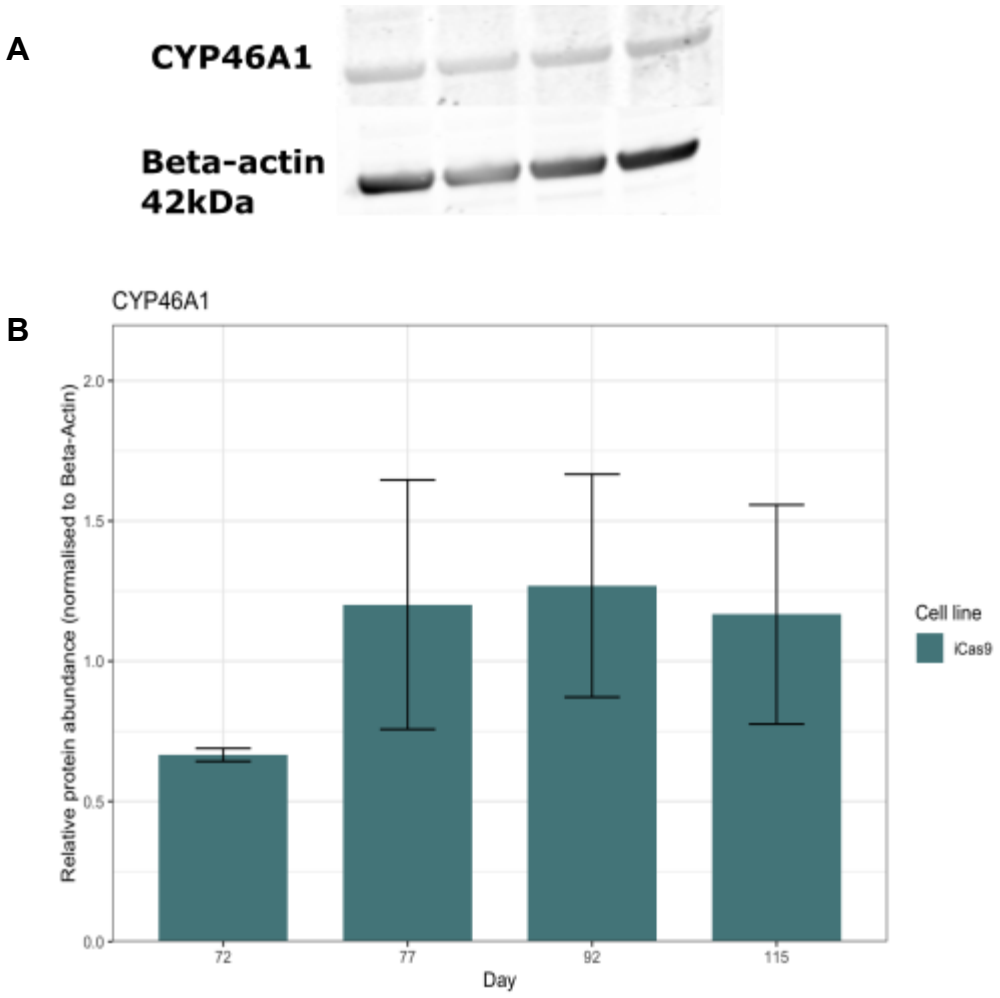

Figure 5.6. CYP46A1 protein expression in hESC-derived cortical astrocyte cultures. (**A**) Bands for CYP46A1 and beta-actin (42kDa). (**B**) Relative protein abundance of CYP46A1 protein was measured in ImageJ and normalised to intensity of beta-actin housekeeper protein on same blot. Data are shown as mean ± SEM of 3 replicate wells collected over 4 time points from a single differentiation experiment. One-way ANOVA, followed by Tukey post-hoc test.

5.3.4. Protein levels of enzymes involved in cholesterol biosynthesis in hESC-derived cortical astrocytic cells

Finally, following the results from our LC-MSn analysis that indicated higher levels of the precursor 8(9)-DHC in our cultures, we aimed to assess the protein level expression of key cholesterol biosynthetic enzymes involved in cholesterol biosynthesis. This would allow us to confirm both overall cholesterol biosynthetic activity and whether the K-R or Bloch biosynthetic pathway appears to be preferred by these cells.

Key enzymes in the cholesterol biosynthetic pathway were selected for analysis, including sterol regulatory element binding protein 2 (SREBP2), the master transcription factor of cholesterol biosynthesis, which controls gene expression of enzymes in the cholesterol biosynthetic pathway. Quantification of both the full-length inactive precursor form of SREBP2 and the cleaved n-terminus of SREBP2 were included in the analysis. We also assessed the expression of hydroxymethylglutaryl-CoA synthase 1 (HMGCS1), the precursor enzyme to the mevalonate pathway and rate limiting enzyme of cholesterol biosynthesis. It was demonstrated that both SREBP2 and HMGCS1 protein expression were detected in the astrocytic progenitors and astrocytic cells following terminal differentiation (**Figure 5.7A & B**).

To confirm our findings following LC-MSn analysis of the immediate precursors to cholesterol, 8(9)-DHC and desmosterol, protein levels were

also assessed for 7-dehydrocholesterol reductase (DHCR7) and 24-dehydrocholesterol reductase (DHCR24), the final enzymes in the Bloch and Kandutsch-Russell (K-R) pathways respectively. This analysis revealed expression of both enzymes in the astrocytic cells, however both enzymes appear to be present at similar levels normalised to the housekeeping gene β-actin and showed no significant changes throughout the differentiation (**Figure 5.7C & D**).

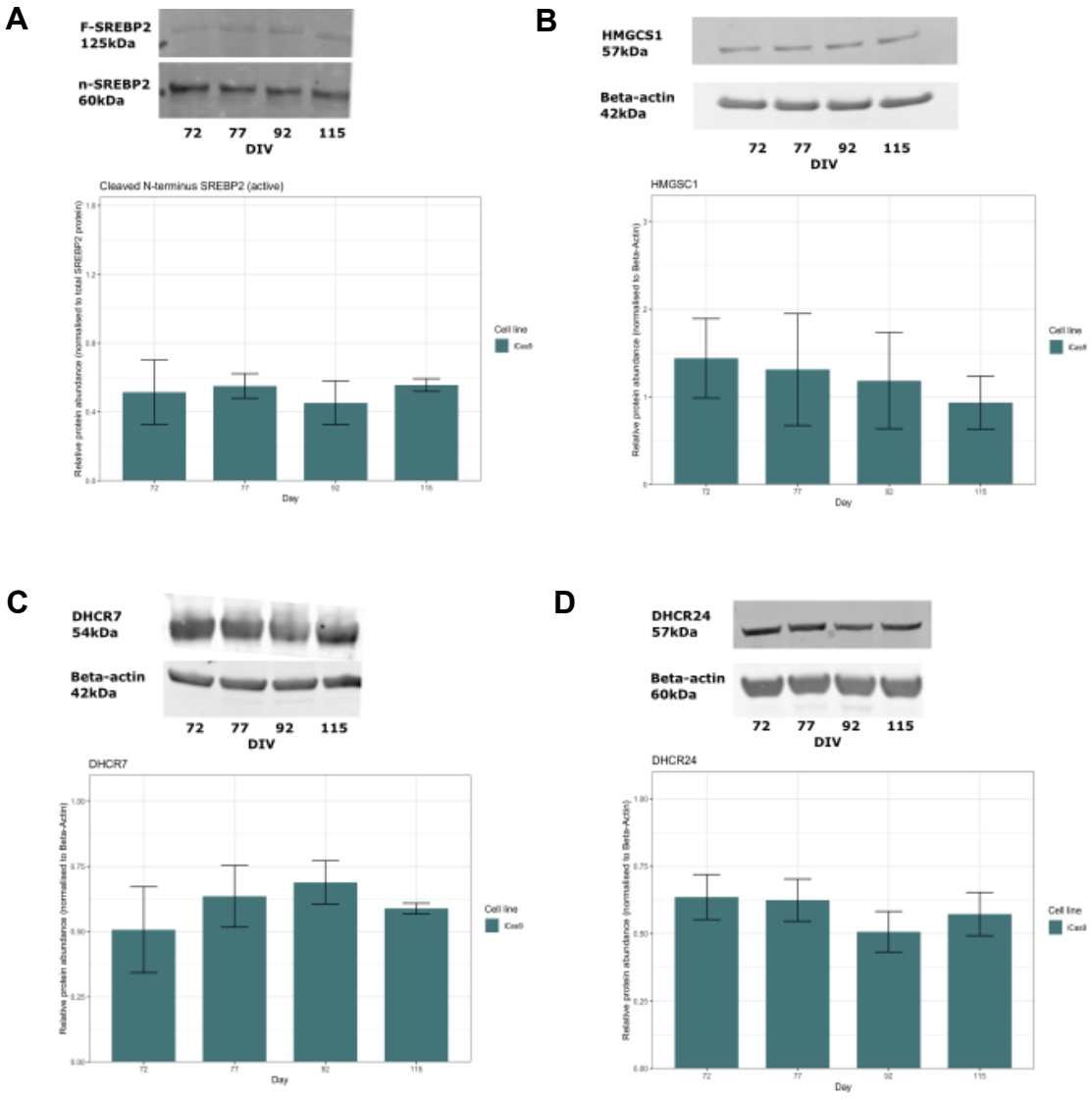

Figure 5.7. Cholesterol biosynthetic enzyme protein expression in hESC-derived astrocytic cultures. (A) SREBP2-cleave n-terminus (60kDa) normalized to total SREBP2 protein expression and beta-actin. **(B)** Total HMGCS1 (57kDa) protein normalized to beta-actin **(C)** Total DHCR7 (54kDa) protein normalized to beta-actin. **(D)** Total DHCR24 (57kDa) protein normalized to beta-actin. Data are shown as mean ± SEM of 3 replicate wells collected over 4 time points from a single differentiation experiment. One-way ANOVA, followed by Tukey post-hoc test.

5.4 Discussion

5.4.1. hESC-derived astrocytes exhibit expression of CYP46A1 and produce 24S-HC

In this work, we have demonstrated using hESC-derived astrocytes as an *in vitro* model of astrogliogenesis, that human astrocytes both express CYP46A1 and produce the bioactive oxysterols 24S-HC and 24S,25-EC. Whilst there is evidence indicating that primary human astrocytes produce 24S,25-EC (Wong et al., 2007), there is so far a lack of evidence that human astrocytes both express CYP46A1 and produce 24S-HC, particularly from a developmental perspective.

Astrocytes play a key function in the brain, with critical roles in synaptic transmission, cognition and behaviour. The regulation of cholesterol metabolism not only in neurons but also in glial cells, including astrocytes, is essential for proper brain functioning. Increasingly, there is a growing recognition for the importance of cross-talk between these cell types in the regulation of cholesterol homeostasis in the brain (Li et al., 2022).

In the adult brain, neurons rely almost entirely on astrocytes for supply of cholesterol (Pfrieger and Ungerer, 2011). Cholesterol produced by astrocytes is bound to the apolipoprotein E (ApoE) and transported by ATP-binding cassette (ABC) transporters, which are then uptaken by neurons via low-density lipoprotein receptors (LDLR) and LDLR-related protein 1 (LRP1). It is thought that neurons are responsible for the turnover of cholesterol due to expression of CYP46A1 being limited to neurons in the

adult brain (Zhang and Liu, 2015). Our work has suggested that in our *in vitro* model of neural development, astrocytes appear to both express CYP46A1 (**Figure 5.5**) and produce 24S-HC (**Figure 5.2**). However, further study into other cholesterol metabolic enzymes as well as the transporters of cholesterol in these cell types would provide a further insight into the ability of these cells to both produce and regulate cholesterol metabolism.

Of note in our analysis is the appearance of CYP46A1 expression and large increase in levels of the oxysterols 24S-HC, 24S,25-EC and 7β-HC at the final timepoint analysed following terminal differentiation of the cultures into astrocytes. Similar increases in cholesterol and its precursors 8(9)-DHC and desmosterol were not observed at this timepoint, whilst the presence of 27-HC was undetectable. Whilst this observation may indeed be due to increased production of these sterols, it should also be considered that the two small molecules introduced to the cultures at this stage of the differentiation may have an effect on cholesterol metabolism themselves. During terminal differentiation, cell media is supplemented with BMP4 and CNTF to promote astrogliogenesis. BMP4 promotes astrocyte differentiation by activating the SMAD1/STAT signallling pathway, leading to the expression of astrocytic markers including GFAP and inhibiting the development of other neural lineages, such as oligodendrocytes (Gomes et al., 2003). CNTF also promotes astrocyte differentiation through its activation of the MAPK and JAK/STAT pathways (Rajan and McKay, 1998). Importantly, both have been shown to affect cholesterol biosynthesis mechanisms, with BMP4 recently evidenced to have an inhibitory effect on cholesterol biosynthesis and shown to downregulate genes encoding for key cholesterol biosynthetic including HMGCS1, HMGCR and SQLE (Chi

et al., 2024). CNTF has also been shown to have a downregulatory effect on SREBP-1 in adipocyte cells (Zvonic et al., 2003). Both factors also cause activation of astrocytes (Hudgins and Levison, 1998; Yang et al., 2019), which therefore may support the previous findings that only reactive astrocytes appear to express CYP46A1 (Brown et al., 2004; Cataldi et al., 2023; TCW et al., 2022).

Whilst 27-HC was found to be present in the astrocytic progenitors, it's production was undetectable following terminal differentiation (**Figure 5.2**). It is also of note that in the iCas9-derived neuronal cultures we were unable to detect 27-HC. The enzyme responsible for 27-HC production, CYP27A1, has been demonstrated to be expressed in rodent astrocytes (Gilardi et al., 2009). Furthermore, the expression of CYP27A1 in astrocytes has been shown to be regulated by LXR signaling, with LXR activation leading to increased CYP27A1 mRNA and protein levels specifically in astrocytes (Gilardi et al., 2009). Alteration to levels of CYP27A1 can disrupt cholesterol handling and delivery to neurons (Gilardi et al., 2009). Interestingly, recent studies have also demonstrated 27-HC to be toxic to astrocytes, by increasing oxidative stress and is linked to astrocytic synaptic dysfunction through the downregulation of glutamate transporters GLAST and GLT-1 (Spanos et al., 2024). Thus, further study of the expression of CYP27A1 in our cultures may help to further elucidate the role of 27-HC in maintaining cholesterol homeostasis between astrocytes and neurons during development.

Interestingly in our analysis we also identified the presence of the oxysterol 7β-hydroxycholesterol (**Figure 5.2**), an oxysterol formed via the

autoxidation of cholesterol, particularly under cases of oxidative stress. With levels of this sterol shown to increase dramatically upon terminal differentiation into astrocytes, this may be an indicator that the cells are under oxidative stress at this timepoint. Interestingly, there is also research that suggests treatment of primary rat astrocytes with 20μM 7β-hydroxycholesterol results in cytotoxicity (Kupferberg et al., 1989).

5.4.2. hESC-derived astrocytes appear to prefer K-R biosynthetic pathway during astrogliosis *in vitro*

With evidence developed following Pfrieger's hypothesis that astrocytes are responsible for the production of cholesterol in the brain postnatally, we aimed to determine if in our *in vitro* model there was any change in cholesterol biosynthesis as hESCs were differentiated from progenitors into astrocytes.

There has previously been evidence that astrocytes and neurons prefer different pathways for cholesterol biosynthesis. Our results here would support the finding that astrocytes have a preference for synthesis of cholesterol via the K-R biosynthetic pathway due to observation of higher levels of 8(9)-DHC, the pathway-specific precursor to cholesterol, compared to desmosterol which forms part of the Bloch pathway (**Figure 5.1**). However, further analysis of protein expression of DHCR24 and DHCR7 did not reveal any significant changes on a protein level of these enzymes as the differentiation progressed. There was however a noted large degree of variation between samples used for the protein analysis, and it should also be considered that these findings are taken from a single

differentiation and would require further independent repeat differentiations in future to confirm our findings.

5.4.3. Impact

This work provides for the first time a characterisation of the temporal sterol profile of a model of human cortical astrogliogenesis *in vitro*. This work develops on the previous chapters, providing information on the sterols produced during human astrocyte development, which can be used to confirm what sterols are produced by astrocytes in comparison to neurons, and whether this is altered between the progenitor and more mature stages of development. Furthermore, this work indicates that astrocytes may indeed be capable of producing 24S-HC, which opens the need for further work in assessing how cholesterol metabolism is regulated during development and potential cross-talk between neurons and astrocytes.

5.4.4. Limitations

Unfortunately we were only able to carry out LC-MS^n analysis using astrocytes from selected timepoints in the differentiation, and not across the entire differentiation paradigm as in the previous chapters examining cortical neuronal differentiations. This is due to the lengthy differentiation protocol required to generate hESC-derived astrocytes and limits on the number of samples we could reasonably analyse on the LC-MS^n within the scope of this project. Due to the similarities in the initial stages of the differentiation to the previously analysed cortical differentiation (**Figure 2.2**) and the emergence of astrocytic-like cells noted around DIV70+ based on

ICC analysis, we reasoned the decision to focus our analysis on these later timepoints to gain the most insight into astrocytic sterol production.

Additionally, we have observed considerable variation within technical replicates, which may influence the robustness of our results. A likely source of this variability is the use of a single cell culture differentiation, with 3 technical well replicates collected per timepoint. This approach may has restrained the biological diversity and introduced culture-specific biases. While such variation isn't uncommon in *in vitro* model systems, this does highlight the need for further work to incorporate multiple independent differentiations to reduce the variability and strengthen the reproducibility of this data.

5.4.5. Further work

Whilst combined ICC and LC-MS^n analysis of cells collected in *in vitro* cell culture conditions provides us with an indication of the sterols produced by the cell population analysed, it is difficult to conclude which individual cell types are responsible for the production of these sterols. A possible approach would be to FACS sort cultures prior to LC-MS^n analysis, however this may reduce the amount of material, which may impede the sterol analysis. With recent advances in single cell lipidomic techniques, such an approach may provide a better idea of the sterolomic profile of individual cells rather than the cell culture population (Li et al., 2021; Tajik et al., 2022).

An additional consideration is the diversity of human astrocytes present in the brain, and if cholesterol biosynthesis and metabolism differs between different astrocyte sub-types (Clavreul et al., 2022). Astrocytes are known to form a heterogenous population in the brain, with recent advances in bulk- and single-cell RNA sequencing further revealing the extent of their diversity (Clavreul et al., 2022).

Whilst we have used *in vitro* cell models for human astrocytes, further confirmation *in vivo* would be required. However, as astrocytes develop postnatally, sourcing human tissue to study this would be extremely difficult. With increasing developments in *in vitro* cell culture models, the possibility of more advanced co-culture, organoid and assembloid models which more closely model the *in vivo* condition (Paşca et al., 2015) would be potential options for further study.

Furthermore, with the observed changes in previous chapters to the sterolomic profiles of neuronal cells derived from CYFIP1-altered hESC and iPSC lines, it would be interesting to investigate if cholesterol metabolism in astrocytes is further impacted. A recent study by (Talvio et al., 2023) has demonstrated dysregulated cholesterol homeostasis in iPSC-derived astrocytes generated from males with fragile X syndrome (FXS), a neurodevelopmental disorder caused by a mutation in the *FMR1* gene encoding the protein FMRP. With the known interaction of CYFIP1 with FMRP, it would be interesting to investigate how altered levels of CYFIP1 may impact astrocytic sterol profiles during astrogliogenesis.

5.4.6. Conclusions

Here we have explored the sterolomic profile of hESC-derived astrocytes in an effort to determine which sterols are produced in these cells during astrogliogenesis and how this changes as cells are terminally differentiated from astrocytic precursor cells to astrocytes. Interestingly, we were able to demonstrate that these cells produce 24S-HC and express the enzyme responsible for its production, CYP46A1. This work highlights the need to further understand not only the sterols produced by neurons in the brain, but in the whole diversity of cells present and how these cells interact to maintain cholesterol homeostasis during human neural development.

Chapter 6
General Discussion

6.1. Summary of Findings

In this thesis, the temporal sterolomic profiles of *in vitro* models of developing human neurons and astrocytes have been generated to investigate how cholesterol homeostasis is regulated and identify the endogenous presence of bioactive sterols implicated in the regulation of key signalling pathways involved in human neural development. From this characterisation we were able to confirm the presence of several oxysterols in the human neuronal cultures, including 24S-HC and 24S,25-EC, that have been evidenced to play a role in neurogenesis. We were able to determine that the predominant oxysterol present in these cultures is 24S-HC, which is also the predominant oxysterol in the adult brain. Additionally, we examined the sterolomic profile of stem cell derived human astrocytes, which revealed these cells produce both 24S-HC and 24S,25-EC as well as evidenced protein expression of the CYP46A1 enzyme. Following the generation of these profiles in control cells, we have then further extended this approach to investigate how altered cholesterol metabolism may impact cortical neurogenesis in a model of neural developmental disorder associated with the 15q11.2 CNV. From this analysis, we were able to confirm significantly altered levels of bioactive oxysterols and enzymes involved in cholesterol biosynthesis. This work both provides evidence of the endogenous presence of bioactive sterols in developing human neural cells and establishes an *in vitro* model framework for the future investigation of how dysregulated cholesterol homeostasis is involved in altered neural development.

6.2. Cholesterol biosynthesis and metabolism during human neural development

This thesis provides the first temporal sterolomic profile of hPSC-derived cells undergoing cortical neurogenesis and astrogliogenesis *in vitro*. In our neuronal cultures, throughout the differentiation we were able to identify the presence of the monohydroxycholesterols 24S-HC, 27-HC, 7-ketocholesterol, 7α-HC, 7β-HC and 6β-HC, 24S,25-EC, the dihydroxycholesterols 7α,26-diHC, cholesterol and its precursors 8(9)-DHC and desmosterol. Of the oxysterols identified, 24S-HC emerged as the predominant oxysterol present, and was shown to increase as neurogenesis progressed, which is in line with evidence that this oxysterol is produced in neurons (Björkhem et al., 1998). This is however in contrast to previous analysis of cortical tissue from embryonic rodent models, which has shown 24S,25-EC to be the predominant sterol during neural development (Wang et al., 2009a). However it is important to note there are differences observed in cholesterol metabolism between humans and various animal species, with rodents evidenced to have a higher basal turnover of cholesterol and bile acids compared to humans (Straniero et al., 2020). Thus, it is crucial to consider this when selecting models for the study of human cholesterol metabolism and biosynthesis. Additionally, it should be considered that the evidence provided in this thesis is derived from monocultures *in vitro*, whereas previous studies have investigated *in vivo* whole tissue samples containing various cell types present in the cortical tissue.

Analysis of the cell media of hPSC-derived cortical cells confirmed the identification of the same sterols as the cell pellet, however also revealed the presence of the more polar cholestenoic acids, (25S)-dihydroxycholestenoic acid and 3β, 7α-dihydroxycholestenoic acid (3β, 7α-diHCA). Bioactive sterols capable of activating LXRs have previously been identified in CSF (Ogundare et al., 2010). Furthermore, cholestenoic acids have previously been implicated in neuronal survival, with 3β, 7α-diHCA shown to promote motor neuron survival via LXR (Theofilopoulos et al., 2014). Additionally, mutations in genes which encode enzymes involved in the metabolism of cholesterol into cholestenoic acids, including CYP7B1 and CYP27A1, are known to result in the neurological conditions hereditary spastic paresis type 5 (SPG5) and cerebrotendinous xanthomatosis (CTX) respectively, with both conditions featuring intellectual disability and behavioural symptoms. Whilst in this study we only initially analysed control cell media, it would be of interest in future sterolomic studies of 15q11.2del patients and other NDDs to assess cholestenoic acid presence in the media collected from these cell cultures.

6.2.1. 24S-HC production in human neural development

24S-HC is produced by the enzyme CYP46A1, and the only 24-OHC stereoisomer present in the human brain, with the 24R-HC stereoisomer only so far only having been identified in mouse brain samples (Griffiths et al., 2019). All 24S-HC present in the circulation is thought to originate from the brain, with this sterol playing an important role in maintaining cholesterol homeostasis across the BBB. However during development, prior to the

formation of the BBB, the exact role of these oxysterols remains unknown. There is additionally a lack of evidence for the endogenous presence of these sterols during human neural development. The characterisation provided in this thesis provides not only insight into the sterols produced during the development of human cortical neurons, but also provides an *in vitro* cell model system for further investigation of how altering cholesterol metabolism may impact neuronal cellular development. Studies have shown that the oxysterols identified in this thesis play a role in neurogenesis, with evidence that 24S,25-EC plays a role in midbrain dopaminergic neurogenesis (Theofilopoulos et al., 2019, 2013) and more recently a study by our lab indicates a role in the regulation of cortical neurogenesis (Fuente et al., 2024). Our subsequent study has suggested that 24S,25-EC promotes cortical neurogenesis through a LXRβ-mediated mechanism (Fuente et al., 2024).

In our analysis we observed increased 24S-HC production in our *in vitro* cultures as the cortical differentiation program progressed and as key neuronal cell marker expression increased. This finding is in line with evidence that 24S-HC is produced by neurons, with the enzyme responsible for its formation, CYP46A1, suggested to be neuronal specific (Lund et al., 2003). 24S-HC is the major oxysterol identified in the human brain, with the oxidation to 24S-HC the major path by which excess cholesterol is eliminated from the brain. However, in recent years 24S-HC has been shown to have further roles in the brain, having both neuromodulatory and transcriptional effects (Shu et al., 2024). 24S-HC has been shown to be a positive allosteric modulator of the NMDA receptors, and been evidenced to have an impact on hippocampal learning and

plasticity in mouse models lacking *Cyp46a1* (Kotti et al., 2006). 24S-HC is also one of the endogenous ligands of the LXRs (Lehmann et al., 1997), and loss of *Cyp46a1* in mouse models has been shown to have a profound transcriptional effect, particularly on genes involved in cholesterol homeostasis (Mast et al., 2017). Whilst shown to be a brain-specific enzyme, there is still a lack of evidence for the impact of cell-type specific knockout of the CYP46A1 enzyme and thus cell-type specific production of 24S-HC, particularly in human cells, with the majority of evidence so far for the role of 24S-HC taken from rodent models. Here, in our work we have been able to confirm 24S-HC production and CYP46A1 expression in cortical neuronal hPSC-derived cell cultures. It would be interesting in future work to investigate the impact of the knockdown of CYP46A1 on hPSC-derived cortical neurogenesis and other neuronal subtypes.

24S-HC levels have previously been shown to be developmentally regulated in mice, with 24S-HC present at lower levels in the embryonic mouse brain and at comparable levels with other oxysterols present (Meljon et al., 2012; Wang et al., 2009a). Further, 24S-HC has a role in regulation of cholesterol transporter and lipoprotein expression in astrocytes (Abildayeva et al., 2006). This indicates a complex system may exist in the form of cross-talk regulation of cholesterol and 24S-HC production between neurons and astrocytes. With our finding that developing astrocytes produce 24S-HC, this highlights the need to further understand how 24S-HC and cholesterol production is regulated throughout development and into the postnatal period, and how this may be impacted in cases of NDD.

6.2.2. Cholesterol metabolism in developing human astrocytes

With increasing evidence for the neuroregulatory role of 24S-HC in the brain, we were interested to look into the role of this oxysterol in other neural cell types, principally astrocytes. There is still debate over the cell type primarily responsible for cholesterol production in the brain, with neurons, astrocytes and oligodendrocytes all considered the likely sources. It is thought that the cell type responsible for cholesterol production may shift during development, with neurons producing their own cholesterol during development and astrocytes thought to be the cell type responsible for the major production of cholesterol in the adult brain, providing neurons with cholesterol via ApoE (Pfrieger, 2003; Pfrieger and Ungerer, 2011). However, there is a lack of evidence for oxysterol production in astrocytes, particularly during neuronal development. We have shown here for the first time that hPSC-derived astrocytes express CYP46A1 and produce both 24S-HC and 24S,25-EC. Whilst a previous study has shown 24S,25-EC production by human primary astrocytes (Wong et al., 2007), there is little evidence that human astrocytes produce 24S-HC, with a single study noting CYP46A1 expression in human post-mortem brain tissue (Brown et al., 2004). It is interesting to speculate that with the identified switch in cholesterol production during development between neurons and astrocytes, that developing astrocytes may also produce 24S-HC whilst this is not the case for postnatal mature astrocytes. However, as the evidence in this thesis is derived from monocultures, further study of co-cultures of

astrocytes and neurons may be able to provide further insight into 24S-HC production and potential crosstalk between these two cell types.

6.3. Dysregulated cholesterol metabolism and altered cortical neurogenesis

Following our characterisation of the sterolome of hPSC-derived cells undergoing cortical neurogenesis *in vitro,* we decided to extend this analysis to a model of a neurodevelopmental disorder caused by the 15q11.2 CNV, that our lab previously found to feature disordered cholesterol metabolism. For this analysis we utilised two pre-existing hESC lines developed by our lab, featuring the knockout and overexpression of the CYFIP1 protein, the candidate gene underlying the neural developmental phenotype observed in affected 15q11.2 CNV carriers, and compared to hPSC lines derived from two 15q11.2del patients to confirm our findings.

From this analysis we were indeed able to confirm that the CYFIP1-altered lines and 15q11.2del patient-derived lines both showed altered sterol profiles compared to their respective control lines. CYFIP1 has been shown to have a role in the regulation of protein translation through interaction with the FMRP-eIF4E protein complex (Napoli et al., 2008). There is evidence for a role for CYFIP1 in regulating cholesterol biosynthesis, with RNA immunoprecipitation sequencing (RIP-Seq) has revealed the master regulator of cholesterol biosynthesis, SREBP2, to be a direct target of

CYFIP1 in the adult mouse cortical and hippocampus tissues (Kim et al., 2022b). Additionally, SREBP2, HMGSC1 and geranylgeranyl diphosphate (GGPS1) have been evidenced to be a target for FMRP in the brain (Darnell et al., 2011b; Sawicka et al., 2019). Our work supports these lines of evidence for a role of CYFIP1 in regulation of cholesterol biosynthesis, with alterations to SREBP2 and HMGSC1 demonstrated on both a RNA and protein level in the CYFIP1-altered neural cells.

A recent study has demonstrated dysregulated cholesterol homeostasis in Fragile X syndrome (FXS) model astrocytes (Talvio et al., 2023), with FXS the most common inherited form of intellectual disability, caused by the absence of FMRP. It would be interesting to investigate the sterolomic profiles of astrocytes derived from the 15q11.2del and CYFIP1-altered lines to determine if a similar disturbance to cholesterol homeostasis is observed.

6.4. Limitations

Whilst we were able to provide a sex-matched healthy control for the 15q11.2del patients, due to the established variation between cell lines identified in Chapter 3, a more appropriate approach for the future analysis of the patient lines would be to correct the patients lines using CRISPR-Cas9 technology to derive isogenic controls for disease modelling, an increasing popular technique in iPSC-derived disease modelling (Burnight et al., 2018; He et al., 2021; Ma et al., 2021). Whilst out of the scope of this project, from the data collected here having demonstrated differences in

sterol profiles between hESC cell lines, it would be important to consider in future experiments utilising patient iPSC lines.

Finally, due to the initial optimisation of the LC-MS^n analysis of the cell pellets, samples collected from the first differentiation analysed required to be pooled and this resulted in the DIV0 and DIV20 timepoints having only 2 technical replicates. From this optimisation we were able to determine that a minimum cell number of ~$0.2x10^6$ cells was required for the sterol extraction in order to obtain a high enough signal for detection in the LC-MS^n analysis. In the repeated analysis we were able to obtain 3 technical replicates, and thus whilst for each timepoint there were 2 biological replicates it must be taken into consideration that for these two timepoints there were a total of 2 technical replicates for the first differentiation compared to 3 technical replicates collected for the remaining timepoints. Additionally, as the findings in this work are derived from 1-2 independent experiments, due to the inherent variability of *in vitro* stem cell models, there is a need for further independent differentiations to confirm these findings.

6.5. Further Directions

This work has provided the first temporal sterol profiling of *in vitro* models of human cortical development and provided a framework for the further study of altered cholesterol homeostasis in models of neural developmental disorder, with the methodology used here to analyse the hPSC-derived cells having potential to be extended to other neurological disorders associated with altered cholesterol biosynthesis and metabolism.

Whilst here we have been able to characterise the bioactive sterols produced during cortical neurogenesis *in vitro*, it would be interesting to further investigate the exact role of these sterols in neurodevelopment. The potential impact of CRISPR-Cas9 knockouts of the enzymes responsible for production of these sterols in *in vitro* models has not yet been investigated, but for certain sterols may be difficult due to shared enzymes leading to the production of various oxysterols. For example, whilst CYP46A1 is responsible for the production of 24S-HC from cholesterol, it is also able to produce 24S,25-EC from desmosterol. There have been various studies looking at the impact of knockout of *Cyp46a1* in mouse models (Ayciriex et al., 2017; Kotti et al., 2006; Lund et al., 2003; Meljon et al., 2012). Interestingly, knockdown of Cyp46a1 has not been shown to alter cholesterol levels, which suggests a robust feedback mechanism in these genetically altered mice (Lund et al., 2003). It would be interesting to assess the impact of *CYP46A1* deletion in both cortical neurons and astrocytes *in vitro*, to assess both the impact on neuronal and astrocytic development as well as the impact on overall cholesterol homeostasis.

Following the identification of bioactive sterols present endogenously in human neural development *in vitro* and various sterols found to be altered in a model of altered cortical neurogenesis, it remains to be confirmed that they are also contributing to neural developmental processes in this *in vitro* model. It would need to be assessed whether altering the levels of these molecules results in changes in expression of key target genes or proteins involved in key neural developmental signalling pathways such as LXR, Hh and Wnt signalling. Conventional knockdown approaches may be difficult, as both cholesterol biosynthesis and metabolic pathways share the same

enzymes to produce various sterols and so this approach may result in the production of multiple sterols being inhibited. There have been further experiments carried out by colleagues in the Li lab to investigate the neurogenic effect of 24S-HC and 24S,25-EC treatment on the development of both cortical and GABAergic neurons [*Unpublished*]. Much evidence so fair indicates oxysterol-LXR mediated regulation of neurogenesis, however possible interaction with Wnt and Shh signalling should not be ruled out in future study, particularly with evidence of a potential crosstalk between oxysterols LXR and Wnt (Makoukji et al., 2011; Shackleford et al., 2013b; Uno et al., 2009).

Using *in vitro* stem cell models, we have developed *in vitro* differentiation protocols that enable us to generate various cell types present in the brain and thus able to assess the impact of altered levels of bioactive sterols on their development. As well as testing developing cells in a 2D monolayer, our lab has additionally developed multiple organoid and assembloid models which could be used to further understand the impact of these sterols in more complex *in vitro* systems more representative of the *in vivo* condition. The use of *in vitro* stem cell models allows for generation of various neuronal cell types to investigate the complexity of NDDs which implicate various cell types in the brain. Ideally these findings would be confirmed *in vivo*, however the restricted access and ethical issues associated with use of human fetal tissue are to be considered.

The work in this thesis provides the first temporal sterol profiling of *in vitro* models of human neurons and astrocyte cultures, however due to the nature of the differentiation the cultures contain mixed populations of

progenitors and post-mitotic neurons and astrocytes. Consequently, in order to interrogate sterol profiles of individual cell types, more targeted approaches such as fluorescence-activated cell sorting (FACS) the cultures could be used prior to sterol analysis to achieve single cell populations. With continuing advancements in single-cell MS techniques (Bennett et al., 2023; Tajik et al., 2022), single-cell LC-MS lipidomics analysis is a rapidly growing approach and could provide individual sterol profiles for different cell types (Kontiza et al., 2025; Li et al., 2021). Unlike bulk analysis which provides average measurements across the cell populations, single-cell techniques allow for analysis of the lipidome of individual cells and provides a powerful tool for understanding cell-specific metabolism. Integrating the EADSA method utilised by our lab with these techniques would be an avenue of interest for the examination of sterols in single-cell resolution.

References

Abildayeva, K., Jansen, P.J., Hirsch-Reinshagen, V., Bloks, V.W., Bakker, A.H.F., Ramaekers, F.C.S., de Vente, J., Groen, A.K., Wellington, C.L., Kuipers, F., Mulder, M., 2006. 24(S)-Hydroxycholesterol Participates in a Liver X Receptor-controlled Pathway in Astrocytes That Regulates Apolipoprotein E-mediated Cholesterol Efflux. J. Biol. Chem. 281, 12799–12808. https://doi.org/10.1074/jbc.M601019200

Alberti, S., Steffensen, K.R., Gustafsson, J.-Å., 2000. Structural characterisation of the mouse nuclear oxysterol receptor genes *LXRα* and *LXRβ*. Gene 243, 93–103. https://doi.org/10.1016/S0378-1119(99)00555-7

Angevine, J.B., Sidman, R.L., 1961. Autoradiographic Study of Cell Migration during Histogenesis of Cerebral Cortex in the Mouse. Nature 192, 766–768. https://doi.org/10.1038/192766b0

Ascano, M., Mukherjee, N., Bandaru, P., Miller, J.B., Nusbaum, J., Corcoran, D.L., Langlois, C., Munschauer, M., Dewell, S., Hafner, M., Williams, Z., Ohler, U., Tuschl, T., 2012. FMR1 targets distinct mRNA sequence elements to regulate protein expression. Nature 492, 382–386. https://doi.org/10.1038/nature11737

Asensio-Ramos, M., Fanali, C., D'Orazio, G., Fanali, S., 2017. Chapter 27 - Nano-liquid chromatography, in: Fanali, S., Haddad, P.R., Poole, C.F., Riekkola, M.-L. (Eds.), Liquid Chromatography (Second Edition). Elsevier, pp. 637–695. https://doi.org/10.1016/B978-0-12-805393-5.00027-0

Audouard, E., Khefif, N., Gillet-Legrand, B., Nobilleau, F., Bouazizi, O., Stanga, S., Despres, G., Alves, S., Lamazière, A., Cartier, N., Piguet, F., 2024. Modulation of Brain Cholesterol Metabolism through CYP46A1 Overexpression for Rett Syndrome. Pharmaceutics 16. https://doi.org/10.3390/pharmaceutics16060756

Ayciriex, S., Djelti, F., Alves, S., Regazzetti, A., Gaudin, M., Varin, J., Langui, D., Bièche, I., Hudry, E., Dargère, D., Aubourg, P., Auzeil, N., Laprévote, O., Cartier, N., 2017. Neuronal Cholesterol Accumulation Induced by Cyp46a1 Down-Regulation in Mouse Hippocampus Disrupts Brain Lipid Homeostasis. Front. Mol. Neurosci. 10. https://doi.org/10.3389/fnmol.2017.00211

Banerjee, S., Mazumdar, S., 2011. Electrospray Ionization Mass Spectrometry: A Technique to Access the Information beyond the

Molecular Weight of the Analyte. Int. J. Anal. Chem. 2012. https://doi.org/10.1155/2012/282574
Barkovich, A.J., Guerrini, R., Kuzniecky, R.I., Jackson, G.D., Dobyns, W.B., 2012. A developmental and genetic classification for malformations of cortical development: update 2012. Brain 135, 1348–1369. https://doi.org/10.1093/brain/aws019
Bauman, M.L., 2010. Medical Comorbidities in Autism: Challenges to Diagnosis and Treatment. Neurotherapeutics, Treatment in Autism 7, 320–327. https://doi.org/10.1016/j.nurt.2010.06.001
Bennett, H.M., Stephenson, W., Rose, C.M., Darmanis, S., 2023. Single-cell proteomics enabled by next-generation sequencing or mass spectrometry. Nat. Methods 20, 363–374. https://doi.org/10.1038/s41592-023-01791-5
Bishop, K.M., Goudreau, G., O'Leary, D.D.M., 2000. Regulation of Area Identity in the Mammalian Neocortex by Emx2 and Pax6. Science 288, 344–349. https://doi.org/10.1126/science.288.5464.344
Björkhem, I., Andersson, U., Ellis, E., Alvelius, G., Ellegård, L., Diczfalusy, U., Sjövall, J., Einarsson, C., 2001a. From Brain to Bile: EVIDENCE THAT CONJUGATION AND ω-HYDROXYLATION ARE IMPORTANT FOR ELIMINATION OF 24S-HYDROXYCHOLESTEROL (CEREBROSTEROL) IN HUMANS*. J. Biol. Chem. 276, 37004–37010. https://doi.org/10.1074/jbc.M103828200
Björkhem, I., Lütjohann, D., Diczfalusy, U., Ståhle, L., Ahlborg, G., Wahren, J., 1998. Cholesterol homeostasis in human brain: turnover of 24S-hydroxycholesterol and evidence for a cerebral origin of most of this oxysterol in the circulation. J. Lipid Res. 39, 1594–1600. https://doi.org/10.1016/S0022-2275(20)32188-X
Björkhem, I., Meaney, S., 2004. Brain Cholesterol: Long Secret Life Behind a Barrier. Arterioscler. Thromb. Vasc. Biol. 24, 806–815. https://doi.org/10.1161/01.ATV.0000120374.59826.1b
Björkhem, I., Starck, L., Andersson, U., Lütjohann, D., Bahr, S. von, Pikuleva, I., Babiker, A., Diczfalusy, U., 2001b. Oxysterols in the circulation of patients with the Smith-Lemli-Opitz syndrome: abnormal levels of 24S- and 27-hydroxycholesterol. J. Lipid Res. 42, 366–371. https://doi.org/10.1016/S0022-2275(20)31660-6
Boyles, J.K., Pitas, R.E., Wilson, E., Mahley, R.W., Taylor, J.M., 1985. Apolipoprotein E associated with astrocytic glia of the central nervous system and with nonmyelinating glia of the peripheral nervous system. J. Clin. Invest. 76, 1501–1513.

Brown, J., Theisler, C., Silberman, S., Magnuson, D., Gottardi-Littell, N., Lee, J.M., Yager, D., Crowley, J., Sambamurti, K., Rahman, M.M., Reiss, A.B., Eckman, C.B., Wolozin, B., 2004. Differential Expression of Cholesterol Hydroxylases in Alzheimer's Disease*. J. Biol. Chem. 279, 34674–34681. https://doi.org/10.1074/jbc.M402324200

Brown, M.S., Goldstein, J.L., 1999. A proteolytic pathway that controls the cholesterol content of membranes, cells, and blood. Proc. Natl. Acad. Sci. U. S. A. 96, 11041–11048.

Burkard, I., von Eckardstein, A., Waeber, G., Vollenweider, P., Rentsch, K.M., 2007. Lipoprotein distribution and biological variation of 24S- and 27-hydroxycholesterol in healthy volunteers. Atherosclerosis 194, 71–78. https://doi.org/10.1016/j.atherosclerosis.2006.09.026

Burnight, E.R., Bohrer, L.R., Giacalone, J.C., Klaahsen, D.L., Daggett, H.T., East, J.S., Madumba, R.A., Worthington, K.S., Mullins, R.F., Stone, E.M., Tucker, B.A., Wiley, L.A., 2018. CRISPR-Cas9-Mediated Correction of the 1.02 kb Common Deletion in CLN3 in Induced Pluripotent Stem Cells from Patients with Batten Disease. CRISPR J. 1, 75–87. https://doi.org/10.1089/crispr.2017.0015

Butler, M.G., 2017. Clinical and Genetic Aspects of the 15q11.2 BP1-BP2 Microdeletion Disorder. J. Intellect. Disabil. Res. JIDR 61, 568–579. https://doi.org/10.1111/jir.12382

Byrne, E.F.X., Sircar, R., Miller, P.S., Hedger, G., Luchetti, G., Nachtergaele, S., Tully, M.D., Mydock-McGrane, L., Covey, D.F., Rambo, R.P., Sansom, M.S.P., Newstead, S., Rohatgi, R., Siebold, C., 2016. Structural basis of Smoothened regulation by its extracellular domains. Nature 535, 517–522. https://doi.org/10.1038/nature18934

Cadwell, C.R., Bhaduri, A., Mostajo-Radji, M.A., Keefe, M.G., Nowakowski, T.J., 2019. Development and Arealization of the Cerebral Cortex. Neuron 103, 980–1004. https://doi.org/10.1016/j.neuron.2019.07.009

Çaku, A., Seidah, N.G., Lortie, A., Gagné, N., Perron, P., Dubé, J., Corbin, F., 2017. New insights of altered lipid profile in Fragile X Syndrome. PLOS ONE 12, e0174301. https://doi.org/10.1371/journal.pone.0174301

Cashikar, A.G., Toral-Rios, D., Timm, D., Romero, J., Strickland, M., Long, J.M., Han, X., Holtzman, D.M., Paul, S.M., 2023. Regulation of astrocyte lipid metabolism and ApoE secretion by the microglial

oxysterol, 25-hydroxycholesterol. J. Lipid Res. 64, 100350. https://doi.org/10.1016/j.jlr.2023.100350
Cataldi, G.G., Elorza, S.D., Toledano-Zaragoza, A., de Olmos, S., Cragnolini, A.B., Martín, M.G., 2023. Cholesterol-24-hydroxylase (CYP46) in the old brain: Analysis of positive populations and factors triggering its expression in astrocytes. J. Comp. Neurol. 531, 486–499. https://doi.org/10.1002/cne.25436
Chen, Z., Borek, D., Padrick, S.B., Gomez, T.S., Metlagel, Z., Ismail, A.M., Umetani, J., Billadeau, D.D., Otwinowski, Z., Rosen, M.K., 2010. Structure and control of the actin regulatory WAVE complex. Nature 468, 533–538. https://doi.org/10.1038/nature09623
Chi, L.H., Redfern, A.D., Lim Kam Sian, T.C.C., Street, I.P., Burrows, A.D., Roslan, S., Daly, R.J., Anderson, R.L., 2024. BMP4-Induced Suppression of Breast Cancer Metastasis Is Associated with Inhibition of Cholesterol Biosynthesis. Int. J. Mol. Sci. 25, 9160. https://doi.org/10.3390/ijms25179160
Chiappelli, J., Quinton, M.S., Volfson, D., Cwik, M., Marshall, W., Bruce, H., Goldwaser, E., Kvarta, M., Summerfelt, A., Kochunov, P., O'Donnell, P., Hong, L.E., 2020. Assessment of brain cholesterol metabolism biomarker 24S-hydroxycholesterol in schizophrenia. Npj Schizophr. 6, 1–6. https://doi.org/10.1038/s41537-020-00121-4
Choudhry, Z., Rikani, A.A., Choudhry, A.M., Tariq, S., Zakaria, F., Asghar, M.W., Sarfraz, M.K., Haider, K., Shafiq, A.A., Mobassarah, N.J., 2014. Sonic hedgehog signalling pathway: a complex network. Ann. Neurosci. 21, 28–31. https://doi.org/10.5214/ans.0972.7531.210109
Clavreul, S., Dumas, L., Loulier, K., 2022. Astrocyte development in the cerebral cortex: Complexity of their origin, genesis, and maturation. https://doi.org/10.3389/fnins.2022.916055
Clifton, N.E., Thomas, K.L., Wilkinson, L.S., Hall, J., Trent, S., 2020. FMRP and CYFIP1 at the Synapse and Their Role in Psychiatric Vulnerability. Complex Psychiatry 6, 5–19. https://doi.org/10.1159/000506858
Corcoran, R.B., Scott, M.P., 2006. Oxysterols stimulate Sonic hedgehog signal transduction and proliferation of medulloblastoma cells. Proc. Natl. Acad. Sci. U. S. A. 103, 8408–8413. https://doi.org/10.1073/pnas.0602852103
Courchesne, E., Mouton, P.R., Calhoun, M.E., Semendeferi, K., Ahrens-Barbeau, C., Hallet, M.J., Barnes, C.C., Pierce, K., 2011. Neuron

Number and Size in Prefrontal Cortex of Children With Autism. JAMA 306, 2001–2010. https://doi.org/10.1001/jama.2011.1638
Crick, P.J., William Bentley, T., Abdel-Khalik, J., Matthews, I., Clayton, P.T., Morris, A.A., Bigger, B.W., Zerbinati, C., Tritapepe, L., Iuliano, L., Wang, Y., Griffiths, W.J., 2015. Quantitative Charge-Tags for Sterol and Oxysterol Analysis. Clin. Chem. 61, 400–411. https://doi.org/10.1373/clinchem.2014.231332
Cyster, J.G., Dang, E.V., Reboldi, A., Yi, T., 2014. 25-Hydroxycholesterols in innate and adaptive immunity. Nat. Rev. Immunol. 14, 731–743. https://doi.org/10.1038/nri3755
Darnell, J.C., Van Driesche, S.J., Zhang, C., Hung, K.Y.S., Mele, A., Fraser, C.E., Stone, E.F., Chen, C., Fak, J.J., Chi, S.W., Licatalosi, D.D., Richter, J.D., Darnell, R.B., 2011a. FMRP Stalls Ribosomal Translocation on mRNAs Linked to Synaptic Function and Autism. Cell 146, 247–261. https://doi.org/10.1016/j.cell.2011.06.013
Darnell, J.C., Van Driesche, S.J., Zhang, C., Hung, K.Y.S., Mele, A., Fraser, C.E., Stone, E.F., Chen, C., Fak, J.J., Chi, S.W., Licatalosi, D.D., Richter, J.D., Darnell, R.B., 2011b. FMRP Stalls Ribosomal Translocation on mRNAs Linked to Synaptic Function and Autism. Cell 146, 247–261. https://doi.org/10.1016/j.cell.2011.06.013
De Wolf, V., Brison, N., Devriendt, K., Peeters, H., 2013. Genetic counseling for susceptibility loci and neurodevelopmental disorders: The del15q11.2 as an example. Am. J. Med. Genet. A. 161, 2846–2854. https://doi.org/10.1002/ajmg.a.36209
DeBarber, A.E., Eroglu, Y., Merkens, L.S., Pappu, A.S., Steiner, R.D., 2011. Smith-Lemli-Opitz Syndrome. Expert Rev. Mol. Med. 13, e24. https://doi.org/10.1017/S146239941100189X
Defesche, J., 2004. Low-density lipoprotein receptor--its structure, function, and mutations. Semin. Vasc. Med. 4 1, 5–11. https://doi.org/10.1055/S-2004-822993
Deshpande, I., Liang, J., Hedeen, D., Roberts, K.J., Zhang, Y., Ha, B., Latorraca, N.R., Faust, B., Dror, R.O., Beachy, P.A., Myers, B.R., Manglik, A., 2019. Smoothened stimulation by membrane sterols drives Hedgehog pathway activity. Nature 571, 284–288. https://doi.org/10.1038/s41586-019-1355-4
Dietschy, J.M., Turley, S.D., 2004. Thematic review series: Brain Lipids. Cholesterol metabolism in the central nervous system during early development and in the mature animal. J. Lipid Res. 45, 1375–1397. https://doi.org/10.1194/jlr.R400004-JLR200

Dietschy, J.M., Turley, S.D., 2001. Cholesterol metabolism in the brain. Curr. Opin. Lipidol. 12, 105–112.
Dwyer, J.R., Sever, N., Carlson, M., Nelson, S.F., Beachy, P.A., Parhami, F., 2007. Oxysterols Are Novel Activators of the Hedgehog Signaling Pathway in Pluripotent Mesenchymal Cells*. J. Biol. Chem. 282, 8959–8968. https://doi.org/10.1074/jbc.M611741200
Fahy, E., Subramaniam, S., Brown, H.A., Glass, C.K., Merrill, A.H., Murphy, R.C., Raetz, C.R.H., Russell, D.W., Seyama, Y., Shaw, W., Shimizu, T., Spener, F., van Meer, G., VanNieuwenhze, M.S., White, S.H., Witztum, J.L., Dennis, E.A., 2005. A comprehensive classification system for lipids1. J. Lipid Res. 46, 839–861. https://doi.org/10.1194/jlr.E400004-JLR200
Fan, X., Kim, H.-J., Bouton, D., Warner, M., Gustafsson, J.-Å., 2008. Expression of liver X receptor β is essential for formation of superficial cortical layers and migration of later-born neurons. Proc. Natl. Acad. Sci. U. S. A. 105, 13445–13450. https://doi.org/10.1073/pnas.0806974105
Felzer-Kim, I.T., Visker, J.R., Ferguson, D.P., Hauck, J.L., 2020. Infant blood lipids: a systematic review of predictive value and influential factors. Expert Rev. Cardiovasc. Ther. 18, 381–394. https://doi.org/10.1080/14779072.2020.1782743
Ferguson-Smith, A.C., 2011. Genomic imprinting: the emergence of an epigenetic paradigm. Nat. Rev. Genet. 12, 565–575. https://doi.org/10.1038/nrg3032
Ferris, H.A., Perry, R.J., Moreira, G.V., Shulman, G.I., Horton, J.D., Kahn, C.R., 2017. Loss of astrocyte cholesterol synthesis disrupts neuronal function and alters whole-body metabolism. Proc. Natl. Acad. Sci. U. S. A. 114, 1189–1194. https://doi.org/10.1073/pnas.1620506114
Fougerousse, F., Bullen, P., Herasse, M., Lindsay, S., Richard, I., Wilson, D., Suel, L., Durand, M., Robson, S., Abitbol, M., Beckmann, J.S., Strachan, T., 2000. Human–mouse differences in the embryonic expression patterns of developmental control genes and disease genes. Hum. Mol. Genet. 9, 165–173. https://doi.org/10.1093/hmg/9.2.165
Francés, L., Quintero, J., Fernández, A., Ruiz, A., Caules, J., Fillon, G., Hervás, A., Soler, C.V., 2022. Current state of knowledge on the prevalence of neurodevelopmental disorders in childhood according to the DSM-5: a systematic review in accordance with

the PRISMA criteria. Child Adolesc. Psychiatry Ment. Health 16, 27. https://doi.org/10.1186/s13034-022-00462-1
Francés, L., Ruiz, A., Soler, C.V., Francés, J., Caules, J., Hervás, A., Carretero, C., Cardona, B., Quezada, E., Fernández, A., Quintero, J., 2023. Prevalence, comorbidities, and profiles of neurodevelopmental disorders according to the DSM-5-TR in children aged 6 years old in a European region. Front. Psychiatry 14. https://doi.org/10.3389/fpsyt.2023.1260747
Francis, K.R., Ton, A.N., Xin, Y., O'Halloran, P.E., Wassif, C.A., Malik, N., Williams, I.M., Cluzeau, C.V., Trivedi, N.S., Pavan, W.J., Cho, W., Westphal, H., Porter, F.D., 2016. Modeling Smith-Lemli-Opitz syndrome with induced pluripotent stem cells reveals a causal role for Wnt/β-catenin defects in neuronal cholesterol synthesis phenotypes. Nat. Med. 22, 388–396. https://doi.org/10.1038/nm.4067
Fuccillo, M., Rallu, M., McMahon, A.P., Fishell, G., 2004. Temporal requirement for hedgehog signaling in ventral telencephalic patterning. Development 131, 5031–5040. https://doi.org/10.1242/dev.01349
Fuente, D.C.D.L., Tamburini, C., Stonelake, E., Andrews, R., Hall, J., Owen, M.J., Linden, D.E.J., Pocklington, A., Li, M., 2024. Impaired oxysterol-liver X receptor signaling underlies aberrant cortical neurogenesis in a stem cell model of neurodevelopmental disorder. Cell Rep. 43. https://doi.org/10.1016/j.celrep.2024.113946
Fukumoto, H., Deng, A., Irizarry, M.C., Fitzgerald, M.L., Rebeck, G.W., 2002. Induction of the Cholesterol Transporter ABCA1 in Central Nervous System Cells by Liver X Receptor Agonists Increases Secreted Aβ Levels*. J. Biol. Chem. 277, 48508–48513. https://doi.org/10.1074/jbc.M209085200
Fünfschilling, U., Jockusch, W.J., Sivakumar, N., Möbius, W., Corthals, K., Li, S., Quintes, S., Kim, Y., Schaap, I.A.T., Rhee, J.-S., Nave, K.-A., Saher, G., 2012. Critical Time Window of Neuronal Cholesterol Synthesis during Neurite Outgrowth. J. Neurosci. 32, 7632–7645. https://doi.org/10.1523/JNEUROSCI.1352-11.2012
Furse, S., Egmond ,Maarten R., and Killian, J.A., 2015. Isolation of lipids from biological samples. Mol. Membr. Biol. 32, 55–64. https://doi.org/10.3109/09687688.2015.1050468
Geiger, T., Wehner, A., Schaab, C., Cox, J., Mann, M., 2012. Comparative Proteomic Analysis of Eleven Common Cell Lines Reveals Ubiquitous but Varying Expression of Most Proteins. Mol. Cell.

Proteomics MCP 11, M111.014050. https://doi.org/10.1074/mcp.M111.014050
Genaro-Mattos, T.C., Anderson, A., Allen, L.B., Korade, Z., Mirnics, K., 2019. Cholesterol Biosynthesis and Uptake in Developing Neurons. ACS Chem. Neurosci. 10, 3671–3681. https://doi.org/10.1021/acschemneuro.9b00248
Gilardi, F., Viviani, B., Galmozzi, A., Boraso, M., Bartesaghi, S., Torri, A., Caruso, D., Crestani, M., Marinovich, M., Fabiani, E. de, 2009. Expression of sterol 27-hydroxylase in glial cells and its regulation by liver X receptor signaling. Neuroscience 164, 530–540. https://doi.org/10.1016/j.neuroscience.2009.08.003
Gold, E.S., Diercks, A.H., Podolsky, I., Podyminogin, R.L., Askovich, P.S., Treuting, P.M., Aderem, A., 2014. 25-Hydroxycholesterol acts as an amplifier of inflammatory signaling. Proc. Natl. Acad. Sci. 111, 10666–10671. https://doi.org/10.1073/pnas.1404271111
Gomes, W.A., Mehler, M.F., Kessler, J.A., 2003. Transgenic overexpression of BMP4 increases astroglial and decreases oligodendroglial lineage commitment. Dev. Biol. 255, 164–177. https://doi.org/10.1016/S0012-1606(02)00037-4
Gordeeva, V., Sharova, E., Arapidi, G., 2022. Progress in Methods for Copy Number Variation Profiling. Int. J. Mol. Sci. 23, 2143. https://doi.org/10.3390/ijms23042143
Goytain, A., Hines, R.M., El-Husseini, A., Quamme, G.A., 2007. *NIPA1*(*SPG6*), the Basis for Autosomal Dominant Form of Hereditary Spastic Paraplegia, Encodes a Functional Mg2+ Transporter*. J. Biol. Chem. 282, 8060–8068. https://doi.org/10.1074/jbc.M610314200
Grayaa, S., Zerbinati, C., Messedi, M., HadjKacem, I., Chtourou, M., Ben Touhemi, D., Naifar, M., Ayadi, H., Ayedi, F., Iuliano, L., 2018. Plasma oxysterol profiling in children reveals 24-hydroxycholesterol as a potential marker for Autism Spectrum Disorders. Biochimie, “Current trends in oxysterols and related sterols”. 153, 80–85. https://doi.org/10.1016/j.biochi.2018.04.026
Griffiths, W.J., Crick, Peter.J., Meljon, A., Theofilopoulos, S., Jonas, A.-K., Yutuc, E., Parker, J.E., Kelly, D., Kelly, S.L., Arenas, E., Wang, Y., 2019. Additional pathways of sterol metabolism: Evidence from analysis of Cyp27a1−/− mouse brain and plasma. BBA - Mol. Cell Biol. Lipid 1864, 191–211.
Griffiths, W.J., Crick, P.J., Wang, Yuchen, Ogundare, M., Tuschl, K., Morris, A.A., Bigger, B.W., Clayton, P.T., Wang, Yuqin, 2013.

Analytical strategies for characterization of oxysterol lipidomes: Liver X receptor ligands in plasma. Free Radic. Biol. Med., Methods in Lipid Oxidation 59, 69–84. https://doi.org/10.1016/j.freeradbiomed.2012.07.027

Griffiths, W.J., Wang, Y., 2021. Sterols, Oxysterols, and Accessible Cholesterol: Signalling for Homeostasis, in Immunity and During Development. Front. Physiol. 12, 723224. https://doi.org/10.3389/fphys.2021.723224

Grosche, J., Matyash, V., Moller, T., Verkhratsky, A., Reichenbach, A., Kettenmann, H., 1999. Microdomains for neuron–glia interaction: parallel fiber signaling to Bergmann glial cells. Nat Neurosci 139–43.

Grove, E.A., Tole, S., Limon, J., Yip, L., Ragsdale, C.W., 1998. The hem of the embryonic cerebral cortex is defined by the expression of multiple Wnt genes and is compromised in Gli3-deficient mice. Development 125, 2315–2325. https://doi.org/10.1242/dev.125.12.2315

Guo, L., Xu, P., Tang, X., Wu, Q., Xing, Y., Gustafsson, J.-A., Xu, H., Fan, X., 2014. Liver X receptor β delays transformation of radial glial cells into astrocytes during mouse cerebral cortical development. Neurochem. Int. 71, 8–16. https://doi.org/10.1016/j.neuint.2014.03.009

Haag, A.M., 2016. Mass Analyzers and Mass Spectrometers. Adv. Exp. Med. Biol. 919, 157–169. https://doi.org/10.1007/978-3-319-41448-5_7

Hagerman, P.J., Hagerman, R., 2021. Fragile X syndrome. Curr. Biol. 31, R273–R275. https://doi.org/10.1016/j.cub.2021.01.043

Halassa, M.M., Fellin, T., Takano, H., Dong, J.H., Haydon, P.G., 2007. Synaptic islands defined by the territory of a single astrocyte. J Neurosci 27, 6473–7.

He, L., Wang, S., Peng, L., Zhao, H., Li, S., Han, X., Habimana, J. de D., Chen, Z., Wang, C., Peng, Y., Peng, H., Xie, Y., Lei, L., Deng, Q., Wan, L., Wan, N., Yuan, H., Gong, Y., Zou, G., Li, Z., Tang, B., Jiang, H., 2021. CRISPR/Cas9 mediated gene correction ameliorates abnormal phenotypes in spinocerebellar ataxia type 3 patient-derived induced pluripotent stem cells. Transl. Psychiatry 11, 479. https://doi.org/10.1038/s41398-021-01605-2

Hennegan, J., Bryant, A.H., Griffiths, L., Trigano, M., Bartley, O.J.M., Bartlett, J.J., Minahan, C., Abreu de Oliveira, W.A., Yutuc, E., Ntikas, S., Bartsocas, C.S., Markouri, M., Antoniadou, E., Laina, I.,

Howell, O.W., Li, M., Wang, Y., Griffiths, W.J., Lane, E.L., Lelos, M.J., Theofilopoulos, S., 2023. Inhibition of 7α,26-dihydroxycholesterol biosynthesis promotes midbrain dopaminergic neuron development. iScience 27, 108670. https://doi.org/10.1016/j.isci.2023.108670

Hirabayashi, Y., Itoh, Y., Tabata, H., Nakajima, K., Akiyama, T., Masuyama, N., Gotoh, Y., 2004. The Wnt/β-catenin pathway directs neuronal differentiation of cortical neural precursor cells. Development 131, 2791–2801. https://doi.org/10.1242/dev.01165

Holčapek, M., Jirásko, R., Lísa, M., 2012. Recent developments in liquid chromatography–mass spectrometry and related techniques. Mass Spectrom. Innov. Appl. Part VII 1259, 3–15. https://doi.org/10.1016/j.chroma.2012.08.072

Huang, P., Nedelcu, D., Watanabe, M., Jao, C., Kim, Y., Liu, J., Salic, A., 2016. Cellular cholesterol directly activates Smoothened in Hedgehog signaling. Cell 166, 1176-1187.e14. https://doi.org/10.1016/j.cell.2016.08.003

Hudgins, S.N., Levison, S.W., 1998. Ciliary Neurotrophic Factor Stimulates Astroglial Hypertrophy*in Vivo*and*in Vitro*. Exp. Neurol. 150, 171–182. https://doi.org/10.1006/exnr.1997.6735

Ingham, P.W., McMahon, A.P., 2001. Hedgehog signaling in animal development: paradigms and principles. Genes Dev. 15, 3059–3087. https://doi.org/10.1101/gad.938601

Isaac, G., Jeannotte, R., Esch, S.W., Welti, R., 2007. New mass-spectrometry-based strategies for lipids. Genet. Eng. (N. Y.) 28, 129–157. https://doi.org/10.1007/978-0-387-34504-8_8

Itel, F., Al-Samir, S., Öberg, F., Chami, M., Kumar, M., Supuran, C.T., Deen, P.M.T., Meier, W., Hedfalk, K., Gros, G., Endeward, V., 2012. CO2 permeability of cell membranes is regulated by membrane cholesterol and protein gas channels. FASEB J. 26, 5182–5191. https://doi.org/10.1096/fj.12-209916

Jessell, T.M., 2000. Neuronal specification in the spinal cord: inductive signals and transcriptional codes. Nat. Rev. Genet. 1, 20–29. https://doi.org/10.1038/35049541

Karten, B., Campenot, R.B., Vance, D.E., Vance, J.E., 2006. Expression of ABCG1, but Not ABCA1, Correlates with Cholesterol Release by Cerebellar Astroglia*. J. Biol. Chem. 281, 4049–4057. https://doi.org/10.1074/jbc.M508915200

Kelley, R., Hennekam, R., 2000. The Smith-Lemli-Opitz syndrome. J. Med. Genet. 37, 321–335. https://doi.org/10.1136/jmg.37.5.321

Kim, A.S., Anderson, S.A., Rubenstein, J.L.R., Lowenstein, D.H., Pleasure, S.J., 2001. Pax-6 Regulates Expression ofSFRP-2 and Wnt-7b in the Developing CNS. J. Neurosci. 21, RC132. https://doi.org/10.1523/JNEUROSCI.21-05-j0002.2001

Kim, N.-S., Ringeling, F.R., Zhou, Y., Nguyen, H.N., Temme, S.J., Lin, Y.-T., Eacker, S., Dawson, V.L., Dawson, T.M., Xiao, B., Hsu, K., Canzar, S., Li, W., Worley, P., Christian, K.M., Yoon, K.-J., Song, H., Ming, G., 2022a. CYFIP1 Dosages Exhibit Divergent Behavioral Impact via Diametric Regulation of NMDA Receptor Complex Translation in Mouse Models of Psychiatric Disorders. Biol. Psychiatry 92, 815–826. https://doi.org/10.1016/j.biopsych.2021.04.023

Kim, N.-S., Ringeling, F.R., Zhou, Y., Nguyen, H.N., Temme, S.J., Lin, Y.-T., Eacker, S., Dawson, V.L., Dawson, T.M., Xiao, B., Hsu, K., Canzar, S., Li, W., Worley, P., Christian, K.M., Yoon, K.-J., Song, H., Ming, G., 2022b. CYFIP1 Dosages Exhibit Divergent Behavioral Impact via Diametric Regulation of NMDA Receptor Complex Translation in Mouse Models of Psychiatric Disorders. Biol. Psychiatry 92, 815–826. https://doi.org/10.1016/j.biopsych.2021.04.023

Kim, S.-M., Kim, B.-Y., Lee, S.-A., Eo, S.-K., Yun, Y., Kim, C.-D., Kim, K., 2014. 27-Hydroxycholesterol and 7alpha-hydroxycholesterol trigger a sequence of events leading to migration of CCR5-expressing Th1 lymphocytes. Toxicol. Appl. Pharmacol. 274, 462–470. https://doi.org/10.1016/j.taap.2013.12.007

Kinnebrew, M., Iverson, E.J., Patel, B.B., Pusapati, G.V., Kong, J.H., Johnson, K.A., Luchetti, G., Eckert, K.M., McDonald, J.G., Covey, D.F., Siebold, C., Radhakrishnan, A., Rohatgi, R., n.d. Cholesterol accessibility at the ciliary membrane controls hedgehog signaling. eLife 8, e50051. https://doi.org/10.7554/eLife.50051

Koldamova, R.P., Lefterov, I.M., Ikonomovic, M.D., Skoko, J., Lefterov, P.I., Isanski, B.A., DeKosky, S.T., Lazo, J.S., 2003. 22*R*-Hydroxycholesterol and 9-*cis*-Retinoic Acid Induce ATP-binding Cassette Transporter A1 Expression and Cholesterol Efflux in Brain Cells and Decrease Amyloid β Secretion*. J. Biol. Chem. 278, 13244–13256. https://doi.org/10.1074/jbc.M300044200

Kontiza, A., Gerichten, J. von, Spick, M., Fraser, E., Costa, C., Saunders, K.D.G., Whetton, A.D., Newman, C.F., Bailey, M.J., 2025. Single-cell lipidomics: protocol development for reliable cellular profiling

using capillary sampling. Analyst 150, 1261–1270. https://doi.org/10.1039/D5AN00037H
Korade, Z., Xu, L., Shelton, R., Porter, N.A., 2010. Biological activities of 7-dehydrocholesterol-derived oxysterols: implications for Smith-Lemli-Opitz syndrome[S]. J. Lipid Res. 51, 3259–3269. https://doi.org/10.1194/jlr.M009365
Kotti, T.J., Ramirez, D.M.O., Pfeiffer, B.E., Huber, K.M., Russell, D.W., 2006. Brain cholesterol turnover required for geranylgeraniol production and learning in mice. Proc. Natl. Acad. Sci. 103, 3869–3874. https://doi.org/10.1073/pnas.0600316103
Krause, M.R., Regen, S.L., 2014. The Structural Role of Cholesterol in Cell Membranes: From Condensed Bilayers to Lipid Rafts. Acc. Chem. Res. 47, 3512–3521. https://doi.org/10.1021/ar500260t
Krysanova, N., Sivko, R., Krupko, O., Borisova, T., 2007. [Methyl-beta-cyclodextrin influences glutamate transport in the rat brain nerve terminals by depletion of membrane cholesterol]. Ukr. Biokhim. Zh. 79 3, 29–37.
Kupferberg, A., Teller, G., Behr, P., Leray, C., Urban, P.F., Vincendon, G., Mersel, M., 1989. Effect of 7β-hydroxycholesterol on astrocyte primary cultures and derived spontaneously transformed cell lines: cytotoxicity and metabolism. Biochim. Biophys. Acta BBA - Mol. Cell Res. 1013, 231–238. https://doi.org/10.1016/0167-4889(89)90140-7
Lee, J.J., Ekker, S.C., von Kessler, D.P., Porter, J.A., Sun, B.I., Beachy, P.A., 1994. Autoproteolysis in hedgehog Protein Biogenesis. Science 266, 1528–1537. https://doi.org/10.1126/science.7985023
Lee, S.M.K., Tole, S., Grove, E.A., McMahon, A.P., 2000. A local Wnt-3a signal is required for development of the mammalian hippocampus. Development 127, 457–467. https://doi.org/10.1242/dev.127.3.457
Lehmann, J.M., Kliewer, S.A., Moore, L.B., Smith-Oliver, T.A., Oliver, B.B., Su, J.-L., Sundseth, S.S., Winegar, D.A., Blanchard, D.E., Spencer, T.A., Willson, T.M., 1997. Activation of the Nuclear Receptor LXR by Oxysterols Defines a New Hormone Response Pathway *. J. Biol. Chem. 272, 3137–3140. https://doi.org/10.1074/jbc.272.6.3137
Li, D., Zhang, J., Liu, Q., 2022. Brain cell type-specific cholesterol metabolism and implications for learning and memory. Trends Neurosci. 45, 401–414. https://doi.org/10.1016/j.tins.2022.01.002
Li, Z., Cardo, L.F., Rokicki, M., Monzón-Sandoval, J., Volpato, V., Wessely, F., Webber, C., Li, M., 2025. Changes in neural progenitor

lineage constituent during astrocytic differentiation of human iPSCs. eLife 13. https://doi.org/10.7554/eLife.96423.2
Li, Z., Cheng, S., Lin, Q., Cao, W., Yang, J., Zhang, M., Shen, A., Zhang, W., Xia, Y., Ma, X., Ouyang, Z., 2021. Single-cell lipidomics with high structural specificity by mass spectrometry. Nat. Commun. 12, 2869. https://doi.org/10.1038/s41467-021-23161-5
Lisik, M.Z., Gutmajster, E., Sieroń, A.L., 2016. Low Levels of HDL in Fragile X Syndrome Patients. Lipids 51, 189–192. https://doi.org/10.1007/s11745-015-4109-6
Liu, J., Xiao, Q., Xiao, J., Niu, C., Li, Y., Zhang, X., Zhou, Z., Shu, G., Yin, G., 2022. Wnt/β-catenin signalling: function, biological mechanisms, and therapeutic opportunities. Signal Transduct. Target. Ther. 7, 1–23. https://doi.org/10.1038/s41392-021-00762-6
Liu, Y., Han, S.S.W., Wu, Y., Tuohy, T.M.F., Xue, H., Cai, J., Back, S.A., Sherman, L.S., Fischer, I., Rao, M.S., 2004. CD44 expression identifies astrocyte-restricted precursor cells. Dev. Biol. 276, 31–46. https://doi.org/10.1016/j.ydbio.2004.08.018
Logan, C.Y., Nusse, R., 2004. The Wnt signaling pathway in development and disease. Annu. Rev. Cell Dev. Biol. 20, 781–810. https://doi.org/10.1146/annurev.cellbio.20.010403.113126
Loomba, S., Straehle, J., Gangadharan, V., Heike, N., Khalifa, A., Motta, A., Ju, N., Sievers, M., Gempt, J., Meyer, H.S., Helmstaedter, M., 2022. Connectomic comparison of mouse and human cortex. Science 377, eabo0924. https://doi.org/10.1126/science.abo0924
Luchetti, G., Sircar, R., Kong, J.H., Nachtergaele, S., Sagner, A., Byrne, E.F., Covey, D.F., Siebold, C., Rohatgi, R., 2016. Cholesterol activates the G-protein coupled receptor Smoothened to promote Hedgehog signaling. eLife 5, e20304. https://doi.org/10.7554/eLife.20304
Lund, E.G., Guileyardo, J.M., Russell, D.W., 1999. cDNA cloning of cholesterol 24-hydroxylase, a mediator of cholesterol homeostasis in the brain. Proc. Natl. Acad. Sci. U. S. A. 96, 7238–7243.
Lund, E.G., Xie, C., Kotti, T., Turley, S.D., Dietschy, J.M., Russell, D.W., 2003. Knockout of the Cholesterol 24-Hydroxylase Gene in Mice Reveals a Brain-specific Mechanism of Cholesterol Turnover*. J. Biol. Chem. 278, 22980–22988. https://doi.org/10.1074/jbc.M303415200
Lütjohann, D., Breuer, O., Ahlborg, G., Nennesmo, I., Sidén, A., Diczfalusy, U., Björkhem, I., 1996. Cholesterol homeostasis in human brain: evidence for an age-dependent flux of 24S-

hydroxycholesterol from the brain into the circulation. Proc. Natl. Acad. Sci. U. S. A. 93, 9799–9804.
Ma, L., Schmidt, M., Morrow, E.M., 2021. Human iPSC lines from a Christianson syndrome patient with NHE6 W523X mutation, a biologically-related control, and CRISPR/Cas9 gene-corrected isogenic controls. Stem Cell Res. 54, 102435. https://doi.org/10.1016/j.scr.2021.102435
Makoukji, J., Shackleford, G., Meffre, D., Grenier, J., Liere, P., Lobaccaro, J.-M.A., Schumacher, M., Massaad, C., 2011. Interplay between LXR and Wnt/ -Catenin Signaling in the Negative Regulation of Peripheral Myelin Genes by Oxysterols. J. Neurosci. 31, 9620–9629. https://doi.org/10.1523/JNEUROSCI.0761-11.2011
Malhotra, D., Sebat, J., 2012. CNVs: Harbinger of a Rare Variant Revolution in Psychiatric Genetics. Cell 148, 1223–1241. https://doi.org/10.1016/j.cell.2012.02.039
Marchetto, M.C., Belinson, H., Tian, Y., Freitas, B.C., Fu, C., Vadodaria, K.C., Beltrao-Braga, P.C., Trujillo, C.A., Mendes, A.P.D., Padmanabhan, K., Nunez, Y., Ou, J., Ghosh, H., Wright, R., Brennand, K.J., Pierce, K., Eichenfield, L., Pramparo, T., Eyler, L.T., Barnes, C.C., Courchesne, E., Geschwind, D.H., Gage, F.H., Wynshaw-Boris, A., Muotri, A.R., 2017. Altered proliferation and networks in neural cells derived from idiopathic autistic individuals. Mol. Psychiatry 22, 820–835. https://doi.org/10.1038/mp.2016.95
Marín, O., Müller, U., 2014. Lineage origins of GABAergic versus glutamatergic neurons in the neocortex. Curr. Opin. Neurobiol., SI: Inhibition: Synapses, Neurons and Circuits 26, 132–141. https://doi.org/10.1016/j.conb.2014.01.015
Martín, M.G., Pfrieger, F., Dotti, C.G., 2014. Cholesterol in brain disease: sometimes determinant and frequently implicated. EMBO Rep. 15, 1036–1052. https://doi.org/10.15252/embr.201439225
Mast, N., Lin, J.B., Anderson, K.W., Bjorkhem, I., Pikuleva, I.A., 2017. Transcriptional and post-translational changes in the brain of mice deficient in cholesterol removal mediated by cytochrome P450 46A1 (CYP46A1). PLOS ONE 12, e0187168. https://doi.org/10.1371/journal.pone.0187168
Mauch, D.H., Nägler, K., Schumacher, S., Göritz, C., Müller, E.-C., Otto, A., Pfrieger, F.W., 2001. CNS Synaptogenesis Promoted by Glia-Derived Cholesterol. Science 294, 1354–1357. https://doi.org/10.1126/science.294.5545.1354

Meaney, S., Hassan, M., Sakinis, A., Lütjohann, D., Von Bergmann, K., Wennmalm, Å., Diczfalusy, U., Björkhem, I., 2001. Evidence that the major oxysterols in human circulation originate from distinct pools of cholesterol: a stable isotope study. J. Lipid Res. 42 1, 70–78.

Meljon, A., Theofilopoulos, S., Shackleton, C.H.L., Watson, G.L., Javitt, N.B., Knölker, H.-J., Saini, R., Arenas, E., Wang, Y., Griffiths, W.J., 2012. Analysis of bioactive oxysterols in newborn mouse brain by LC/MS. J. Lipid Res. 53, 2469–2483. https://doi.org/10.1194/jlr.D028233

Menteşe Babayiğit, T., Gümüş-Akay, G., Uytun, M.Ç., Doğan, Ö., Serdar, M.A., Efendi, G.Y., Erman, A.G., Yürümez, E., Öztop, D.B., 2024. Investigation of Liver X Receptor Gene Variants and Oxysterol Dysregulation in Autism Spectrum Disorder. Children 11, 551. https://doi.org/10.3390/children11050551

Messedi, M., Makni-Ayadi, F., 2024. 24S-Hydroxycholesterol in Neuropsychiatric Diseases: Schizophrenia, Autism Spectrum Disorder, and Bipolar Disorder, in: Lizard, G. (Ed.), Implication of Oxysterols and Phytosterols in Aging and Human Diseases. Springer International Publishing, Cham, pp. 293–304. https://doi.org/10.1007/978-3-031-43883-7_15

Mitroi, D.N., Pereyra-Gómez, G., Soto-Huelin, B., Senovilla, F., Kobayashi, T., Esteban, J.A., Ledesma, M.D., 2019. NPC1 enables cholesterol mobilization during long-term potentiation that can be restored in Niemann–Pick disease type C by CYP46A1 activation. EMBO Rep. 20, e48143. https://doi.org/10.15252/embr.201948143

Moreno, M.B.T., Singulani, M.P., van de Bilt, M.T., Loch, A.A., Gattaz, W.F., Talib, L.L., 2025. Cholesterol metabolism and its implications in psychotic disorders: a comparative study of individuals at ultra high risk and control groups. Eur. Arch. Psychiatry Clin. Neurosci. https://doi.org/10.1007/s00406-025-01966-5

Mukhtar, T., Taylor, V., 2018. Untangling Cortical Complexity During Development. J. Exp. Neurosci. 12, 1179069518759332. https://doi.org/10.1177/1179069518759332

Mutka, A.-L., Lusa, S., Linder, M.D., Jokitalo, E., Kopra, O., Jauhiainen, M., Ikonen, E., 2004. Secretion of Sterols and the NPC2 Protein from Primary Astrocytes*. J. Biol. Chem. 279, 48654–48662. https://doi.org/10.1074/jbc.M405345200

Myers, B.R., Sever, N., Chong, Y.C., Kim, J., Belani, J.D., Rychnovsky, S., Bazan, J.F., Beachy, P.A., 2013. Hedgehog pathway modulation by

multiple lipid binding sites on the smoothened effector of signal response. Dev. Cell 26, 346–357. https://doi.org/10.1016/j.devcel.2013.07.015
Nachtergaele, S., Whalen, D.M., Mydock, L.K., Zhao, Z., Malinauskas, T., Krishnan, K., Ingham, P.W., Covey, D.F., Siebold, C., Rohatgi, R., 2013. Structure and function of the Smoothened extracellular domain in vertebrate Hedgehog signaling. eLife 2, e01340. https://doi.org/10.7554/eLife.01340
Napoli, I., Mercaldo, V., Boyl, P.P., Eleuteri, B., Zalfa, F., De Rubeis, S., Di Marino, D., Mohr, E., Massimi, M., Falconi, M., Witke, W., Costa-Mattioli, M., Sonenberg, N., Achsel, T., Bagni, C., 2008. The Fragile X Syndrome Protein Represses Activity-Dependent Translation through CYFIP1, a New 4E-BP. Cell 134, 1042–1054. https://doi.org/10.1016/j.cell.2008.07.031
Nedelcu, D., Liu, J., Xu, Y., Jao, C., Salic, A., 2013. Oxysterol binding to the extracellular domain of Smoothened in Hedgehog signaling. Nat. Chem. Biol. 9, 557–564. https://doi.org/10.1038/nchembio.1290
Nieuwenhuis, E., Hui, C., 2005. Hedgehog signaling and congenital malformations. Clin. Genet. 67, 193–208. https://doi.org/10.1111/j.1399-0004.2004.00360.x
Nieweg, K., Schaller, H., Pfrieger, F.W., 2009. Marked differences in cholesterol synthesis between neurons and glial cells from postnatal rats. J. Neurochem. 109, 125–134. https://doi.org/10.1111/j.1471-4159.2009.05917.x
Ogata, K., Kosaka, T., 2002. Structural and quantitative analysis of astrocytes in the mouse hippocampus. Neuroscience 113, 221–33.
Ogundare, M., Theofilopoulos, S., Lockhart, A., Hall, L.J., Arenas, E., Sjövall, J., Brenton, A.G., Wang, Y., Griffiths, W.J., 2010. Cerebrospinal Fluid Steroidomics: Are Bioactive Bile Acids Present in Brain? 2. J. Biol. Chem. 285, 4666–4679. https://doi.org/10.1074/jbc.M109.086678
Olzmann, J.A., Carvalho, P., 2019. Dynamics and functions of lipid droplets. Nat. Rev. Mol. Cell Biol. 20, 137–155. https://doi.org/10.1038/s41580-018-0085-z
Parente, M., Tonini, C., Buzzelli, V., Carbone, E., Trezza, V., Pallottini, V., 2022. Brain Cholesterol Biosynthetic Pathway Is Altered in a Preclinical Model of Fragile X Syndrome. Int. J. Mol. Sci. 23, 3408. https://doi.org/10.3390/ijms23063408

Parrado-Fernandez, C., Leoni, V., Saeed, A., Rodriguez-Rodriguez, P., Sandebring-Matton, A., Córdoba-Beldad, C.M., Bueno, P., Gali, C.C., Panzenboeck, U., Cedazo-Minguez, A., Björkhem, I., 2021. Sex difference in flux of 27-hydroxycholesterol into the brain. Br. J. Pharmacol. 178, 3194–3204. https://doi.org/10.1111/bph.15353

Paşca, A.M., Sloan, S.A., Clarke, L.E., Tian, Y., Makinson, C.D., Huber, N., Kim, C.H., Park, J.-Y., O'Rourke, N.A., Nguyen, K.D., Smith, S.J., Huguenard, J.R., Geschwind, D.H., Barres, B.A., Paşca, S.P., 2015. Functional cortical neurons and astrocytes from human pluripotent stem cells in 3D culture. Nat. Methods 12, 671–678. https://doi.org/10.1038/nmeth.3415

Paul, S.M., Doherty, J.J., Robichaud, A.J., Belfort, G.M., Chow, B.Y., Hammond, R.S., Crawford, D.C., Linsenbardt, A.J., Shu, H.-J., Izumi, Y., Mennerick, S.J., Zorumski, C.F., 2013. The Major Brain Cholesterol Metabolite 24(S)-Hydroxycholesterol Is a Potent Allosteric Modulator of N-Methyl-d-Aspartate Receptors. J. Neurosci. 33, 17290–17300. https://doi.org/10.1523/JNEUROSCI.2619-13.2013

Paulsen, B., Velasco, S., Kedaigle, A.J., Pigoni, M., Quadrato, G., Deo, A.J., Adiconis, X., Uzquiano, A., Sartore, R., Yang, S.M., Simmons, S.K., Symvoulidis, P., Kim, K., Tsafou, K., Podury, A., Abbate, C., Tucewicz, A., Smith, S.N., Albanese, A., Barrett, L., Sanjana, N.E., Shi, X., Chung, K., Lage, K., Boyden, E.S., Regev, A., Levin, J.Z., Arlotta, P., 2022. Autism genes converge on asynchronous development of shared neuron classes. Nature 602, 268–273. https://doi.org/10.1038/s41586-021-04358-6

Pepinsky, R.B., Zeng, C., Wen, D., Rayhorn, P., Baker, D.P., Williams, K.P., Bixler, S.A., Ambrose, C.M., Garber, E.A., Miatkowski, K., Taylor, F.R., Wang, E.A., Galdes, A., 1998. Identification of a Palmitic Acid-modified Form of Human Sonic hedgehog*. J. Biol. Chem. 273, 14037–14045. https://doi.org/10.1074/jbc.273.22.14037

Pfrieger, Frank W., 2003. Outsourcing in the brain: Do neurons depend on cholesterol delivery by astrocytes? BioEssays 25, 72–78. https://doi.org/10.1002/bies.10195

Pfrieger, Frank W, 2003. Role of cholesterol in synapse formation and function. Cholest.-Rich Domains 1610, 271–280. https://doi.org/10.1016/S0005-2736(03)00024-5

Pfrieger, F.W., Ungerer, N., 2011. Cholesterol metabolism in neurons and astrocytes. Prog. Lipid Res. 50, 357–371. https://doi.org/10.1016/j.plipres.2011.06.002
Porter, F.D., Herman, G.E., 2011. Malformation syndromes caused by disorders of cholesterol synthesis. J. Lipid Res. 52, 6–34. https://doi.org/10.1194/jlr.R009548
Porter, J.A., Young, K.E., Beachy, P.A., 1996. Cholesterol Modification of Hedgehog Signaling Proteins in Animal Development. Science. https://doi.org/10.1126/science.274.5285.255
Qi, X., Friedberg, L., De Bose-Boyd, R., Long, T., Li, X., 2020. Sterols in an intramolecular channel of Smoothened mediate Hedgehog signaling. Nat. Chem. Biol. 16, 1368–1375. https://doi.org/10.1038/s41589-020-0646-2
Qi, X., Liu, H., Thompson, B., McDonald, J., Zhang, C., Li, X., 2019. Cryo-EM structure of oxysterol-bound human Smoothened coupled to a heterotrimeric Gi. Nature 571, 279–283. https://doi.org/10.1038/s41586-019-1286-0
Radhakrishnan, A., Rohatgi, R., Siebold, C., 2020. Cholesterol access in cellular membranes controls Hedgehog signaling. Nat. Chem. Biol. 16, 1303–1313. https://doi.org/10.1038/s41589-020-00678-2
Rajan, P., McKay, R.D.G., 1998. Multiple Routes to Astrocytic Differentiation in the CNS. J. Neurosci. 18, 3620–3629. https://doi.org/10.1523/JNEUROSCI.18-10-03620.1998
Rakic, P., 1974. Neurons in Rhesus Monkey Visual Cortex: Systematic Relation between Time of Origin and Eventual Disposition. Science 183, 425–427. https://doi.org/10.1126/science.183.4123.425
Raleigh, D.R., Sever, N., Choksi, P.K., Sigg, M.A., Hines, K.M., Thompson, B.M., Elnatan, D., Jaishankar, P., Bisignano, P., Garcia-Gonzalo, F.R., Krup, A.L., Eberl, M., Byrne, E.F.X., Siebold, C., Wong, S.Y., Renslo, A.R., Grabe, M., McDonald, J.G., Xu, L., Beachy, P.A., Reiter, J.F., 2018. Cilia-Associated Oxysterols Activate Smoothened. Mol. Cell 72, 316-327.e5. https://doi.org/10.1016/j.molcel.2018.08.034
Redcay, E., Courchesne, E., 2005. When Is the Brain Enlarged in Autism? A Meta-Analysis of All Brain Size Reports. Biol. Psychiatry 58, 1–9. https://doi.org/10.1016/j.biopsych.2005.03.026
Repa, J.J., Mangelsdorf, D.J., 2000a. The Role of Orphan Nuclear Receptors in the Regulation of Cholesterol Homeostasis. Annu. Rev. Cell Dev. Biol. 16, 459–481. https://doi.org/10.1146/annurev.cellbio.16.1.459

Repa, J.J., Mangelsdorf, D.J., 2000b. The Role of Orphan Nuclear Receptors in the Regulation of Cholesterol Homeostasis. Annu. Rev. Cell Dev. Biol. 16, 459–481. https://doi.org/10.1146/annurev.cellbio.16.1.459

Saher, G., Brügger, B., Lappe-Siefke, C., Möbius, W., Tozawa, R., Wehr, M.C., Wieland, F., Ishibashi, S., Nave, K.-A., 2005. High cholesterol level is essential for myelin membrane growth. Nat. Neurosci. 8, 468–475. https://doi.org/10.1038/nn1426

Sakashita, N., Miyazaki, A., Takeya, M., Horiuchi, S., Chang, C.C.Y., Chang, T.-Y., Takahashi, K., 2000. Localization of Human Acyl-Coenzyme A:Cholesterol Acyltransferase-1 (ACAT-1) in Macrophages and in Various Tissues. Am. J. Pathol. 156, 227–236. https://doi.org/10.1016/S0002-9440(10)64723-2

Sato, R., 2010. Sterol metabolism and SREBP activation. Arch. Biochem. Biophys. 501, 177–181. https://doi.org/10.1016/j.abb.2010.06.004

Sawicka, K., Hale, C.R., Park, C.Y., Fak, J.J., Gresack, J.E., Van Driesche, S.J., Kang, J.J., Darnell, J.C., Darnell, R.B., 2019. FMRP has a cell-type-specific role in CA1 pyramidal neurons to regulate autism-related transcripts and circadian memory. eLife 8, e46919. https://doi.org/10.7554/eLife.46919

Schenck, A., Bardoni, B., Moro, A., Bagni, C., Mandel, J.-L., 2001. A highly conserved protein family interacting with the fragile X mental retardation protein (FMRP) and displaying selective interactions with FMRP-related proteins FXR1P and FXR2P. Proc. Natl. Acad. Sci. U. S. A. 98, 8844–8849. https://doi.org/10.1073/pnas.151231598

Schroepfer, G.J., 2000. Oxysterols: Modulators of Cholesterol Metabolism and Other Processes | Physiological Reviews [WWW Document]. URL https://journals.physiology.org/doi/full/10.1152/physrev.2000.80.1.361?rfr_dat=cr_pub++0pubmed&url_ver=Z39.88-2003&rfr_id=ori%3Arid%3Acrossref.org (accessed 12.3.24).

Shackleford, G., Makoukji, J., Grenier, J., Liere, P., Meffre, D., Massaad, C., 2013a. Differential regulation of Wnt/beta-catenin signaling by Liver X Receptors in Schwann cells and oligodendrocytes. Biochem. Pharmacol., European Network for Oxysterol Research 86, 106–114. https://doi.org/10.1016/j.bcp.2013.02.036

Shackleford, G., Makoukji, J., Grenier, J., Liere, P., Meffre, D., Massaad, C., 2013b. Differential regulation of Wnt/beta-catenin signaling by Liver X Receptors in Schwann cells and oligodendrocytes.

Biochem. Pharmacol., European Network for Oxysterol Research 86, 106–114. https://doi.org/10.1016/j.bcp.2013.02.036
Shackleton, C., Pozo, Ó., Marcos, J., 2018. GC/MS in Recent Years Has Defined the Normal and Clinically Disordered Steroidome: Will It Soon Be Surpassed by LC/Tandem MS in This Role? J. Endocr. Soc. 2, 974–996. https://doi.org/10.1210/js.2018-00135
Sharpe, H.J., Wang, W., Hannoush, R.N., de Sauvage, F.J., 2015. Regulation of the oncoprotein Smoothened by small molecules. Nat. Chem. Biol. 11, 246–255. https://doi.org/10.1038/nchembio.1776
Sheng, R., Kim, H., Lee, H., Xin, Y., Chen, Y., Tian, W., Cui, Y., Choi, J.-C., Doh, J., Han, J.-K., Cho, W., 2014. Cholesterol selectively activates canonical Wnt signalling over non-canonical Wnt signalling. Nat. Commun. 5, 4393. https://doi.org/10.1038/ncomms5393
Shu, H.-J., Ziolkowski, L.H., Salvatore, S.V., Benz, A.M., Wozniak, D.F., Yuede, C.M., Paul, S.M., Zorumski, C.F., Mennerick, S., 2024. Effects of Complete and Partial Loss of the 24S-Hydroxycholesterol-Generating Enzyme Cyp46a1 on Behavior and Hippocampal Transcription in Mouse. Biomolecules 14, 254. https://doi.org/10.3390/biom14030254
Smiljanic, K., Lavrnja, I., Mladenovic Djordjevic, A., Ruzdijic, S., Stojiljkovic, M., Pekovic, S., Kanazir, S., 2010. Brain injury induces cholesterol 24-hydroxylase (Cyp46) expression in glial cells in a time-dependent manner. Histochem. Cell Biol. 134, 159–169. https://doi.org/10.1007/s00418-010-0718-6
Son, Y., Kim, S.-M., Lee, S.-A., Eo, S.-K., Kim, K., 2013. Oxysterols induce transition of monocytic cells to phenotypically mature dendritic cell-like cells. Biochem. Biophys. Res. Commun. 438, 161–168. https://doi.org/10.1016/j.bbrc.2013.07.046
Song, H.-R., Gonzalez-Gomez, I., Suh, G.S., Commins, D.L., Sposto, R., Gilles, F.H., Deneen, B., Erdreich-Epstein, A., 2010. Nuclear factor IA is expressed in astrocytomas and is associated with improved survival. Neuro-Oncol. 12, 122–132. https://doi.org/10.1093/neuonc/nop044
Spanos, F., Gerenu, G., Goikolea, J., Latorre-Leal, M., Balleza-Tapia, H., Gomez, K., Álvarez-Jiménez, L., Piras, A., Gómez-Galán, M., Fisahn, A., Cedazo-Minguez, A., Maioli, S., Loera-Valencia, R., 2024. Impaired astrocytic synaptic function by peripheral cholesterol metabolite 27-hydroxycholesterol. Front. Cell. Neurosci. 18, 1347535. https://doi.org/10.3389/fncel.2024.1347535

Stoner Rich, Chow Maggie L., Boyle Maureen P., Sunkin Susan M., Mouton Peter R., Roy Subhojit, Wynshaw-Boris Anthony, Colamarino Sophia A., Lein Ed S., Courchesne Eric, n.d. Patches of Disorganization in the Neocortex of Children with Autism. N. Engl. J. Med. 370, 1209–1219. https://doi.org/10.1056/NEJMoa1307491

Straniero, S., Laskar, A., Savva, C., Härdfeldt, J., Angelin, B., Rudling, M., 2020. Of mice and men: murine bile acids explain species differences in the regulation of bile acid and cholesterol metabolism. J. Lipid Res. 61, 480–491. https://doi.org/10.1194/jlr.RA119000307

Subramanian, L., Calcagnotto, M.E., Paredes, M.F., 2020. Cortical Malformations: Lessons in Human Brain Development. Front. Cell. Neurosci. 13. https://doi.org/10.3389/fncel.2019.00576

Sun, W., Cornwell, A., Li, J., Peng, S., Osorio, M.J., Aalling, N., Wang, S., Benraiss, A., Lou, N., Goldman, S.A., Nedergaard, M., 2017. SOX9 Is an Astrocyte-Specific Nuclear Marker in the Adult Brain Outside the Neurogenic Regions. J. Neurosci. 37, 4493–4507. https://doi.org/10.1523/JNEUROSCI.3199-16.2017

Sun, Z., Zhao, L., Bo, Q., Mao, Z., He, Y., Jiang, T., Li, Y., Wang, C., Li, R., 2021. Brain-Specific Oxysterols and Risk of Schizophrenia in Clinical High-Risk Subjects and Patients With Schizophrenia. Front. Psychiatry 12. https://doi.org/10.3389/fpsyt.2021.711734

Sur, M., Rubenstein, J.L.R., 2005. Patterning and Plasticity of the Cerebral Cortex. Science 310, 805–810. https://doi.org/10.1126/science.1112070

Suzuki, R., Lee, K., Jing, E., Biddinger, S.B., McDonald, J.G., Montine, T.J., Craft, S., Kahn, C.R., 2010. Diabetes and Insulin in Regulation of Brain Cholesterol Metabolism. Cell Metab. 12, 567–579. https://doi.org/10.1016/j.cmet.2010.11.006

Tachikawa, M., Watanabe, M., Hori, S., Fukaya, M., Ohtsuki, S., Asashima, T., Terasaki, T., 2005. Distinct spatio-temporal expression of ABCA and ABCG transporters in the developing and adult mouse brain. J. Neurochem. 95, 294–304. https://doi.org/10.1111/j.1471-4159.2005.03369.x

Tajik, M., Baharfar, M., Donald, W.A., 2022. Single-cell mass spectrometry. Trends Biotechnol. 40, 1374–1392. https://doi.org/10.1016/j.tibtech.2022.04.004

Talvio, K., Wagner, V.A., Minkeviciene, R., Kirkwood, J.S., Kulinich, A.O., Umemori, J., Bhatia, A., Hur, M., Käkelä, R., Ethell, I.M., Castrén,

M.L., 2023. An iPSC-derived astrocyte model of fragile X syndrome exhibits dysregulated cholesterol homeostasis. Commun. Biol. 6, 789. https://doi.org/10.1038/s42003-023-05147-9

TCW, J., Qian, L., Pipalia, N.H., Chao, M.J., Liang, S.A., Shi, Y., Jain, B.R., Bertelsen, S.E., Kapoor, M., Marcora, E., Sikora, E., Andrews, E.J., Martini, A.C., Karch, C.M., Head, E., Holtzman, D.M., Zhang, B., Wang, M., Maxfield, F.R., Poon, W.W., Goate, A.M., 2022. Cholesterol and matrisome pathways dysregulated in astrocytes and microglia. Cell 185, 2213-2233.e25. https://doi.org/10.1016/j.cell.2022.05.017

Teboul, M., Enmark, E., Li, Q., Wikström, A.C., Pelto-Huikko, M., Gustafsson, J.A., 1995. OR-1, a member of the nuclear receptor superfamily that interacts with the 9-cis-retinoic acid receptor. Proc. Natl. Acad. Sci. 92, 2096–2100. https://doi.org/10.1073/pnas.92.6.2096

Theofilopoulos, S., Abreu de Oliveira, W.A., Yang, S., Yutuc, E., Saeed, A., Abdel-Khalik, J., Ullgren, A., Cedazo-Minguez, A., Björkhem, I., Wang, Y., Griffiths, W.J., Arenas, E., 2019. 24(S),25-Epoxycholesterol and cholesterol 24S-hydroxylase (CYP46A1) overexpression promote midbrain dopaminergic neurogenesis in vivo. J. Biol. Chem. 294, 4169–4176. https://doi.org/10.1074/jbc.RA118.005639

Theofilopoulos, S., Griffiths, W.J., Crick, P.J., Yang, S., Meljon, A., Ogundare, M., Kitambi, S.S., Lockhart, A., Tuschl, K., Clayton, P.T., Morris, A.A., Martinez, A., Reddy, M.A., Martinuzzi, A., Bassi, M.T., Honda, A., Mizuochi, T., Kimura, A., Nittono, H., De Michele, G., Carbone, R., Criscuolo, C., Yau, J.L., Seckl, J.R., Schüle, R., Schöls, L., Sailer, A.W., Kuhle, J., Fraidakis, M.J., Gustafsson, J.-Å., Steffensen, K.R., Björkhem, I., Ernfors, P., Sjövall, J., Arenas, E., Wang, Y., 2014. Cholestenoic acids regulate motor neuron survival via liver X receptors. J. Clin. Invest. 124, 4829–4842. https://doi.org/10.1172/JCI68506

Theofilopoulos, S., Wang, Y., Kitambi, S.S., Sacchetti, P., Sousa, K.M., Bodin, K., Kirk, J., Saltó, C., Gustafsson, M., Toledo, E.M., Karu, K., Gustafsson, J.-Å., Steffensen, K.R., Ernfors, P., Sjövall, J., Griffiths, W.J., Arenas, E., 2013. Brain endogenous liver X receptor ligands selectively promote midbrain neurogenesis. Nat. Chem. Biol. 9, 126–133. https://doi.org/10.1038/nchembio.1156

Tierney, E., Bukelis, I., Thompson, R.E., Ahmed, K., Aneja, A., Kratz, L., Kelley, R.I., 2006. Abnormalities of cholesterol metabolism in

autism spectrum disorders. Am. J. Med. Genet. B Neuropsychiatr. Genet. 141B, 666–668. https://doi.org/10.1002/ajmg.b.30368
Tierney, E., Remaley, A.T., Thurm, A., Jager, L.R., Wassif, C.A., Kratz, L.E., Bailey-Wilson, J.E., Bukelis, I., Sarphare, G., Jung, E.S., Brand, B., Noah, K.K., Porter, F.D., 2021. Sterol and lipid analyses identifies hypolipidemia and apolipoprotein disorders in autism associated with adaptive functioning deficits. Transl. Psychiatry 11, 471. https://doi.org/10.1038/s41398-021-01580-8
Tint, G.S., Yu, H., Shang, Q., Xu, G., Patel, S.B., 2006. The use of the Dhcr7 knockout mouse to accurately determine the origin of fetal sterols. J. Lipid Res. 47, 1535–1541. https://doi.org/10.1194/jlr.M600141-JLR200
Tomita, H., Hines, K.M., Herron, J.M., Li, A., Baggett, D.W., Xu, L., n.d. 7-Dehydrocholesterol-derived oxysterols cause neurogenic defects in Smith-Lemli-Opitz syndrome. eLife 11, e67141. https://doi.org/10.7554/eLife.67141
Toppozini, L., Meinhardt, S., Armstrong, C.L., Yamani, Z., Kučerka, N., Schmid, F., Rheinstädter, M.C., 2014. Structure of Cholesterol in Lipid Rafts. Phys. Rev. Lett. 113, 228101. https://doi.org/10.1103/PhysRevLett.113.228101
Tozawa, R., Ishibashi, S., Osuga, J., Yagyu, H., Oka, T., Chen, Z., Ohashi, K., Perrey, S., Shionoiri, F., Yahagi, N., Harada, K., Gotoda, T., Yazaki, Y., Yamada, N., 1999. Embryonic Lethality and Defective Neural Tube Closure in Mice Lacking Squalene Synthase*. J. Biol. Chem. 274, 30843–30848. https://doi.org/10.1074/jbc.274.43.30843
Uno, S., Endo, K., Jeong, Y., Kawana, K., Miyachi, H., Hashimoto, Y., Makishima, M., 2009. Suppression of β-catenin signaling by liver X receptor ligands. Biochem. Pharmacol. 77, 186–195. https://doi.org/10.1016/j.bcp.2008.10.007
van der Zwaag, B., Staal, W.G., Hochstenbach, R., Poot, M., Spierenburg, H.A., de Jonge, M.V., Verbeek, N.E., van ’t Slot, R., van Es, M.A., Staal, F.J., Freitag, C.M., Buizer-Voskamp, J.E., Nelen, M.R., van den Berg, L.H., van Amstel, H.K.P., van Engeland, H., Burbach, J.P.H., 2010. A Co-segregating Microduplication of Chromosome 15q11.2 Pinpoints Two Risk Genes for Autism Spectrum Disorder. Am. J. Med. Genet. Part B Neuropsychiatr. Genet. Off. Publ. Int. Soc. Psychiatr. Genet. 153B, 960–966. https://doi.org/10.1002/ajmg.b.31055

Villalba, A., Götz, M., Borrell, V., 2021. Chapter One - The regulation of cortical neurogenesis, in: Bashaw, G.J. (Ed.), Current Topics in Developmental Biology, Molecular Mechanisms of Neural Development and Insights into Disease. Academic Press, pp. 1–66. https://doi.org/10.1016/bs.ctdb.2020.10.003

Wang, N., Yvan-Charvet, L., Lütjohann, D., Mulder, M., Vanmierlo, T., Kim, T.-W., Tall, A.R., 2008. ATP-binding cassette transporters G1 and G4 mediate cholesterol and desmosterol efflux to HDL and regulate sterol accumulation in the brain. FASEB J. 22, 1073–1082. https://doi.org/10.1096/fj.07-9944com

Wang, Y., Sousa, K.M., Bodin, K., Theofilopoulos, S., Sacchetti, P., Hornshaw, M., Woffendin, G., Karu, K., Sjövall, J., Arenas, E., Griffiths, W.J., 2009a. Targeted Lipidomic Analysis of Oxysterols in the Embryonic Central Nervous System. Mol. Biosyst. 5, 529–541. https://doi.org/10.1039/b819502a

Wang, Y., Sousa, K.M., Bodin, K., Theofilopoulos, S., Sacchetti, P., Hornshaw, M., Woffendin, G., Karu, K., Sjövall, J., Arenas, E., Griffiths, W.J., 2009b. Targeted lipidomic analysis of oxysterols in the embryonic central nervous system. Mol. Biosyst. 5, 529–541. https://doi.org/10.1039/b819502a

Wang, Y., Yutuc, E., Griffiths, W.J., 2021. Neuro-oxysterols and neuro-sterols as ligands to nuclear receptors, GPCRs, ligand-gated ion channels and other protein receptors. Br. J. Pharmacol. 178, 3176–3193. https://doi.org/10.1111/bph.15191

Wellington, C.L., Walker, E.K.Y., Suarez, A., Kwok, A., Bissada, N., Singaraja, R., Yang, Y.-Z., Zhang, L.-H., James, E., Wilson, J.E., Francone, O., McManus, B.M., Hayden, M.R., 2002. ABCA1 mRNA and Protein Distribution Patterns Predict Multiple Different Roles and Levels of Regulation. Lab. Invest. 82, 273–283. https://doi.org/10.1038/labinvest.3780421

Willert, K., Brown, J.D., Danenberg, E., Duncan, A.W., Weissman, I.L., Reya, T., Yates, J.R., Nusse, R., 2003. Wnt proteins are lipid-modified and can act as stem cell growth factors. Nature 423, 448–452. https://doi.org/10.1038/nature01611

Wong, F., Fei, J., Mora-Bermúdez, F., Taverna, E., Haffner, C., Fu, J., Anastassiadis, K., Stewart, A., Huttner, W., 2015. Sustained Pax6 Expression Generates Primate-like Basal Radial Glia in Developing Mouse Neocortex. PLoS Biol. 13. https://doi.org/10.1371/journal.pbio.1002217

Wong, J., Quinn, C.M., Guillemin, G., Brown, A.J., 2007. Primary human astrocytes produce 24(S),25-epoxycholesterol with implications for brain cholesterol homeostasis. J. Neurochem. 103, 1764–1773. https://doi.org/10.1111/j.1471-4159.2007.04913.x

Yang, L., Liu, S., Wang, Y., 2019. Role of bone morphogenetic protein-2/4 in astrocyte activation in neuropathic pain. Mol. Pain 15, 1744806919892100. https://doi.org/10.1177/1744806919892100

Yoon, K.-J., Nguyen, H.N., Ursini, G., Zhang, F., Kim, N.-S., Wen, Z., Makri, G., Nauen, D., Shin, J.H., Park, Y., Chung, R., Pekle, E., Zhang, C., Towe, M., Mohammed Qasim Hussaini, S., Lee, Y., Rujescu, D., St. Clair, D., Kleinman, J.E., Hyde, T.M., Krauss, G., Christian, K.M., Rapoport, J.L., Weinberger, D.R., Song, H., Ming, G., 2014. Modeling a genetic risk for schizophrenia in iPSCs and mice reveals neural stem cell deficits associated with adherens junctions and polarity. Cell Stem Cell 15, 79–91. https://doi.org/10.1016/j.stem.2014.05.003

Yutuc, E., Angelini, R., Baumert, M., Mast, N., Pikuleva, I., Newton, J., Clench, M.R., Skibinski, D.O.F., Howell, O.W., Wang, Y., Griffiths, W.J., 2020. Localization of sterols and oxysterols in mouse brain reveals distinct spatial cholesterol metabolism. Proc. Natl. Acad. Sci. U. S. A. 117, 5749–5760. https://doi.org/10.1073/pnas.1917421117

Zerbinati, C., Iuliano, L., 2017. Cholesterol and related sterols autoxidation. Free Radic. Biol. Med., 4-Hydroxynonenal and Related Lipid Peroxidation Products 111, 151–155. https://doi.org/10.1016/j.freeradbiomed.2017.04.013

Zhang, J., Liu, Q., 2015. Cholesterol metabolism and homeostasis in the brain. Protein Cell 6, 254–264. https://doi.org/10.1007/s13238-014-0131-3

Zvonic, S., Cornelius, P., Stewart, W.C., Mynatt, R.L., Stephens, J.M., 2003. The Regulation and Activation of Ciliary Neurotrophic Factor Signaling Proteins in Adipocytes *. J. Biol. Chem. 278, 2228–2235. https://doi.org/10.1074/jbc.M205871200

Chapter 7
Appendix

Publications related to thesis

De La Fuente, D.C.F., Tamburini, C., Stonelake, E., *et al*. (2024). Impaired oxysterol-liver X receptor signaling underlies aberrant cortical neurogenesis in a stem cell model of neurodevelopmental disorder. Cell Reports. Vol. 43, Issue 3.

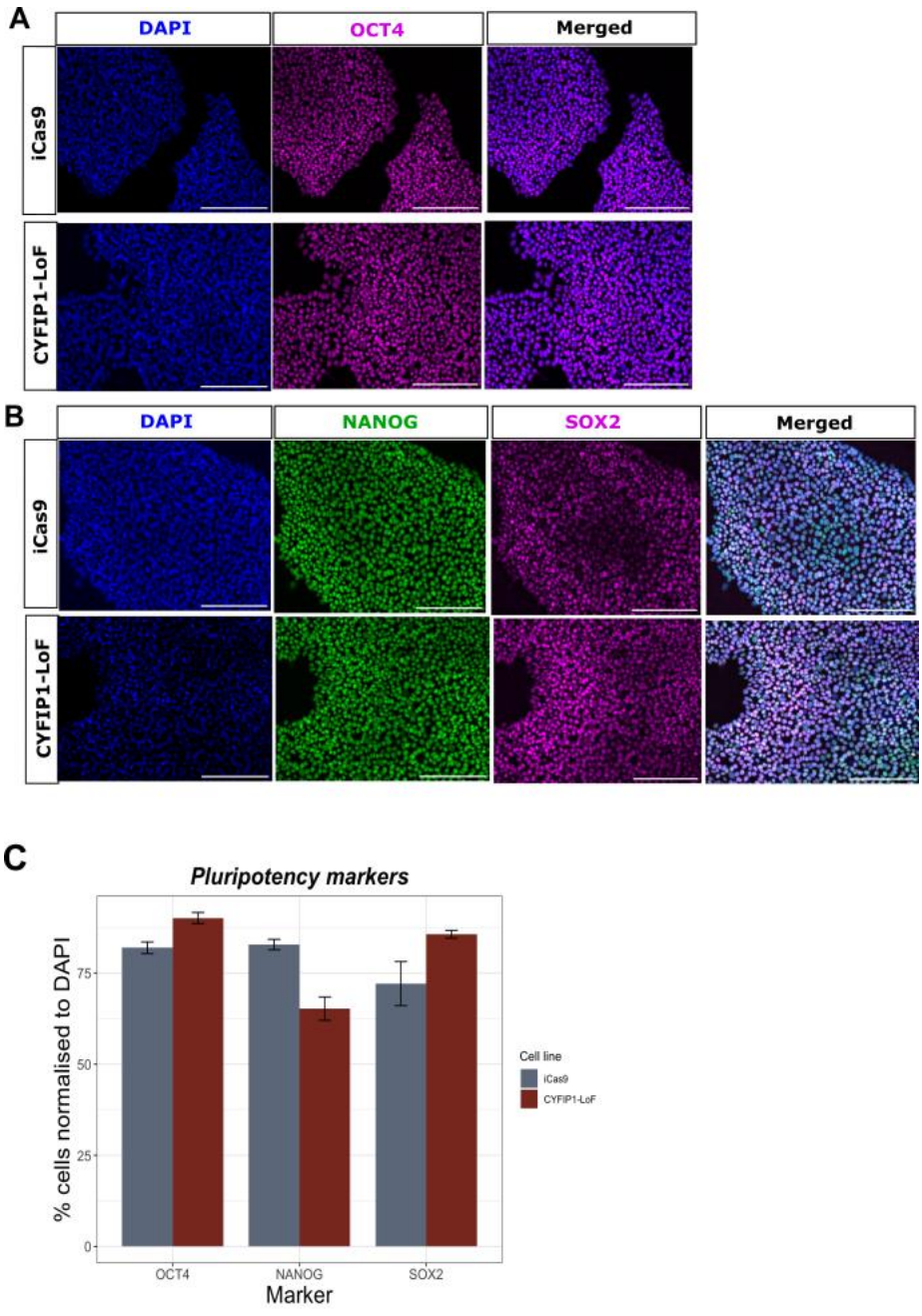

Figure 7.1. Pluripotency of CYFIP1-LoF and iCas9 hESC cultures. 20X magnification. Scale bar = 200μM. n=3, count average from 10 fields of view.

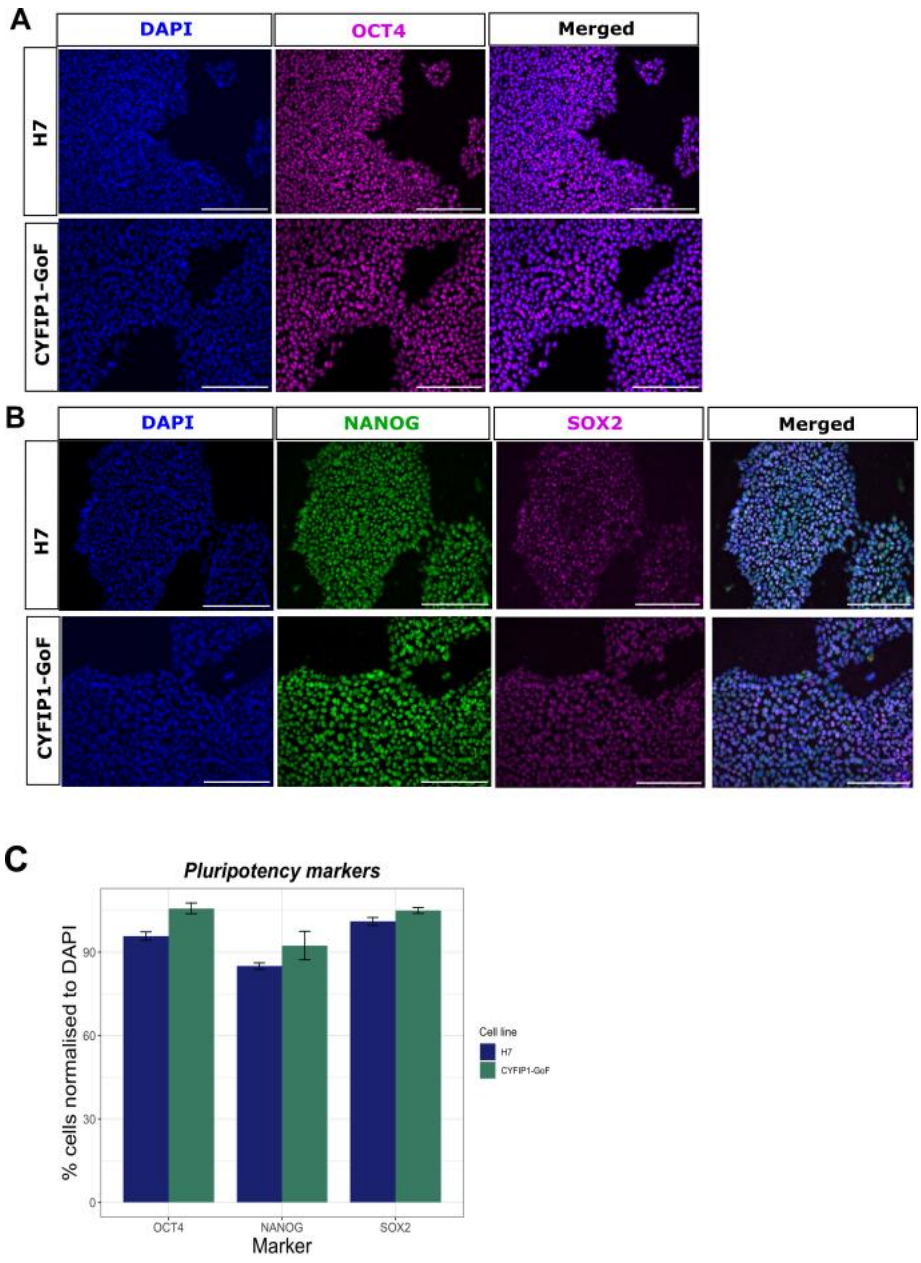

Figure 7.2. Pluripotency of CYFIP1-GoF and H7 hESC cultures. 20X magnification. Scale bar = 200μM. n=3, count average from 10 fields of view.

Table 7.1. Monohydroxycholesterol LC-MS^3 method specification. Mass inclusion list and analysis time.

Precursor ion [M+] (m/z)	IT-MS mass (MS^2 transition) (m/z)	Time (min)
534.4054	455.3632	37
539.4368	455.3632	37
540.4431	461.4009	37
545.4745	461.4009	37
546.4807	462.4071	37

Table 7.2. Dihydroxycholesterol LC-MS^3 method specification. Mass inclusion list and analysis time

Precursor ion [M+] (m/z)	IT-MS mass (MS^2 transition) (m/z)	Time (min)
550.4003	471.3581	17
555.4317	471.3581	17
561.4694	477.3958	17
532.3898	453.3476	17
537.4212	453.3476	17

Table 7.3. Methoxyhydroxycholesterol and cholestenoic acids LC-MS^3 method specification. Mass inclusion list and analysis time.

Precursor ion [M+] (m/z)	IT-MS mass (MS^2 transition) (m/z)	Time (min)
564.3796	485.3374	17
569.411	485.3374	17
567.3984	488.3562	17
572.4298	488.3562	17
548.3847	469.3425	17
553.4161	469.3425	17

Table 7.4. Cholesterol LC-MS3 method specification. Mass inclusion list and analysis time.

Precursor ion [M+] (m/z)	IT-MS mass (MS^2 transition) (m/z)	Time (min)
518.4105	439.3683	17
523.4419	439.3683	17
525.4544	446.4122	17
530.4858	446.4122	17

Table 7.5. Cholesterol precursor LC-MS3 method specification. Mass inclusion list and analysis time.

Precursor ion [M+] (m/z)	IT-MS mass (MS^2 transition) (m/z)	Time (min)
516.3948	437.3526	17
521.4262	437.3526	17
527.3639	443.2904	17
514.3792	435.337	17
519.4106	435.337	17

Table 7.6. Internal standards used in sample iSTD mastermix.

Internal standard	Cat. number
24R/S-HC-D6	700018
7α-HC-D7	LM-4103
7-OC-D7	LM-4107
22S-3O-HC-D7	700051P
7α,25-DiHC-D6	111117P
3β-HCA-D5	700151P
7αH,3O-HCA-D3	700194P
Desmosterol-D6	700040P
Cholesterol-D7	700041P

Table 7.7. Composition of iSTDs mastermix for analysis of hPSC pellet.

Endogenous sterol		iSTD quantified against	Amount per sample (ng)
Systemic name	**Common name**		
Cholest-5-en-3β,24S-diol	24S-hydroxycholesterol	24R/S-HC-D6	2
Cholest-5-en-3β,(25R)26-diol	27-hydroxycholesterol	24R/S-HC-D6	2
Cholest-5-en-3β,7α-diol	7α-hydroxycholesterol	7α-HC-D7	2
Cholest-5-en-3β,7β-diol	7β-hydroxycholesterol	7α-HC-D7	2
3β-Hydroxycholest-5-en-24-one	24-one	7α,25-DiHC-D6	1
Cholesta-4,6-diene-3β,24(or25)-diol	24S,25-dehydrocholesterol	7α,25-DiHC-D6	1
Cholest-5-en-3β,24,25-triol	24S,25-dihydroxycholesterol	7α,25-DiHC-D6	1
Cholest-5-en-3β,7α,26-triol	7α, 26-dihydroxycholesterol	7α,25-DiHC-D6	1
3β-Hydroxycholesta-5-en-(25R)26-oic acid	(25S)-cholestenoic acid	7αH,3O-HCA-D3	2
3β,7α-Dihydroxycholest-5-en-26-oic acid	3β, 7α-dihydroxycholestenoic acid	7αH,3O-HCA-D3	2

3β,24-Dihydroxycholest-5-en-25-methoxide	24S,25-methoxyhydroxycholesterol	7αH,3O-HCA-D3	2
Cholesta-5,24-dien-3β-ol	Desmosterol	Desmosterol-D6	2
Cholesta-5,8(9)-dien-3β-ol	8(9)-dehydrocholesterol	Desmosterol-D6	2
Cholest-5-en-3β-ol	Cholesterol	Cholesterol-D7	200

Table 7.8. Composition of iSTDs mastermix for analysis of hPSC media.

Endogenous sterol		iSTD quantified against	Amount per sample (ng)
Systemic name	**Common name**		
Cholest-5-en-3β,24S-diol	24S-hydroxycholesterol	24R/S-HC-D6	1
Cholest-5-en-3β,(25R)26-diol	27-hydroxycholesterol	24R/S-HC-D6	1
Cholest-5-en-3β,7α-diol	7α-hydroxycholesterol	7α-HC-D7	1
Cholest-5-en-3β,7β-diol	7β-hydroxycholesterol	7α-HC-D7	1
3β-Hydroxycholest-5-en-24-one	24-one	7α,25-DiHC-D6	0.5
Cholesta-4,6-diene-3β,24(or25)-diol	24S,25-dehydrocholesterol	7α,25-DiHC-D6	0.5
Cholest-5-en-3β,24,25-triol	24S,25-dihydroxycholesterol	7α,25-DiHC-D6	0.5

Cholest-5-en-3β,7α,26-triol	7α, 26-dihydroxycholesterol	7α,25-DiHC-D6	0.5
3β-Hydroxycholesta-5-en-(25R)26-oic acid	(25S)-cholestenoic acid	7αH,3O-HCA-D3	1
3β,7α-Dihydroxycholest-5-en-26-oic acid	3β, 7α-dihydroxycholestenoic acid	7αH,3O-HCA-D3	1
3β,24-Dihydroxycholest-5-en-25-methoxide	24S,25-methoxyhydroxycholesterol	7αH,3O-HCA-D3	1

Table 7.9. 15q11.2del patient-derived cells demonstrate differences in cortical neurogenesis. Quantification of neural progenitor marker PAX6 and cortical markers CTIP2 and TBR1 expression.

Cell line	Marker	DIV	Mean	SD
900	PAX6	35	28.74	5.27
EA008	PAX6	35	20.43	4.86
EA062	PAX6	35	19.75	6.31
900	TBR1	20	4.82	3.81
EA008	TBR1	20	6.92	4.03
EA062	TBR1	20	7.15	2.34
900	TBR1	30	32.13	7.24
EA008	TBR1	30	50.05	8.48
EA062	TBR1	30	32.79	13.26
900	TBR1	40	19.68	9.63
EA008	TBR1	40	30.2	13.52
EA062	TBR1	40	32.79	13.26
900	CTIP2	20	3.82	0.6
EA008	CTIP2	20	3.82	3.00
EA062	CTIP2	20	9.31	3.39
900	CTIP2	30	38.27	11.13
EA008	CTIP2	30	43.13	5.44
EA062	CTIP2	30	58.87	9.55
900	CTIP2	40	22.32	9.54
EA008	CTIP2	40	39.13	14.81
EA062	CTIP2	40	31.01	16.09

Table 7.10. Sterols identified in LC-MS^n analysis of hPSC-derived cell samples. Details of all sterols quantified in name, systemic name, chemical formula, exact mass before derivatisation and following derivatisation with GP-d5 and GP-d0, structure and ion trap fragmentation (ITMS^3) spectra.

Sterol	Systematic Name	Chemical formula	Structure mass (m/z)	GPd0 m/z	GPd5 m/z	Structure	ITMS^3 spectra
Cholesterol	Cholest-5-en-3β -ol	$C_{27}H_{46}O$	386.3549	518.4105	523.4414	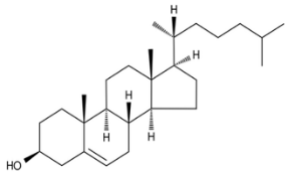	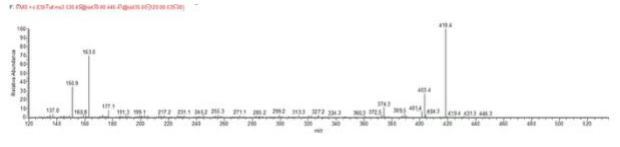
Desmosterol	Cholest-5,24-dien-3β-ol	$C_{27}H_{44}O$	384.3392	516.3950	521.4262	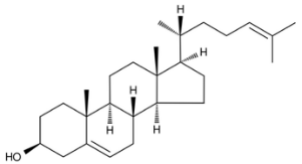	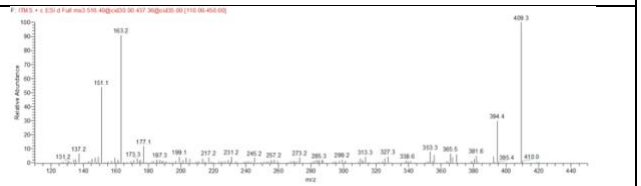
8(9)-DHC	Cholest-5,8-dien-3β-ol	$C_{27}H_{44}0$	384.3392	516.3950	521.4262	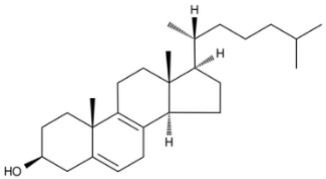	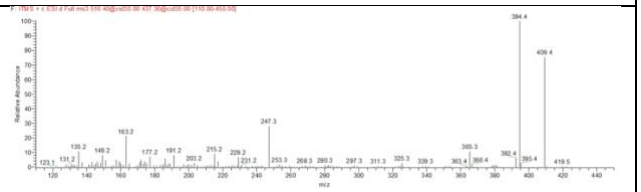

24S,25-EC	24S,25-epoxycholest-5-ene 3β-ol	$C_{27}H_{44}O_2$	400.3341	532.3898	537.4206	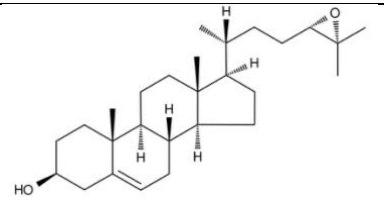	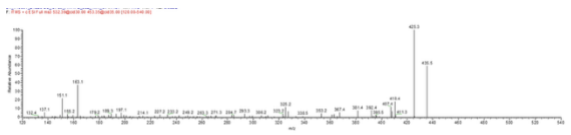
24S-HC	Cholest-5-ene-3β,24S-diol	$C_{27}H_{46}O_2$	402.3498	N/A	539.4368	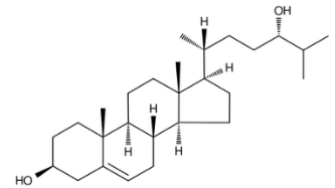	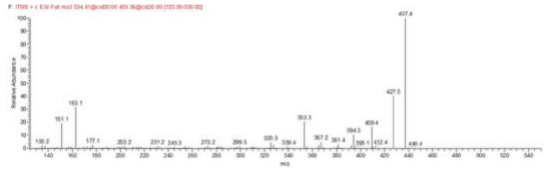
27-HC	Cholest-5-en-3β,26-diol	$C_{27}H_{46}O_2$	402.3498	N/A	539.4368	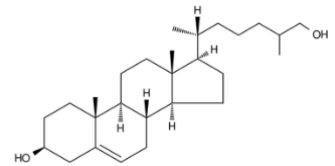	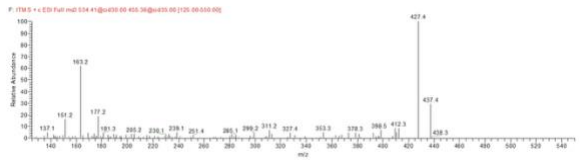
7-keto-cholesterol	3β-Hydroxycholest-5-en-7-one	$C_{27}H_{44}O_2$	400.3341	534.4054	N/A	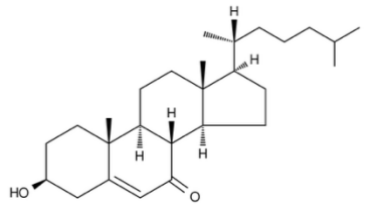	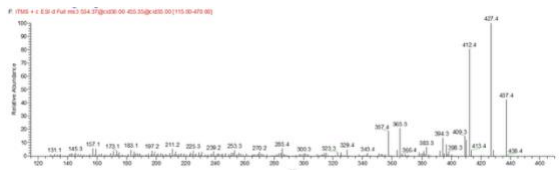

7α-HC	Cholest-5-ene-3β,7α-diol	$C_{27}H_{46}O_2$	402.3498	N/A	539.4368	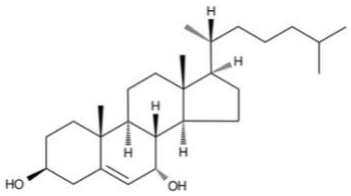	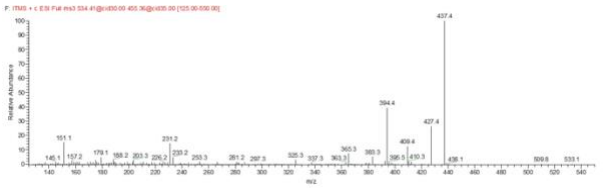
7β-HC	Cholest-5-ene-3β,7β-diol	$C_{27}H_{46}O_2$	402.3498	534.4054	539.4368	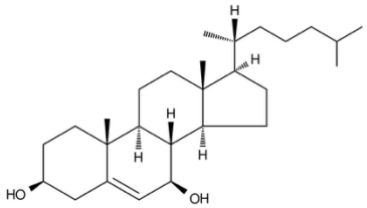	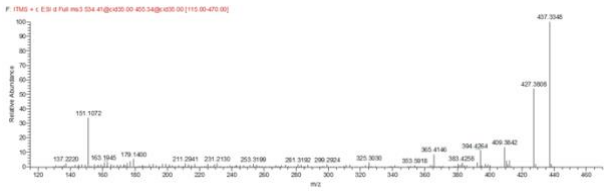
7α, 26-diHC	Cholest-5-ene-3β,7α,(25R)26-triol	$C_{27}H_{46}O_3$	418.3447	N/A	555.4317	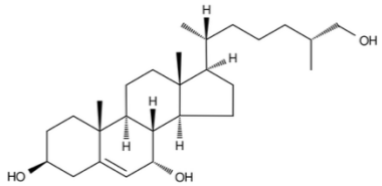	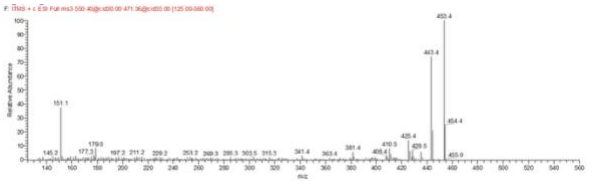

Table 7.11. Quantification of sterol content of neural cell pellets from derived from hESC lines determined by LC-MS^n analysis. Mean of 2 independent experiments, n=5-6. N/D = Not detected.

Cell line	Sterol	Day *In Vitro* (DIV)	Mean Concentration (ng/x10^6 cells)	S.E.M.
H7	24S-HC	10	0.886	0.0554
		20	0.209	0.0616
		30	0.366	0.0242
		40	2.37	0.433
		50	5.00	0.332
H7	24S,25-EC	10	0.919	0.0763
		20	0.413	0.124
		30	0.366	0.0443
		40	0.713	0.114
		50	0.394	0.0221
H7	27-HC	10	0.413	0.0663
		20	N/D	N/D
		30	N/D	N/D
		40	N/D	N/D
		50	0.0814	0.00543
H7	7α-HC	10	0.161	0.0195
		20	0.0711	0.0141
		30	0.0296	0.00129
		40	0.0299	0.00474
		50	0.0590	0.00685
H7		10	0.128	0.0175

	7β-HC	20	0.0633	0.0171
		30	0.0318	0.00391
		40	0.0813	0.0185
		50	0.115	0.0160
H7	7-ketocholesterol	10	1.54	0.263
		20	0.502	0.0677
		30	0.493	0.113
		40	0.712	0.144
		50	1.37	0.122
H7	6β-HC	10	0.193	0.0512
		20	0.107	0.00554
		30	0.0710	0.0189
		40	0.00207	0
		50	0.106	0.0250
H7	7α, 26-diHC	10	0.0623	0.00766
		20	0.0334	0.00637
		30	0.000997	0.000173
		40	0.00215	0.000439
		50	0.00255	0.000141
H7	Cholesterol	10	6590	0.935
		20	2650	0.556
		30	3010	0.240
		40	4620	0.597
		50	6950	0.549
H7	Desmosterol	10	27.8	3.64
		20	5.74	1.37
		30	8.50	0.649

		40	30.1	3.02
		50	49.7	2.41
H7	8(9)-DHC	10	28.2	5.52
		20	15.1	3.78
		30	14.9	1.62
		40	31.3	4.35
		50	63.6	4.52
iCas9	24S-HC	10	0.0474	0.00343
		20	0.269	0.0262
		30	0.366	0.0146
		40	0.823	0.0776
		50	0.652	0.192
iCas9	24S,25-EC	10	0.143	0.0111
		20	0.406	0.0648
		30	0.277	0.0148
		40	0.932	0.0809
		50	0.531	0.151
iCas9	27-HC	10	N/D	N/D
		20	N/D	N/D
		30	N/D	N/D
		40	N/D	N/D
		50	N/D	N/D
iCas9	7α-HC	10	0.0101	0.000562
		20	0.0958	0.0315
		30	0.0588	0.0254
		40	0.0859	0.00815
		50	0.0327	0.0107

iCas9	7β-HC	10	0.0212	0.00137
		20	0.165	0.0601
		30	0.0581	0.0274
		40	0.105	0.00643
		50	0.0698	0.0267
iCas9	7-ketocholesterol	10	0.125	0.0106
		20	1.35	0.305
		30	1.14	0.533
		40	1.58	0.0529
		50	0.539	0.213
iCas9	6β-HC	10	0.0175	0.00436
		20	0.128	0.0366
		30	0.0884	0.0302
		40	0.100	0.00585
		50	0.0527	0.0199
iCas9	7α, 26-diHC	10	N/D	N/D
		20	0.0257	0.00970
		30	N/D	N/D
		40	N/D	N/D
		50	N/D	N/D
iCas9	Cholesterol	10	437	0.0376
		20	1260	0.148
		30	1360	0.0216
		40	2090	0.134
		50	1430	0.392
iCas9	Desmosterol	10	1.10	0.133
		20	4.60	0.376

		30	7.49	0.0857
		40	19.4	8.38
		50	3.99	1.18
iCas9	8(9)-DHC	10	3.46	0.207
		20	6.23	0.946
		30	6.52	0.0996
		40	19.5	9.18
		50	8.16	2.53
CYFIP1-GoF	24S-HC	10	1.10	0.0554
		20	0.163	0.0390
		30	1.08	0.142
		40	2.74	0.362
		50	3.98	0.462
CYFIP1-GoF	24S,25-EC	10	2.47	0.232
		20	0.245	0.0443
		30	0.311	0.0746
		40	0.389	0.0437
		50	0.159	0.0138
CYFIP1-GoF	27-HC	10	0.474	0.108
		20	N/D	N/D
		30	N/D	N/D
		40	0.697	0.0238
		50	1.16	0.153
CYFIP1-GoF	7α-HC	10	0.229	0.0114
		20	0.0684	0.0336
		30	0.0392	0.00473
		40	0.0266	0.00198

		50	0.0461	0.00887
CYFIP1-GoF	7β-HC	10	0.182	0.00735
		20	0.0622	0.0243
		30	0.0980	0.0108
		40	0.137	0.0101
		50	0.126	0.0147
CYFIP1-GoF	7-ketocholesterol	10	2.68	0.312
		20	0.640	0.105
		30	0.516	0.0893
		40	0.176	0.0161
		50	0.246	0.0352
CYFIP1-GoF	6β-HC	10	0.217	0.00752
		20	0.194	0.103
		30	0.0415	0.00299
		40	0.000247	0.000247
		50	0.144	0.0416
CYFIP1-GoF	7α, 26-diHC	10	0.0561	0.00746
		20	0.0534	0.0122
		30	0.0125	0.00114
		40	0.0217	0.00238
		50	0.0137	0.00126
CYFIP1-GoF	Cholesterol	10	7600	0.401
		20	2800	0.634
		30	5630	0.692
		40	8590	0.407
		50	9160	0.828
	Desmosterol	10	28.8	1.63

CYFIP1-GoF		20	8.24	2.37
		30	6.84	1.44
		40	7.80	1.10
		50	7.87	0.211
CYFIP1-GoF	8(9)-DHC	10	38.6	4.15
		20	13.2	3.93
		30	16.7	1.97
		40	26.4	2.73
		50	31.3	2.61
CYFIP1-LoF	24S-HC	10	0.128	0.0221
		20	0.244	0.0333
		30	0.482	0.0629
		40	0.576	0.0150
		50	0.468	0.0682
CYFIP1-LoF	24S,25-EC	10	0.378	0.0793
		20	0.458	0.0345
		30	0.419	0.0561
		40	0.736	0.0294
		50	0.360	0.0702
CYFIP1-LoF	27-HC	10	N/D	N/D
		20	N/D	N/D
		30	N/D	N/D
		40	N/D	N/D
		50	N/D	N/D
CYFIP1-LoF	7α-HC	10	0.0284	0.00255
		20	0.221	0.0118
		30	0.0405	0.00197

		40	0.0827	0.0649
		50	0.0680	0.0127
CYFIP1-LoF	7β-HC	10	0.0623	0.0113
		20	0.251	0.0245
		30	0.0964	0.00326
		40	0.144	0.00277
		50	0.149	0.0188
CYFIP1-LoF	7-ketocholesterol	10	0.472	0.0860
		20	2.46	0.170
		30	0.804	0.0630
		40	1.72	0.0986
		50	1.24	0.167
CYFIP1-LoF	6β-HC	10	0.0355	0.00816
		20	0.280	0.0188
		30	0.0759	0.0226
		40	0.108	0.0176
		50	0.127	0.0397
CYFIP1-LoF	7α, 26-diHC	10	N/D	N/D
		20	0.0372	0.00297
		30	N/D	N/D
		40	N/D	N/D
		50	N/D	N/D
CYFIP1-LoF	Cholesterol	10	1360	0.235
		20	1740	0.0984
		30	2070	0.197
		40	1720	0.0890
		50	1320	0.196

CYFIP1-LoF	Desmosterol	10	3.33	0.686
		20	11.5	1.17
		30	28.1	5.28
		40	15.4	0.156
		50	1.47	0.182
CYFIP1-LoF	8(9)-DHC	10	10.4	2.10
		20	10.7	0.428
		30	12.4	1.27
		40	12.0	1.02
		50	7.44	0.917

Table 7.12. Quantification of sterol content of neural cell media determined by LC-MS^n analysis.

Mean result of 1 independent differentiation, n=3.

Cell line	Sterol	Day *In Vitro* (DIV)	Mean Concentration (ng/x10^6 cells)	S.E.M.
H7	24S-HC	10	0.359	0.180
		20	0.432	0.141
		30	0.428	0.062
		40	0.659	0.084
		50	0.958	0.129
H7	24S,25-EC	10	0.418	0.088
		20	0.470	0.193
		30	0.199	0.020
		40	0.077	0.013
		50	0.078	0.008
H7	27-HC	10	0.573	0.289
		20	0.356	0.130
		30	0.086	0.015
		40	0.055	0.009
		50	0.085	0.012
H7	7α-HC	10	0.048	0.013
		20	0.277	0.157
		30	0.214	0.022
		40	0.180	0.068
		50	0.051	0.011

H7	7β-HC	10	0.039	0.010
		20	0.064	0.005
		30	0.042	0.012
		40	0.044	0.013
		50	0.027	0.005
H7	7-ketocholesterol	10	0.140	0.015
		20	0.426	0.069
		30	0.519	0.154
		40	0.345	0.020
		50	0.100	0.002
H7	6β-HC	10	0.038	0.006
		20	0.352	0.080
		30	0.255	0.061
		40	0.148	0.040
		50	0.091	0.052
H7	7α, 26-diHC	10	1.500	0.343
		20	0.317	0.102
		30	0.064	0.012
		40	0.034	0.005
		50	0.066	0.007
H7	25S-cholestenoic acid	10	2.28	0.772
		20	0.166	0.066
		30	0.070	0.016
		40	0.070	0.008
		50	0.072	0.014
H7	3β,7α-cholestenoic acid	10	8.39	1.880
		20	0.271	0.039

		30	0.088	0.014
		40	0.035	0.004
		50	0.157	0.031

Table 7.13. Quantification of sterol content of neural cell pellets from derived from iPSC lines determined by LC-MS^n analysis. Mean of 1 independent experiment, n=3. N/D = Not detected.

Cell line	Sterol	Day *In Vitro* (DIV)	Mean Concentration (ng/x10^6 cells)	S.E.M.
900	24S-HC	10	0.494	0.0478
		20	0.340	0.00254
		30	0.760	0.0583
		40	2.64	0.378
		50	4.67	1.30
900	24S,25-EC	10	0.873	0.0533
		20	0.795	0.0124
		30	0.577	0.0294
		40	0.457	0.0314
		50	0.816	0.0795
900	27-HC	10	N/D	N/D
		20	N/D	N/D
		30	N/D	N/D
		40	N/D	N/D
		50	N/D	N/D
900	7α-HC	10	0.0248	0.00350
		20	0.0443	0.00541

		30	0.121	0.0135
		40	0.0554	0.00488
		50	0.687	0.346
900	7β-HC	10	0.102	0.0155
		20	0.0448	0.00162
		30	0.0991	0.0112
		40	0.209	0.0311
		50	0.460	0.231
900	7-ketocholesterol	10	1.23	0.116
		20	0.615	0.0297
		30	1.71	0.105
		40	2.39	0.242
		50	3.49	1.79
900	6β-HC	10	0.0746	0.00536
		20	0.0597	0.00307
		30	0.102	0.00789
		40	0.123	0.0267
		50	0.594	0.303
900	7α, 26-diHC	10	0.0714	0.0117
		20	0.0492	0.00313
		30	N/D	N/D
		40	0.00983	0.000691
		50	N/D	N/D
900	Cholesterol	10	3120	0.285
		20	2480	0.0461
		30	3350	0.189
		40	4580	0.358

		50	17200	3.83
900	Desmosterol	10	1.47	0.134
		20	5.81	0.131
		30	34.7	4.15
		40	34.8	0.549
		50	12.1	0.199
900	8(9)-DHC	10	21.8	2.02
		20	10.6	0.201
		30	22.4	1.35
		40	32.5	1.76
		50	44.5	5.84
EA008.4	24S-HC	10	0.517	0.149
		20	0.585	0.095
		30	0.147	0.0133
		40	0.71	0.179
		50	0.980	0.148
EA008.4	24S,25-EC	10	0.473	0.142
		20	1.50	0.105
		30	0.49	0.0681
		40	0.45	0.102
		50	0.172	0.00716
EA008.4	27-HC	10	N/D	N/D
		20	N/D	N/D
		30	N/D	N/D
		40	N/D	N/D
		50	N/D	N/D
EA008.4		10	0.0196	0.0105

	7α-HC	20	0.115	0.0664
		30	0.0666	0.00454
		40	0.349	0.0457
		50	0.572	0.0502
EA008.4	7β-HC	10	0.0771	0.0428
		20	0.110	0.0564
		30	0.0464	0.00505
		40	0.276	0.0582
		50	0.240	0.0175
EA008.4	7-ketocholesterol	10	0.565	0.300
		20	1.56	1.05
		30	0.998	0.0620
		40	6.31	0.760
		50	3.57	0.532
EA008.4	6β-HC	10	0.0561	0.0290
		20	0.104	0.0573
		30	0.192	0.0292
		40	0.260	0.0399
		50	0.776	0.0889
EA008.4	7α, 26-diHC	10	0.00864	0.000742
		20	0.0623	0.0184
		30	0.0384	0.0366
		40	0.00234	0.000496
		50	N/D	N/D
EA008.4	Cholesterol	10	3780	0.955
		20	4460	0.315
		30	2390	0.200

		40	3790	0.710
		50	4930	0.552
EA008.4	Desmosterol	10	1.53	0.416
		20	6.04	0.58
		30	5.53	2.28
		40	16.4	3.63
		50	3.15	0.235
EA008.4	8(9)-DHC	10	32.4	3.26
		20	16.7	1.35
		30	33.4	6.89
		40	49.4	3.63
		50	48.3	24.6
EA008.21	24S-HC	10	0.557	0.0318
		20	0.53	0.0889
		30	0.0933	0.00882
		40	0.453	0.144
		50	0.453	0.121
EA008.21	24S,25-EC	10	0.32	0.0153
		20	1.67	0.155
		30	0.37	0.0252
		40	0.28	0.0520
		50	0.153	0.0897
EA008.21	27-HC	10	N/D	N/D
		20	N/D	N/D
		30	N/D	N/D
		40	N/D	N/D
		50	N/D	N/D

EA008.21	7α-HC	10	0.0222	0.00196
		20	0.140	0.0150
		30	0.103	0.0177
		40	0.109	0.0706
		50	0.762	0.264
EA008.21	7β-HC	10	0.0841	0.00125
		20	0.128	0.00299
		30	0.0773	0.0217
		40	0.0963	0.0679
		50	0.194	0.0264
EA008.21	7-ketocholesterol	10	1.02	0.0530
		20	1.24	0.250
		30	1.37	0.0817
		40	2.53	1.54
		50	2.95	1.15
EA008.21	6β-HC	10	0.133	0.00961
		20	0.136	0.0117
		30	0.373	0.0551
		40	0.254	0.163
		50	1.31	0.364
EA008.21	7α, 26-diHC	10	0.0262	0.00371
		20	0.438	0.0298
		30	1.17	0.106
		40	1.27	0.0776
		50	N/D	N/D
	Cholesterol	10	4070	0.166
		20	4610	0.596

EA008.21		30	2420	0.271
		40	2770	0.740
		50	3020	0.617
EA008.21	Desmosterol	10	1.47	0.152
		20	6.64	0.178
		30	3.00	1.26
		40	15.3	7.65
		50	3.89	1.04
EA008.21	8(9)-DHC	10	45.2	2.09
		20	21.4	3.07
		30	39.8	4.04
		40	64.9	14.2
		50	56.6	21.7
EA062.13	24S-HC	10	1.13	0.0624
		20	0.709	0.0271
		30	0.939	0.0802
		40	1.81	0.386
		50	4.56	1.01
EA062.13	24S,25-EC	10	4.44	0.337
		20	1.13	0.0548
		30	1.59	0.263
		40	1.12	0.247
		50	1.66	0.460
EA062.13	27-HC	10	N/D	N/D
		20	N/D	N/D
		30	N/D	N/D
		40	N/D	N/D

		50	N/D	N/D
EA062.13	7α-HC	10	0.183	0.0485
		20	0.0557	0.00700
		30	0.0418	0.00610
		40	0.0226	0.00345
		50	0.209	0.0273
EA062.13	7β-HC	10	0.288	0.0116
		20	0.167	0.0117
		30	0.0657	0.00476
		40	0.0992	0.0210
		50	0.475	0.144
EA062.13	7-ketocholesterol	10	2.62	0.228
		20	1.13	0.0941
		30	1.24	0.0446
		40	1.19	0.644
		50	3.75	1.20
EA062.13	6β-HC	10	0.204	0.00847
		20	0.0836	0.00320
		30	0.109	0.00434
		40	0.0892	0.00825
		50	0.655	0.0645
EA062.13	7α, 26-diHC	10	0.0175	0.00164
		20	0.0200	0.00208
		30	0.0219	0.0198
		40	0.00113	0.000429
		50	N/D	N/D
	Cholesterol	10	6300	0.368

EA062.13		20	4250	0.103
		30	4130	0.330
		40	3830	0.688
		50	746	0.166
EA062.13	Desmosterol	10	7.32	0.420
		20	8.57	0.461
		30	70.2	8.12
		40	106.0	23.8
		50	121.0	28.1
EA062.13	8(9)-DHC	10	59.1	2.43
		20	10.1	0.370
		30	18.0	1.84
		40	35.2	9.00
		50	93.8	22.4
EA062.19	24S-HC	10	0.802	0.0671
		20	0.624	0.0373
		30	0.510	0.0168
		40	1.74	0.109
		50	2.69	0.490
EA062.19	24S,25-EC	10	2.03	0.207
		20	0.376	0.0168
		30	0.0851	0.0102
		40	0.120	0.00785
		50	0.217	0.0364
EA062.19	27-HC	10	N/D	N/D
		20	N/D	N/D
		30	N/D	N/D

		40	N/D	N/D
		50	N/D	N/D
EA062.19	7α-HC	10	0.0351	0.00840
		20	0.0319	0.00166
		30	0.0200	0.00107
		40	0.00677	0.000747
		50	0.185	0.0702
EA062.19	7β-HC	10	0.179	0.0196
		20	0.0882	0.000507
		30	0.0330	0.000323
		40	0.0386	0.00434
		50	3.70	0.471
EA062.19	7-ketocholesterol	10	0.995	0.100
		20	0.352	0.0571
		30	0.0793	0.00945
		40	0.0765	0.0204
		50	4.24	0.731
EA062.19	6β-HC	10	0.0901	0.00562
		20	0.0815	0.0121
		30	0.0462	0.00149
		40	0.0336	0.00505
		50	1.53	0.307
EA062.19	7α, 26-diHC	10	0.0237	0.00262
		20	0.131	0.00196
		30	0.159	0.00306
		40	0.425	0.0264
		50	N/D	N/D

EA062.19	Cholesterol	10	4270	0.499
		20	4130	0.106
		30	3730	0.118
		40	4190	0.276
		50	898	0.130
EA062.19	Desmosterol	10	5.29	0.520
		20	2.96	0.172
		30	0.649	0.0668
		40	2.06	0.124
		50	5.13	0.426
EA062.19	8(9)-DHC	10	45.8	5.29
		20	10.3	0.555
		30	4.98	0.246
		40	9.04	0.678
		50	37.2	4.79

Table 7.14. Quantification of sterol content of astrocyte cell pellets determined by LC-MS^n analysis. N/D = Not detected.

Cell line	Sterol	Day *In Vitro* (DIV)	Mean Concentration (ng/x10^6 cells)	S.E.M.
iCas9	24S-HC	70	0.133	0.015
		80	0.170	0.020
		90	0.190	0.040
		110	5.220	0.207
iCas9	24S,25-EC	70	1.38	0.185
		80	2.13	0.298
		90	1.52	0.223
		110	20.5	1.38
iCas9	27-HC	70	0.300	0.062
		80	0.623	0.073
		90	0.300	0.010
		110	N/D	N/D
iCas9	7β-HC	70	0.323	0.012
		80	0.490	0.090
		90	0.314	0.073
		110	30.1	0.325
iCas9	7-ketocholesterol	70	0.420	0.070
		80	0.909	0.132
		90	1.85	0.273
		110	N/D	N/D
iCas9	Cholesterol	70	2.84	0.162
		80	4.56	0.744

		90	3.05	0.148
		110	7.30	0.333
iCas9	Desmosterol	70	4.97	0.762
		80	8.04	1.14
		90	7.04	0.163
		110	4.27	0.108
iCas9	8(9)-DHC	70	37.0	0.686
		80	52.7	9.24
		90	20.7	1.58
		110	46.9	3.94

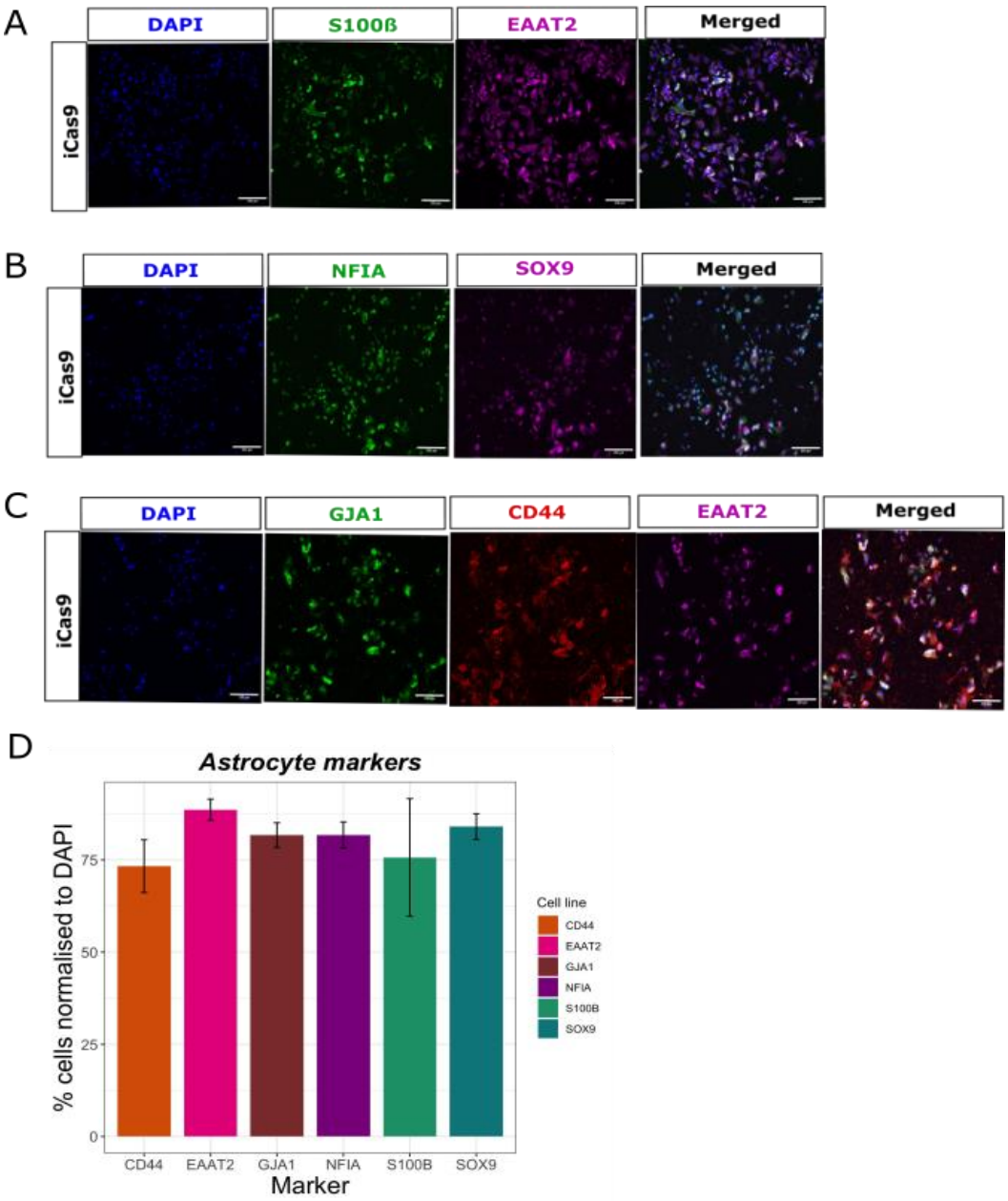

Figure 7.3. Astrocytic marker expression in terminally differentiated astrocyte cultures at DIV110. (**A**) Expression of markers S100β and EAAT2. (**B**) Expression of markers NFIA and SOX9. (**C**) Expression of markers GJA1, CD44 and EAAT2. Scale bar = 200μM, 10X objective.